Royal Holloway
University of London
Department of Earth Sciences

An investigation of tropical Holocene speleothems and their relationship to modern local precipitation

Marianne Brett

Submitted in part fulfilment of the requirements for the degree of
Doctor of Philosophy in Earth Sciences of the University of London
September 2017

Abstract

Holocene speleothems from NE India and the South Pacific were analysed using a robust multi-proxy approach, with contextual environmental monitoring and daily resolution local precipitation. This study compares intraseasonal and interannual variations in precipitation amount and isotopic signature with proxy capture in speleothems to improve methods in climate reconstruction from speleothem proxies, and presents novel records from India and the South Pacific.

Krem Umsynrang cave, in NE India, is located in the core region of the Indian Summer Monsoon, a highly seasonal environment where the controls on interannual precipitation intensity are complex and remain to be fully understood. In the first part of this thesis, I present a new speleothem record spanning the late Holocene, characterise seasonal proxy capture and analyse local precipitation isotopes. The study highlights the importance of fabric studies to construct reliable age models and interpret hydrological changes recorded in the proxy record.

Cave sites in the South Pacific afford the opportunity to reconstruct precipitation records of a tropical maritime environment strongly influenced by the position of the ITCZ and the state of ENSO. I report the results of a detailed analysis of daily precipitation isotopes from Suva, Fiji, and present a new speleothem record from nearby island, Vatulele, as well as pilot studies from the island of Atiu, Cook Islands. These combine to make a novel dataset: the first proxy record to show interdecadal- and centennial-scale variability of the SSouth Pacific Convergence Zone.

The results argue that an interpretation of "the amount effect", which underpins many palaeoclimate reconstructions from speleothem proxies, is belied by complex behaviour of oxygen isotopes, hence, a simple transfer function from speleothem calcite to rainfall amount requires corroboration from local precipitation data. The research emphasises a multi-proxy approach, supported by cave monitoring and study of local rainfall, is crucial for palaeoclimatic reconstruction from speleothem records.

Acknowledgements

I would like to express sincere gratitude and appreciation to:

- The Natural Environment Research Council for funding my doctoral training, and the Royal Holloway Research Committee for providing additional funding for conferences and study visits.

- Prof Dave Mattey & Prof Nigel Harris for supervision, teaching and encouragement with additional scientific support from Prof. Wolfgang Muller. Thanks also to Dr Silvia Frisia, a great scientist and role model, and Dr Andrea Borsato, especially for photography, and to my co-authors and collaborators.

- Dr Steph Walker, Dr Maxim Lamare, Dr Amy Gough and Dr Dave Gold; my stalwart colleagues in the department keeping me on the straight and narrow and Humarrah Sheikh for sterling work in proof-reading the entire thesis!

- The "Stalgossip" group: Dr Bob Jamieson, Dr Monika Markowska, Dr Pete Akers and Dr Nick Scroxton; some amazing stalagmite discussion and conferences together.

- Dr Seb Zimmerman and the circus society; Dan Parsonage and the touch rugby people, for getting me out of the office and teaching me new skills.

- The Evans family and Liam Glen for housing me in my time of need.

- Flo Glen, Jenty Burrill, Tom Fackrell, and my wonderful family, for their endless support, patience and unswerving belief. There's no better support network, I love and appreciate you all, thank you.

Dedication

This thesis is dedicated to the memory of Sir Terry Pratchett, whose writing accompanied me throughout my formative years until the commencement of my doctoral training. He will always inspire me to look at the world from new perspectives and to be endlessly curious. Thank you, and rest in peace.

"If you trust in yourself.... and believe in your dreams.... and follow your star... you'll still get beaten by people who spent their time working hard and learning things and weren't so lazy."

Sir Terence David John Pratchett, OBE - in "The Wee Free Men"

Contents

List of Tables

List of Figures

Chapter 1

Introduction

1.1 The Indo-Pacific Warm Pool: driver of global climate

The Indo-Pacific Warm Pool (IPWP) is a large (>30×10^6 km^2), non-static area of ocean where surface temperatures remain >28 °C, and has been recognised as the primary source of heat for the atmosphere, driving the global climate system. The IPWP spans the western Pacific and eastern Indian oceans, with water transferred through the Indonesian archipelago. It forms part of the global thermohaline circulation and provides an important coupling between ocean and atmosphere via the formation of high convective clouds, supplying the atmosphere with water vapour and heat. Warm pool associated oceanic and atmospheric currents provide important mechanisms for zonal and meridional mass transport, but there is an inherent difficulty in isolating part of a highly complex global system, with continual temporal and spatial variability, and attempting to quantify it in a meaningful way. However, long term weather and climate forecasting depend heavily on current understanding of IPWP processes and teleconnections, thus it is an endeavour deemed well worth pursuing.

Large variations (up to 25% variance) in the spatial extent of the IPWP have been observed on timescales from seasonal to decadal in the instrumental record (Wang and Mehta, 2008), and longer in proxy records (Oppo et al., 2009). These changes locally alter divergent flow in the atmosphere, affecting the Hadley circulation, of which the Intertropical Convergent Zone (ITCZ) is the ascending member, and the Walker circulation, the zonal atmospheric overturning above the tropical Pacific, with global consequences.

The IPWP interacts with several large scale weather-climate systems, including the El Niño - Southern Oscillation (ENSO) (Brijker et al., 2007), the Madden Julian Oscillation (MJO) (Madden and Julian, 1994; Chen and Houze Jr, 1997), the Indian Ocean Dipole (IOD) (Saji et al., 1999) and the Asian and Indian monsoons, but the relationships are complex and appear to be non-static and difficult to model reliably (Annamalai, 1995; Gao et al., 2006). Recent studies suggest climate change is having a profound impact on the IPWP, with the spatial extent and internal sea surface temperatures steadily increasing since the 1980s, slowing down the Walker circulation (Tokinaga et al., 2012), raising sea levels (Weller et al., 2016), and weakening of established modes such as the India Summer Monsoon with ENSO (Kumar, 1999; Ham et al., 2017). Concerns are also raised about intensification of regional monsoon extremes and tropical cyclone (TC) genesis (De Deckker, 2016). The consequences of these changes in the IPWP are as yet unknown but are cause for concern among the international community, as a huge swath of the global population are at risk from the aforementioned impacts. Perturbations in the Asian, Indian and East African monsoons have brought devastating flooding and droughts in recent decades, which in turn bring about economic and humanitarian instability. These areas produce much of the raw and manufactured goods that are traded internationally, as well as hosting large and high density populations. Human activities only serve to exacerbate climate change related disasters, with large cities on coastlines at risk from sea level rise, intense tropical cyclone activities, coastal erosion and sedimentation of waterways. In

the future, these events could lead to the mass migration of people, destabilising the geopolitical situation in affected areas and further afield. It has been argued that the Syrian civil war and mass movement of people escaping the conflict are a direct result of an unusual and prolonged drought that resulted in famine, migration and thus destabilised the formerly thriving country. Thus additional data from centre-of action areas, especially focussed on past perturbations of climate and the IPWP, as well as mechanisms and teleconnections, are of great value for forecasting and planning for mitigation of IPWP related disasters.

An important and well known part of the IPWP is ENSO, which is a quasi-regular ocean-atmosphere coupled oscillatory mode which dominates the inter-annual - decadal variability in rainfall anomalies around the world, especially affecting landmasses adjoining the Pacific ocean (Dai and Wigley, 2000). An extensive body of literature concerning ENSO has built up in recent decades, yet prediction remains elusive prior to the indicative warming(cooling) of the equatorial Pacific signalling onset of El Niño (La Niña) conditions.

This is partially due to the nature of investigating complex systems in a changing climate, and also due to the spatial and temporal bias (Gergis et al., 2006; Rehfeld et al., 2012) in instrumental data (Hausfather et al., 2013), historic documentation and archaeological evidence, which is somewhat Eurasian-centric and predominantly within the Northern Hemisphere. General circulation models (GCMs) and proxy records are extending scientific understanding, but the spatial bias continues (Vilhena and Smith, 2013): the IPWP drives the ocean-atmosphere circulation, yet there are still few high-resolution well-constrained palaeoclimate reconstructions from centre of action locations (Deininger, 2013). Proxy records that record centre-of-action ENSO variability are challenging to establish as sampling opportunities are sparse. With deep ocean and few terrestrial areas suitable, proxy records are limited to a few short speleothem and coral records, along with low resolution lake and ocean cores.

The South Pacific Convergence Zone is a branch of the ITCZ which extends from the main zone in the west equatorial pacific diagonally south east across the south Pacific. It is strongly influenced by ENSO and is of vital importance to the Pacific islands nations being the primary driver of rainfall in the area, yet it is difficult for GCMs to model (Brown et al., 2013), as well as having few reliable proxy records due to the sparse nature of land in this region.

Palaeoclimate reconstructions are sought after for characterisation of climate variability in the pre-instrumental era, with a view to investigating long term and pre-anthropogenic teleconnections, leads, lags and feedbacks between different components of the global climate system, and responses to internal and external forcings. They also provide a framework for the disentangling impacts of anthropogenic activities from long term natural variability, and for testing the validity of GCMs used for predicting weather and future climate.

Proxy records, including lake and ocean sediments, ice cores, pack rat middens, corals and speleothems, are archives of local or regional conditions, or both. Many projects (e.g. Pfeiffer et al., 2006; Cosford et al., 2009; Nehme et al., 2015; Stolper et al., 2016) focus on singular or few samples from a small area, which provide useful and interesting information about past environmental change in that region, but suffer somewhat from being isolated from a regional or global perspective. The palaeoclimate community is increasingly moving towards a cross-disciplinary integrated approach, comparing multiple records together to identify common events, drivers or teleconnections on a hemispheric or global scale (e.g. Gergis et al., 2006; Liang et al., 2015; Akers et al., 2016). As records accumulate, compilations with coherent trends increasingly support palaeoclimate interpretations. However, proxy records must be shown to be robust and reproducible archives of regional change, and on appropriate timescales which can be difficult to achieve. Speleothems are inherently complex and care must be taken to isolate the regional signal from the local.

This project seeks to contribute to this effort by gathering, constructing and

interpreting novel speleothem proxy records from teleconnected areas of interest in the IPWP, where detailed proxy records are yet sparse, and making them available to the community at large, following the standards agreed in the Speleothem Isotopes Synthesis and Analysis Working Group (SISAL).

1.2 Speleothems as palaeoclimate proxies

Over the last two decades, speleothems have become widely recognised as valuable archives of terrestrial palaeoclimate data due to their unique combination of properties: they can be precisely dated, record climate signals continuously over prolonged periods of time and are found in terrestrial locations throughout the world, at diverse latitudes and altitudes. Coupled with the advance in imaging and mass spectrometry, allowing precise and accurate geochemistry to be carried out at high resolution, speleothem have the potential to provide detailed insights into past climate and global teleconnections.

Speleothem are formed as deposits of calcium carbonate in karstified limestone terrains. Rain water dissolves CO_2 from the atmosphere and, at higher partial pressures during infiltration, from respiration products of plants and microorganisms in the soil zone (Baldini et al., 2008; Meyer et al., 2014)and karst (Mattey et al., 2016), thus forming an aqueous solution of weakly dissociating carbonic acid and conjugate base:

$$H_2O_{(l)} + CO_{2(g)} \rightleftharpoons H_2CO_{3(aq)} \rightleftharpoons HCO^-_{3(aq)} + H^+_{(aq)}$$

This provides a solvent to the karst which dissolves $CaCO_3$ from the host rock, usually limestone or dolomite, with some impurities, forming a calcium bicarbonate solution:

$$H_2O_{(l)} + CO_{2(aq)} + Ca^+_{2(aq)} + CO^{2-}_{3(aq)} \rightleftharpoons Ca(HCO_3)^2_{(aq)}$$

As the calcium bicarbonate solution leaves the aquifer and enters the cave, the lower partial pressure of carbon dioxide causes the excess to exsolve from

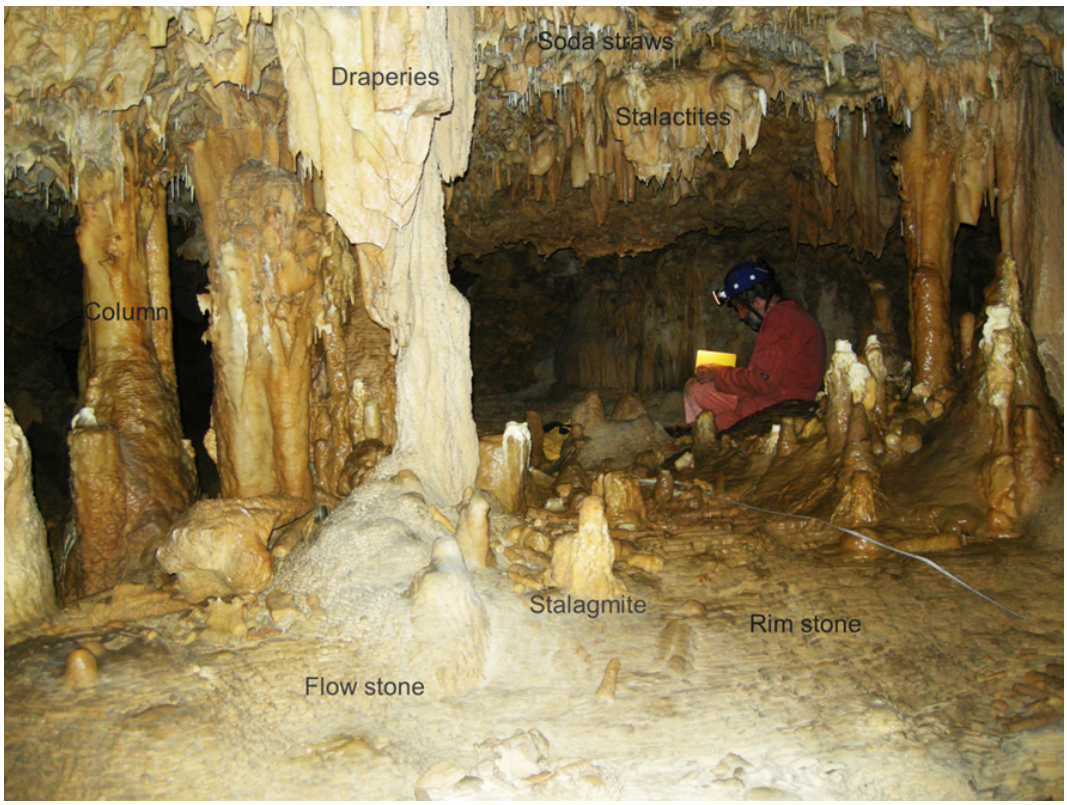

Figure 1.1: Examples of speleothem types, Puatea Cave, Fiji. A large active drapery leads to an active flowstone, and broken, fossil stalagmites are covered in a brown detrital layer. Similar coloured stalactites are visible, many broken at head height, alongside clean, white soda straws feeding the new "parasitic" or "baby" stalagmites forming on the bases where large stalagmites have been broken. All this shows active speleothem growth and is discussed in Chapter 5. Photograph by A. Borsato.

solution:

$$Ca(HCO_3)^2_{(aq)} \rightarrow H_2O_{(l)} + CO_{2(g)} + CaCO_3(s)$$

Within a cave system there are a number of speleothem types formed in this way (Fairchild et al., 2006), with the morphology very much dependent on the partial pressure of the cave CO_2, and the flow regime of the aqueous calcium bicarbonate solution (aka drip water) entering the cave. Laminar flow creates flow stones and drapes, ceiling drips form stalactites (Short et al., 2005)and stalagmites, and, where the liquid pools, features such as cave pearls, rimstones and moonmilk (Alonso-Zarza et al., 2011). There are many other morphologies, but in this thesis we will focus exclusively on stalagmites.

Of all the cave deposits, stalagmites are the most popular to use for palaeocli-

mate research, because they generally have a more simplistic growth history than other speleothem types (Fairchild et al., 2007). Since stalagmites grow dripwise from base to tip, even without a chronology, the researcher can be certain that the stalagmite is younging upward, whereas other cave deposits are more complex in their growth systematics. Additionally, the feeder drips may continue, albeit at a lower rate, during dry seasons or droughts when a flowstone is more likely to be starved of water, especially where the feeder stalactite is supplied by seepage, or diffuse flow of groundwater (Baker and Brunsdon, 2003; McDonald and Drysdale, 2007). Conversely, flood events may well sequentially cover flow stones with sediment, whereas the growing tip of a speleothem may escape from damage or deposits, although not always. Flow stones are also spatially extensive, and have been used for palaeoclimatology work (Boch and Spötl, 2011), but they are spatially heterogenous, providing a challenge for sampling consistency, whereas a stalagmite morphology may be examined to some extent prior to sampling. Another unique property of stalagmites is that the morphology of an individual can indicate the changing environment over time, since changing cave conditions will promote or inhibit faster or slower growth, or a wider or narrower calcite deposit (Dreybrodt, 1999).

Over the last decades, the predominant geochemical investigation carried out using stalagmites has been focused on stable isotopes, specifically those of carbon and oxygen (Harmon et al., 2004; McDermott, 2004). They have been used extensively for attempting to reconstruct a range of parameters, with some examples detailed in Table 1.1.

Speleothem oxygen isotope records are particularly good for providing precise timing and duration of major climatic changes or events that had previously be difficult to date independently, and had relied upon "tuned" age models from sediment or ice cores. Examples include the 8.2ka event (Wu et al., 2012), glacial-interglacial transitions (Mehterian et al., 2017), and Dansgaard-Oeschger events (Spötl and Mangini, 2002). These are large-scale hemispheric

Reconstruction	Isotope	Research example(s)
palaeotemperature	oxygen	Gascoyne (1992); Winograd et al. (1992)
tropical storms	oxygen	Frappier et al. (2007)
vegetation type	carbon	Denniston et al. (1999); Dorale et al. (1998)
biological productivity	carbon	Baldini et al. (2005); Cosford et al. (2009)
sociopolitical changes	oxygen, carbon	Medina-Elizalde et al. (2010); Akers et al. (2016)
solar/orbital forcing	oxygen	Wang et al. (2008); Yuan et al. (2004); Asmerom et al. (2007)
Indian Monsoons	oxygen	Fleitmann et al. (2007); Gupta et al. (2003); Liang et al. (2015)
Asian Monsoons	oxygen, carbon	Wang and Mehta (2008); Li et al. (2011); Cosford et al. (2009)
ENSO	oxygen	Lachniet et al. (2004); Rasbury and Aharon (2006)
palaeorainfall amount	oxygen	Maupin et al. (2014); Partin et al. (2013)

Table 1.1: Some examples of different uses of oxygen and carbon isotope proxy records in speleothems for various climatic and environmental reconstructions. This table is far from exhaustive and serves to give a flavour of the breadth of research within the field.

- global events, so their presence (or absence) in suites of coeval speleothem records of suitable age provides important understanding about teleconnections in the past.

The effort to use speleothems to reconstruct more regional climate signals, such as ENSO, the Atlantic Multidecadal Oscillation (AMO) and the position of the ITCZ, or the jet streams provide different challenges, with an increasing emphasis on using a "multi-proxy approach". This relies on the use of a suite of trace elements (Fairchild and Treble, 2009), or various imaging techniques (Baker et al., 2008), to unpick the local signal from the regional climatic or meteorological variability, and then comparing with existing published records for speleothems or other archives such as historical data, ice cores and tree rings.

While a large body of published research is now available, there are still questions being asked, and gaps in knowledge. For many speleothem papers, the link between oxygen isotopes and climate is somewhat qualitative, and only a few authors have proposed a quantitative relationship between their proxy record and it's environmental driver (Maupin et al., 2014; Partin et al., 2013). Along the same vein, oxygen isotopes of rainfall are often assumed to be primarily controlled by "the amount effect" following (Dansgaard, 1964), in locations where little or no local precipitation isotope data is available (Yadava and Ramesh, 2005; Sinha et al., 2007; Berkelhammer et al., 2010). Within this study, we seek to understand better whether these assumptions are valid for speleothem studies by including detailed precipitation sampling and analysis, in our investigations, and studying two very different hydrological regimes.

There are two areas of interest for this research: i) the complex, continental, orographic Indian monsoonal region, which has a large population, global economic consequences, and produces runoff into Brahmaputra and Ganges rivers that provides important sediment input to Indian Ocean; and ii) Tiny islands in the Pacific Ocean with seasonal convective rainfall.

Both of these are teleconnected with the IPWP and ENSO, have tropical climates and highly seasonal rainfall, yet the hydrological regimes for delivery of moisture are very different and yet to be fully understood.

The South Pacific Convergence Zone (SPCZ) is the most important southern hemisphere expression of the ITCZ, yet an area with very sparse records, either historical or from palaeoclimate reconstruction, and GCMs do not yet resolve it well (Lintner et al., 2016). Within this study we contribute to understanding the SPCZ, by producing new coeval speleothem proxy records of the SPCZ.

1.3 Research aims and objectives

The aim of this research is to produce a suite of novel speleothem proxy records from sites influenced by the IPWP and assess

1. their relationship with local precipitation based on local rainfall isotope data;
2. the extent to which they preserve environmental signals; and
3. their significance as archives of regional environmental change.

In order to achieve the overall research aim, specific research objectives were laid out as outlined below:-

- Test and validate the relationships between rainfall amount and oxygen isotope signatures in both a complex monsoonal region, and the “simple” convective system of an isolated tropical island.
- Use event-resolved rainfall and cave monitoring to establish a framework for interpretation of speleothem proxy time series for each location.
- Build indicative chronologies using targeted U-Th series dating and complementary techniques to model extension rate of selected speleothem samples.

- Create high resolution oxygen and carbon isotopes times eries, supported by trace elements and microstratographic analysis, producing proxy time series' as tools for palaeoclimate reconstruction.

- Compare proxy records to pick out regionally coherent signals.

Chapter	*Title*	*Description*
2	Analytical methods	This chapter details all of the samples and analytical methods used in this research, including field work undertaken, laboratory equipment, set up and work flows. It is written to allow the reader to replicate the experiments while avoiding those techniques that proved less useful.
3	Paper: Annually Laminated Speleothem from NE India: a case study in proxy complexity	This co-authored paper takes the place of a chapter, and presents a new speleothem record from NE India alongside event-resolved rainfall samples. The paper is in final manuscript form and will be submitted to QSR pending final co-author approval.
4	Paper: Oxygen isotopes of Fiji rainfall	This co-authored paper takes the place of a chapter, and presents a new event-resolved rainfall isotope datset from Vitu Levu in Fiji, investigating the controls on oxygen isotopes with respect to rainfall amount and regional convection. This manuscript has been submitted to JGR:Atmos as seen here.
5	Variability of the SPCZ recorded in South Pacific speleothems	This chapter presents new speleothem proxy records from the South Pacific, and discusses how they can preserve a record of the variability of the position of the South Pacific Convergence Zone through the spatiality of rainfall anomaly in the region.
6	Critical analysis	This chapter evaluates the samples, methods, data and conclusions of the work presented in chapters 2-5, to assess the strengths and weaknesses therein, and, with hindsight, what could have been improved. It also discusses the caveats and limitations of the work, where not already discussed within the previous chapters.
7	Synthesis and conclusions	This chapter presents a synthesis of the work, referring back to the aims and objectives of the project, and presents the overall conclusions and implications, along with a summary of achievements, applications and further work.

Table 1.2: Thesis overview: Summary outline of chapters and papers within this thesis.

Chapter 2

Analytical Methods

Methods for extracting proxy records of environmental change from speleothem are developing rapidly, as they become increasingly popular within the palaeoclimate research community. As with many developing fields, there is an element of trial and error, and this is especially the case with stalagmites, as specimens can range widely in size, density, composition and geochemical properties.

A multi-proxy approach underpinned the sampling strategy employed in this research project, with experimental design discussed in Chapters 1 and 6. Reported here are various methods employed in this research project to extract information from Holocene speleothems from the Indo-Pacific Warm Pool, in an attempt to reconstruct palaeo-precipitation, and teleconnections between the South Pacific Convergence Zone (SPCZ) and the Indian Summer Monsoon (ISM).

2.1 Heritage samples used in this research

Some "heritage" samples, that had been previously collected and worked on, were made available at the commencement of this project. They are described

below with appropriate credits.

2.1.1 Samples from India

Precipitation samples from Shillong Plateau

Dr Seb Breitenbach (Cambridge University) arranged collection of rain water samples from Cherrapunjee Holiday Resort (50 km SSW of Shillong, Figure 2.1) in the Meghalaya region of India for his thesis and analysed the oxygen isotopes therein (Breitenbach, 2010). Subsequently, Dr Bijay Mipun collected rainwater samples for this group from the North-Eastern Hill University, Shillong, Megahalaya, which were shipped to Royal Holloway University of London. All fieldwork in India was arranged as a collaboration between Prof Dave Mattey (Royal Holloway University of London), Prof Nigel Harris (The Open University), Prof Talat Ahmad (University of Delhi), Dr Bijay Mipan (North-Eastern Hill University), and Dr Seb Breitenbach (Cambridge), preceding my involvement in the project.

UMS10: Stalagmite from Shillong Plateau

UMS10 is a 604 mm tall stalagmite from Krem Ums Synrang cave, near Shillong, in the Meghalaya region of India. The location and site are described in detail in Chapter 3. UMS10 was found in 6 pieces on the floor of the cave and collected from there, so was assumed to be inactive at the time of collection. The cause of the stalagmite destruction is unclear, however the region is seismically active, so the stalagmite may have been displaced during an earthquake. The pieces are labeled as sections 1 through 6, with the basal section as Section 1. Section 4 has since been cut into two, sections 4a and 4b for precessing into thin sections. Subsequently, much of the stalagmite has been dissected through creation of thin and thick sections, and drilling (See Section 2.3.3).

Figure 2.1: The Indian subcontinent, and inset, the Shillong Plateau region, Meghalaya, with (dark blue) rain water sampling locations and (purple) cave sites.

Investigations of UMS10 commenced in 2010 with a series of U-Th dating at the Open University and a low resolution isotope traverse carried out by N. Grassineau. D. Hodkin studied the visible layering within UMS10, and with D. Mattey, ascertained that they may be interpreted as annual layers indicating cyclicity between layers.

Type	*Provenance*	*Resolution*	*n*	*Collector*
Rain	University of the South Pacific, Suva Campus	Event based Jan - Sept 2012	126	M. Stephens
Rain	University of the South Pacific, Suva Campus	Event based January - July 2013	80	M. Stephens
Drip	Volivoli cave	Sometimes	33	Multiple

Table 2.1: Fiji water samples collection summary

2.1.2 Samples from Fiji

Water samples from Fiji

Water samples were collected in Fiji over a number of years, from several different locations (see Chapter 4, Figure 1) and by multiple collaborators (Table 2.1)). Dr Mark Stephens (previously at University of the South Pacific, now at University of Botswana) collected rain water samples from the Suva Campus of the University of the South Pacific, in one or two aliquots of the mixed rainfall for the preceding 24 hours. He also recorded meterological conditions and total rainfall volume. Sampling did not take place from September 2012 - January 2013. Cave drip waters were collected approximately every 2 months by Dr Stephens or local collaborator and village leader Tuinayava Baleiva Bea. Additional drip water samples were obtained by Mattey and others during maintenance visits to Volivoli cave.

Fiji cave sites

Two caves in Fiji are referenced in this study:

1. Volivoli cave is on Vitu Levu, close to Kings road, located in the cliff above Volivoli village at 18.161°S 177.481°E. Cave monitoring was set up in 2010 and is ongoing (see Chapter 5 Section 2.2). Sample VV10 was obtained from here, and is being studied alongside but not within this

work.

2. Vatulele (18.547°S, 177.617°E) is a small island to the south of Vitu Levu, with dense forest cover and extensive makatea-type limestone which inhibits exploration. The field observations are described in Chapter 5, section 2.1. There are extensive caves within the karst although access is limited. Several samples were retrieved from Vatulele as detailed below in section 2.4. Sample Vat13a was sourced from Vatulele Island in 2013.

2.2 Field campaign for this research

The 2014 field season involved travel to Fiji and the Cook Islands, via the Karst Record VII conference in Melbourne, from September 13th to October 23rd. The objectives of the trip were to follow up previous work done in Volivoli, Fiji, and establish a new field site on Atiu, Cook Islands, along with local collaborators in both locations. The field campaign involved researchers from five institutions from around the world:, myself, Prof Tim Atkinson (University College London), Prof Silvia Frisia (The University of Newcastle, NSW), Dr Andrea Borsato (The University of Newcastle, NSW), Dr Dan Sinclair (Victoria University of Wellington) and Dr Jon Cunningham (Birkbeck, University of London), led by Prof Dave Mattey (Royal Holloway University of London).

2.2.1 Field observation methods

Cave mapping

Satellite images, soil maps and published papers were used prior to commencement of the field work to identify areas of interest. On arrival to the islands, local guides were employed to lead us to known cave entrances. GPS transects were taken of all accessible entrances and exits. Once inside, each “chamber”

was measured by afixing a candle to a point, and measuring long and short axes from there with a long measuring tape and compass. This process was repeated with a digital laser distance measure. Sketch maps were also drawn as caves were explored, with locations of interesting or important features marked.

CO_2 logging

CO_2 was logged, both continuously and as spot measurements, using a hand-held Vaisala CO_2 logger encased in a modified plastic box for ruggedness and some protection from water damage. The first and last measurements of each expedition were outside the cave but nearby the entrance to establish a base-line. Within the cave, the bearer of the Vaisala had to intrepidly lead the way into new areas, before the rest of the team entered, to ensure the measured CO_2 was not artificially elevated by the exhalations of the scientists.

Ventilation dynamics

A smoke pen was used to identify ventilation patterns within the caves, and provide a target for the Vaisala. In some caves, ventilation differed between the ceiling and floor, with great differences in carbon dioxide concentration, between inflowing and outward flowing air. In some caves, the air flow was a very strong breeze, whereas in others, the smoke pen was a vital tool to ascertain any movement of air.

Water chemistry in the field

In the field, samples were taken from rain, drip, standing pools, lakes and sea for immediate chemical analysis: pH, using a meter and standards in sachets, total alkalinity by sulphuric acid titration, and conductivity, using a meter.

Selecting and removing speleothem samples

Promising speleothem samples were identified through a set of criteria:

Active growth: If the speleothem is wet on the tip, and has evidence of an active drip from the feeder stalactite, it is likely that it is undergoing active growth. This is beneficial if targeting modern samples and allows the top date to be constrained to the time of collection.

Colour: If the stalagmite appears white, or translucent, then it may have low detrital content, which allows a higher chance of precise U-Th dating. Potential samples were tested by attempting to shine light through the calcite. Any transmission of light indicates a low number of detrital or porous layers.

Morphology: A stalagmite with a regular morphology will be more likely to have experienced low drip variability, hence a lower risk of the local conditions overpowering the regional signal (Fairchild and Baker, 2012). It is also more probable that irregularly shaped speleothem have multiple growth axes, changes in growth regime and pockets of dendritic calcite. We targeted the most regularly shaped speleothem, predominantly candleform and "boss" stalagmites, but also small parasitic speleothem growing on vandalised fossil speleothems. The latter provide verification of the growth rate of calcite since the destruction event, and modern environmental conditions.

Once promising speleothems had been identified, they were removed at the base using hammer and chisel for candleform specimens, and a large coring drill lubricated and cooled by local water, for boss type speleothem. All the necessary consultations and permissions were sought and received prior to any fieldwork commencing.

Establishing low maintenance ongoing cave monitoring

Low maintenance cave monitoring was established with TinyTag (Gemini Data Loggers) temperature and relative humidity monitors, and Stalagmate drip loggers (Collister and Mattey, 2008). Tinytags were placed in carefully chosen locations, hidden from the casual visitor to the cave, but marked by coloured ropes to aid retrieval. Tinytags were generally suspended from the cave ceiling, and one within a tree near to the cave entrance to enable future comparion between external and in-cave conditions. Stalagmate drip loggers were placed on the stumps of sampled speleothems cushioned by socks filled with sand. All loggers were cleaned prior to emplacement due to the prevalence of large cave crabs and their attraction to any "food" type scent.

Establishing local environmental monitoring

Samples of rainwater are being collected daily in pre labelled Exetainer vials by Mr Roger Malcolm of Atiu Villas, a weather observer for the New Zealand MetService. Additionally we collected water samples from cave drips, the local saline lake, Lake Tiroto, sea water and every 30 minutes of rainfall through a 12 hour storm event (Figure 2.2).

2.2.

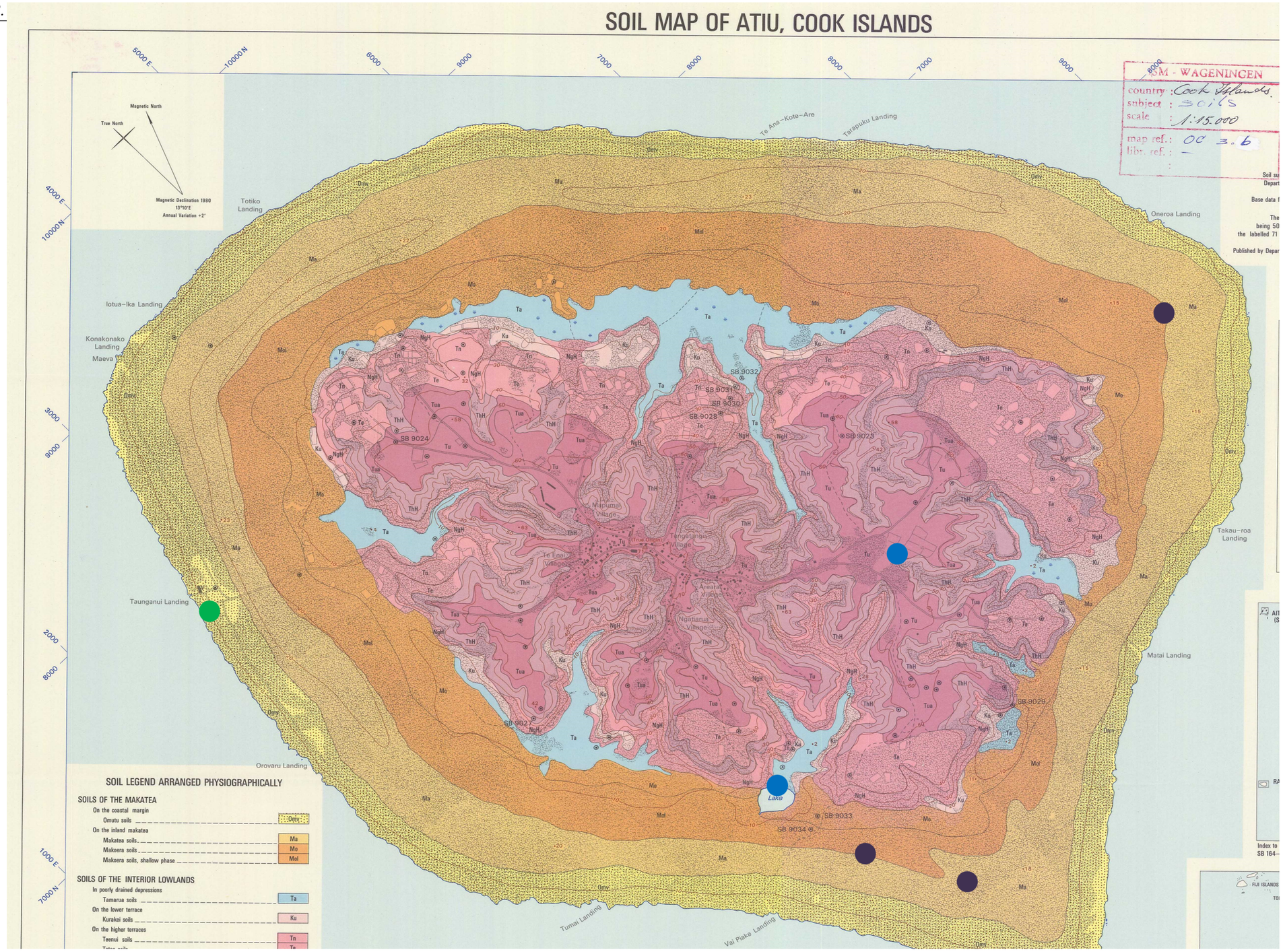

Figure 2.2: Atiu soil map modified from Campbell et al. (1980) with (blue) rain water sampling sites during the aforemetioned storm event, (purple) cave sites and (green) sea water sampling sites.

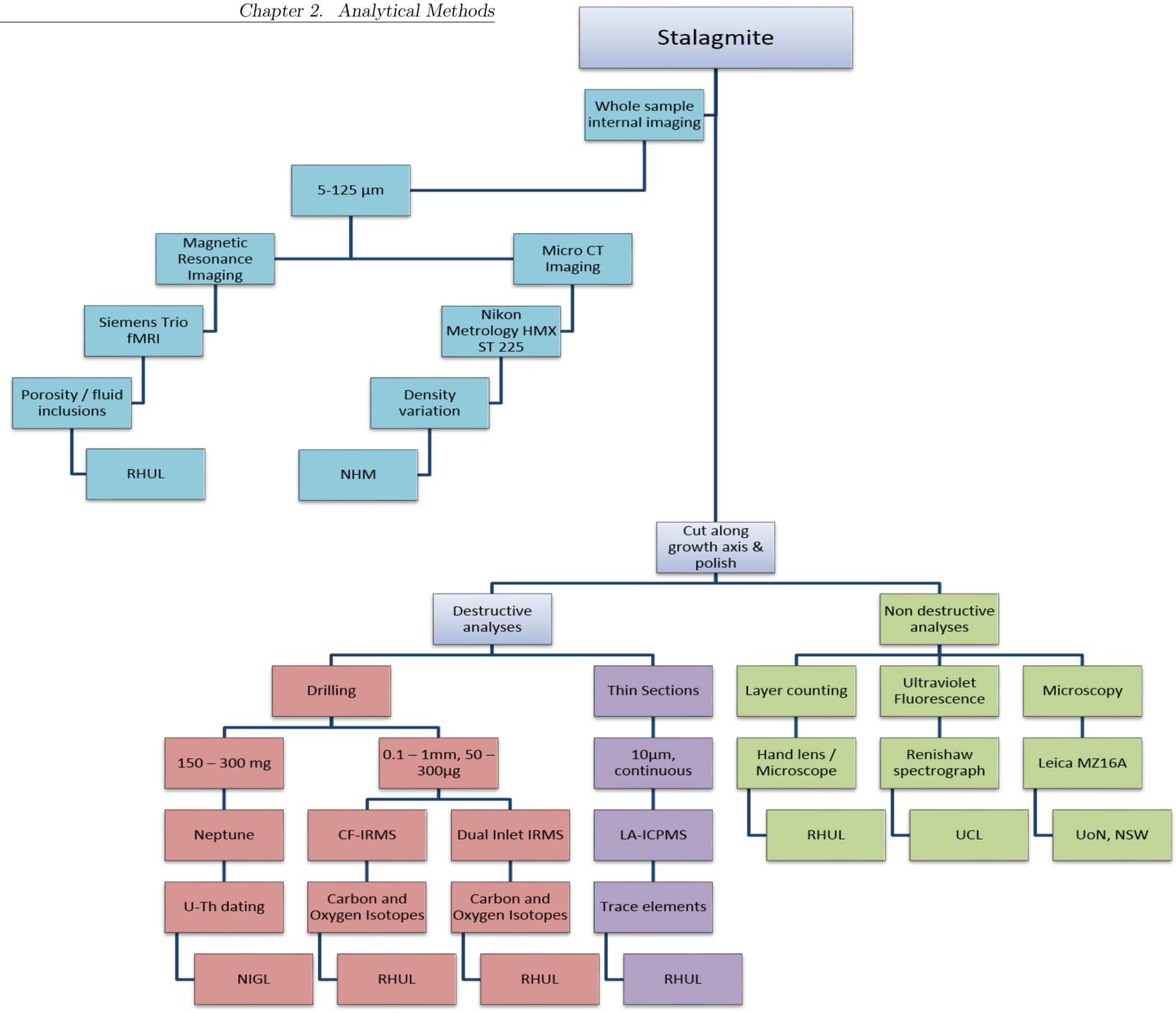

Figure 2.3: Speleothem laboratory processes undertaken in the course of this research. Hierarchy: Resolution; Analysis type; Instrument; Target proxy; Laboratory.

2.3 Speleothem sample preparations

Non destructive means of studying whole stalagmites were attempted, as there is a growing awareness among the speleothem-focused scientific community of the need for cave conservation. Ideally, researchers would remove only a stalagmite core, or work on the sample in such a way that it could be later replaced. We attempted two forms of non-destructive analysis, both of which indicated that destructive testing was necessary. Fortunately, the conservation aspect is unnecessary in our Atiu cave site due to local practices of removing stalagmites.

2.3.1 Functional magnetic resonance imaging

fMRI scans of samples PU7 and PU11 were attempted in the Psychology Department of Royal Holloway University of London, using a 3.0T fMRI scanner, to identify and locate fluid inclusions within the samples (Muñoz-García et al., 2012; Zisu et al., 2012). Stalagmites were wrapped in moistened cloth to ensure that the surface was easily visible in the scan, and a cod liver oil was used as a reference marker as this provides a high contrast area on the scan (Figure 2.4). The scan revealed that there was only one small area that fluid inclusions might be found: at the join of two growth axes of PU11. This indicated a high density/low porosity sample.

2.3.2 Micro-computed tomography imaging

A high resolution (5-125 μm) micro-computed tomography (CT) scan was attempted of PU7 (following Walczak et al., 2015), the most promising whole sample from Atiu, at the Natural History Museum Imaging and Analysis Centre. However, the density was so great that sample was opaque to transmission of x-rays. This indicated that the stalagmite was extremely compact with no

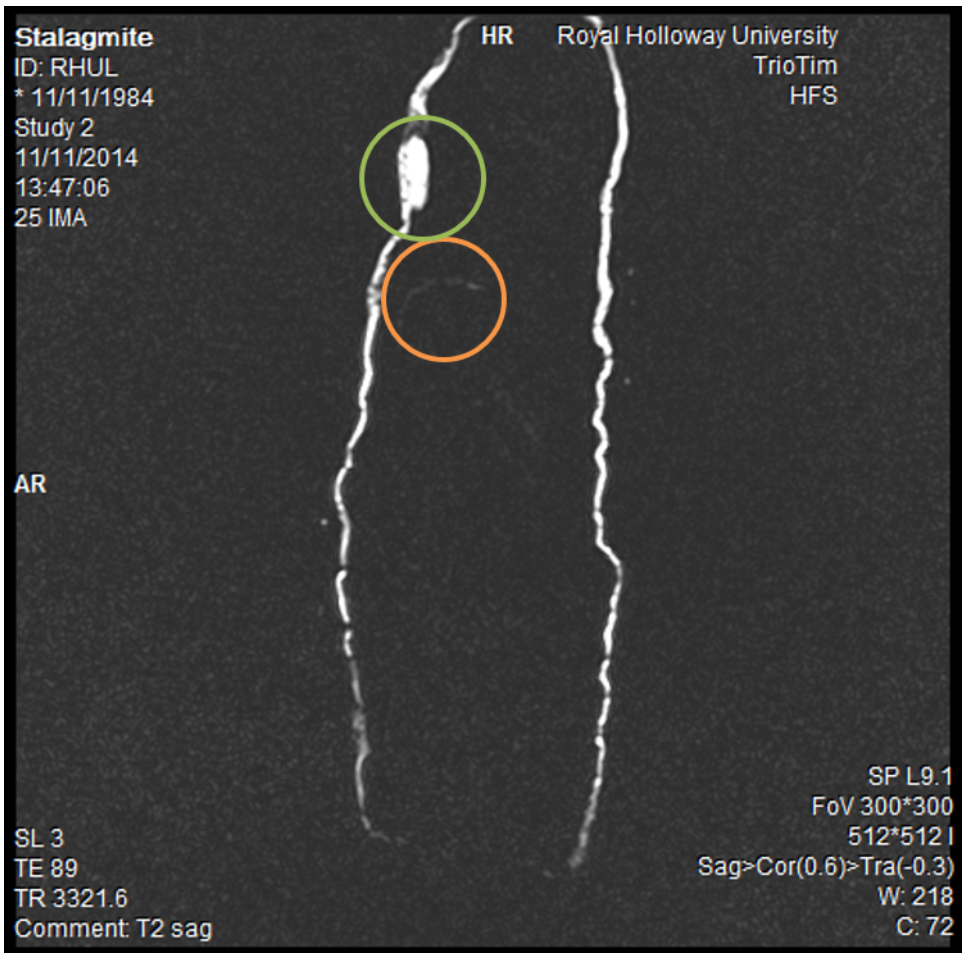

Figure 2.4: fMRI scan example: PU11 with cod liver oil reference (indicated by green circle) and fluid inclusion rich lamina (orange circle).

changes of density within and no possibility for non destructive analysis or fluid inclusion work.

2.3.3 Preparation for geochemical analyses

Each speleothem was cut along the growth axis, with one half preserved (where possible) as an archive, and the other further split into slabs using a diamond band saw. Sections were made by the in house specialist at RHUL, mounted with crystal bond on glass slides: thick sections (2-3 mm) for micromilling, and thin sections for LA-ICPMS and microstratigraphic logging. Sections were polished using increasing grades of diamond lapping plate on Knuth-Rotor 2. With the very compact or sparry samples, some plucking occurred resulting in an imperfect polishing finish. Polishing with silicon carbide grits was an option and may have resulted in a smoother polish, however they could be retained inside macropores and interfere with other analyses, so this option was not used in preparation of samples discussed in this thesis.

2.4 Sample Descriptions

2.4.1 Stalagmite from Meghalaya, India

UMS10 is a 604mm candleform stalagmite. A full description can be found in Chapter 3.

2.4.2 Stalagmites from Vatulele, Fiji

Vat13a

Vat13a (Figure 2.5) is a visibly laminated stalagmite from Vatulele Island, to the south of Vitu Levu, in Fiji. The stalagmite is calcitic and formed of

layers of open and compact calcite, with some stratigraphic discontinuities associated with thin detrital deposits, and a significant amount of dendritic calcite. The main body of Vat13a remained in the University of the South Pacific, Suva, while one slab was brought to Royal Holloway University of London for investigation. A full discussion and images of this sample are in Chapter 5.

Vat13b

Vat13b is an off-axis speleothem core sampled from Vatulele in 2013. The basal flowstone is visible, with decreaing detrital component in the younging direction, and is inconsistently laminated, with some similar characteristics as Vat13a. Calcite varies from compact to highly porous, with some possible dendritic areas. This speleothem is delicate and prone to disintegrate during preparation for analyses so only preliminary work has been carried out on this sample.

Vat13c

Vat13c is a speleothem with an unusual morphology sampled nearby to Vat13a and Vat13b, but in an area of cave with high concentration of upwelling CO_2 (Figure 5.2), resulting in convoluted growth that can not be described as lamina, and large holes with detrital content. Vat13c was not used for palaeoclimate reconstruction.

2.4.3 Cook Islands

PU2

PU2 is a laminated core (Figure 5.15b) sampled from Puatea Cave, Atiu, primarily composed of compact calcite with some open and some dendritic

Figure 2.5: Vat13a: Cut slab of speleothem from Vatulele Island, Fiji collected in 2013 by D. Mattey

areas. The lamina change aspect frequently, sometimes becoming concave downwards indicating limited splashcup behaviour. There is some evidence for organic content, in the slight yellow colour of the calcite, but detrital and particulate-rich lamina are not evident.

PU7

PU7 is a complete sparry compact calcitic 220 mm length speleothem collected from Puatea Cave, Atiu. At the growth axis and the top 50 mm, it is predominantly transparent, with very faintly visible lamina. From 50 mm to the base, there is a significant amount of red clay incorporated into the speleothem, but only away from the growth axis, so does not appear to negatively impact on the compact growth of the calcite. There is one visible hiatus at the transition from "detritally associated" to "clean" calcite at 50 mm from tip, where the detrital component coats the stalagmite and there has been crystal renucleation.

PU11

PU11 presented with a non-symmetrical growth regime suggesting two growth axes. The MRI scan, whilst otherwise inconclusive, confirmed this. The sample was cut open through both growth axes, rather than attempting to separate the axes into two incomplete samples. The cause of the change in growth axis is yet undetermined, however the calcite is generally clean, sparry and with low detrital content, except for the outer cortex.

2.5 Stable Isotope Analyses

All stable isotope analysis was carried out in the Stable Isotope Laboratory at Royal Holloway University of London, under the supervision of and with

Figure 2.6: Stalagmite core PU2 collected in Puatea cave on Atiu island. PU2 displays irregular, concave laminae, macropores and disrupted calcite nearby the growth axis and small pockets of dendritic calcite on the right hand side of the core in this image.

(a) PU7 polished archive half with scale (cm) Note the large individual calcite spar crystals at the growth axis, and the distribution of detrital material away from the growth axis but clearly visible due to clarity of crystal lattice.

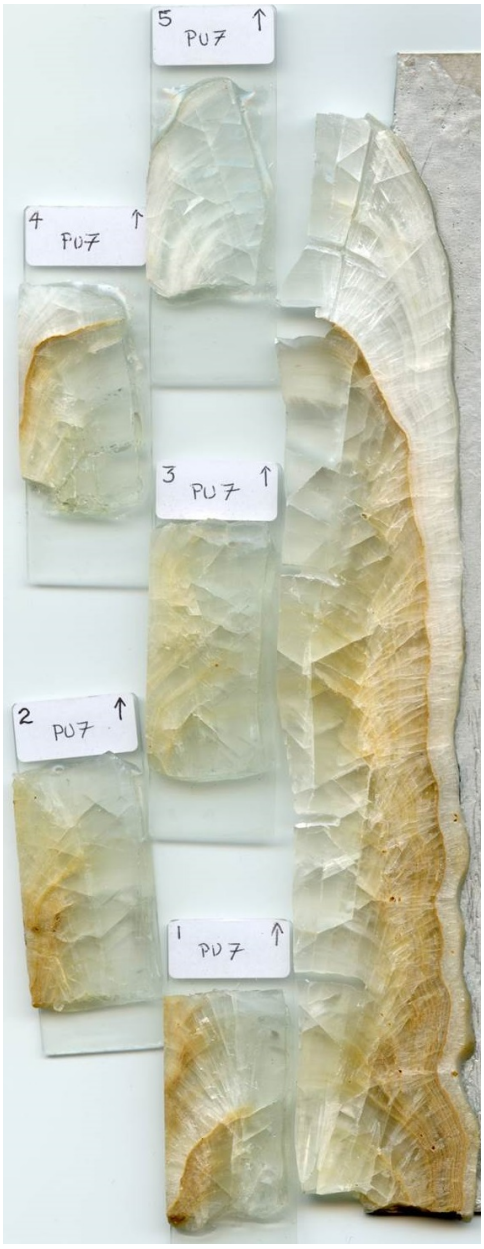

(b) PU7 prepared for analysis: with thick sections for micromilling and laser ablation, and a polished slab for cutting U-Th samples. Thin sections have also been prepared.

Figure 2.7: PU7: sparry speleothem from Puatea cave, Atiu. This sample was found in situ and with an active soda straw above, and translucent to torch light. A drip logger is now located at the sample site (Figure 5.8) for ongoing environmental monitoring.

training from Prof. Dave Mattey and Prof. Dave Lowry. All results are reported using the standard δ notation, which is used to express small relative differences between samples and internationally agreed upon standards. A detailed explanation and discussion can be found in Sharp (2017).

2.5.1 Calcite sample preparation for IRMS

Sample preparation of calcite for analysis by Isotope Ratio Mass Spectrometer (IRMS) analysis was by two methods: hand drill and precision micromill.

Hand drill traverse

A Proxxon Micromot 50/E hand drill with tungsten carbide burr was used for pilot and low resolution traverses of stalagmites. After polishing, the sample was cleaned with distilled water to remove dust, calcite dust or other particles, then dried with acetone. The desired distance was then measured and marked by scalpel scratch along the sample from the stalagmite tip, or from the middle of the growth axis at the "young end" for sections. The drill bit was cleaned every 10 samples with distilled water and dried with acetone. The sample and the drill bit were cleaned between every sample with a dry paintbrush to remove residual loose calcite powder.

For each sample, the drill bit was positioned with the measured mark at the centre, and a small amount of calcite removed, and brushed away to minimise surface or polishing contamination. Subsequently the sample was drilled, at the same point, with resulting powder retained until the desired weight was reached. These weights were: 100 - 150 µg for the Dual Inlet and 250 - 350 µg for the CF-IRMS (See section 2.5.3). The samples were then categorised into batches by sample weight, to allow samples of very similar yields to be run together, and to ensure they were broadly not in stratigraphic order.

Traverses of 1 mm were sampled contiguously to avoid aliased data, but lower

resolution were not sampled contiguously due to the radius of the drill bit. Where calcite was evidently disrupted, due to macroporosity, splash cupping, or significant non calcitic detritus, sampling traverses were offset from the centre of growth for the extent of the interruption, then returned to the growth axis. Hendy Tests (Hendy, 1971; Dorale and Liu, 2009), sampling along lamina, were carried out to ensure no persistent or progressive isotopic fractionation away from the growth axis. (Figure 2.8).

Micromill traverse

High resolution isotope samples were taken using a NewWave Micromill compute controlled high precision drill. This system allows calcite to be sampled along precisely controlled tracks, defined by the user via proprietary software. Samples were prepared into thick sections and polished, scanned and matched to hand specimens. Micromill tracks were defined as curves to match the lamina contours, and shifted along the growth axis every 0.1 mm, or 0.05 mm for very high resolution work. Surfaces heights were defined approximately every 10 samples, but drill depth varied to allow for changes in calcite density, which would otherwise yield different powder weights.

Every sample was weighed individually to confirm sufficient mass for confident analysis, and the section was cleaned with a dry brush between each sample collection to remove any remaining loose calcite powder.

2.5.2 Calcite isotopic analysis using Isoprime Dual Inlet IRMS

Small calcite samples, 100 - 150 µg, were analysed using an IonVantage driven MultiCarb autosampling system linked to an Isoprime 100 Dual Inlet Isotope Ratio Mass Spectrometer. Samples are introduced to the system in vacuum enabled vials with self sealing septa and additional polymer septa that seal

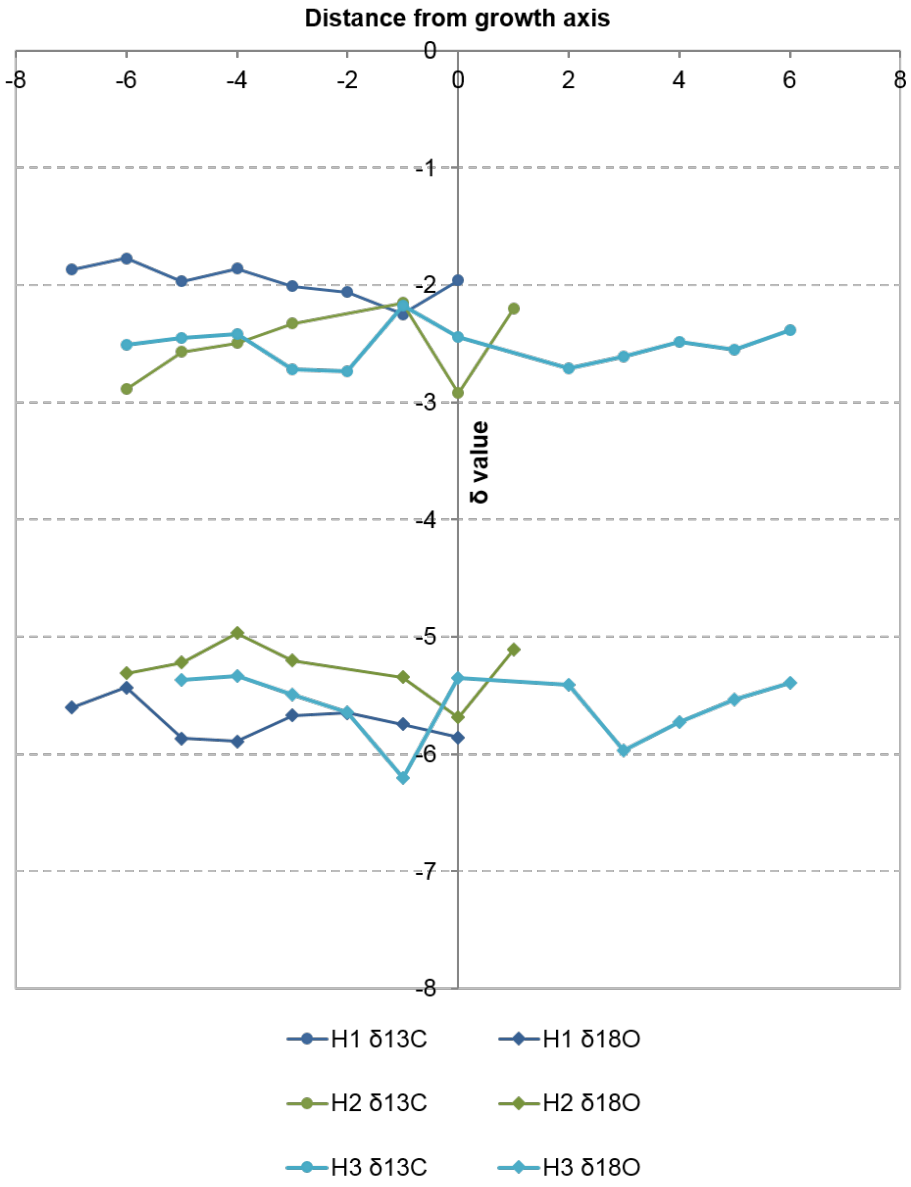

Figure 2.8: Hendy test results for UMS10. The growth axis is defined as x = 0, with samples taken outward fron the growth axis. There is some variation on isotopic value but it is not systematic. H1 targeted a lamina of "normal" calcite, which for this sample is spherulitic with elongate pores. H2 followed a lamina of more dense calcite, and H3 was sampled from a lamina with very large pores with crystal tips clearly visible. The results indicate that the more porous the lamina, the more variable are the isotopes along the lamina.

to the glass when brought up to 90°C in the sampling tray. Vials are first evacuated to 6.8x10^{-2} mbar, then 2 strokes 103% orthophosphoric acid is introduced. The reaction is allowed to continue for 8 minutes, after which the sample is introduced to the mass spectrometer via cryogenic coldfinger. These sample sizes produce a double coldfinger volume with a yield of approx 4.8. All samples are standardised to NBS-19 (Friedman et al., 1982) and an internal standard for run monitoring.

Specifics for carbonate analysis using DI-IRMS:

Autosampler type: IsoPrime MultiCarb

Sample sizes: 100 - 150 µg

Tray temperature: 90°C

Vacuum pressure: 6.8x10^{-2} mbar

Acid volume: 2 strokes

Reaction time: 900 sec

Sample beam: 4.5x10^{-9} - 1.5x10^{-8}

2.5.3 Calcite stable isotope analysis using CF-IRMS

Two similar IRMS systems were used: both modified Multi-Prep autosamplers coupled to a gas chromatography column, and introduced by Helium flow to an Isoprime IRMS.

Specifics for carbonate stable isotope analysis:

Autosampler type: Gilson with Multiprep

Sample sizes: 250 - 400 µg calcite powder sorted into batches by weight

Standards: NBS-19, LSVEC, RHBNC

Tray temperature: 90°C

Helium flush flow: 90cc

Helium flush time: 210 seconds

Acid volume: ≈ 0.3 ml

Reaction time: 3 hours

Peak heights: 5 - 11 nA

2.5.4 Oxygen isotopic analysis of water samples using CF-IRMS

Analysis of $\delta^{18}O$ of precipitation was carried out at Royal Holloway University of London in the Stable Isotope Laboratory using a Multiflow system connected to an IsoPrime Continuous Flow Isotope Ratio Mass Spectrometer. 200 µl of each water sample were decanted to new Exetainer vials, and then flushed with a mixture of Helium and CO_2 gas of known composition at 40 cc for 210 seconds. These were allowed to equilibrate for 3 hours at 40°C. Linearity tests indicated that peak heights below 5 nA or above 12 nA behave non-linearly, forcing exclusion of these samples. Precision varied with this technique, so some precipitation samples were measured up to 12 times, to get a reasonable average measurement. All water samples were standardised (see section 6.2 using V-SMOW2 (Gröning et al., 2007)), GISP (Hut, 1987) and SLAP2 (Gröning et al., 2007), as well as an in house standard for run monitoring.

Specifics for water stable isotope analysis:

Autosampler type: Gilson with Multiprep

Sample sizes: 200 µl water

Standards: NBS-19, LSVEC, RHBNC

Tray temperature: 40°C

Mix gas components: 98% He, 2% CO_2

Mix gas flow: 40cc

Mix gas flow time: 210 seconds

Reaction time: 3 hours

Peak heights: 6-11 nA

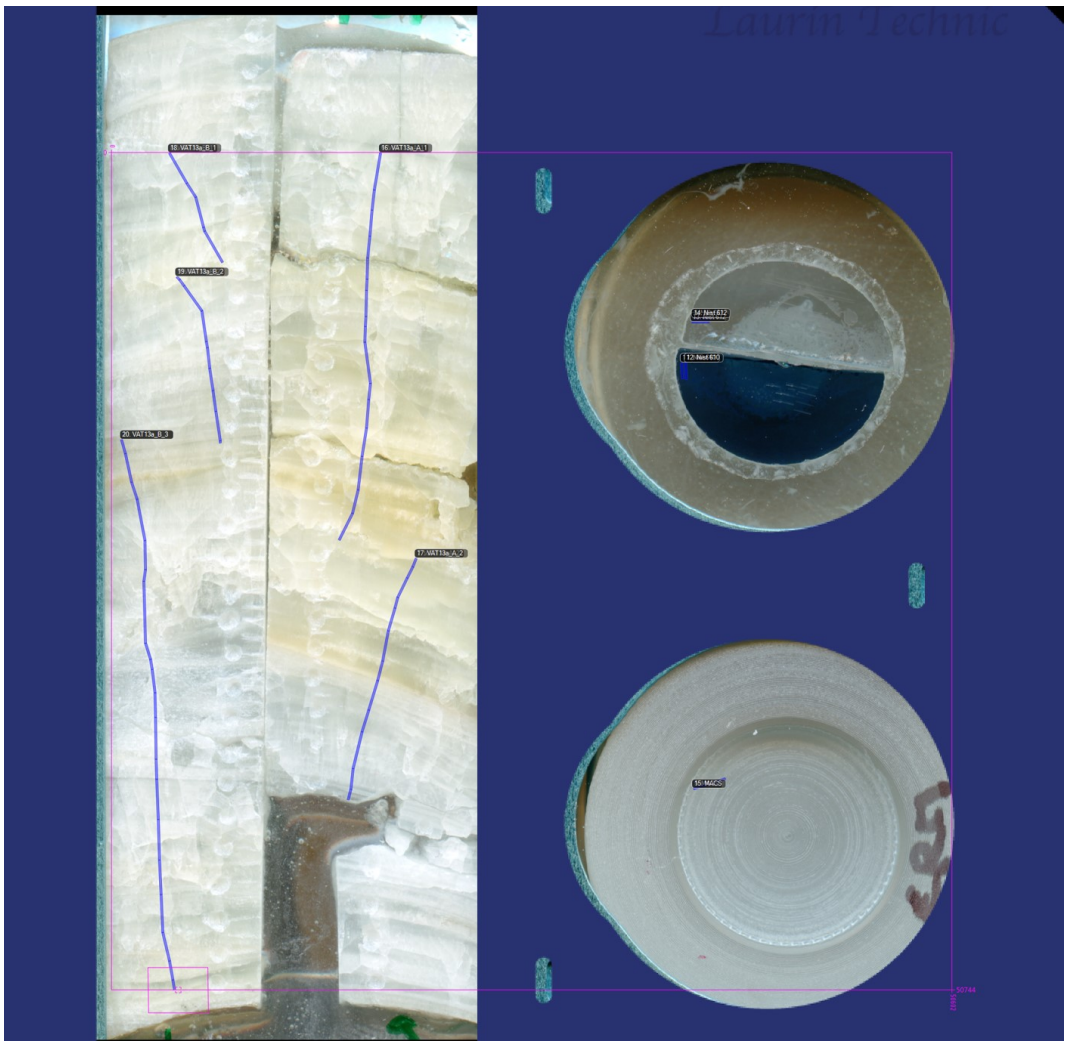

Figure 2.9: Example set-up for laser ablation ICPMS to analyse trace elements in speleothem. Vat13a thick sections (L) are loaded into a special holder along with reference materials: NIST glasses at top right, and a space for MACS powder. Intended tracks for the laser are shown in blue, crosscutting perpendicular to lamina for maximum precision. The field of view is shown as a pink rectangle, and any sample material outside of this cannot be sampled in this run.

2.6 Trace element analysis by LA-ICPMS

Trace element analyses were targeted to specific areas of the stalagmite where fabrics indicated a change in growth regime and analysed by LA-ICPMS. These sections were prepared into thick sections and polished to allow the laser to focus consistently. Analysis was carried out at RHUL by myself, under the direction and supervision of Dr Viola Warter and Dr Wolfgang Müller, using a 193 nm excimer laser-ablation cell coupled by SQUID inline signal smoothing device (Evans and Muller, 2013) to an Agilent 7500ce/cs quadrupole Induc-

tively Coupled Quadrapole Plasma Mass Spectrometer, with a letterbox aperture designed for speleothem analysis. Trace element data were standardised to MACS and NIST 610 and 612 glasses (updated to Jochum et al., 2012) and processed using the Iolite package in Igor. Following Fairchild and Treble (2009), trace elements analysed were: Na, Mg, Al, P, Mn, Fe, Zn, Br, Sr, Y, Ba, Ce, Pb, Th, U. This suite of elements should provide information about a wide range of environmental processes recorded in the speleothem.

Some papers (e.g. Griffiths et al., 2010) use Mg/Ca and Sr/Ca when reporting speleothem trace elements, primarily when solution geochemistry is used for analysis. Since this research uses laser ablation ICPMS, and all data are normalised to the total beam, this is unnecessary. However, prior to interpretation of results, trace elements (ppm) and trace elements ratio to counts per second of calcium were compared, with no significant differences apparent. Therefore the decision to report in ppm rather than a ratio to calcium is retained.

2.7 Age determination and modelling

2.7.1 U/Th disequilibrium dating

Sampling for U/Th dating:

1. Hand drill "powder method":

   200 mg calcite samples were required for U-Th column chemistry due to the low uranium content of the samples (0.2 -0.6 ppm) and the young age. The large pit left by this sampling technique increases the uncertainty of each reported age, therefore, the distance from the stalagmite datum to each side of the dating pit is measured, and the midpoint found. The final date is then tied to this midpoint, with distances above and below this propagated as uncertainties within the final modelling procedure.

2. Wire saw

   The wire saw was employed for cutting very fine segments of speleothem calcite, targeting specifically chosen individual layers for U-Th dating. The polished samples are attached to a stand and gently introduced to the cutting wire. The precision of this technique is limited by the stand which only allows cutting in two planes, with no gradational changes, making it suitable only where the lamina are perpendicular with the cut edge. If that criteria, is met, this is an effective and accurate sampling technique.

3. Proxxon Typ MBS 240/E Diamond band saw

   The diamond band saw was used in a similar way to the wire saw: to remove small samples of calcite from a prepared slab for U-Th dating.

Dating was possible due to a NERC Small Grant awarded for a collaboration with the National Isotope Geochemistry Laboratory. Chemical separation followed an established method of microresin column separation to isolate the uranium and thorium from calcite dissolved in nitric acid. A calibrated Uranium spike was used to standardise samples and were analysed using a Neptune Plus high-sensitivity MC-ICP-MS. For detail of analytical procedures, please see the supplementary information to Smith et al. (2016). I visited Diana Sahy and Steve Noble at NIGL, part of BGS Keyworth w/c 5/10/15 to learn about the chemistry required to prepare these samples and assist with the lab work.

2.7.2 Layer counting

Following Smith et al. (2009) and Domínguez-Villar et al. (2012), layer counting can be used as a complementary age modelling technique if there is evidence for annual laminae, or seasonal couplets within the sample. In the case of UMS10, David Hodkin was responsible for identifying annual couplets and performing layer counting as his MSci research. His work has contributed to

the age modelling for sample UMS10.

2.7.3 Age modelling: the battle of the algorithms

StalAge

StalAge is an age modelling algorithm which uses R and is freely available for use (Scholz and Hoffmann, 2011). The authors describe the model thus:

> "Firstly, major outliers are identified. Secondly, age data are screened for minor outliers and age inversions, and the uncertainty of potential outliers is increased using an iterative procedure. Finally, the age model and corresponding 95% confidence limits are calculated by a Monte-Carlo simulation fitting ensembles of straight lines to sub-sets of the age data."

However, StalAge requires that at least 3 U-Th dates lie on a consistent slope, between any growth rate change or hiatus, to allow the fitting of the cubic spline throughout. Scholz proposed that StalAge is not suitable for samples which have few dates, and many changes of growth rate, and suggested that more U-Th dates be obtained if these criteria are not met. For samples discussed here, StalAge rejects most dates as outliers and forces cubic splines through the data with the fewest gradient changes. This results in an age model unlikely to be an appropriate representation of reality, for the samples that have evidence for hiatuses: UMS10 and PU7.

"Constructing proxy records from age models (COPRA)"

COPRA (Breitenbach et al., 2012) is an alternative age modelling package written for MatLab, with the code available to researchers on request. It is designed to allow detection of hiatuses and incorporation of layer counted intervals. MonteCarlo simulation and translation create suggested time scales

for proxy data. This results in a curved age model and assigns uncertainties to the proxy rather than to the ages. COPRA was used for preliminary age modelling where the layers are thought to be annual and the output appears to resolve some of the hiatuses and layer counting intervals.

2.7.4 Creating a composite age model

A composite age model was constructed using elements from different techniques. Where annual couplets were visible and verified, these provided the extension rate for that part of the speleothem. This series of floating chronologies was then pinned to best available U-Th dates following (Domínguez-Villar et al., 2012). COPRA age modelling was used for parts of the record without visible annual couplets. This composite technique was only used where annual laminae were present, in this case on sample UMS10 Further discussion is found in Chapter 6.

2.8 Fabric analysis

Fabric analysis has been shown to be a productive addition to speleothem analysis (Frisia and Borsato, 2000; Fairchild et al., 2007; Baker et al., 2008; Belli et al., 2013). The following fabric types were identified and logged.

2.8.1 Determination of fabric types

Columnar calcite

Columnar calcite exists in several types which are defined by their size, number, size and location of pores, and optical properties. These are described in detail in (Frisia and Borsato, 2000). Columnar calcite grows upward perpendicular from the substrate. Crystals compete as they grow away from the nucleation

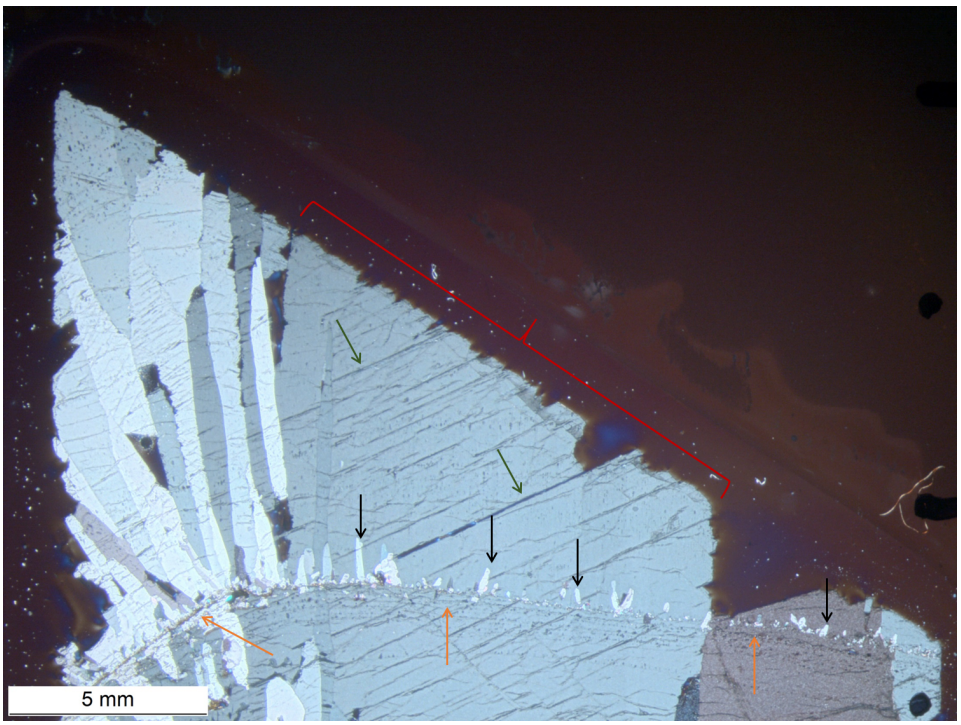

(a) Compact columnar calcite with stratigraphic discontinuity (PU7). Red bracket indicates the extent of one crystal. Green arrows indicates cleavage planes, Orange arrows indicates microporosity approaching the stratigraphic discontinuity, Black arrows indicates crystal renucleation on top of the stratigraphic discontinuity, before the main growth orientation is reestablished.

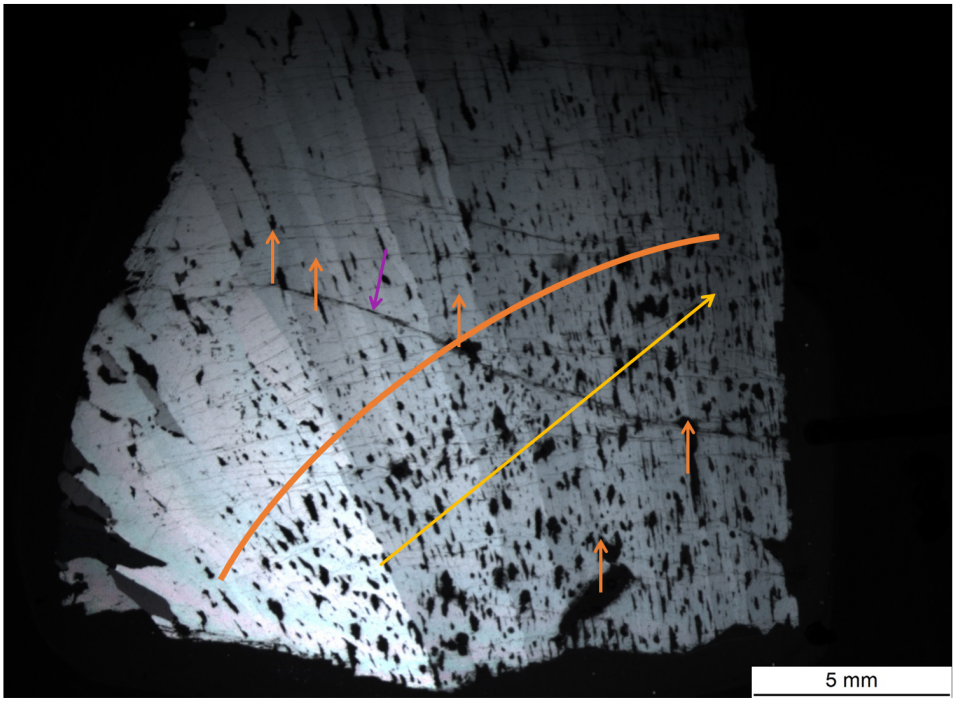

(b) XPL micrograph of fascicular optic calcite with interconnected porosity (UMS10). This is a type of columnar spherulitic calcite that grows in a spiral lattice. In this example there is a great deal of interconnected porosity, examples indicated by orange arrows. Where these pores form a lineation, a lamina of "white" lower density calcite is visible in thin section. An example is shown by the orange line. Fascicular optic calcite has undulose extinction, indicated by yellow arrows. Purple arrow indicates cracked calcite that may act as a fluid conduit.

Figure 2.10: Examples of compact columnar, and fascicular optic fabric types observed in thin section.

point on the substrate, with the ones with the fastest growth vector away from the substrate "winning".

Examples of calcite types encountered in our samples are summarised below:

Columnar compact: PU7 is made entirely of compact calcite (Figure 2.10a). Porosity is minimal and cleavage is evident under the microscope. Crystals may be euhedral or subhedral, and elongate, where aspect ratio exceeds 4:1.

Columnar open: Similar to compact, except that there is room for porosity, commonly where crystal edges do not grow precisely together. Microporosity may also form lamina bands visible in hand specimen.

Columnar elongated: Similar to columnar compact, but each crystal is elongated along the c axis.

Columnar spherulitic: UMS10 (Figure 2.10b) displays spherulitic fabric for much of the length. This is of the type "fascicular optic". It is identified by spiral extinction when viewed in thin section.

Dendritic fabric

Dendritic calcite is a primary fabric (Figure 2.11b), consisting of interconnected rod-like crystals with high intercrystalline porosity. These pores allow inclusions of particles, fluids and detrital material, or can allow post-depositional cementation with silicates or carbonates, making this a complex fabric with potential for misleading geochemical data. There is also growing evidence that in some cases, the dendritic fabric may be biologically mediated (Cailleau et al., 2009), displaying higher δ^{13}C than surrounding columnar type calcite.

Since dendritic calcite may host particles containing detrital thorium, or have post depostional calcite cement in the inter-crystalline pore spaces, calcite should not be sampled from this fabric type for U-Th dating. While den-

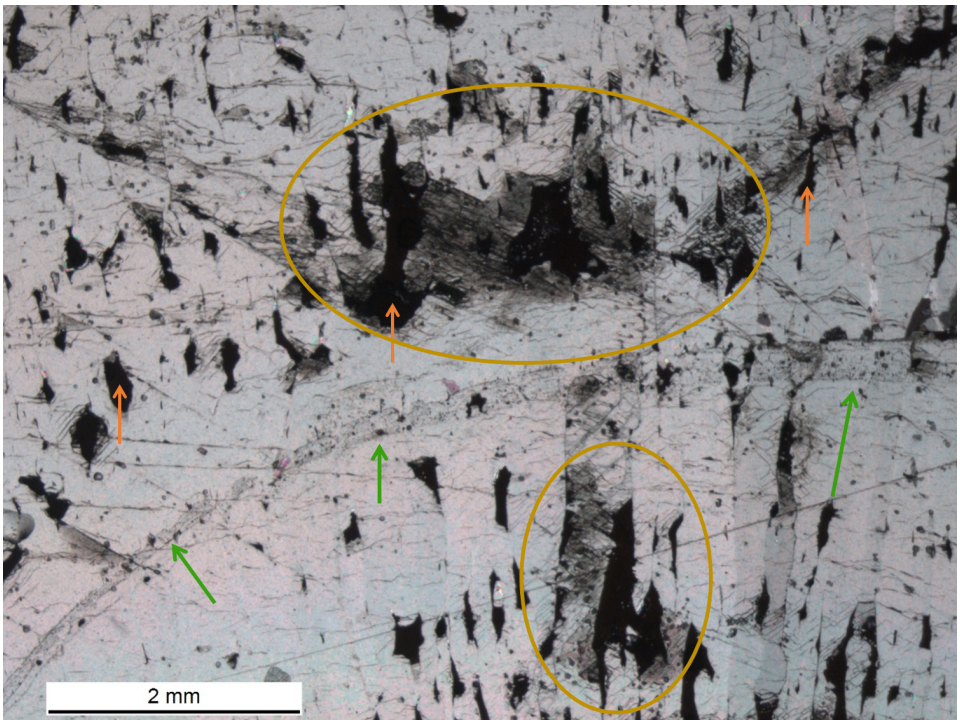

(a) PPL micrograph of corroded calcite with interconnect porosity and stratigraphic discontinuity (UMS10). Orange arrows indicate examples of porosity which may have previously contained fluid. Green arrows points towards stratigraphic discontinuity with corroded crystal tips, and yellow circles indicate areas of corroded calcite, possibly from movement of water through the pores.

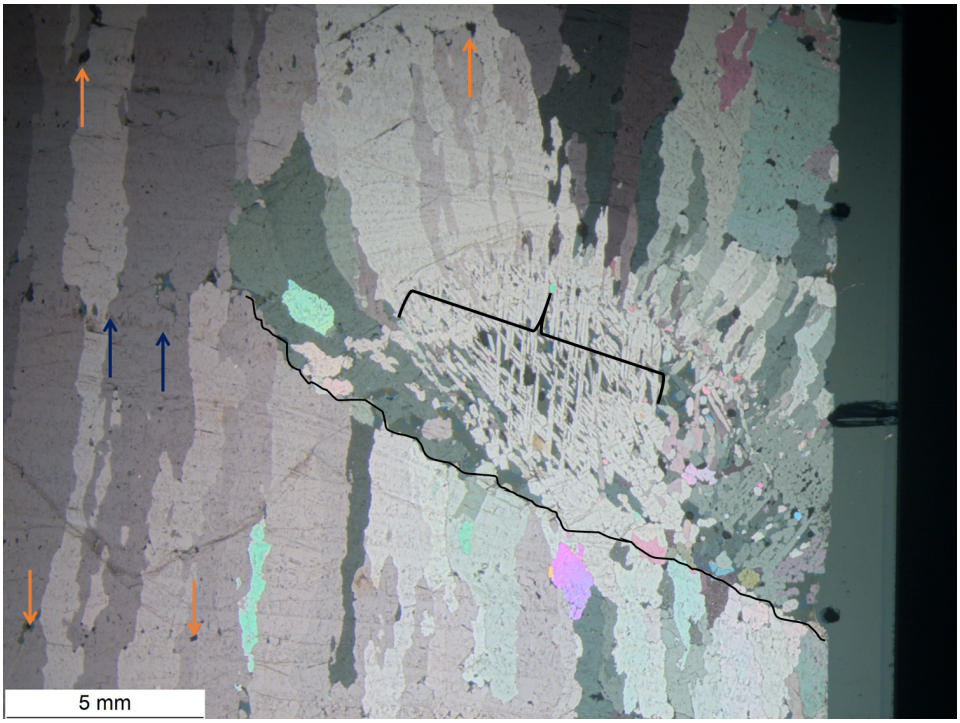

(b) XPL micrograph of compact columnar calcite with dendritic pocket and organics (PU2). Orange arrows show examples of pores which may have contained fluid; in this example, these pores form a lineation which would appear in hand specimen as a less transparent lamina. Blue arrows point towards a layer of organic staining tracing where the crystal tips once were but not disrupting growth at the left-hand side of this image. At the right-hand side growth disruption takes place along the black line resulting in a pocket of dendritic calcite indicated by black bracket.

Figure 2.11: Examples of undesirable fabric types observed in thin section.

dritic calcite can be identified in hand specimen, verification is facilitated by examination in thin section.

Diagenetic fabrics and their problems

Calcite can be diagenetic for two main reasons: Neomorphism of aragonite or micrite, or dissolution and reprecipitation of existing calcite (Perrin et al., 2014). Aragonite is an unstable polymorph of calcite deposited in high Mg environments, and micrite is an collection of tiny, unstable, often biologically mediated calcite crystals, which are unstable due to their high surface area to volume ratio. Both types undergo aggrading neomorphism to microsparite. The second type, mosaic calcite, occurs when an influx of understaurated water dissolves the primary fabric and reprecipitates sub-euhedral crystals. This results in loss of primary calcite, and the more euhedral calcite is also likely to lose trace elements, such as uranium, that incorporate into calcite at crystal defect sites and are water soluble (De Boever et al., 2017).

In both cases, there is a loss of primary fabric (e.g. Figure 2.11a), facilitating a possible disruption of trace elements, since partition coefficients differ between aragonite and calcite, and fewer defects in crystal lattices remain, rejecting elements with large ionic radii. The loss or movement of uranium is particularly problematic, as it introduces gross errors to U-Th data, providing anomalous and misleading results.

Identifying areas of open-system calcite allows targeted sampling for U-Th analysis, giving a higher probability of reliable dates being obtained (Ortega et al., 2005).

2.8.2 Microstratigraphic Logging

Speleothem fabrics record hydrologically and biologically influenced deposition processes, as well as post-depositional changes (Fairchild and Baker, 2012).

They can be a valuable counterpart to geochemical paleo-proxy data, and provide additional information to reduce assumptions and errors within proxy interpretation.

Microstratigraphic logging (Frisia, 2015) provides a method to systematically analyse speleothem fabrics in a manner that may be compared to other speleothem records. It is a relatively new technique, but has been extremely valuable in the course of this research, in highlighting areas of diagenetic or dendritic calcite, that are not suitable for U-Th dating, and identifying stratigraphic discontinuities.

Microstratigraphic logging was carried out in the University of Newcastle, New South Wales, under the supervision of Dr Silvia Frisia,using a Leica stereomicroscope. Thin sections were prepared with diagonal slicing, to ensure overlap of lamina between the sections. These were labelled from top to base, and systematically examined frrom the top, to identify fabric type and aspect, any stratigraphic discontinuity, detrital component, or organic staining. These were then attributed a value to allow for graphing comparison with other proxy metrics (See Chapter 5, Figure 5.17).

2.8.3 Ultra-violet fluorescence

UV induced fluorescence scans were carried out at University College London Materials Chemistry Centre using an advanced micro-Raman spectroscopy system used in a wide range of materials characterisation experiments. It consists of a Renishaw spectrograph system based on use of Kayser™ notch filters with a sensitive CCD detector coupled to a microscope for point-by-point analyses. Incident lasers for Raman scattering and fluorescence measurements range from the near-infrared (785 nm) through the visible (442, 514 nm) to the UV (325 nm). Polished thick section samples were prepared for this, however the sample surfaces were not sufficiently flat for very high resolution analysis, and organic content was low. The resulting data were resolved to 1 pixel = 142

nm.

2.8.4 Additional datasets

Additional datasets were of great importance to this work. Please find them detailed in:

- Supplementary Information of Chapter 3
- Acknowledgements of Chapter 4
- Detailed in the appendices

Chapter 3

Paper: Annually Laminated Speleothem from NE India: a case study of proxy complexity

Authors: M Brett, S Breitenbach, N Harris, T Ahmad, N Grassineau, S Noble, S Frisia, D Mattey

This co-authored paper manuscript is submitted as substitution for a similar thesis chapter.

I certify that I made the following original and independent contributions to the paper manuscript:

- 1 mm isotope traverse data & microstratigraphic data
- All figures except 2, 5, DR2, DR3, DR4
- The entire first manuscript draft and implementing subsequent edits

Annually Laminated Speleothem from NE India: a case study of proxy complexity

M Brett[a], S Breitenbach[b], N Harris[c], T Ahmad[d], N Grassineau[a], S Noble[e], S Frisia[f], D Mattey[a]

[a]*Department of Earth Sciences, Royal Holloway, University of London, Egham, TW20 0EX UK*
[b]*Department of Earth Sciences, University of Cambridge, Cambridge, CB2 3EQ UK*
[c]*School of Environmental, Earth and Ecosystem Sciences, Open University, Milton Keynes MK7 6AA, U.K.*
[d]*Department of Geology, University of Delhi, New Delhi 110007, India (presently at JMI University, New Delhi 1100025*
[e]*National Isotopes Geochemistry Laboratory, British Geological Survey, Nicker Hill, Keyworth, Nottingham NG12 5GG UK*
[f]*School of Environmental and Life Sciences, The University of Newcastle, University Dr, Callaghan NSW 2308, Australia*

Abstract

A candleform stalagmite from NE India highlights the innate complexity of speleothem records, and provides a cautionary tale for other speleothem researchers. Using a multiproxy approach, we attempted to characterise changes in Indian Summer Monsoon intensity over the formation period of our annually laminated sample, taken from a region of exceptionally high seasonal precipitation. Stable isotope analyses, trace element data and U-Th dating, along with consistent visible laminae for much of the length of the sample, and trace element data have allowed us to build a detailed understanding of the varied and complex processes that affect this sample and have identified hydrological changes that affected the cave system. However, the degree of uncertainty within the data does not allow a meaningful proxy record to be reconstructed from this sample. This study highlights the need

for a multiproxy approach, and confirms that, for speleothem data to be related to the historical record, the age model must fall within acceptable levels of uncertainty for robust conclusions to be supported.
Keywords: Speleothem, India, Precipitation, Isotopes, Amount effect, Monsoon

1. Introduction

Speleothems are now widely used as palaeoclimate proxies due to their unique nature as high-resolution terrestrial archives of environmental data. They are remarkably complex and their interpretation can be challenging without taking a multi proxy approach [12]. In this study we present a record from the Shillong Plateau, using a candleform stalagmite which exhibits visible paired laminae, and little perceptible detritus in hand specimen, making it an attractive specimen for a detailed investigation.

Speleothems have provided iconic proxy records of the East Asian Summer Monsoon from caves in China indicating that, on an glacial-interglacial timescale, summer insolation at 65°N has a controlling influence on the intensity of the East Asian monsoon in response to ice sheet extent in the Northern Hemisphere [24, 27, 26, 25]. Yancheva et al. [30] argue that speleothems are biased towards recording the summer monsoon, and use lake sediments to suggest that when the summer monsoon weakens, the winter monsoon becomes more intense. They link this to the movement of the Intertropical Convergence Zone (ITCZ) and suggest that changes in monsoon intensity may destabilise established civilisations, which provides incentive for further research.

1.1. Climatic Setting

The Indian Summer Monsoon (ISM) is the primary climate system affecting the Indian subcontinent and controls the water resources of the one of the most densely populated areas in the world. It is so important to the area that extremes of the ISM, droughts and floods, affect the global economy [15]. More than 1 billion people rely upon the ISM, as agriculture and associated industries are important economic drivers in the subcontinent. The ISM is characterised by the annual variation in wind and rainfall [28] and has two distinct pathways from the Indian Ocean to the centre of the subcontinent; the Bay of Bengal and the Arabian Sea branches (Fig. 1). The seasonal migration of the ITCZ is generally understood to be the primary factor determining the timing and intensity of the ISM, but a number of further climate phenomena control this. The winter high-pressure conditions over Central Asia must decay before the ITCZ can migrate northward, allowing the Indian Ocean Dipole (IOD) and the El Niño - Southern Oscillation (ENSO) to subsequently either modulate and intensify the monsoon. The role of these climate systems and the influence of the westerlies are not well understood, as they appear to vary considerably over time and instrumental records are both sparse and short. Furthermore, the instrumental record available is only within the anthropogenic era, and may not be indicative on the "natural" long-term variability of the ISM. Some researchers have suggested that the ISM has become increasingly decoupled from ENSO in recent years [18]. Speleothem records, being high resolution, terrestrial archives of environmental change, may provide insights into the long term behaviour of the ISM.

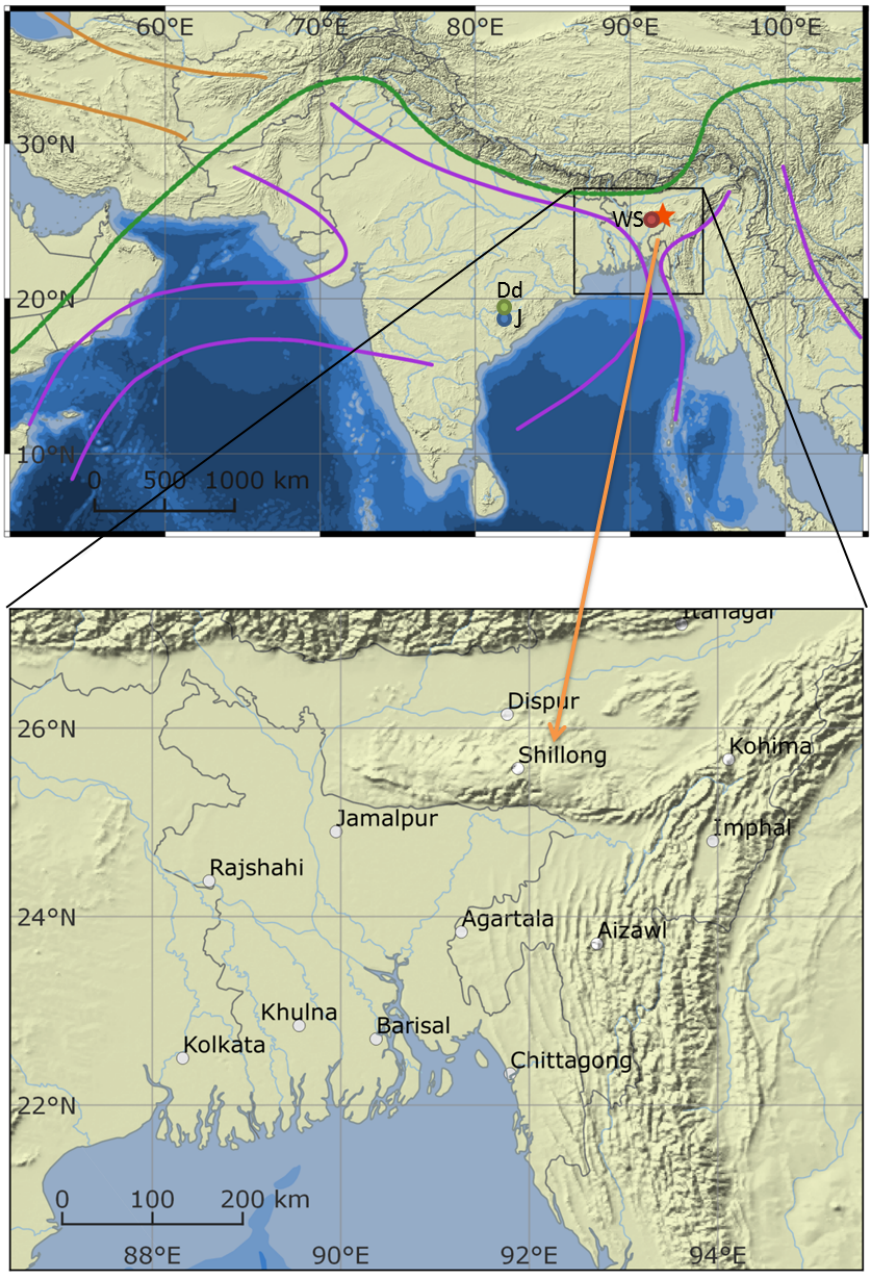

Figure 1: (Top) Physical map of South Asia showing prevailing ITCZ wind directions (green); winds from south (purple) and from north (orange). Previously published speleothem locations at Dandak cave (green dot) and Jhumar cave (blue dot) [2, 23].(Zoom) Detailed map of Shillong Plateau (rectangle indicated in A). Orange star shows Krem Umsynrang (this study), red dot shows location of Wah Shikar cave [23].

1.1.1. Proxy Records

Palaeoclimate records of the ISM are somewhat sporadic, both spatially and temporally. Well-resolved stalagmite records from the Common Era exist from Dandak [2], Jhumar, and Wah-Shikar [23] caves (Fig. 1), on the Indian Subcontinent, as well as an ISM proxy from Oman [13]. While these records are well resolved, they span a short time scale, are from individual stalagmites, and only report the δ^{18}O rather than a multi proxy record (Figure 4). If a longer proxy record could be produced, which both corroborated and extended these previous studies, longer timescale cycles and oscillations would be seen more clearly, as well as allowing increased confidence in the use of speleothems for ISM reconstructions.

For these studies, there is an inherent requirement for understanding the relationship between proxy records and local weather systems and climate. There are few studies integrating detailed research of local precipitation with cave monitoring, to provide a framework to identify and interpret a climate record from the ISM. An understanding of how isotopes vary between individual rain events, reveals how weather patterns influence the overall annual and interannual isotopic signature of bulk water in the region, and give a basis for interpreting climate from δ^{18}O of speleothem calcite in well studied cave sites.

1.1.2. Oxygen isotopes in precipitation

The isotopic signature of precipitation at any given location is influenced by several factors [9]: the "amount effect", where the isotopic ratio is negatively correlated with the precipitation amount; the "temperature effect" where the isotopes change proportionately with surface temperature, and

the "altitude effect" where increasing altitude causes isotopic depletion of precipitation. Additionally there is the "rainout effect"; Rayleigh type distillation causing lighter isotopic ratios further from the moisture source, as well as local effects such as continental recycling of moisture. Due to these effects, in a given location, the precipitation from each branch of the ISM should display distinct signatures. In areas of the Indian subcontinent that are affected by both arms, the isotopic signature of a specific rainfall event will be controlled by which front is dominant in that area, and the seasonal average will depend on which arm was dominant over the season, or an average of both "arms". Breitenbach et al. [6] postulate that rainfall in the Shillong Plateau is delivered by the Bay of Bengal branch only, so changes in isotopic signature here will not suffer from this further convolution, but will also not be comparable with data from central India, in either amount or isotopic signature.

In the monsoon season of 2013, Peethambaran and Ghosh [21] collected monsoon rainfall and water vapour from Bangalore and found a mean δ^{18}O difference of -13.3 $\pm$ 2.5 ‰between liquid and vapour, with the most enriched samples during pre-monsoon months, and most depleted during the post-monsoon periods. They attribute this to a change in prevailing wind from southwest to northeast, which is in disagreement with Breitenbach [6] who proposed that a similar effect observed in Meghalaya (the Indian State encompassing the Shillong Plateau) was due to the freshening of the Bay of Bengal during the course of the ISM. The Online Isotopes in Precipitation Calculator (OIPC) [3] uses an algorithm to calculate expected isotopic signature based on geographic coordinates and altitude. The OIPC calculated

δ^{18}O monthly averages for Bangalore (12.97° N, 77.59° E, 914m a.s.l.) vary from -2.9 ‰ in June to -9.2 ‰ in November whilst those for Shillong (25.56° N, 91.88° E, 1507m a.s.l.) vary from -2.6 ‰ in April to -10.9 ‰ in September. Breitenbach et al. [5] reports measured δ^{18}O values from Meghalaya varying from +0.8 ‰ (April) to -18.8 ‰ (September) so local effects, or regional forcing, unaccounted for by OIPC, must be a significant factor of rainfall δ^{18}O signature here.

1.2. Objectives of this study

This study presents new speleothem and modern precipitation records from NE India, to explore the relationship between regional weather systems, precipitation, and preservation of the signal within the proxy record. A speleothem, UMS10, was sampled from Krem Umsynrang, a cave in the Shillong Plateau, which is located at the core of the ISM. The cave underwent some limited but valuable monitoring which can be related to seasonal variability in precipitation isotopes, following Mattey [19]. New data for ISM rainfall over 2 years, combined with data published by Breitenbach, provides a detailed record sampled at daily to weekly resolution.

1.3. Krem Umsynrang: regional setting and cave environment

The Shillong Plateau is in the Meghalaya province in NE India, directly due north of the Bay of Bengal (Fig. 1). It rises to >1500 m above sea level (a.s.l.) in less than 10 km, and is the first significant elevation change to stand in the way of the northward moving monsoon winds, causing orographic uplift and hence a large amount of rain during the ISM. The Shillong Plateau receives on average 11.5 m of rainfall per year, >70% of that during the three

monsoon months, yet the karst drainage is so efficient that water shortages often occur during the dry season. Karstified Eocene limestone [5] forms the southern perimeter of the plateau, overlain by interbedded sandstone and coal seams [22] which have been exploited for mining. Many caves have been discovered in Meghalaya [5], with some used as underground water reservoirs, or exploited for domestic purposes. Human habitation in the area is believed to date back several thousand years, and in recent years, there has been extensive deforestation for agriculture and mining. The highly seasonal nature of precipitation in this area, coupled with extensive karst and minor annual temperature range, 19-28°C, makes it promising for useful speleothem records, although the anthropogenic influence on vegetation, water flow and geology, through mining, introduce potential interpretation complexities.

Krem Umsynrang (25 °13' N, 92 °21' E; 825 m a.s.l. (25.21 °N 92.35 °E) is a previously studied (Breitenbach 2010) cave, 25 km SE of Jowai, on the Shillong Plateau, Meghalaya, NE India (Fig. 1). It consists of a 5.6 km length network of well-decorated passages within the Lakadong member of the Shella formation of Eocene limestone, with active erosion by a small watercourse in the lowest of three levels [details and maps in ref 6, p6&37]. Sandstone and a 50 cm thick coal seam overlie the horizontal passages, with grassland and tropical forest on the surface. Active and inactive speleothems are found on every level, and broken or crooked stalagmites indicate seismic activity within the region, rather than vandalism, as the cave is somewhat inaccessible.

Cave monitoring was first established in 2006, with temperature and drip loggers deployed. The mean air temperature of the cave, 20.6 °C ± 0.6 °C, is

lower than the mean surface temperature of 25 °C, but the passages display different annual temperature changes. The lower passage varies smoothly from 19.8 °C to 21.5 °C, whereas the upper passage varies only from 21.0 °C to 21.5 °C but with more small-scale variability across the year. Drips per month vary from ≈ 2000 to ≈ 24000 across the year, peaking in September, 4 months after the average peak in monsoon rainfall volume.

2. Analytical Methods

2.1. Rainwater sampling and isotopic analysis

Rainwater samples were collected at daily "event resolution" from North Eastern Hill University during the monsoon seasons of 2010, 2011 and 2012, together with volume of rain. Although at this point the units are unknown, it does allow for comparison between rain amount and isotope values. Water samples were shipped to Royal Holloway University of London, and 200 µl aliquots were analysed following the standard CO_2 equilibration method using a continuous flow isotope ratio mass spectrometer (CF-IRMS), standardised to V-SMOW, SLAP and GISP.

2.2. Stable isotope analyses of speleothem calcite

Stable isotope analysis of speleothem calcite was performed in three stages: an initial 4 mm traverse was analysed by reaction with orthophosphoric acid, using continuous flow introduction to Isoprime IRMS, followed by 0.1 mm resolution micromilled traverses over selected areas of UMS10, with aliquots analysed using orthophosphoric acid reaction with an Isoprime Multicarb system linked to a Dual Inlet IRMS. In the third stage, 100 - 150 µg calcite

was sampled contiguously at a 1 mm resolution for the length of the stalagmite, deviating from the growth axis only where a drip cup had formed. The resulting powders were analysed using the Dual Inlet IRMS system. In all stable isotope analyses, NBS19 was used as the international standard, as well as an in-house standard for run monitoring. Hendy tests [16, 11] indicate isotopes do not change systematically away from the growth axis.

2.3. Trace element analyses

Trace element analyses were targeted to specific areas of the stalagmite where fabrics indicated a change in growth regime. These sections were prepared into thick sections and polished to allow the laser to focus consistently. Analysis was carried out using a 193 nm excimer laser-ablation system coupled to an Agilent 7500ce/cs quadrupole ICPMS system, with a letterbox aperture designed for speleothem analysis. These data are extremely high resolution but suffer from two key issues: the difficulties of tying the laser traverse to the isotope traverse due to resolution differences, and the problem of the porous fabric. Since trace elements are heterogeneously included within calcite crystals, traversing crystal boundaries can introduce misleading results within the laser data. Trace element data were standardised to MACS, and NIST 610 and 612 glasses.

2.4. U/Th disequilibrium dating

The age model for UMS10 was established using U/Th disequilibrium dating (4). As the U content is $\approx$ 0.6 ppm, large aliquots of 200 mg are required for the analysis, producing an inherent sampling precision uncertainty within the ages. Samples were taken by identifying specific laminae

and drilling calcite from that target area. However, as a large amount of calcite was needed for these analyses, material from several laminae were required for most samples. U/Th dating proceeded in a number of phases. Initially 11 powders were analysed in 2010 by the Open University dating lab with the tip dated at 1996 CE ± 2 years and the base at 972 BCE ± 90 years. This initial round of dating targeted each side of the fabric anomalies (Section 3.2) and suggested a "step-wise" growth regime. Further dating produced 30 ages in 2014 from the NERC Isotope Geochemistry Lab at the British Geological Survey, Keyworth, UK. For the purposes of age modelling, ages with large uncertainties or where high detrital thorium was identified during analysis, are also excluded, as well as dates that are reported with good precision but plot as significant outliers.

2.5. Ultraviolet Fluorescence

Organic molecules are often incorporated into speleothem calcite, and display fluorescence under UV light. Since these molecules would be produced and transported differentially depending on the season, annual layers may be recorded in different concentrations of these fluorescing molecules. To investigate the transition between the visible couplet laminations, and the "hiatuses", polished sections of UMS10 were scanned them high resolution with UVF confocal microscopy. While this method is often productive for speleothem analysis [1], the porous nature of UMS10, and the low organic content did not yield conclusive results.

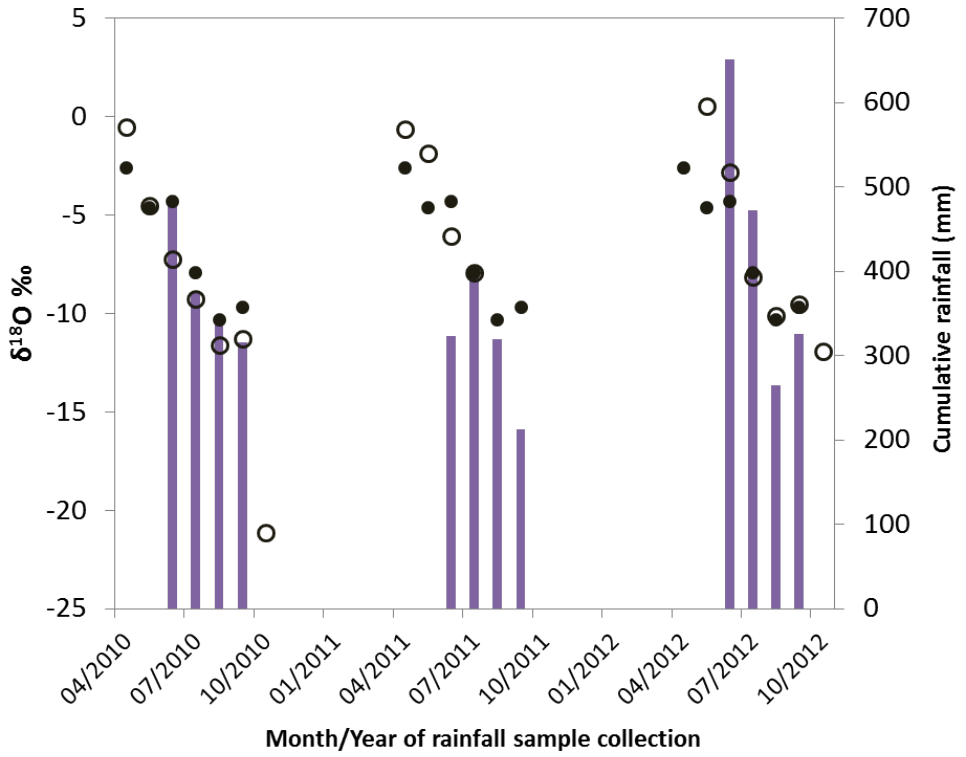

Figure 2: Monthly rainfall amounts (purple bars) with calculated oxygen isotopes (solid circles) and measured oxygen isotopes (open circles) for rainfall during monsoon seasons of 2010 and 2011 ([4], and 2012 (collected at NEHU, Shillong, Fig. 1)).

3. Results

3.1. Precipitation isotopes

Rainwater collected for three consecutive monsoon seasons (2010-2011 data previously published by Breitenbach [4]) from Cherra Lodge Resort, to the SE of the cave site, reveals systematic isotopic evolution of rainfall during the course of each monsoon. Using weekly and monthly composites of rainfall amount and isotopic signatures, as well as data published by NOAA and the Indian Meteorological Department, we can identify the primary controls on modern monsoon rainfall in Shillong. Rainfall measurements from North East Hill University span 2010 - 2012, although with some gaps in the data.

Rainfall samples from Shillong plateau reveal a remarkably consistent progressive depletion of heavy isotopes during each monsoon season (Fig. 2). This phenomenon is repeated in all three sampled years, as well as within the historic data from Shillong published on the GNIP database. The range of isotopes varies slightly each year: the most depleted monthly rainfall sampled was δ^{18}O = -21.13‰ in October 2010, and the least depleted was May 2012 when δ^{18}O = 0.53‰ . The range in signatures here is greater than calculated by OIPC, which suggests between -2.6‰ in April and -10.3‰ in September each year. These values are calculated following Bowen and Wilkinson [3] based on location and altitude of a location, in this case, 25.56 °N, 91.88 °E, 1507 m a.s.l.

The Indian Meteorological Department (IMD) publishes an annual "monsoon report" with key observations and statistics, including cumulative monthly rainfall reported on a "regional" basis, with Shillong in the "Meghalaya and Assam" region. To compare these regional data with our own Shillong data,

we have compiled the latter into weighted monthly averages. The IMD data are especially interesting as they indicate that the rainfall experienced across NE India, including "Meghalaya and Assam" follows a different pattern then the rest of India. To analyse these differences further we have compared IMD data with our measurements from Shillong, OIPC calculated δ^{18}O, GNIP historical data, the Multivariate ENSO Index (MEI) and back trajectory analyses performed on NOAA's Hybrid Single Particle Lagrangian Integrated Trajectory Model (HYSPLIT).

Both in the new Shillong data, and the historic Shillong data from GNIP, there is no significant relationship between precipitation amount and δ^{18}O, with correlations of $R^2 = 0.0024$, n = 16 and $R^2 = 0.16$, (n = 31), respectively, indicating that the "amount effect" is not a significant influence on δ^{18}O evolution through the monsoon in this area. However, the correlation between "Meghalaya and Assam" cumulative regional rainfall as reported by IMD, and observed δ^{18}O is much stronger, $R^2 = 0.62$, (n = 10), but cannot be taken as statistical significance due to the low number of data points. Where local surface temperature data are available in the GNIP dataset, there is no correlation with δ^{18}O and the correlation of δ^{18}O with MEI is weak: $R^2 = 0.26$, (n = 17).

3.2. Petrography and speleothem sample description

UMS10 (Fig. 4) is a 604 mm laminated candle form stalagmite collected in 2010 from the upper level of Krem Umsynrang. The stalagmite was found broken into 6 sections on the floor of the cave, possibly as the result of seismic activity, and brought to Royal Holloway University of London for analysis. UMS10 is a highly porous calcitic stalagmite with visible laminations and

several layers of denser calcite that appear darker then the surrounding calcite. In the middle section, there is evidence of splash cups indicating a faster, or slightly less supersaturated, drip. The growth axis is not entirely straight, but the sample has a relatively consistent width tapering towards the tip.

UMS10 has been examined in both hand specimen and thin section, the latter at University of Newcastle, New South Wales using confocal microscopy for microstratigraphic logging as described by Frisia [14]. Much of the length of UMS10 exhibits paired couplets of alternating visually grey and white lamina (Fig. 5). When examined in thin section, it is evident that these layers are the result of varying fabric densities, with the lighter coloured part of the pair exhibiting higher porosity than the laminae which appear grey in hand specimen. These distinct paired couplets are typically formed due to annual changes in stalagmite growth regime and are consistent with the highly seasonal nature of the region.

There are six distinct stratigraphic discontinuities spaced along the stalagmite, characterised by a fade out of the paired couplets leading up to a denser layer, and then the abrupt resumption of the paired couplets (Fig. 5). These characteristics indicate a change in environmental conditions, gradually inhibiting calcite deposition for an indeterminate amount of time, followed by an abrupt return to previous, more optimal conditions. When examined in thin sections, there is a suggestion of dissolution fronts, fabric perturbations cross cutting the normal fabric, indicating that some of the stratigraphic discontinuities were associated with more aggressive waters, and that some calcite was precipitated and subsequently dissolved. In others, there is a

small amount of detrital material associated with the stratigraphic discontinuity, suggesting flooding of the cave above the level of stalagmite growth, an interpretation consistent with rainfall and drainage characteristics during monsoon months.

Calcite crystals forming the core of UMS10 grow in an unusual form, characterised by spiral extinction and highly elongate form; termed "Columnar Fascicular Optic" following [14] (Fig. 3a). This fabric has been previously understood to form from (i) low drip rate or (ii) lamina flow conditions, (iii) within caves formed in dolomitic formations, where (iv) the Mg/Ca ratio of the parent water is typically greater than 0.35, prior calcite precipitation is active, and/or prolonged water/rock interaction increases the saturation index to 0.5 or greater. However, this is not consistent with the environment of Krem Umsynrang, where drip rates vary from ≈ 2000 to ≈ 24000 per month: reaching two drips per minute during higher flow regimes.

The porosity of UMS10 is high, and macropores are visible in hand specimen with the naked eye and, when examined in thin section, there is clear evidence of interconnected porosity for much of the length, with complete permeability hindered only by the high-density areas around the aforementioned stratigraphic discontinuities. It is therefore possible for water to migrate within this stalagmite, and there is evidence of open system behaviour, with mosaic calcite, a diagenetic crystal type, forming part of the lower portion (Fig. 4b). This has implications for U-Th dating of this section, where evidence for open system behaviour allows the possibility of uranium leaching, resulting in a misleading result.

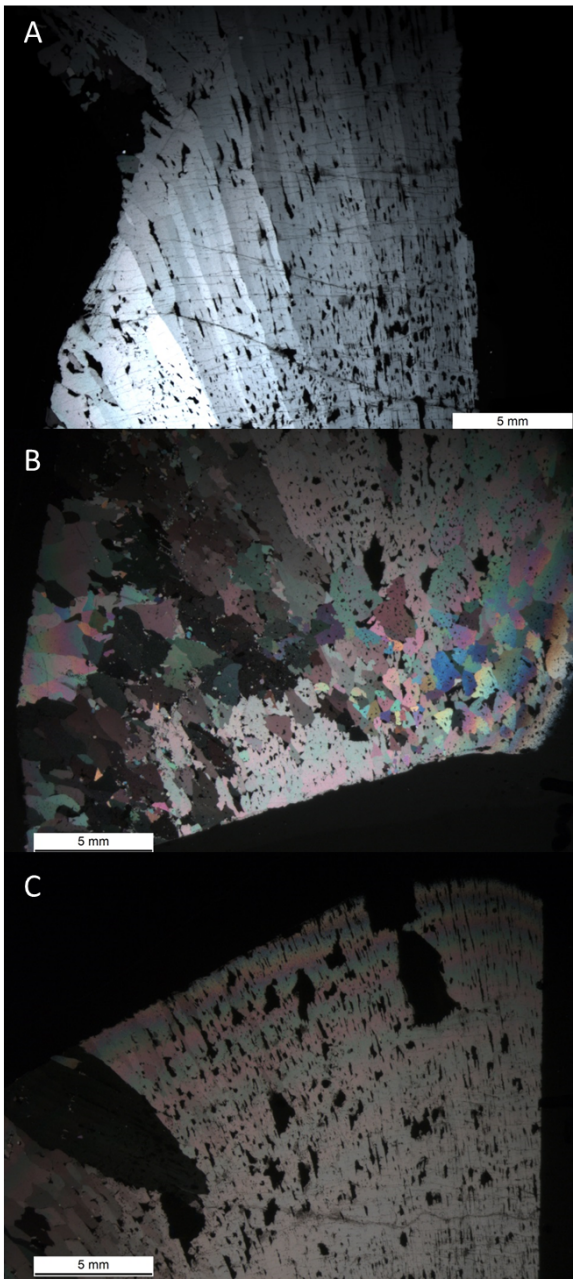

Figure 3: Calcite types found within UMS10 viewed in thin section (XPL). A) Fascicular optic calcite, the typical fabric of this stalagmite. B) Mosaic calcite indicating recrystallisation. C) Calcite overgrowths and a stratigraphic discontinuity

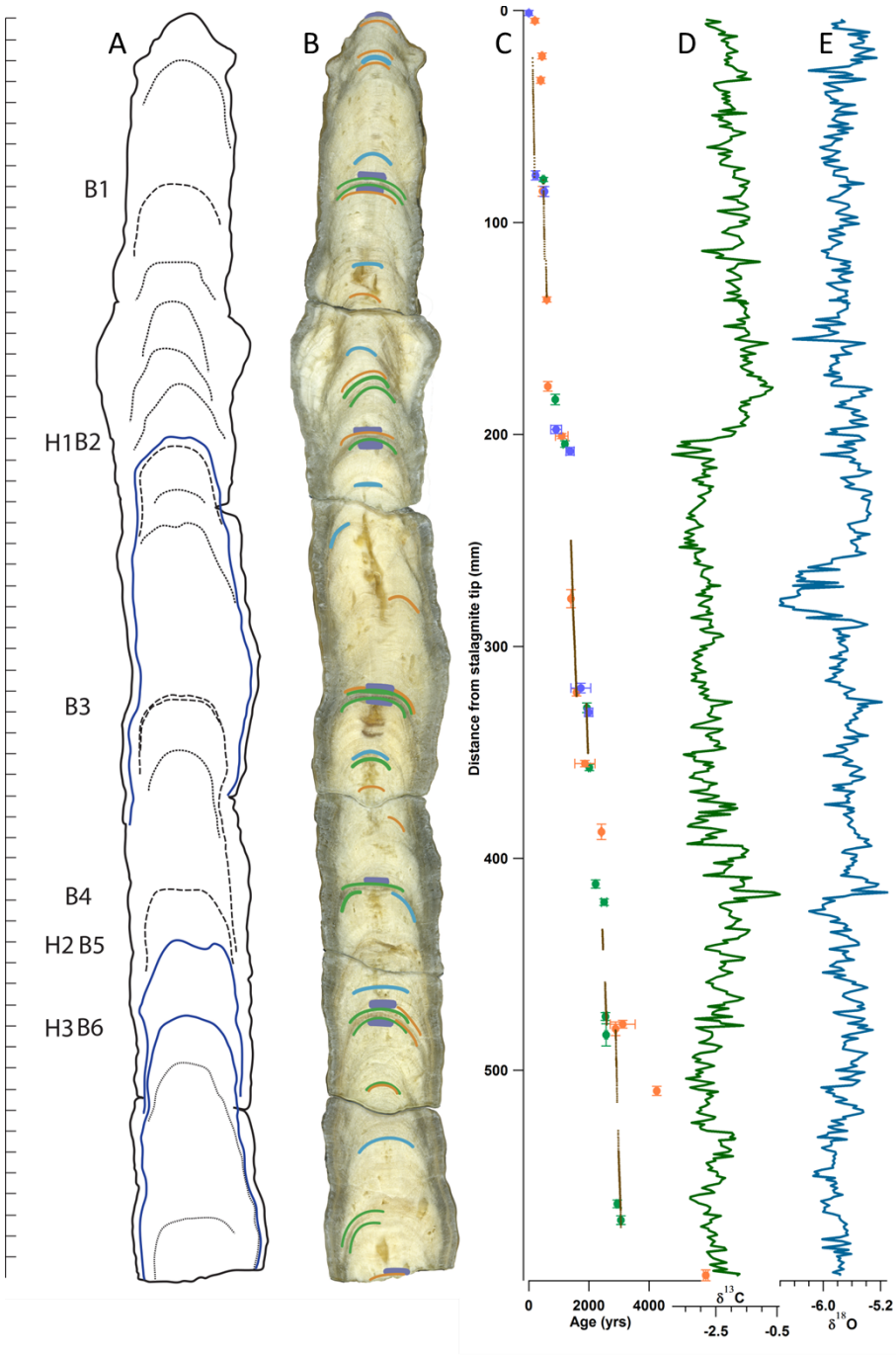

Figure 4: Stalagmite UMS10: A) schematic diagram of significant hiatuses and dense bands. B) sample scan with U-Th sample sites indicated; colours indicate dating batch C) U-dates (coloured) and annual layers (lines) colour matching with overlay bands on B. D) carbon isotopes, E) oxygen isotopes aligned with B.

3.3. Carbon and oxygen isotope results

A specific strategy was followed for the isotope analysis phase as described in section 2.2. Initially a 4 mm pilot study was carried out, followed by a 1 mm resolution contiguous traverse. Subsequently, selected regions of interested were sampled at 0.1 mm resolution, again contiguously. These regions include an annually laminated area, and cross two stratigraphic discontinuities.

The 4 mm and 1 mm isotope traverses are consistent for the length of the stalagmite, with the 1 mm sampling being contiguous, representing true point-to-point variance, removing the concerns of aliasing. In both δ^{13}C and δ^{18}O, we observe rapid, short lived excursions, represented by only between 1 and 3 samples. These are real excursions that were reproduced in subsequent resampling of the same laminae. The excursions account for much of the overall range of the isotopes measured in this sample. δ^{13}C ranges between -3.93‰ and -0.41‰ , with a mean of -2.39‰ and standard deviation of 0.62‰ over the whole record, but should be considered in two major sections; from the tip to 190 mm, δ^{13}C is less depleted, with an average of -1.83‰ and exhibits a rising trend. At 190 mm from the tip, over the subsequent 10 mm, the δ^{13}C abruptly and rapidly drops, from -1 ‰ to nearly -4‰.This change occurs within highly porous laminated fabric immediately preceding a major stratigraphic discontinuity. From this point to the stalagmite tip, δ^{13}C averages -2.63‰ , and exhibits a single waveform in a long period cycle.

δ^{18}O does not behave in a similar way to δ^{13}C at this scale (Fig. 4). There is no evidence of an abrupt change at 190 mm, and instead the most obvious δ^{18}O perturbation is between 264 mm and 283 mm from the tip.

Here the oxygen isotopes are up to 1‰ more depleted than average, and the most depleted δ^{18}O measured throughout the stalagmite. This perturbation matches with a highly corroded calcite fabric identified in microstratigraphic logging, with interconnected macropores up to 4x2 mm. Although there is no appreciable change in δ^{13}C here, this section is again immediately preceding a stratigraphic discontinuity. δ^{18}O ranges between -6.61 and -5.06 ‰ with a mean of -5.72 and a standard deviation of 0.22.

Over the whole record, we consider δ^{13}C independent from δ^{18}O which is supported by an R^2 of 0.003, and, the lack of correlation seen in the high resolution isotope traverses discussed in section 3.3. When analysing short sections of the isotope data individually, R^2 improves up to 0.21, however, the evidence for a common driver is meagre.

The high-resolution isotope traverses reveal distinct, regular and consistent cycles within δ^{13}C, which are in accordance with the visible paired couplets (Fig. 5). Cave monitoring data reveal that the cave environment changes seasonally, with a 4 month lag of peak drip rate to peak rainfall, and a smoothly varying temperature. These cycles suggest a seasonally driven signature, with the peak of each δ^{13}C cycle corresponding to the lowest annual drip rate, which we propose is equal to mid-dry season plus 4 months. This is consistent with the paired laminae corresponding to annual layers driven by the highly seasonal climate, as seen in other records [19, 17]. δ^{18}O is decoupled from δ^{13}C during these high-resolution traverses, which indicates that interpreting climatic significance of δ^{18}O is acceptable, as local processes that would disrupt this would also respond to seasonal forcing and thus correspond to δ^{13}C cycles. In some cases there are progressive depletions

within the δ^{18}O series that are reminiscent of the incoming rainfall isotope data but these are not persistent, indicating a degree of mixing and storage within the karst, in agreement with our cave monitoring data.

The high-resolution isotope traverse across the "stratigraphic discontinuity" (Fig. 5) indicates a rapid but smooth change in local environmental conditions. The δ^{13}C cycles fade out and carbon isotopes rise to above 0‰ for the dense calcite of the stratigraphic feature, before dropping back down to continue the regular cycles. There is no abrupt jump, indicating that this is not caused by a catastrophic event, or drip switching, turning the stalagmite drip "off". Indeed, during this perturbation, the δ^{18}O more closely resembles δ^{13}C than at other times, indicating a change in drip rate and/or PCP as well as any regional change. This suggests a period of low water input to the karst.

While each stratigraphic discontinuity measured in this way is somewhat distinct, most exhibit a fade out of the δ^{13}C cycles, then an upward progression, followed by a smooth drop and resumed cycles. The exception is "dark band 2" where δ^{13}C cycles, fade out but rather than enrichment of δ^{13}C, and instead, there is a jump in δ^{18}O. This dark band also has evidence of dissolution fronts when examined in thin section, and the "dark band" cross cuts the annual lamina, suggesting that a period of more aggressive dripwater has dissolved some calcite, before normal growth resumes. We suggest that this is therefore a period of elevated rainfall leading to, either lower supersaturation of drip water, or raising of the river levels, and flooding the cave with more aggressive water which degraded the stalagmite.

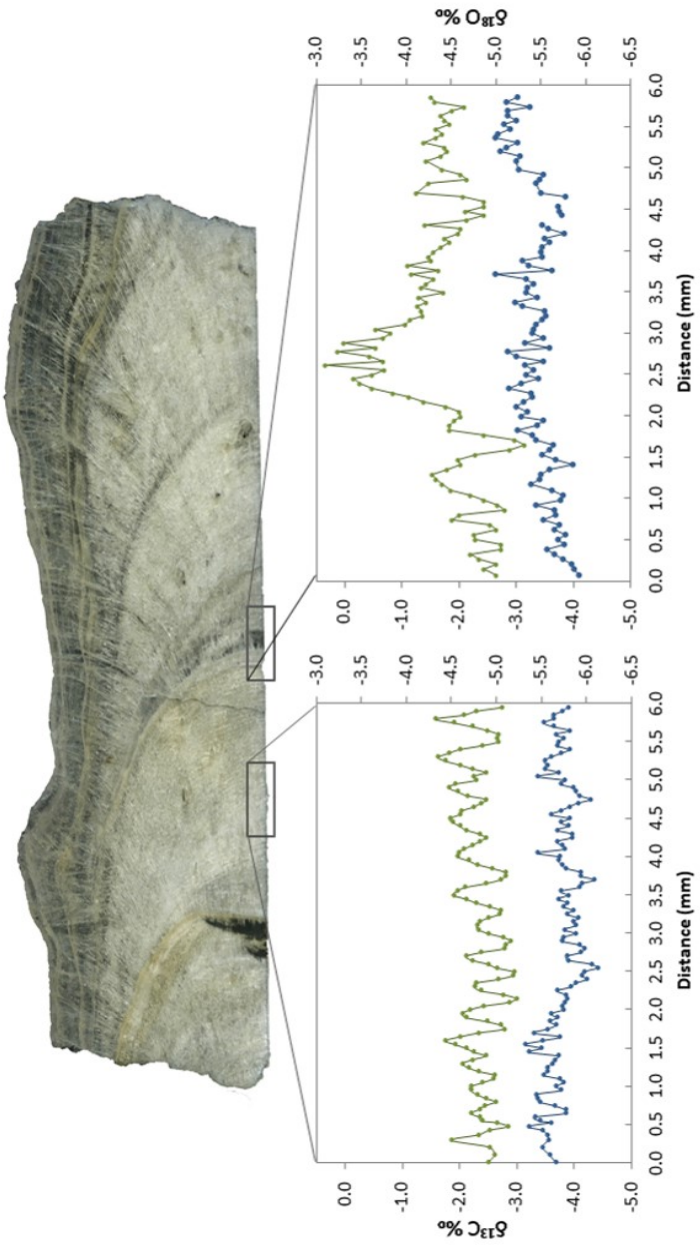

Figure 5: High-resolution stable isotope (δ^{13}C in green, δ^{18}O in blue) traverses: A) along annually laminated sections, B) across a stratigraphic discontinuity. Locations of traverses shown in C taken across stratigraphic discontinuity labelled B3 on Fig. 4, part A. Figure from David Hodkin (MSc thesis)

Element	*Relation to annual laminae*
Mg	irregular
Ba	peaks in low density fabric, also displays multiannual cyclicity
Sr	peaks in low density fabric, also displays multiannual cyclicity
Y	peaks in dense calcite, also displays multiannual cyclicity
P	peaks in dense calcite
Zn	peaks with U minima
U	mini peaks correspond to low density calcite but the main variability is longer time scale.

Table 1: Trace element characteristics in laminated section

3.4. Trace elements

Trace element analysis was targeted on three key areas: one 5 mm traverse of an regularly laminated section of the speleothem, and two traverses across stratigraphic discontinuities that appear different from each other in hand specimen. The laminated section revealed cyclicities within certain trace elements, detailed in Table 1 (and Fig. DR3 in the supplementary information). Note that in this section, there are also regular, well-resolved δ^{13}C cycles determined by high-resolution isotope analysis. During the cycle at which δ^{13}C is least depleted, P and Zn also peak. The prominent Y peak is concurrent with minima in Mg, Sr, Ba and U, but with no change in Zn and P. All Zn peaks above baseline correspond with U minima. This trace element traverse is assumed to be representative of the laminated areas of the speleothem due to the similarities in growth rate, fabrics and colour, throughout the speleothem. This does not include the section which displays mosaic-type calcite that has undergone diagenesis. Principal Component

Analysis of trace element data result in three significant Principle Components (PC) (Fig. 6). PC1 reveals strong negative correlation with Sr, Ba and U, and to a lesser degree to Mg, while Al, Zn and P are strongly positively correlated with PC1. PC2 is of lower significance than PC1, but all trace elements measured, except Br, are positively correlated with PC2, with Sr, Ba and U at R^2 = >0.5. When plotted against each other (Fig. 6), these clearly separate the colloidal and detrital elements, from the large ionic radii elements which compete for defect spots in the crystal lattice.

3.5. U-Th dating and age modelling

Age determinations either side of " dark bands" indicates that they are significant growth slowdowns or hiatuses, but with the limited U/Th ages, a widely used age modelling algorithm, StalAge (Scholz et al.), does not allow many of these suspected hiatuses, and so suggests a consistent growth rate for much of the stalagmite. Another algorithm: COPRA [7], does allow hiatuses, but introduces smooth curves between points, which again may not be representative of the real growth rate with so few U-Th dates. When each of these are applied to the isotope data, there are large differences in the resulting time series, with individual samples being displaced up to 200 years each way, and big differences in dates of important excursions. Regular cycles in $\delta^{13}C$, visible fabric couplets, and trace element peaks all indicate that annual layering is present within UMS10. When all the visible couplets are analysed as "annual", the resulting extension rate is not in agreement with that indicated by U-Th dates. The latter indicate $\approx$ 0.17 mm yr^{-1}, whereas the layer counting (DR2), assuming annual couplets, indicates a growth rate of between 0.3 – 0.9 mm yr^{-1}.

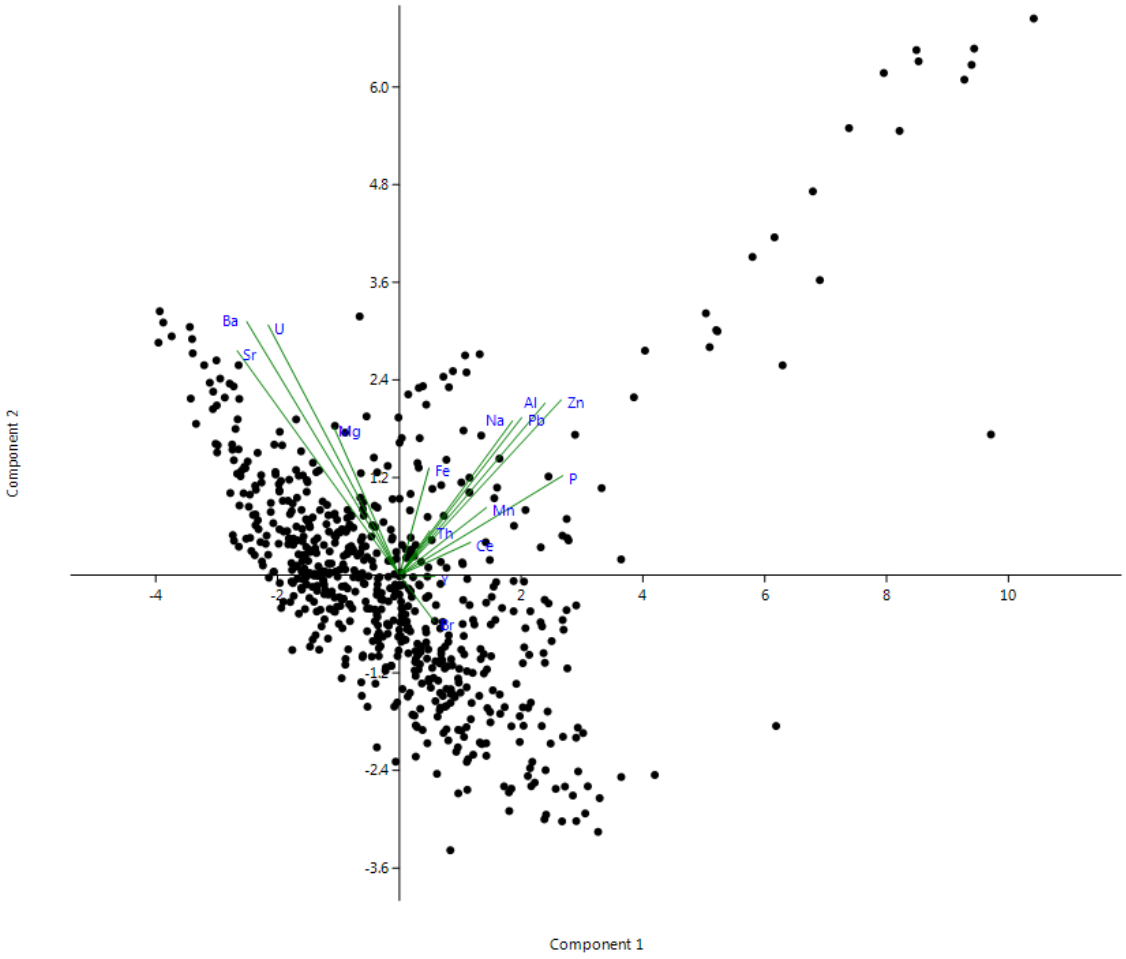

Figure 6: Principal Components Analysis; PCA 1, elements incorporated into the crystal lattice (Mg, Sr, Ba & U) vs 2, elements associated with colloids or detrital materials (Fe, Na, Al, Zn, Pb, Mn, Ce, P).

A hypothetical age model (Fig. 7) was calculated for each paired couplet representing one year of calcite deposition. When the resulting growth rates are compared with those indicated by U-Th dating, it is clear that they are inconsistent over the whole stalagmite, indicating that, if these are indeed annual, significant hiatuses must occur to allow both fabric and U-Th dates to co-exist. The visible laminations fade out when approaching a "dark band" but resume immediately after, rather than fading back in. This fabric suggests that a growth slowdown occurs up to the "dark band", then a cessation of growth, and finally an abrupt restart of "normal" layered calcite deposition. If we then assume that all major "dark bands" must be stratigraphic discontinuities, and pin the layer counting to available U-Th dates, the resulting composite age model is stepped, in a similar manner to the COPRA age model. Since the U-Th dates are not in stratigraphic order, some dates are necessarily excluded from the age model; this represents "best understanding" of the stalagmite's growth history, based on all available evidence.

4. Discussion

4.1. Characteristics of UMS10

UMS10 has periods of steady, seasonally modulated growth punctuated by changes in hydrological regimes resulting in visible stratigraphic discontinuities. Trace elements and carbon isotopes reveal annual laminations with prior calcite precipitation markers Sr and Mg coincident with porous fabrics and less depleted δ^{13}C. These indicate that, in general, shifts in carbon isotopes towards lighter values indicate drier or more ventilated conditions.

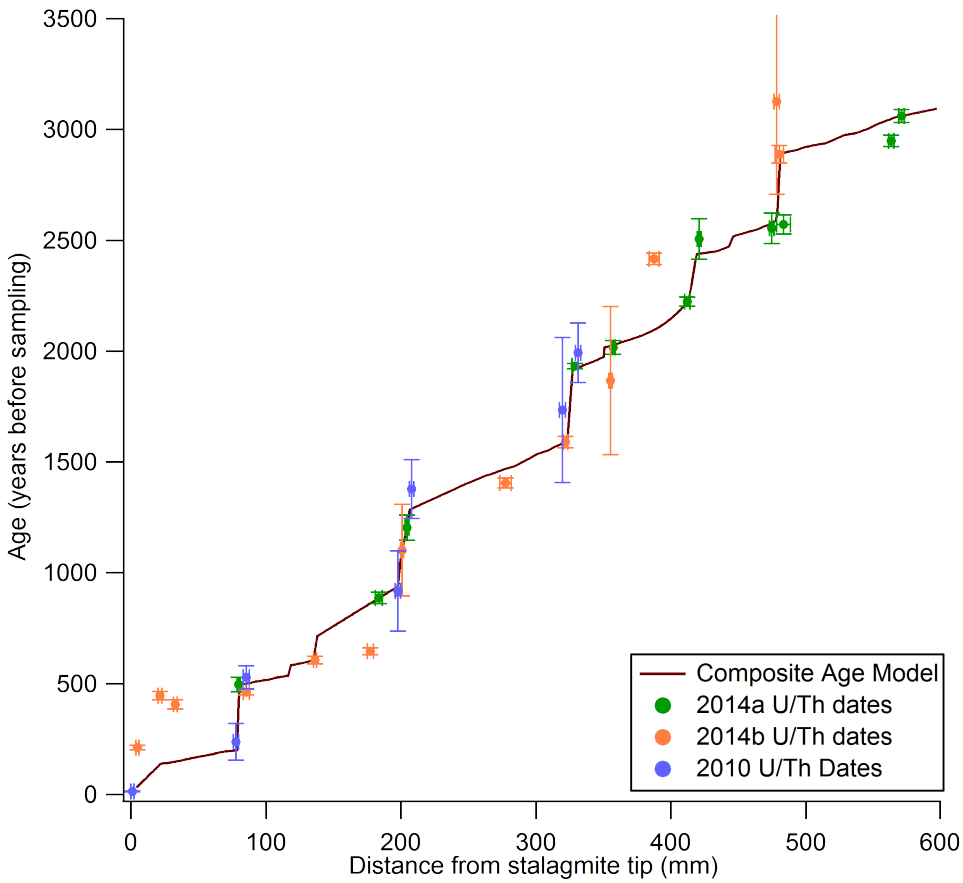

Figure 7: Composite age model based on annual layers and stratigraphic discontinuities pinned by U-Th dating. The three batches of analyses are indicated by colour.

Y is the main "autumnal flush" element we have analysed and spikes when PCP indicators drop, so we attribute this to the onset of the monsoon. P also peaks in dense calcite lamina, during the monsoon when bioproductivity will be increased. So, in general, changes in δ^{13}C, within the record, should indicate changes in karst water balance.

The δ^{18}O record is quite consistent throughout the whole speleothem, with one deviation to more negative values coincidental with splash-cup type fabrics, which may indicate a faster drip rate, although δ^{13}C does not have a concurrent excursion here. δ^{18}O is likely to be driven by changes in hydrological regime, by both changes in isotopic signature of local rainfall, and karst flow regimes. There is a significant regime change at one third of the length, where δ^{13}C becomes significantly reduced.

4.2. Controls on local rainfall oxygen isotopes

Breitenbach et al. [6] interpret the observed progressive depletion of rain δ^{18}O, to be attributable to freshening of the Bay of Bengal through the monsoon season from the discharge of the Ganges and Brahmaputra rivers, changing the δ^{18}O of the source water and hence allowing the observed phenomena. However, this is not consistent with HYSPLIT back trajectory analyses (see Fig. DR1 in Supplementary Info), which indicate that, while some moisture is sourced from Bay of Bengal, there are a variety of other sources, including from the Arabian Sea arm of the ISM, North Africa and East, from China and Myanmar.

The Multivariate ENSO index [29] indicates that, in 2010, La Niña conditions prevailed; in 2011, ENSO was in a neutral to slightly cooled state, and in 2012, weak El Niño-like conditions were observed. IMD Long Period

Average (LPA) data, records all three sampling years as significantly drier than usual, and that only two months out of the sampling period had higher than average rainfall, suggesting that rainfall amount across Meghalaya, is independent from ENSO.

Since there is no measurable amount effect in these data, this conclusion does not preclude the possibility of a causal link between ENSO and δ^{18}O rainfall. Indeed IMD regional rainfall data correlate with δ^{18}O, and the discrepancy between calculated δ^{18}O from the Oxygen Isotopes in Precipitation Calculator (OIPC) and observed δ^{18}O can be linked back to the MEI values for these years. In 2010, when La Niña conditions prevailed, measured δ^{18}O was generally more depleted than calculated estimates. In 2011, with mainly neutral phase MEI, there was no systematic shift of measured from calculated δ^{18}O, and overall they match quite closely. In 2012, when the MEI shifts to a more El Niño-like state, the measured δ^{18}O shifts to be slightly less depleted than expected, including one month where δ^{18}O is measured as enriched relative to V-SMOW (Fig. 2). While the progressive depletion of δ^{18}O exhibits the same trend for each year, ENSO does appear to be able to shift the entire range. This is of course a preliminary interpretation based on pilot study data.

ENSO exerts one control on the position of the Intertropical Convergence Zone (ITCZ), which is pushed northward in the northern hemisphere summer months [30]. The ISM onsets once the Tibetan High degrades and allows northward movement of air [10]. The onset of the ISM is therefore to some extent controlled by the balance between the position of the ITCZ and the state of the Tibetan High, although this is not yet fully understood. So the

position of the ITCZ has an inherent causal influence on the movement of air masses across the Indian subcontinent.

HYSPLIT back trajectory analyses indicate that rainfall over the Shillong Plateau originates from a number of sources and takes different paths, and that this is variable year on year. In 2010, during La Niña conditions, the air mass trajectories generally originated from off the Horn of Africa, and skirted around the south of the Indian subcontinent before moving up over the Bay of Bengal and Bangladesh, with only a more minor contribution from the Indian subcontinent. In 2012, the El Niño-like phase, the air masses come from two sources: 1) from north of Madagascar cutting across the mid-point of the Indian subcontinent to reach the Bay of Bengal; 2) from the Mediterranean or Arabian Seas, following the base of the Himalayas to reach Meghalaya. In 2011, the neutral phase of ENSO, air mass trajectories are generally split, with some coming from east along the base of the Himalayas, some from the Arabian sea cutting across the subcontinent, some across the Bay of Bengal and even, in October at the end of the monsoon, originating in China.

These observations may provide an explanation for an ENSO link to the ISM on an interannual scale, but they do not address the seasonal progressive depletion of the isotopes. We have ruled out amount effect, a systematic change in moisture source, and temperature as controls on a seasonal scale. There must be a gradual process that allows this very distinct phenomenon, and we suggest that it is the progressive "wettening" of the region. Water drains very efficiently in this region, allowing the Shillong plateau to dry so much during the winter that water shortages often occur. This creates low relative humidity and water deficits. When the first rain arrives, relative

humidity is well below 100% resulting in many of the droplets re-evaporating as they fall, with a much higher proportion of ^{18}O enriched droplets "making it" to ground level than ^{16}O enriched droplets, due to the preference for lower energy state. In this case δ^{18}O of rainfall exhibits less negative values. As the monsoon progresses, the ground becomes more saturated, plants grow vigorously, making evapotranspiration high, and relative humidity rises. As relative humidity progressively rises towards 100%, a higher proportion of raindrops reach the ground surface without being evaporated, making the δ^{18}O signature of that rain event more depleted.

In summary, rainfall isotopes in this area are not controlled by the amount effect, but rather, on an annual scale, by evaporation of raindrops, and on an inter-annual scale, by the position of the ITCZ and its influence on air mass trajectories. We suggest that there is also a longer periodicity controlling overall rainfall amount, but dataset does not cover a sufficieant time span to address this.

4.3. Implications for time-integrated $\delta^{18}O$ in speleothems

This event-resolved precipitation study carries implications for interpretation of δ^{18}O in speleothem calcite. If the calcite was recording rainfall at high resolution, we could expect to see a similar systematic sawtooth pattern within the calcite δ^{18}O. However, at the highest resolution (Fig. 5), there are only hints of this, indicating that karst and mixing processes provide an inconsistent low-pass filtering of the rainfall signalling, recording instead the seasonal signal. In this case the volume of rainfall, evapotranspiration and infiltration characteristics are important as they influence the overall δ^{18}O of the water that finally reaches the cave to form the calcite.

The dry season and wet season contributions will also differ, as during the dry season there will generally be a slower drip rate and be more supersaturated, whereas wet season drip rate will be higher and less supersaturated. This is apparent from the cave monitoring data (See Fig. DR4), with variable drip rates reflecting a piston flow regime through the karst.

To reiterate; $\delta^{18}O$ of the calcite reflects a seasonal average of rainfall, with different dry and wet season characteristics dependent of the flow rate of water through the karst, but since our sampling resolution for the entire traverse is too low for seasonal or annual signals then our isotopes are essentially showing a 3-5 year average; over the same time frame as ENSO and other climate oscillations.

4.4. Stratigraphic discontinuities

Stratigraphic discontinuities are described in Table 2 and can been attributed to two different scenarios:

1. Failure of the Indian Summer Monsoon, causing low drip rate and depositing "dry season type" calcite.
2. Prolonged high rainfall, initially causing low supersaturation and a cessation of calcite growth, becoming increasingly aggressive and hence, resulting in dissolution at the stalagmite tip rather than calcite deposition. The evidence for this includes dissolution fronts seen in thin section analysis, and crosscutting of previous annual lamina by the stratigraphic discontinuity. Additionally the trace element data and the isotope response to these discontinuities are inconsistent. We can therefore relate these to extremes of the Indian Summer Monsoon intensity.

"Dry type" stratigraphic discontinuities initially appear as an extended drought, lasting several decades, but it is unlikely that the Indian Summer Monsoon totally failed for this period of time, due to historic records of continuous settlement of the area. And, unlike the "wet type" stratigraphic discontinuities, there is no evidence for lost calcite. However, it is not necessary for the monsoon to stop altogether, but rather, that the volume of rainfall decreases enough that the water balance of the karst is not fully recharged from the monsoon. In this situation, the δ^{13}C would rise, as observed. This could happen if the ISM regime shifted to bring the air masses more across the Indian subcontinent before reaching the Shilling Plateau, as the orographic change would have a less profound effect on the rainfall volume after traversing the continent. For this to happen, the Bay of Bengal Arm would have to be weakened or shifted for a prolonged period of time, allowing the Arabian Sea arm to dominate. This effect could be achieved in a number of ways, including a shift in the Tibetan High, or prolonging the Tibetan High for a longer proportion of the year; a shift in the annual range of the ITCZ to the South, or a change in the weather systems over the Mediterranean sea.

ID	*Distance*	*Hiatus*	*Type*	$\delta^{13}C$	$\delta^{18}O$	*Fabric characteristics*
Sd1	20-21	unclear	Abrupt	-ve excursion	+ve excursion	minor dissolution front
Sd2	78-80	199-495	Abrupt	change to increased values	no change	corroded crystal tips, dissolution front
Sd3	117-119	539-584	Abrupt	sharp +ve excursion	abrupt minor change	dissolution front cross cuts lamina. dendritic pocket on top. Wet type
Sd4	136-140	605-724	Gradual	-ve excursion	minor negative excursion	Intersects with M3. Associated splash cup & corroded calcite
Sd5	197-209	939-1293	Gradual	loss of cyclicity, no excursion, change to -ve	rapid +ve change at onset	Cessation of fabric, dissolution front. Fossil surface with corroded crystal tips & crystal renucleation
Sd6	323-327	1593-1920	Unclear	+ve excursion, then drops	+ve then drops to more -ve	Annual laminae above, bifurcate band: dense-porous-dense. splash cup and lamina below
Sd7	350-352	1975-2018	Abrupt	decreases	decreases	
Sd8	413-418	2237-2406	Gradual	major +ve excursion	+ve excursion	
Sd9	443-448	2472-2520	Abrupt	loss of seasonality, +ve excursion	+ve, rapid change near finish	upper boundary of mosaic calcite
Sd10	478-481	2587-2889	Abrupt	+ve excursion & partial seasonality loss	no change	bifurcate band. lower boundary of mosaic calcite

Table 2: Stratigraphic Discontinuities: characteristics and comparisons. Distance = Distance from tip in mm. Hiatus = estimated timing of hiatus (years BP). Type = type of cessation

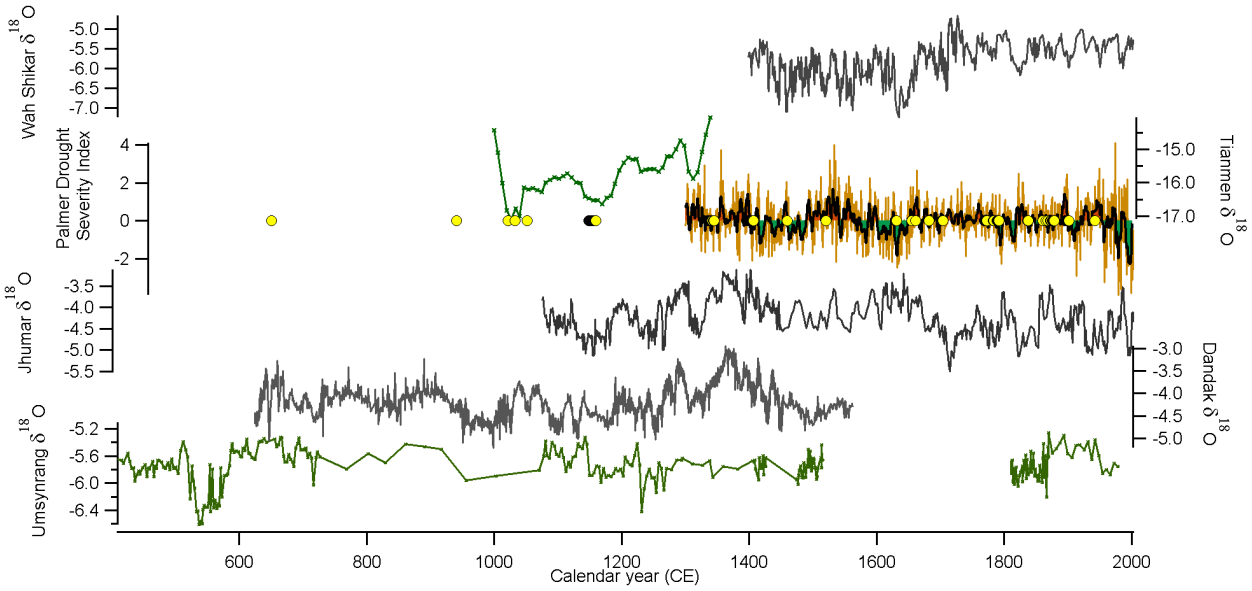

Figure 8: Compiled oxygen isotope records from: Umsynrang (this study, assuming age model of Fig.7) compared with Jhumar [23], Tianmen [8], Dandak [2] and Wah Shikar [23]. Also shown is Palmer Drought Severity Index (brown) [20] and historically reported drought events (yellow dots) (see supplementary information)

While hypothetically, the stratigraphic discontinuities could provide information about regional climate perturbations, in reality, stratigraphic discontinuities, both major and minor occur throughout the stalagmite without any consistent changes in other proxies. Additionally the U-Th dating is of insufficient quantity and quality to constrain all the hiatuses appropriately for detailed palaeomonsoon reconstruction. However, it is clear that this record indicates extended periods of time where the monsoon intensity is regular, interspersed with significant changes in the hydrological regimes, either regional or local, which affect stalagmite growth over decades to centuries (dry type discontinutities) or are shorter very wet events which dissolve large amounts of calcite from the stalagmite.

4.5. Significance of results for regional climate events

The UMS10 proxy timeseries was compared to published coeval speleothem studies from eastern India: Wah Shikar [23], Tianmen[8], Jhumar [23] and Dandak [2] cave records, as well as the Palmer Drought Severity Index, and historical drought events. While there are clear similarities between Tianmen, Jhumar and Dandak, the relationship with the UMS10 record is less clear. There are some suggestions of similarities with Dandak in the earlier part of the record, and Jhumar in the later part, but uncertainties in the age modelling are too great for statistical analyses. Interestingly, these proxy records show no obvious correspondence to recorded famine events from historical documents. Indeed the decadal-long drought events in the historical record between 1350 and 1450 CE discussed by Sinha et al. [23] in the context of oxygen-isotope timeseries from a single speleothem from Dandak (eastern India) are not recognised within our record from the Shillong plateau.In view

of this we suggest that the wet-dry paradigm for interpretation of $\delta^{18}O$ in ISM regions may not be sustainable without improvement to the accuracy of speleothem age models in this region.

5. Conclusions

Event-resolved rainfall isotope data reveal a systematic shift in the isotopic signature throughout the monsoon, which is related to the progressive amounts of available moisture contributing to higher relative humidity over the Indian subcontinent as the monsoon progresses. This reveals a new understanding of rainfall isotopes systematic in the core of the Indian Summer Monsoon, and provides a framework for interpreting oxygen isotopic signature in terms other than "the amount effect".

The proxy record from Krem Umsynrang highlights the complexities of speleothems as archives of proxy data; using a multiproxy approach has revealed details that could have been overlooked if only oxygen isotopes were considered, and this has provided us with a greater understanding of the general moisture dynamics is this locality, even with the uncertainties of the age models.

While regional coherence of proxy records provides information about the variability of the ISM, the "amount effect interpretation is not the sole control precipitation isotopes and their capture in speleothem proxies and the concept of "monsoon intensity is yet to be properly defined.

Acknowledgements

The authors would like to gratefully acknowledge the valuable input of Dr. Bijay Mipun, Dept. of Geography, North Eastern Hill University, and Dave Hodkin (MSci). as well as the Natural Environment Research Council UK for funding this research through grants: *Speleothem records of monsoon intensity: evaluating proxy fidelity via cave process monitoring in the Shillong plateau, NE India* PI Mattey, D. Co I Harris Natural Envt Research Council (NERC): 1/04/09 - 1/10/10 and *U-series dating of speleothem calcite and evaluation of climate recording of S. Asian monsoon intensity in Mawmluh Cave, Cherrapunji, NE India.* Mattey, D. Natural Environment Research Council (NERC): 1/09/10 - 31/08/11 and *A 3000 year annually resolved speleothem record of monsoon intensity from the Shillong plateau, NE India: frequency and duration of drought and teleconnections to regional climate modes* (NERC IP-1551-0515)

References

[1] Akers, P. D., Brook, G. A., Railsback, L. B., Liang, F., Iannone, G., Webster, J. W., Reeder, P. P., Cheng, H., Edwards, R. L., 2016. An extended and higher-resolution record of climate and land use from stalagmite mc01 from macal chasm, belize, revealing connections between major dry events, overall climate variability, and maya sociopolitical changes. Palaeogeography, Palaeoclimatology, Palaeoecology 459, 268–288.

[2] Berkelhammer, M., Sinha, A., Mudelsee, M., Cheng, H., Edwards, R. L.,

Cannariato, K., 2010. Persistent multidecadal power of the Indian Summer Monsoon. Earth and Planetary Science Letters 290 (1), 166–172.

[3] Bowen, G. J., Wilkinson, B., 2002. Spatial distribution of delta O-18 in meteoric precipitation. Geology 30 (4), 315–318.

[4] Breitenbach, S., 2010. Changes in Monsoonal Precipitation and Atmospheric Circulation During the Holocene Reconstructed from Stalagmites from Northeastern India. Ph.D. thesis, Deutsches GeoForschungsZentrum GFZ.

[5] Breitenbach, S. F., Adkins, J. F., Meyer, H., Marwan, N., Kumar, K. K., Haug, G. H., mar 2010. Strong influence of water vapor source dynamics on stable isotopes in precipitation observed in Southern Meghalaya, NE India. Earth and Planetary Science Letters 292 (1-2), 212–220.

[6] Breitenbach, S. F., Donges, J. F., Kharpran Daly, B., Kohn, T., Kohn, T., 2010. Two sandstone caves on the southern edge of the Meghalaya Plateau, India. Cave and Karst Science 37 (2), 49–52.

[7] Breitenbach, S. F. M., Rehfeld, K., Goswami, B., Baldini, J. U. L., Ridley, H. E., Kennett, D. J., Prufer, K. M., Aquino, V. V., Asmerom, Y., Polyak, V. J., Cheng, H., Kurths, J., Marwan, N., 2012. Constructing proxy records from age models (COPRA). Climate of the Past 8 (5), 1765–1779.

[8] Cai, Y., Zhang, H., Cheng, H., An, Z., Edwards, R. L., Wang, X., Tan, L., Liang, F., Wang, J., Kelly, M., 2012. The holocene indian monsoon

variability over the southern tibetan plateau and its teleconnections. Earth and Planetary Science Letters 335, 135–144.

[9] Dansgaard, W., 1964. Stable isotopes in precipitation. Tellus A.

[10] Dixit, Y., Tandon, S. K., 2016. Hydroclimatic variability on the indian subcontinent in the past millennium: Review and assessment. Earth-Science Reviews 161, 1–15.

[11] Dorale, J. A., Liu, Z., 2009. Limitations of hendy test criteria in judging the palaeoclimatic suitability of speleothems and the need for replication. Journal of Cave and Karst Studies 71 (1), 73–80.

[12] Fairchild, I. J., Treble, P. C., mar 2009. Trace elements in speleothems as recorders of environmental change. Quaternary Science Reviews 28 (5-6), 449–468.

[13] Fleitmann, D., Burns, S. J., Mangini, A., Mudelsee, M., Kramers, J., Villa, I., Neff, U., Al-Subbary, A. A., Buettner, A., Hippler, D., Matter, A., jan 2007. Holocene ITCZ and Indian monsoon dynamics recorded in stalagmites from Oman and Yemen (Socotra). Quaternary Science Reviews 26 (1-2), 170–188.

[14] Frisia, S., 2015. Microstratigraphic logging of calcite fabrics in speleothems as tool for palaeoclimate studies. International Journal of Speleology.

[15] Gadgil, S., 2004. Extremes of the Indian summer monsoon rainfall, ENSO and equatorial Indian Ocean oscillation. Geophysical Research Letters 31.

[16] Hendy, C. H., 1971. The isotopic geochemistry of speleothems-I . The calculation of the effects of different modes of formation on the isotopic composition of speleothems and their applicability as palaeoclimatic indicators. Geochimica et Cosmochimica Acta 35 (386).

[17] Johnson, K. R., Ingram, B. L., Sharp, W. D., Zhang, P., 2006. East asian summer monsoon variability during marine isotope stage 5 based on speleothem δ 18 o records from wanxiang cave, central china. Palaeogeography, Palaeoclimatology, Palaeoecology 236 (1), 5–19.

[18] Kumar, K. K., 1999. On the Weakening Relationship Between the Indian Monsoon and ENSO.

[19] Mattey, D., Lowry, D., Duffet, J., Fisher, R., Hodge, E., Frisia, S., may 2008. A 53year seasonally resolved oxygen and carbon isotope record from a modern Gibraltar speleothem: Reconstructed drip water and relationship to local precipitation. Earth and Planetary Science Letters 269 (1-2), 80–95.

[20] Palmer, W., 1965. Meteorological Drought.

[21] Peethambaran, R., Ghosh, P., 2015. Stable isotope ratios in rainfall and water vapour at Bangalore , Southern India during the monsoon period of 2013. In: EGU. Vol. 17. p. 2015.

[22] Singh, M. P., Singh, A. K., 2000. Petrographic characteristics and depositional conditions of Eocene coals of platform basins, Meghalaya, India. International Journal of Coal Geology 42 (4), 315–356.

[23] Sinha, A., Berkelhammer, M., Stott, L., Mudelsee, M., Cheng, H., Biswas, J., 2011. The leading mode of Indian Summer Monsoon precipitation variability during the last millennium. Geophysical Research Letters 38 (15), 2–6.

[24] Wang, B., Wu, R., Lau, K. M., 2001. Interannual Variability of the Asian Summer Monsoon : Contrasts between the Indian and the Western North Pacific East Asian Monsoons *. American Meterological Society, 4073–4090.

[25] Wang, B., Wu, R., Lau, K. M., 2008. How to Measure the Strength of the East Asian Summer Monsoon. American Meterological Society, 4449–4463.

[26] Wang, Y., Cheng, H., Edwards, R. L., Kong, X., Shao, X., Chen, S., Wu, J., Jiang, X., Wang, X., An, Z., 2008. Millennial- and orbital-scale changes in the East Asian monsoon over the past 224 , 000 years. Nature 451 (February), 18–21.

[27] Wang, Y. J., Cheng, H., Edwards, R., He, Y. Q., G, K. X., An, Z., Kelly, M. J., Dykoski, C. A., Li, X. D., 2005. The Holocene Asian monsoon : links to solar changes and North Atlantic climate . Science 308 (June), 854–857.

[28] Webster, P. J., 1987. The Elementary Monsoon. In: Fein, J., Stephens, P. (Eds.), Monsoon. John Wiley, New York, pp. 3–32.

[29] Wolter, K., Timlin, M. S., 2011. El Niño/Southern Oscillation behaviour

since 1871 as diagnosed in an extended multivariate ENSO index (MEI. ext). International Journal of Climatology 31 (7), 1074–1087.

[30] Yancheva, G., Nowaczyk, N. R., Mingram, J., Dulski, P., Schettler, G., Liu, J., Sigman, D. M., Peterson, L. C., Haug, G. H., 2007. Influence of the intertropical convergence zone on the East Asian monsoon. Nature 445 (January), 3–6.

Supplementary Information

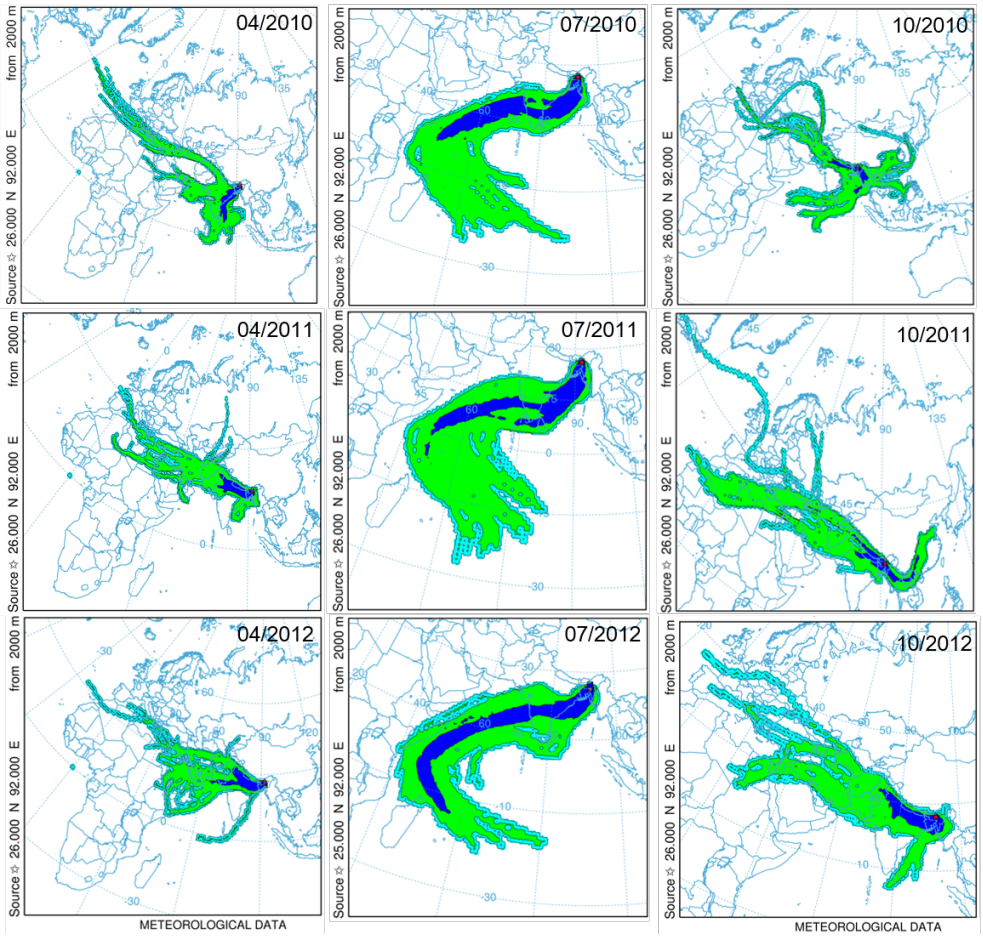

Figure DR1: Monthly composite HYSPLIT Back Trajectory Analyses: Star = origin of calculation, blue = greater than 10%, green = greater than 1%. turquoise = greater than 0.1% contribution to air mass trajectories calculated from the origin at intervals of 6 hours for the entire month.

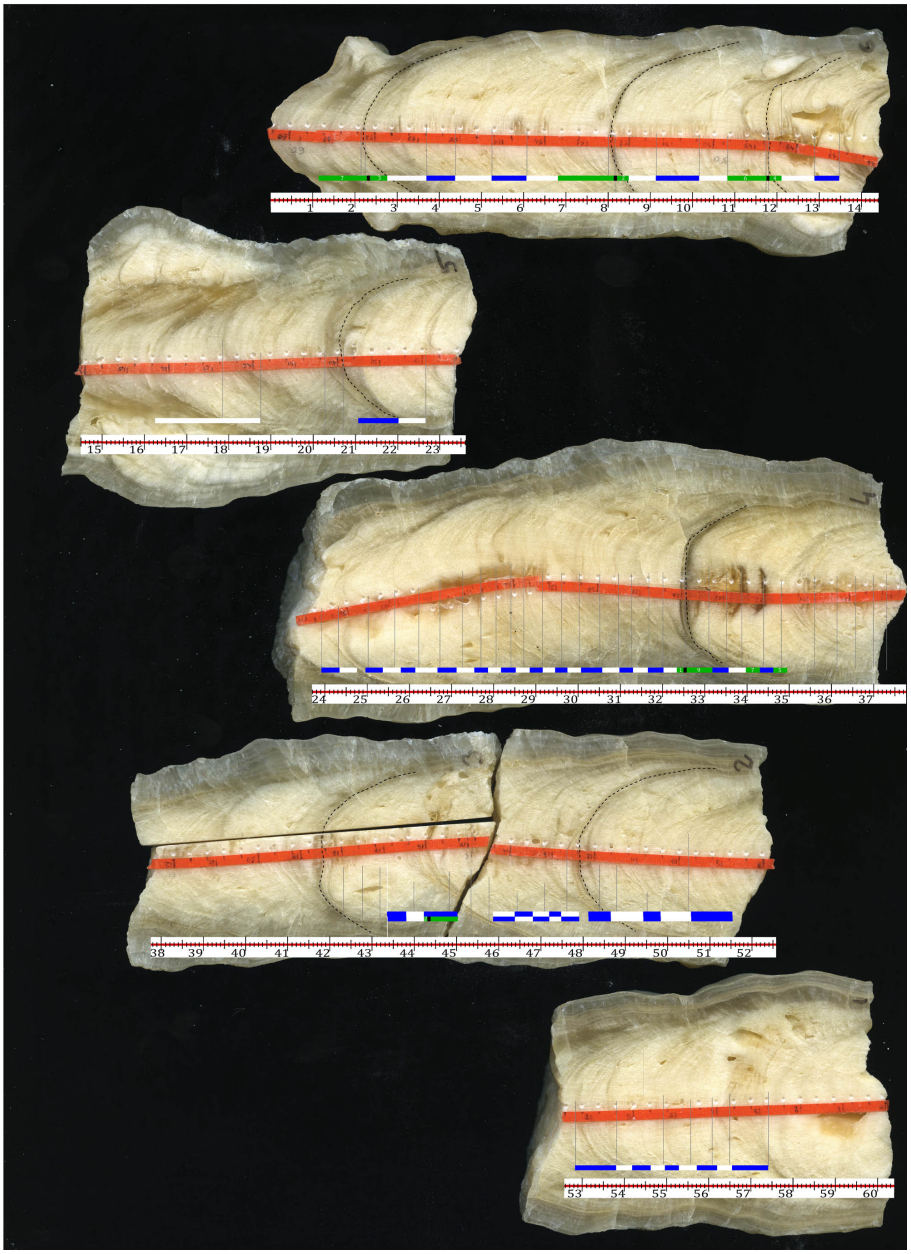

Figure DR2: Layer counting figure (Dave Hodkins), each coloured bar represents 10 couplets. Extension rate is remarkably consistent for much of the stalagmite but punctuated with growth discontinuities.

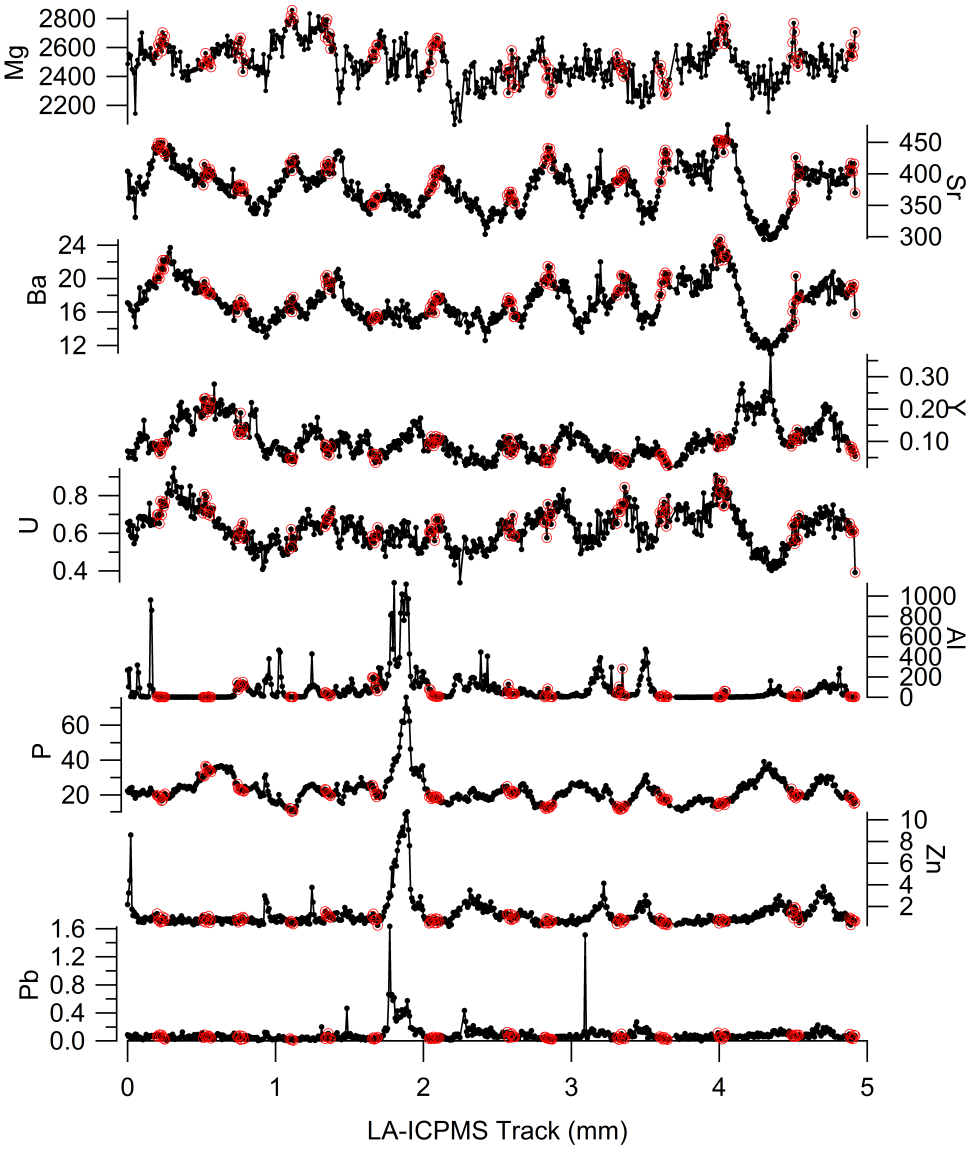

Figure DR3: Trace elements corrected to Ca43 CPS, sampled by LA-ICPMS along a 5mm track of an annually laminated section. All units in ppm, red markers indicate low density calcite.

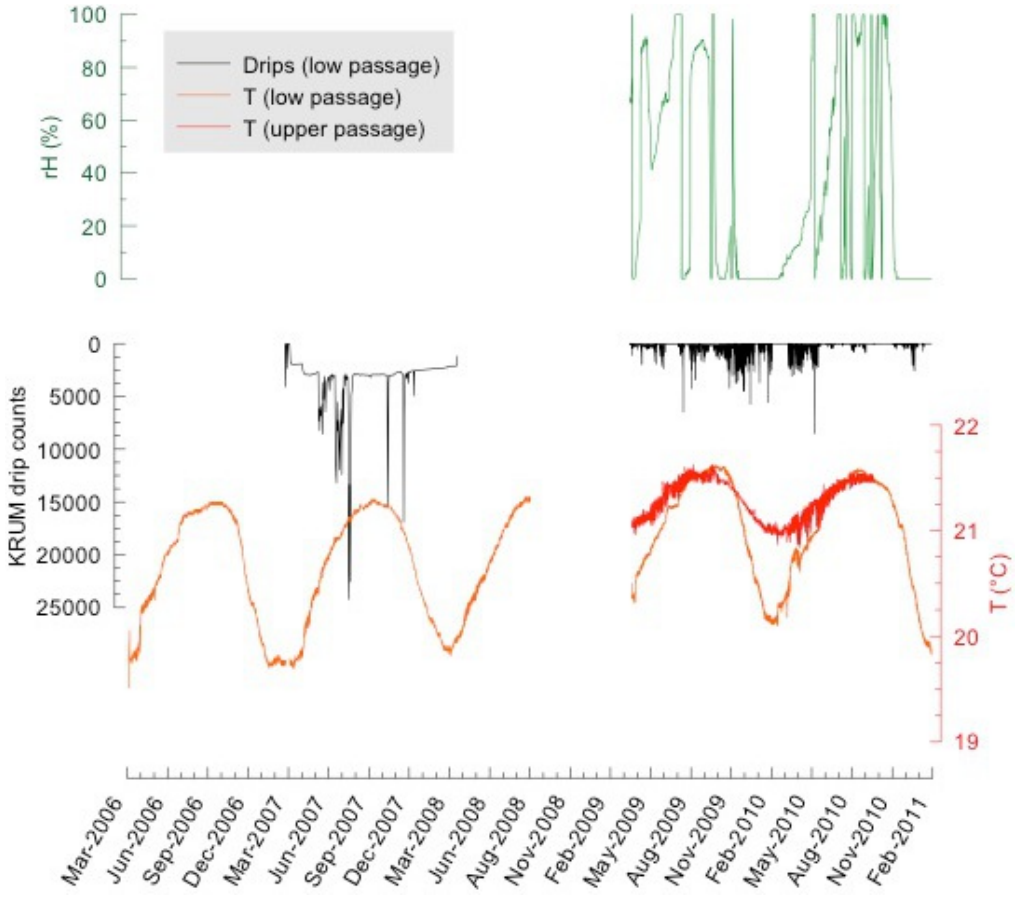

Figure DR4: Monitoring summary of Krems Umsynrang: Relative humidity (green), Daily drip counts (black), temperature in cave passageways: upper (red) and lower (orange).

Data set	Source	Reference
Global Network of Isotopes in Precipitation	International Atomic Energy Agency	IAEA/WMO (2017). Global Network of Isotopes in Precipitation. The GNIP Database.
Oxygen Isotopes in Precipitation Calculator	Centre for High Performance Computing, University of Utah, USA	Bowen G. J. and Revenaugh J. (2003) Interpolating the isotopic composition of modern meteoric precipitation. Water Resources Research 39(10), 1299
Dai Palmer Drought Severity Index	NCAR's CGD (Climate and Global Dynamics Division) PDSI webpage	Dai, A., K. E. Trenberth, and T. Qian, 2004: A global data set of Palmer Drought Severity Index for 1870-2002: Relationship with soil moisture and effects of surface warming. J. Hydrometeorology, 5, 1117-1130.
Jhumar and Wah Shikar Caves Stalagmite Oxygen Isotope Data	Sinha, A., et al. 2011. Central and Northeast India 1000 Year Stalagmite Oxygen Isotope Data	Sinha, A., M. Berkelhammer, L. Stott, M. Mudelsee, H. Cheng, and J. Biswas. 2011. The leading mode of Indian Summer Monsoon precipitation variability during the last millennium. Geophysical Research Letters, Vol. 38, L15703,
Dandak Cave, India Speleothem Oxygen Isotope Data	Berkelhammer, M., et al. 2010. Dandak Cave, India Speleothem Oxygen Isotope Data.	Berkelhammer, M., A. Sinha, M. Mudelsee, H. Cheng, R.L. Edwards, and K. Cannariato. 2010. Persistent multidecadal power of the Indian Summer Monsoon. Earth and Planetary Science Letters, Vol. 290, Issues 1-2, pp. 166-172
Hybrid Single Particle Lagrangian Integrated Trajectory Model (HYSPLIT)	NOAA Air Resources Laboratory	Stein, A.F., Draxler, R.R, Rolph, G.D., Stunder, B.J.B., Cohen, M.D., and Ngan, F., (2015). NOAA's HYSPLIT atmospheric transport and dispersion modeling system, Bull. Amer. Meteor. Soc., 96, 2059-2077
Multivariate ENSO Index	NOAA Earth Systems Research Laboratory, Physical Sciences Division	Wolter, K., and M. S. Timlin, 2011: El Niño/Southern Oscillation behaviour since 1871 as diagnosed in an extended multivariate ENSO index (MEI.ext). Intl. J. Climatology, 31, 14pp., 1074-1087

Table 3: Additional data sets were important additions to this research and are detailed above.

Chapter 4

Paper: Oxygen isotope composition of Fiji precipitation

Authors: M Brett, D Mattey & M Stephens

Submitted to Journal of Geophysical Research: Atmospheres

This co-authored paper manuscript is submitted as substitution for a similar thesis chapter.

I certify that I made the following original and independent contributions to the paper manuscript:

- All isotope data laboratory analysis
- All modelling as described within
- All figures
- The entire first manuscript draft and implementation of subsequent edits

Oxygen isotopes of Fiji rainfall

Marianne Brett[1], **Dave Mattey**[1], **Mark Stephens**[2 3]

[1]Department of Earth Sciences, Royal Holloway University of London, Egham, UK
[2]Department of Environmental Science, Faculty of Science, University of Botswana, P/Bag UB00704, Gaborone, Botswana.
[3]School of Geography, Earth Science and Environment, Faculty of Science, Technology and Environment, The University of the South Pacific, Suva, Fiji.

Key Points:

- Event resolved precipitation samples from Fiji
- Rainfall amount does not predict oxygen isotope signature
- δ^{18}O reflects the position of the SPCZ as a function of the zonal sea surface temperature gradient

Corresponding author: M Brett, marianne.brett.2013@live.rhul.ac.uk

Abstract

Precipitation was sampled in Suva, Fiji, for two years at an event resolution and analysed for $\delta^{18}O$. The "amount effect" accounts for around 20% of the variance in the $\delta^{18}O$ record, but the relationship is neither static, nor reproducible on any timescale within this sampling period. A simple transfer function cannot successfully predict the rainfall amount based on the $\delta^{18}O$ of that event. However, the $\delta^{18}O$ on a monthly or seasonal timescale is representative of the position of the South Pacific Convergence Zone via the zonal sea surface temperature gradient driving air mass trajectories. This finding indicates that the oceanic conditions of the regional hydrological system drive the atmospheric component observed in rainfall amount and isotope signature.

1 Introduction

1.1 Research Motivation

The motivation for this research lies in the need to calibrate and quantify controls on rainfall isotopes in a tropical island setting using current observations and historical data, to allow greater understanding of the implications of $\delta^{18}O$ in terrestrial proxy records such as speleothems [*Stephens and Rose*, 2005]. Speleothems are popular as palaeoclimate proxy hosts, as they occur around the globe, from the tropics to the high latitudes, and from low lying islands to high mountain ranges, giving a broad coverage of terrestrial environments [*Baker et al.*, 2008].

They can provide information at a range of timescales, from daily (in rare cases) to continuous records over thousands of years. The proxy record can include temperature change, rainfall amount, sea level change, tropical cyclone intensity, changes in land use, and flooding events [*Baker et al.*, 2008]). However, speleothem systems are highly complex and localised palaeoclimate archives and so it is absolutely fundamental for speleothem research, and climate science at a wider context, that speleothem data are carefully scrutinised and robustly calibrated, to ensure maximum confidence in the research outcomes.

Speleothem $\delta^{18}O$ is directly affected by the $\delta^{18}O$ of rainfall, moisture uptake by plants, temperature, karst dissolution, and kinetic and disequilibrium fractionation in the cave [*Lachniet*, 2009]. Hence the extent to which rainfall $\delta^{18}O$ is preserved in the stalagmite must be determined in order to distinguish between controls. However the water cycle controls on isotopes in meteoric water are still not well understood, despite $\delta^{18}O$ being used qualitatively in most carbonate palaeoclimate proxy studies. *Dansgaard* [1964], *Rozanski et al.* [1993] and *Gonfiantini et al.* [2001] discuss the negative relationship between stable isotope ratios in precipitation and rainfall amount, known as “the amount effect”. Further work is required to obtain quantitative meteorological data from speleothems.

Precipitation $\delta^{18}O(\delta^{18}O_{precip})$ may be preserved in the stalagmite record and therefore, quantifying the processes controlling different timescales of $\delta^{18}O_{precip}$ give a direct aid to interpreting proxy records. In many places, accessing the Global Network of Isotopes in Precipitation (GNIP) database provides sufficient data to constrain this variable, however, currently available GNIP data from Fiji consists solely of 45 deuterium measurements between 1966 and 1974. GNIP data are available for other Pacific Islands; within the southern part of the West Pacific Warm Pool, these are Rarotonga and Samoa, however, these are monthly composites and do not record details of the synoptic scale controls on precipitation $\delta^{18}O$. Here we have collected precipitation at daily resolution which provides a detailed record of $\delta^{18}O$ associated with local weather.

1.2 Controls on tropical precipition

The “amount effect” was first observed by Dansgaard (1964), who discussed the empirical negative correlation between $\delta^{18}O_{precip}$ and rainfall amount. This observation has since

been studied at various spatial and temporal scales but the mechanisms that lead to this effect are yet to be fully constrained. Fractionation processes on both local [*Lee et al.*, 2005] and regional [*Baldini et al.*, 2010; *Breitenbach et al.*, 2010; *Scholl et al.*, 2007; *Chakraborty et al.*, 2016], scales have been postulated as controlling the "amount effect", but there are several prevailing hypotheses about the exact mechanisms involved, based on both models and observed data. *Rozanski et al.* [1993], and *Yoshimura et al.* [2003] favour the "rain out" effect as a key operator, where the isotopic signature of a convective air mass is controlled by three primary factors; moisture flux, evaporation, and precipitation.

Deep convective clouds in the Intertropical Convergence Zone (ITCZ) form storm clouds, producing more or less intense rain storms. The δ^{18}O of the moisture remaining in the air mass is controlled by the intensity of the initial rain, and the extent of transport and mixing with other moist air masses of different compositions (moisture flux). *Bony et al.* [2008] and *Risi et al.* [2008] argue that, in the tropics, the observed "amount effect" is a result of effects of unsaturated downdrafts within the convective system, although their model does not allow horizontal advection of air masses of different isotopic signatures.

Unsaturated downdrafts have two mechanisms for affecting water isotopes; re-evaporation and equilibration of falling rain by diffusion, and recycling of the subcloud layer vapour, which injects isotopically depleted water vapour back into the convective system. *Moore et al.* [2014], developed a further model for seasonal and longer timescales, studying δD of clouds and rain, and conclude that moisture convergence is central in controlling the strength of the amount effect in steady state, and that these processes may also be applicable to individual storm events as well as seasonal rainfall.

Several studies suggest that the "amount effect" is more strongly related to regional rather than local rainfall amount [*Breitenbach et al.*, 2010; *Kurita*, 2013; *Lekshmy et al.*, 2014], proposing that the isotopic variations in precipitation are a result of regional rain-out processes. One of these regional convective processes, that affects intraseasonal rainfall variability in the tropics, is the Madden-Julian Oscillation (MJO) which is defined by eastward propagation of enhanced or reduced convection, dissipating in the western or central Pacific, typically with a periodicity of 30 – 60 days. *Kurita et al.* [2011] and *Moerman et al.* [2013] suggest that the MJO has a significant impact on precipitation isotope variability in Northern Borneo, with very negative δ^{18}O excursions associated with wet phases of the MJO.

There is also a temperature effect to consider [*Dansgaard*, 1964], not only the temperature during the rainfall event, but the temperature at which clouds form. In the tropics, higher cloud tops, measured by low outgoing longwave radiation (OLR), indicate a lower condensation temperature. Thus a part of the seasonal $\delta^{18}O_{precip}$ variability corresponds to cloud heights associated with seasonal climates patterns [*Scholl et al.*, 2009].

1.3 Previous daily resolution $\delta^{18}O_{precip}$ studies

The majority of $\delta^{18}O_{precip}$ studies published thus far deal with monthly, seasonal or annual δ^{18}O composite measurements rather than daily or event-based collections (e.g.[*Gonfiantini et al.*, 2001; *Yoshimura et al.*, 2003]. $\delta^{18}O_{precip}$ at daily or event resolution provides a means to distinguish effects connected with specific synoptic weather patterns and, as an input to aquifer models, provides more insight into effects of storage and mixing of rainfall when reconstructing groundwater ^{18}O time series [*Baker and Bradley*, 2010]. *Baldini et al.* [2010] analysed event-resolved rainfall in the maritime section of the North Atlantic. They found that on an event-scale, only 20% of the δ^{18}O variability was due to the amount effect, 7% to the temperature effect, while on a monthly or longer timescale, the North Atlantic Oscillation was responsible for 40% of the δ^{18}O variability, with amount and temperature effects being insignificant.

From a speleothem-proxy perspective, this is an important finding as it strongly highlights the importance of understanding controls on precipitation isotopes at different timescales

to interpret precipitation archives in speleothem. A linear relationship between "the amount effect" and $\delta^{18}O_{speleothem}$ is unlikely to be a robust means of reconstructing palaeorainfall in mid-latitude maritime settings [*Baldini et al.*, 2008] but studies in tropical continental settings reveal a different set of complexities.

Breitenbach et al. [2010]) collected event resolution precipitation samples in the Indian Summer Monsoon (ISM) region north of the Bay of Bengal (BoB) in 2007 and 2008, and found a strong seasonal signal with $\delta^{18}O_{precip}$ exhibiting three components of variability: transport distance during the ISM, isotopic changes in the BoB and vapour re-equilibration with rain droplets. The amount effect is not a main control in this region where the $\delta^{18}O$ of source regions is complex. *Kurita et al.* [2009] used daily precipitation sampling from a network of eight stations in South East Asia, "the Maritime Continent". They found only a weak "amount effect" on a station specific, event resolved basis, and reported differing correlations on a monthly timescale at each station, with coastal regions displaying a stronger "amount effect" correlation. *Kurita et al.* [2009] ascribe their findings to regional scale rain out from atmospheric circulation over the tropics.

Moerman et al. [2013] published a 5-year long, daily resolved rainfall oxygen isotope record from northern Borneo and found a weak but significant inverse relationship with local precipitation amount at daily resolution, consistent with the tropical amount effect. However, they report that daily $\delta^{18}O$ variability has a strong and significant correlation to the regional precipitation amount in the preceding week, and conclude that regional scale convective activity is the primary control on $\delta^{18}O_{precip}$ in that location. *Permana et al.* [2016] conducted a similar study in the southern Papua area of Indonesia from January 2013 to September 2015 at different elevations, and found an altitude effect, as well as a regional convective control on daily $\delta^{18}O_{precip}$ variability and propose that major $\delta^{18}O$ depletion events are related to active MJO phases.

These recent, high resolution rainfall isotope studies all found weak or insignificant correlations between $\delta^{18}O_{precip}$ and precipitation amount, and the most common finding was "regional scale convective activity", indicating that a simple "amount effect" correction for palaeoclimate $\delta^{18}O$ proxy records may be simplistic in these complex regions influenced by large land masses.

1.4 Climate Setting

Fiji is located in the South Pacific, lying to the north of New Zealand, east of Australia and south of the Equator. It is isolated from large land masses, with only other small ocean islands in the area. The major meteorological influences here are the South Pacific Convergence Zone (SPCZ), Pacific Decadal Oscillation (PDO), Madden Julian Oscillation (MJO) and tropical cyclones (TCs).

The Republic of Fiji is an archipelago in the South Pacific, consisting of over 330 islands. The largest of these, Vitu Levu (17°48'S 178°0'E), is 146 x 106 km, with Mt Tomanivi, it's highest peak, in the northern highlands reaching 1394 m. There are two distinct seasons, based on precipitation amount. The "wet season" occurs in the austral summer, with the majority of rain falling between November and April, in the form of brief, local showers. Annual total precipitation is highly variable, with up to ±40% departure from the 1961-2003 mean. *Mataki et al.* [2006], and for this reason, the Fiji Meteorological Service (FMS) advise that seasonal averages are non-useful as a forecast for rain volume [*FMS*, 2006; *Mataki et al.*, 2006].

1.4.1 The South Pacific Convergence Zone

The South Pacific Convergence Zone (SPCZ) was first described from surface measurements by*Bergeron* [1930] and from satellite images by *Hubert et al.* [1969], as a persistent cloud and precipitation band in the South Pacific. *Trenberth* [1976] described it as a

"quasi-permanent feature of cloud distribution" and coined the phrase "South Pacific Convergence Zone". The SPCZ is divided into two sectors, the Zonal sector; over the Western Pacific Warm Pool, and the Diagonal sector, orientated northwest-southeast from the Solomon Islands to French Polynesia [*Vincent*, 1994]. The position of each sector is related to sea surface temperatures (SST) and SST gradients in the Pacific [*Takahashi and Battisti*, 2007; *Vincent et al.*, 2009; *Cai et al.*, 2012; *Matthews*, 2012; *Chung and Li*, 2013].

The processes behind the position and maintenance of the diagonal sector of the SPCZ are not well understood, but appear to reflect the preferred storm tracks propagating from low to high latitudes across western and central Pacific [*Widlansky et al.*, 2011], with land-sea distribution also affecting the slope and position of the SPCZ [*Matthews*, 2012]. The zonal sector is subject to convective pulses from the Madden Julian Oscillation (MJO) [*Matthews and Li*, 2005], which may also propagate along the diagonal sector, reaching the subtropics [*Matthews*, 2012].

The SPCZ varies seasonally, with the cloud band being most extensive during the austral summer; November to April [*Meehl*, 1987], when peak negative anomalies in surface pressure, minimum OLR, maximum precipitation and low level convergence occur: "wet season" in the South Pacific. In the austral winter the SPCZ contracts towards the Solomon Islands and exhibits a decreased angle of incidence [*Widlansky et al.*, 2011], however interannual variability of the SPCZ is high, as it also relates to the Interdecadal Pacific Oscillation and the state of El Niño Southern Oscillation (ENSO). [*Lorrey et al.*, 2012; *Folland*, 2002]. ENSO is a quasi-regular linked atmospheric and oceanic phenomenon that affects the global climate, and is characterised by pressure changes in the equatorial Pacific and associated thermocline perturbations [*Trenberth*, 1997]. The diagnostic features are sea surface temperature anomalies spanning the equatorial Pacific, and measured pressure anomalies between Darwin (Australia) and Tahiti [*Wolter and Timlin*, 2011].

ENSO has a profound effect on the position and angle of the SPCZ [*Lorrey et al.*, 2012], as well as global weather systems, such as the Indian Summer Monsoon, and propagates to high latitudes by reorganization of global jet streams. ENSO is well studied in the instrumental era, although not yet fully understood, but attempts to reconstruct behavior in the pre-instrumental era face multiple challenges [*Gergis et al.*, 2006; *Wilson et al.*, 2010].

There are few direct records of the atmospheric component of ENSO, and proxy records of ENSO may be discontinuous, such as corals [*Cobb et al.*, 2003], reliant on low resolution dating [*Conroy et al.*, 2008; *Brijker et al.*, 2007], located in teleconnected areas, bordering the system rather than centre-of-action [*Brook et al.*, 1999] or a combination of these [*Zinke et al.*, 2004]. Few of these records are sufficiently well dated or temporally resolved to inform of decadal scale ocean-atmosphere coupling of ENSO before instrumental data.

1.4.2 Rainfall in Fiji

ENSO exerts an influence on rainfall amount and timing by affecting the position of the Intertropical Convergence Zone (ITCZ), of which the southernmost arm, the South Pacific Convergence Zone (SPCZ) (Fig.1), is the most significant for Fiji. During the dry season, Austral winter, the SPCZ is located more towards the northwest, towards the equator, whereas during wet season, Austral summer, the SPCZ moves south, overlying or passing over Fiji, bringing the rainfall that the population relies upon for irrigation and potable water.

ENSO influences the SPCZ in similar ways: during El Niño, the SPCZ is displaced further to the northwest, causing anomalously low rainfall during "wet season" in Fiji, and during a La Niña event, the SPCZ moves further south, causing winds to arrive in Fiji from the North, and anomalously high rainfall.

Kumar et al. [2013] used instrumental records from weather stations and sugar mills to analyse rainfall amount dynamics, variability and controls. They show that the ENSO has a

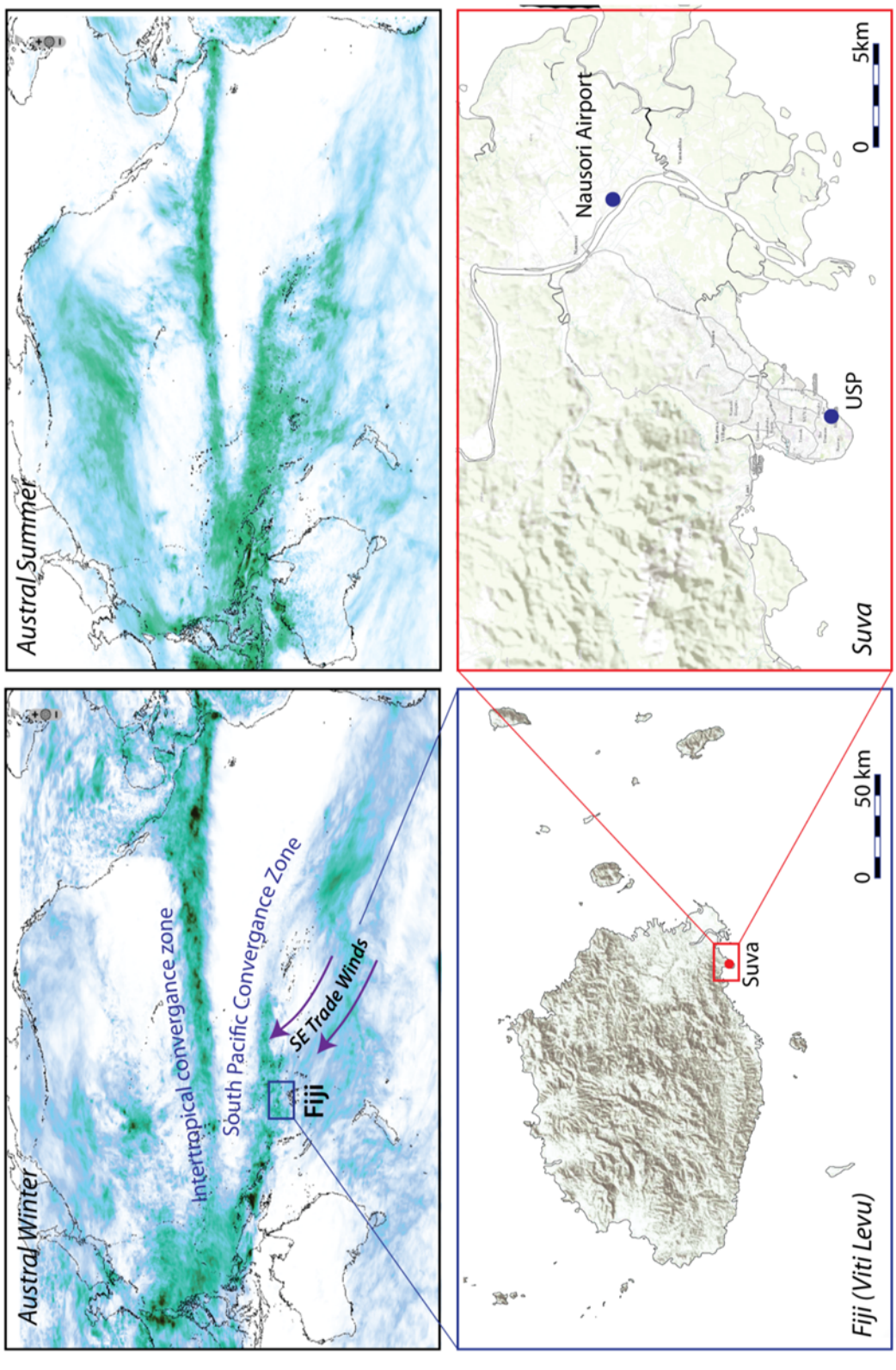

Figure 1. The ITCZ and SPCZ during austral winter and austral summer and the relative location of Fiji and capital city Suva. Note how the SPCZ lies further to the south and is a wider and denser band in austral summer than winter. USP = University of the South Pacific, the location for rain water sampling.

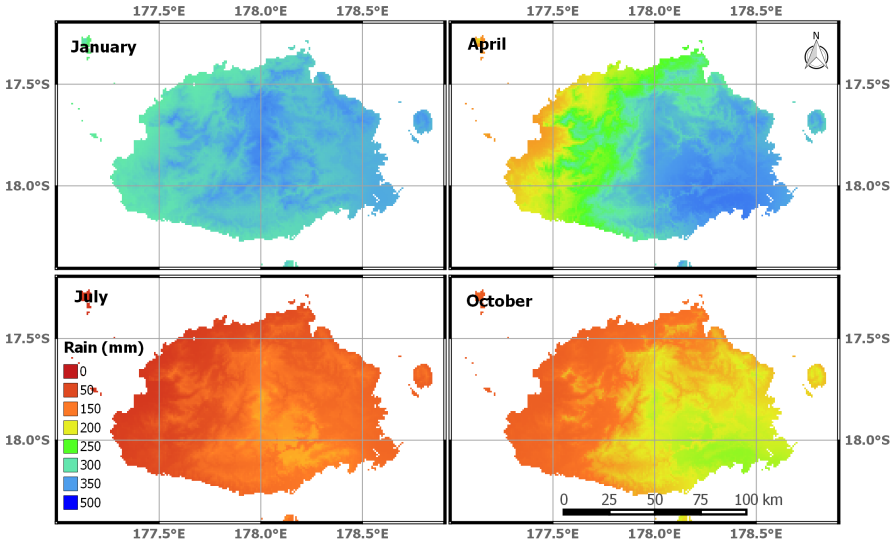

Figure 2. Interpolated monthly precipitation, data from WorldClim [*Hijmans et al.*, 2005], representative of 1950 to 2000 CE. A systematic pattern of drying SE-NW is visible, with the Suva peninsula being the wettest place and Nadi in the northwest, the driest. The mountainous terrain is also visible by rainfall patterns, and it is also apparent that there is some small scale heterogeneity, even when averaged on a 50 year timescale.

significant influence on the rainfall amount in Fiji, and that there is no evidence of modulation by the Interdecadal Pacific Oscillation. Additionally, although Fiji has high interannual rainfall variability, there is no statistically significant change or trend over the last 100 years [*Kumar et al.*, 2013].

1.5 Objectives of this study

In a tropical island setting, the precipitation is governed by a relatively simple system making it an ideal natural laboratory for studying the "amount effect" of precipitation isotopes in a pure natural setting. The objective of this study is to examine the synoptic scale, meteorological controls on precipitation oxygen isotopes. Here we present a daily resolution rainfall isotope record spanning much of 2012 – 2013 CE. We examine the relative importance of precipitation amount, moisture source region, Nino4 SST, and air mass trajectory direction in controlling precipitation oxygen isotopes. This work provides a background to ongoing research in Volivoli cave, which is a speleothem research cave on south-west Vitu Levu [*Stephens et al.*, 2013].

2 Methodology

2.1 Precipitation sampling

The precipitation sampling station for this study was located at the University of the South Pacific (USP), in the capital city, Suva, on a small peninsula extending from the south east of Vitu Levu (Fig. 1). Suva receives the highest volume of rainfall on Vitu Levu (Fig. 2), with annual rainfall between 1.8 m and 4.3 m of precipitation per year, contrasting with Nadi, which receives between 0.8 m and 2.9 m per year *Mataki et al.* [2006]. This discrepancy is due to Suva being located directly in the path of the prevailing wind, and on the windward side of the topographic high, receiving plenty of orographically induced precipitation.

The rain water samples were collected between 19th January 2012 and 15th September 2013 from a standard metal rain gauge on the Lower Campus of USP, based in Suva, Fiji. The rain gauge was located in the middle of the grass lawn in front of the Marine Science building at coordinates 18.91°S 178.45°E. The rain gauge consists of an outer cylinder 13 cm diameter with a funnel top and an inner cylinder 7.5 cm diameter. Collections were made in the morning at around 9 am and the water was measured by removing the inner cylinder from inside the standard rain gauge (outer cylinder). The collected water therefore represents rain that fell in the previous 24 hours. Any collected rainfall was carefully poured into a graduated measuring cylinder where the volume of water was recorded in millilitres and stored in duplicate in Exetainer vials with no head space, and shipped in batches to Royal Holloway University of London (RHUL) for analysis..

2.2 Isotope analyses

205 rainwater samples were analysed for $\delta^{18}O$ at the Stable Isotope Laboratory at RHUL. $\delta^{18}O$ values were determined by standard CO_2 equilibration using an Isoprime continuous flow isotope ratio mass spectrometer (CFIRMS) optimised for water isotope analysis. After each analysis, the reference gas was measured for comparison. δ values were determined relative to an internal standard calibrated to VSMOW, GISP and SLAP standards with precision of ±0.1‰.

2.3 Validation with local meteorological data

Local meteorological data (precipitation amount, maximum and minimum temperatures, relative humidity, mean sea level pressure, and wind speed and direction) are supplied by the Fiji Meterological Service (FMS) from weather stations at Nadi Airport and Nacocolevu Research Station (NRS) and used to test whether the collection from Suva were representative of "normal" rainfall. The NRS data span January 2008 to August 2014, at daily resolution, but with some missing and accumulated values. All data is missing from January to June 2011, as well as July and August 2012. The Nadi Airport data span the same time frame but are more complete, missing only one data point.

Additional precipitation data were obtained from the Nausori Airport weather station, near Suva, to compare with the USP data, however, there are a number of records which indicate that rain occurred here but report 0 mm of precipitation. Rainfall observations from a total five locations are included in this study and comparison between them indicate that rainfall in Fiji is distinctly heterogeneous, being orographically influenced.

Gridded monthly average interpolated precipitation data were obtained from the WorldClim project [*Hijmans et al.*, 2005], sea surface temperature and sea surface salinity data from NASA Jet Propulsion Laboratory, NCEP/NCAR Reanalysis and Niño 3.4, ONI and multivariate ENSO index (MEI) data from the United States' National Oceanic and Atmospheric Administration (NOAA).

2.4 Back trajectory and synoptic analyses

The air mass history of each precipitation event was modelled using 24 hour kinematic back trajectories originating at the USP, Lower Campus (-18.91°S 178.45°W) for 3 different starting heights; 500 m, 1000 m and 2000 m above ground level (agl), using the Hybrid Single Particle Lagrangian Integrated Trajectory (HYSPLIT) Model (Version 4), developed by the NOAA Air Resources Laboratory (NOAA ARL). Suva is located on a small peninsula to the south-east of Vitu Levu, where the trade winds arrive first for much of the year.

Since the precipitation samples were collected at Suva, air mass trajectories were also calculated from here. HYSPLIT computes forward and back trajectories using synoptic scale wind fields generated by the National Center for Environmental Predictions (NCEP) global

data assimilation system (GDAS) forecast/analysis model. The HYSPLIT model provides the horizontal and vertical coordinates for every hour along the trajectory, but has limitations in this situation by the modelled parameter being air mass movement rather than moisture source region or moisture uptake.

Additionally, *Stohl* [1998] highlights the large uncertainties associated with some back trajectory modelling, hence to scrutinise these we have also obtained "NCEP/NCAR 20th Century Reanalysis data (V2c)" from the NOAA Earth System Research Laboratory, Physical Services Division (PSD) [*Compo et al.*, 2011]. These data are created by assimilating climate and meteorological observations from many different sources, using the same climate model throughout the entire reanalysis period, in order to reduce the effects of modeling changes on climate statistics, and are widely used in climate and weather related research. Precipitable water, Vertical wind velocity (Ω) at 500 hPa and OLR, as well as vector magnitude of u-wind and v-wind, have been plotted for the region 40°S, 10°N, 160°E, 160°W, at daily resolution. The back trajectories modelled by HYSPLIT are consistent with the wind fields assimilated by the reanalysis data, and rain events, except for missing data, are consistent with OLR maps.

For the majority of back trajectories, the tracks at all three levels were similar, indicating resolution error to be minor and atmospheric shearing to be insubstantial at these levels. However, general circulation models (GCMs) have difficulty simulating a diagonal SPCZ [*Brown et al.*, 2013; *Niznik et al.*, 2015], thus the GCMs involved in both reanalysis assimilation and back trajectory modelling may introduce some anomalous results. This is checked against satellite data e.g. OLR, which is independent of these GCMs, but may suffer from calibration issues.

3 Results

3.1 Precipitation

3.1.1 Spatial and temporal rainfall amount

Precipitation amount in Vitu Levu is spatially heterogeneous on daily and seasonal timescales due to the prevailing wind direction and topography of the volcanic island. The western side of the island experiences much less rainfall then the eastern side, where the USP campus is located (Fig.2). Mount Tomanivi (1324 m), an extinct volcano, in the northern highlands, has a significant orographic effect on the rainfall regimes of Vitu Levu which is visible in Fig 2. Additionally, it appears that rainfall in Vitu Levu is very localised, with weather stations, even within a few km, reporting orders of magnitude variation of rainfall in the same day, with more than 100 mm of rainfall recorded in a location and less than 20 mm in other locations on the same day.

For 3 out of 4 rainfall events reported as over 150 mm in 24 hours, at least one other weather station recorded rainfall above 100 mm, indicating a more regional event. Large rainfall events are not coincident with recorded TCs in the region. However, on weekly timescales, rainfall recorded across the island exhibits similar patterns, indicating a regional as well as local control on the timing and amount of precipitation. Inter-annual variation 2012 – 2014 is marked: 2012 and 2014 exhibit fewer overall rain events, but more events have higher intensity, whereas in 2013, more rain days are recorded, but in general lower daily rainfall volume.

3.1.2 Temporal $\delta^{18}O$ variability

$\delta^{18}O_{precip}$ exhibited high temporal variability of -18.8‰ to +1.6‰ over the sampling period (mean = -4.66 ‰, 2σ = 7.1 ‰; n= 202) with both extremes occurring in 2013 (Fig. 3). Monthly $\delta^{18}O$ values (n = 7) (Fig. 4) exhibit reduced variability compared to the event based data, with weighted means ranging between -11.0‰ (March) and -1.7‰ (July), how-

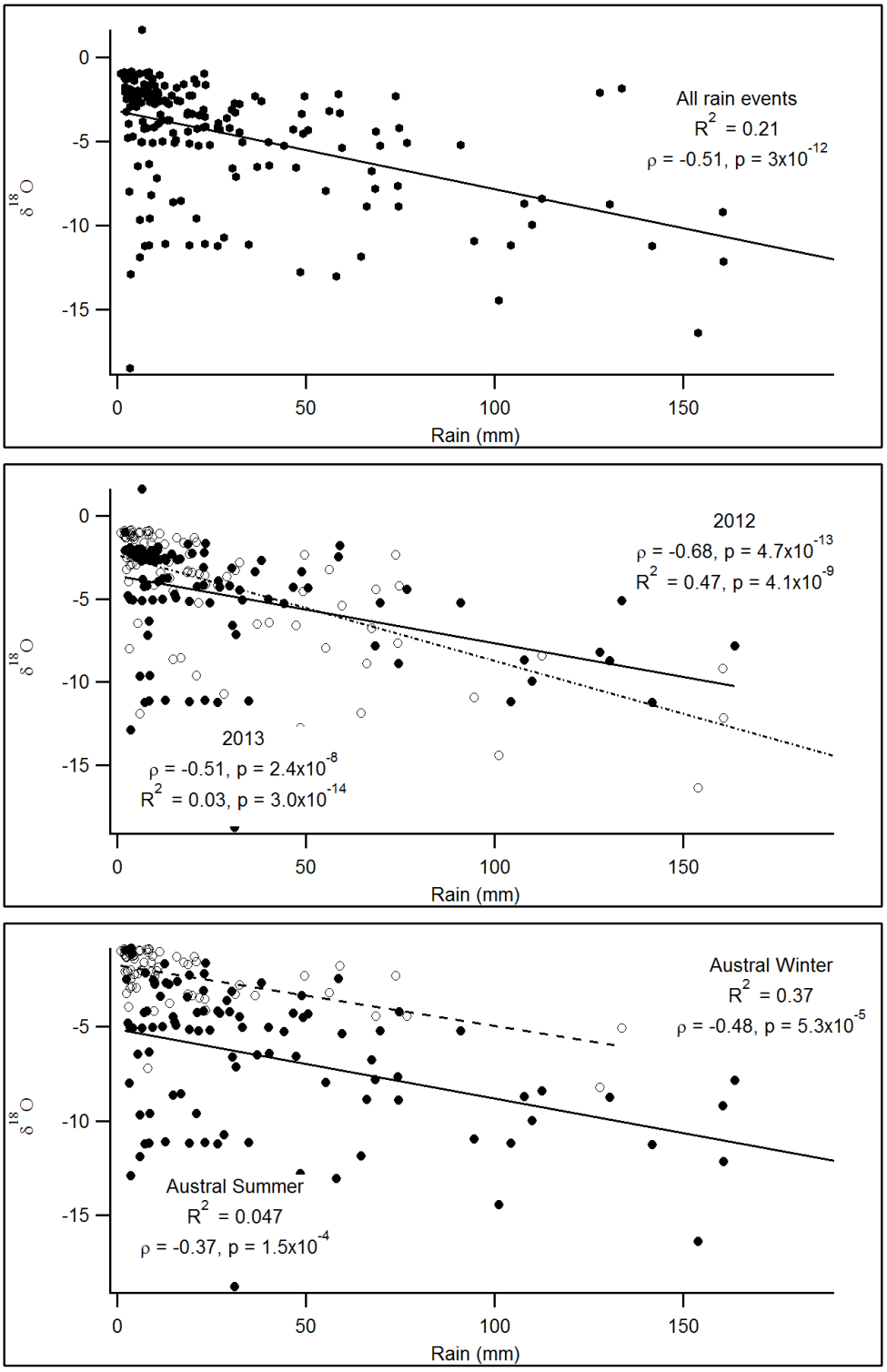

Figure 3. The "amount effect": all samples (top), annual (middle) and seasonal (lower) differences. 2012 / winter data in open circles and dashed lines. 2013 / summer data in filled circles and solid lines. R^2 = Partial Least Squares regression, ρ = Spearmans Rank Correlation Coefficient. P values indicate statistically significant relationships between rainfall amount and isotopic signature, but strength of correlation is variable.

ever, the relatively depleted $\delta^{18}O$ value for March is dominated by four days of measured high volume, highly depleted precipitation, which is not reported as an extreme weather event such as a tropical storm or tropical depression. September – January (inclusive) are missing precipitation amount values thus weighted means are only available for 7 months.

When $\delta^{18}O$ values are binned monthly, it is evident that $\delta^{18}O$ varies throughout the year, with each month displaying a different correlation between amount and isotopic signature (Fig. 4). $\delta^{18}O_{precip}$ displays a seasonal pattern of changes in variability: January – April of both 2012, and 2013, $\delta^{18}O_{precip}$ is highly variable, ranging between -18 ‰ and -1 ‰ with seasonal averages of -7.1 ‰ (2012) and -6.4 ‰ (2013). In contrast, during May – September, $\delta^{18}O_{precip}$ ranges between -4.5 ‰ and +1 ‰ with seasonal averages of -2‰ (2012) and -3‰ (2013) respectively. This indicates a regime change between wet season (austral summer) and dry season (austral winter), and is reflected in both rainfall amount and $\delta^{18}O_{precip}$. Rainfall isotope values are unavailable for September – December of either year, however, independent rainfall records from Nacocolevu Research Station and Nausori Airport, Suva, indicate that rainfall in December is similar to January, and that September and October are similar to August, although again with marked inter-annual variability.

3.2 Synoptic analyses

Synoptic analysis was carried out to assess controls on weather patterns for Fiji during the sampling period. Although the regional system has been extensively described in previous research [*Folland*, 2002; *Linsley et al.*, 2006; *Vincent et al.*, 2009; *Matthews*, 2012; *van der Wiel et al.*, 2015], it is useful to focus on specific events that appear prominently within the $\delta^{18}O_{precip}$ record, to assess any special circumstances present, such as TCs. In 2012-2013, 5 TCs were recorded in the South Pacific basin, but none of these appear within our records as anomalous rainfall peaks in Fiji, or very negative $\delta^{18}O_{precip}$, so our data is representative of "normal" precipitation events. However, much of the rain does coincide with low pressure systems moving across the Pacific and which may contribute to varying $\delta^{18}O$ values.

Wind fields were reconstructed using vector magnitudes of daily mean V-wind and U-wind from publically available NOAA datasets. South westerly trade winds dominate for much of the year, but with significant days of slack wind and more northerly winds. Wind field varies with both the position of the SPCZ, and the occurrence of TCs, both nearby and up to several hundred km distant.

3.2.1 Nino4 and the ITCZ

It is well established that the position of the SPCZ is linked to the position of the ITCZ, as they are understood to be part of the same system, and the El Niño Southern Oscillation exerts a great influence on both. Using Nino4 temperature anomaly as an estimation for the relative position of the ITCZ, we found that there is a significant relationship between $\delta^{18}O_{precip}$ variability and Nino4 temperature anomaly.

As Nino4 is only available at weekly intervals, the correlation is perhaps less statistically significant than it could be. Within the sampling period of this study, Niño 4 temperature was measured across a range of 26.9 to 29.3°C. A La Niña event was concluding in early 2012, with January – March still within the Oceanic Niño Index definition of La Niña, and the remainder of the precipitation sampling was during neutral ENSO conditions.

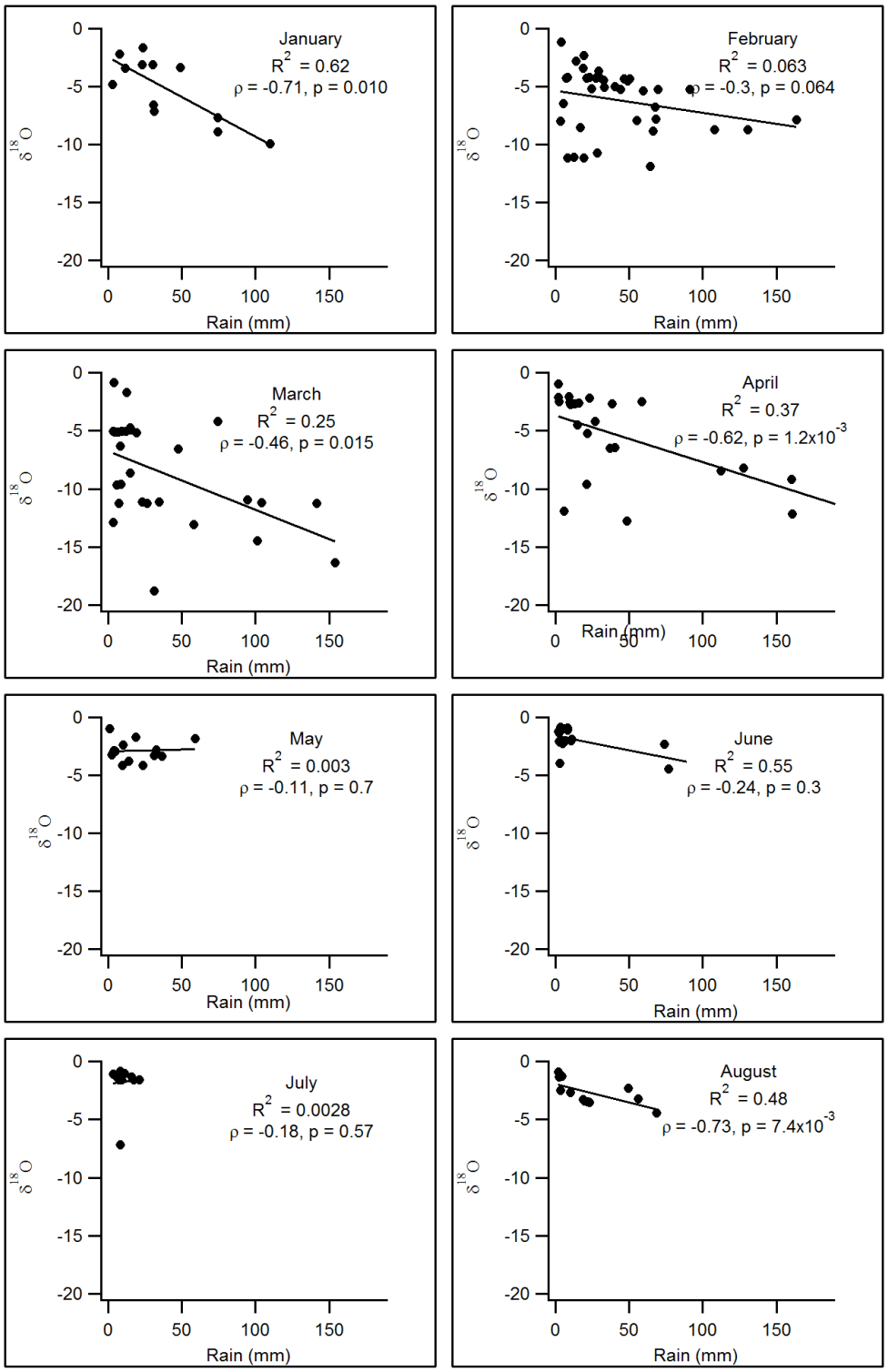

Figure 4. Monthly δ^{18}O vs rainfall amount (mm) show a weak but statistically significant correlation for data from January, March, April and August when separated monthly, however, the other months have p values above 0.05, indicating no significant "amount effect" signature.

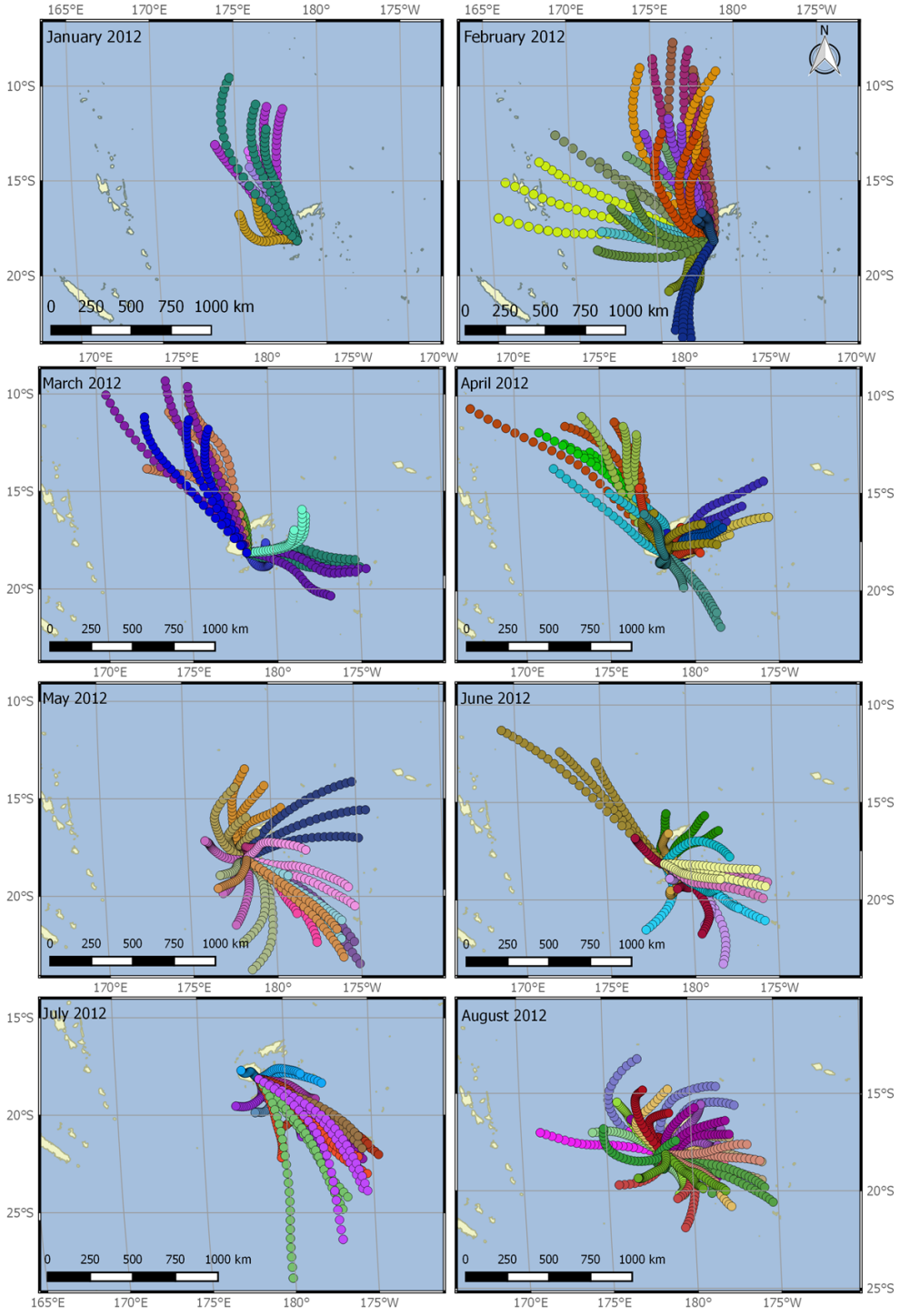

Figure 5. HYSPLIT back trajectory analyses for rain days in 2012, with three trajectories calculated for each day, as denoted by colour.

4 Discussion

4.1 Controls on oxygen isotopes in daily precipitation in Fiji

The $\delta^{18}O$ signature of rainfall is related to amount of rain in our data set, with Spearman's rank for non-parametric data, giving a statistically significant correlation of -0.504 ($p = 3.16 \times 10^{-9}$). However, since this explains less than a quarter of the overall variance observed, we also investigated other controls on rainfall isotope signature. HYSPLIT back trajectory analyses reveal that air masses bringing rain to Fiji arrive mainly from the southeast but with important contributions from the north, and some events from the northeast and south (Fig. 5). $\delta^{18}O$ and rainfall amount data daily values were binned by wind direction; north, northeast, southeast and south-southeast (Fig. 6). For the "north bin" 325° to 15°, there is no statistically significant correlation between $\delta^{18}O$ and precipitation amount. For the other three bins, = -0.53 ± 0.01, $p < 0.0001$. We suggest that the discrepancy between the north bin and the other three, is most likely due to the orographic rainout across the northern highlands.

Within the northeast, southeast and south-southeast bins, while the correlations to the precipitation amounts are similar, each bin shows different characteristics. In the northeast bin (25° – 85°), the average rainfall amount is 31 mm, with a weighted average $\delta^{18}O$ of -6.08 ‰. For the southeast bin, 85°-125°, where the majority of rain events fall, the average is 14 mm, and weighted average $\delta^{18}O$ of -3.0‰. For the final bin, 125° - 180°, the average rainfall event is 32 mm, with a weighted average $\delta^{18}O$ of -7.3‰. This bin also shows a statistically significant correlation with air temperature at Nausori airport: =-0.41, p=0.006, n=45. These similar correlations, but different means, and rainfall amount dynamics, indicate that the "amount effect" is exerting a similar influence on rain from all directions, but that the there is an additional factor causing the $\delta^{18}O$ discrepancies related to wind direction.

Previous similar research (see section 1.3) suggests that regional convection exerts a control on rainfall isotopes and regional wind fields, indicating that these factors may be related. HYSPLIT back trajectory analyses return a marked difference in the air mass movements from north or southeast trajectories. When winds come from the north, air masses typically move approximately twice as fast as when the wind is from the south east, indicating a slightly different moisture source and greater distance over which fractionation processes and interactions with other air masses may occur (Fig. 5).

The variability of the range of isotopes varies according to the difference between Nino4 SST (NOAA) and SST around Fiji (Aquarius), referred to as the zonal sea surface temperature gradient: zΔSST for this study (Fig. 7). When SST in Fiji is greater than at Nino4, zSST < 0, and rainfall isotopes in Suva have a large range, -2 to – 18‰, as a greater contribution of rainfall comes from the north. When SST_{Fiji} is cooler than Nino4, zΔSST > 0, and $\delta^{18}O_{precip}$ range only between +1 and -5 ‰, this is typical of Austral winter, when the SPCZ is generally located to the north of Fiji, allowing the South-easterly trade winds to dominate. Rainfall events can be divided into zΔSST > 0 and zΔSST < 0 (Fig. 7), with each displaying the characteristics expected on dry and wet seasons respectively. This is expected, as previous research (e.g. *Vincent et al.* [2009]; *Widlansky et al.* [2011]) shows that in Austral Winter, the SPCZ moves further north, allowing dry trade winds to dominate Fiji's weather.

However, our data indicate that the period of time where zΔSST > 0, and isotopes show the wet season "Austral summer" signature, is contracted to only 5 months of the year: December – April (Fig. 7), whereas "wet season" is usually recognised as October – April. During the La Niña period of our data set, the zΔSST > 0 persisted for longer than in the ENSO neutral phase in 2013. Correlation PCA of $\delta^{18}O$, rainfall amount and Niño 4 SST, returns three principle components, with PC1 explaining 58.8% of the variance, PC2 at 27.5% and PC3 at 13.6%. Since Nino 4 SST is essentially the independent variable with this, the high value of PC1 indicates that Nino4 SST, or the position of the ITCZ, is the regional forc-

ing for both $\delta^{18}O$ and rainfall amount, which is in agreement with the observed variability of rainfall amount and $\delta^{18}O$ depending on wind direction.

An additional factor complicating this interpretation is the occurrence of TCs. The intense moisture uptake and heavy rainfall within a tropical cyclone produces highly depleted rainfall, which could distort correlations and seasonal, and annual averages. Within our sampling period, five tropical cyclones passed over or nearby Fiji, but we do not have samples or amounts from these events, we do see heavy rainfall events within our data and they fall along the expected regression.

In this case we know that this dataset, while incomplete, is not skewed by these extreme events, and we are understanding the general context. In Suva, therefore, we propose that rainfall isotopes are a determined by air mass trajectory responding to regional convective processes, and amount of rainfall, following Raleigh fractionation, and that these are controlled by the relative position of the SPCZ as it moves according to seasonal SST variability.

4.2 Synthesis

The "amount effect" can be shown to explain about 20% of the variance within the data: a simple linear regression gives r^2=0.207(partial least squares) p=8.4E^{-10}, Pearson r = -0.455 p=8E^{-10}, and Spearman's ρ = -0.509 p=3E^{-12}. The third is statistically the best method for these data as they are non parametric and non normal. This establishes that there is a monotonic relationship between $\delta^{18}O$ and rainfall amount but it explains no more that one quarter of the observed variance. Additionally, the relationship is not stable at any timescale that we can study within the sampling period. Looking at a monthly, seasonal, or annual timescale, the relationship between $\delta^{18}O$ and rainfall amount is neither static nor reproducible: both slope and intercept of regression change.

In this case, it is not feasible to apply a simple transfer function to a $\delta^{18}O$ value to come up with an "amount" of rainfall. In contrast to other studies [*Partin et al.*, 2013; *Maupin et al.*, 2014], a simple transfer function cannot successfully predict the rainfall amount based purely on $\delta^{18}O$, since 80% of the variance is independent of rainfall amount. Fiji is a relatively simple system compared with more continental or coastal sites, so we propose that, if it can not be done here, then it does not stand up in more complicated systems either. Indeed, *Vuille et al.* [2005], argue that there are only a few places that are "amount effect dominated" according to their combined analyses of GNIP data with climate models, and GNIP data are notoriously sparse. This position, while maybe controversial within some parts of the speleothem community, is supported by other high resolution studies of rainfall isotope variability, as detailed in section 1.2.

When plotted as a time series, the isotope data exhibit a clear bimodal pattern which follows austral summer and winter, and could be misconstrued as evidence for the amount effect. However, one must be cautious of making a regressive fallacy: correlation is not causation, and in this case, they are both dependent variables of a third factor which is controlling the bimodal pattern of rainfall amount and isotopic behaviour: the seasons. Notice that the two parts to the pattern are not "isotope values" but "range of isotope values". If we take an individual event value between -5 ‰ and -1 ‰, we cannot be sure which time of year it fell, or whether it was raining heavily or lightly. However, if the event value is between -7 and -20 ‰, we can be reasonably sure that it fell in austral summer.

In the austral winter, the SST around Fiji is cool, providing less energy for evaporation and convective storms. The SPCZ sits to the north, allowing the southeast trade winds to dominate across Fiji. According to the HYSPLIT back trajectory analyses, most rain comes from the nearby ocean, and mainly from south east of Fiji. Additionally, relative humidity is low, allowing reevaporation of droplets before they reach the surface, which favours an enriched, "heavy" signature.

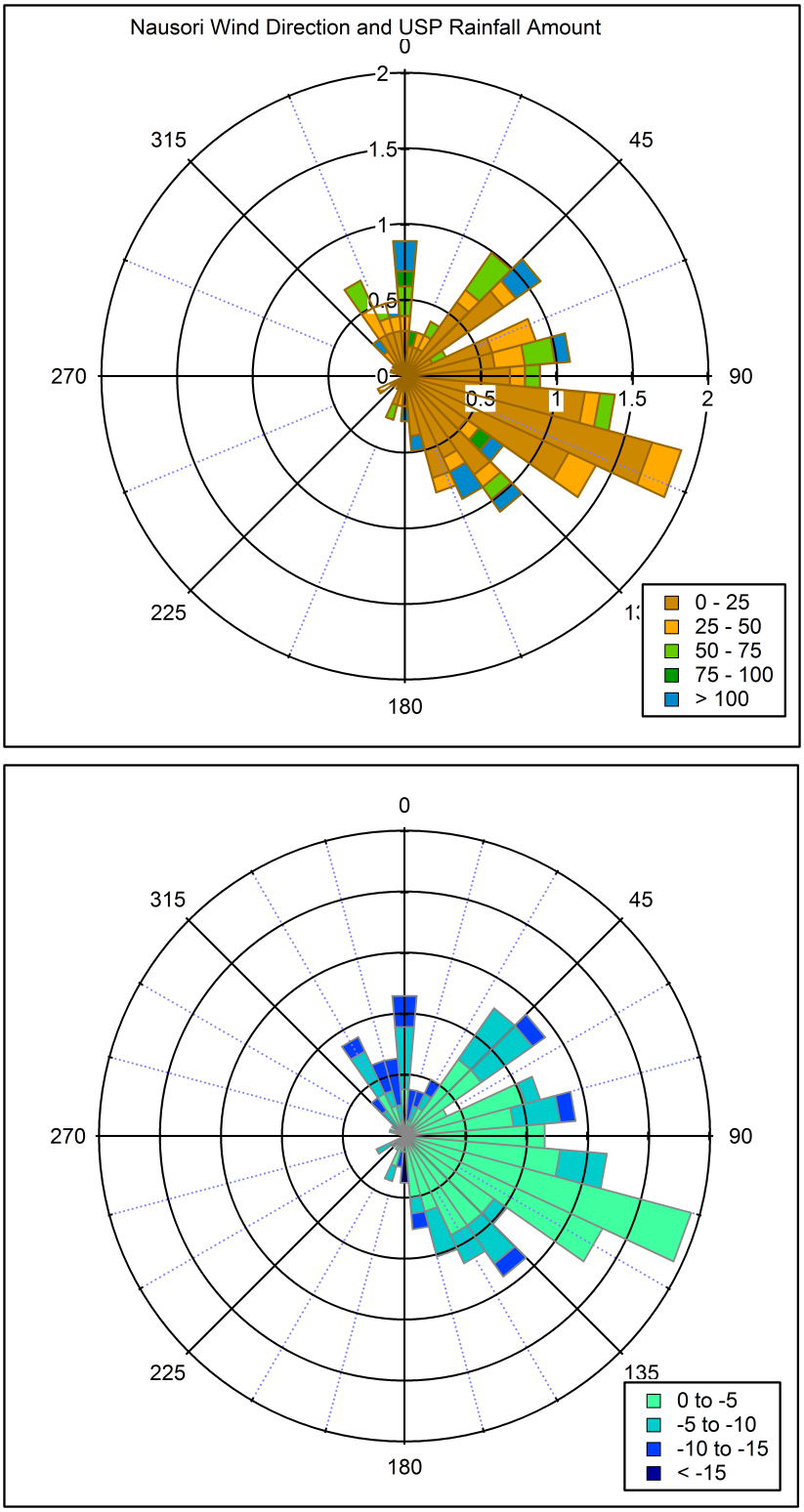

Figure 6. Polar graphs of rainfall amounts (upper) and δ^{18}O (lower) plotted with respect to wind direction (USP Lower Campus data). Light colours refer to low amount or less negative events. Dark colours indicate high volume or more depleted events.

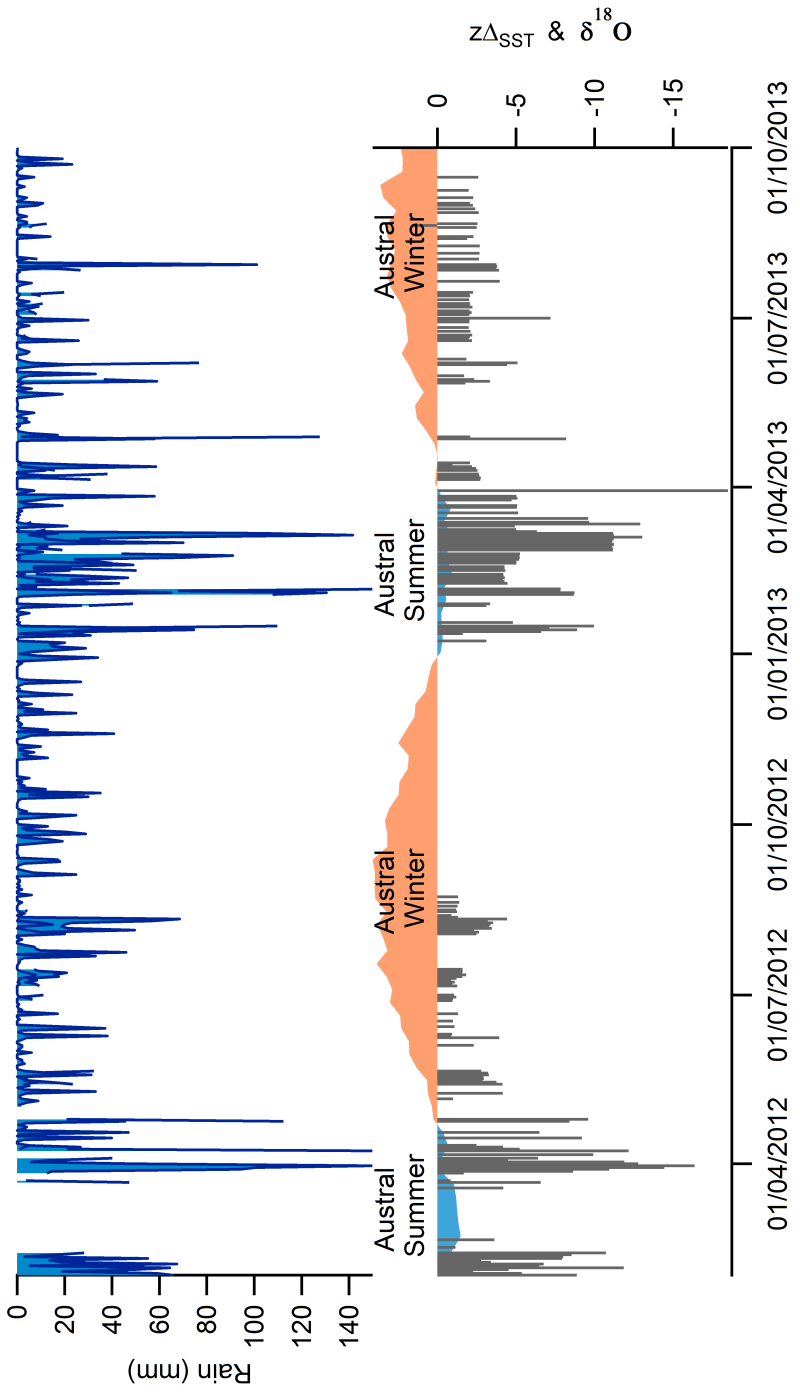

Figure 7. Precipitation in Suva (mm) (left axis), and δ^{18}O (‰) and zδSST (right axis). In Austral summer, zδSST is negative (blue), δ^{18}O displays high variability and precipitation increases. In Austral winter zδSST is positive, δ^{18}O remains mainly within -5 ‰ and precipitation volume is low.

In the austral summer, the sea surface around Fiji becomes warmer, and if it becomes hotter than the equatorial ocean surface, the zonal sea surface temperature anomaly (zΔSST) becomes negative, pulling the SPCZ to the south, and broadening it's influence. At this point airmasses can move south across Fiji, bringing rain from over 1000 km further north. The warm SST also encourages strong evaporation and convection, causing intense local thunderstorms and flash flooding. Therefore, during Austral summer, there are more diverse systems bringing rainfall to Fiji, resulting in a greater variance of isotopic signature, which are only loosely related to rainfall amount. In this way, the oceanic component of the hydrological system, drives the atmospheric conditions observed.

5 Implications and conclusions

Although this study argues that, even in this relatively simple system, δ^{18}O cannot alone allow calculation of the amount of rain occurring, it is still a useful measure for palaeoclimate studies, if interpreted carefully. In this case, the changing δ^{18}O signature of a proxy record capturing meteoric δ^{18}O would reflect the relative position of the SPCZ in relation to Fiji. In years where the δ^{18}O is more depeleted, it can be argued that the SPCZ was positioned further to the south for a longer portion of the year, than if the δ^{18}O is less depleted. Since the position of the SPCZ is dependent on the zonal SST gradient, which is a function of ENSO, the longer term variability of the δ^{18}O provides information about the the state of ENSO over growth period of that proxy.

The isotopic signature of the rainfall in Fiji is controlled both by the position of the SPCZ and the amount of rainfall, the latter which is itself a product of the position of the SPCZ. Isotopic signature of the rainfall is highly variable, but on average more depleted in Austral summer (wet season). The change in the position of the SPCZ is a function of the zonal sea surface temperature gradient, so the seasonal or annual δ^{18}O value, reflects the oceanic compenent of the regional hydrological system.

Acknowledgments

The authors are very grateful for the diligent precipitation sampling by Mr. Albert Whippy and Mr. Soropepeli Seru, postgraduate students (USP). Precipitation sampling was generously funded by a research grant from The Faculty of Science, Technology and Environment of The University of the South Pacific. We also gratefully acknowledge the support of the Fiji Meteorological Service and specifically Mr Ravind Kumar for providing additional meteorological data for this study. This research is part of a NERC funded PhD scholarship.

References

Baker, A., and C. Bradley (2010), Modern stalagmite δ18O: Instrumental calibration and forward modelling, *Global and Planetary Change*, *71*(3-4), 201–206, doi: 10.1016/j.gloplacha.2009.05.002.

Baker, A., C. L. Smith, C. Jex, I. J. Fairchild, D. Genty, and L. Fuller (2008), Annually laminated speleothems: A review, *International Journal of Speleology*, *37*(3), 193–206, doi: 10.5038/1827-806X.37.3.4.

Baldini, L. M., F. McDermott, A. M. Foley, and J. U. L. Baldani (2008), Spatial variability in the European winter precipitation δ18O-NAO relationship: Implications for reconstructing NAO-mode climate variability in the Holocene, *Geophysical Research Letters*, *35*(4), doi: 10.1029/2007GL032027.

Baldini, L. M., F. McDermott, J. U. L. Baldini, M. J. Fischer, and M. Möllhoff (2010), An investigation of the controls on Irish precipitation δ18O values on monthly and event timescales, *Climate Dynamics*, *35*(6), 977–993, doi:10.1007/s00382-010-0774-6.

Bergeron, T. (1930), Richtlinien einer dynamischen Klimatologie, *Meteorologische Zeitschrift*, *47*, 246—-262.

Bony, S., C. Risi, and F. Vimeux (2008), Influence of convective processes on the isotopic composition (δ18O and δD) of precipitation and water vapor in the tropics: 1. Radiative-convective equilibrium and Tropical Ocean-Global Atmosphere-Coupled Ocean-Atmosphere Response Experiment, *Journal of Geophysical Research: Atmospheres*, *113*(19), 1–21, doi:10.1029/2008JD009942.

Breitenbach, S. F., J. F. Adkins, H. Meyer, N. Marwan, K. K. Kumar, and G. H. Haug (2010), Strong influence of water vapor source dynamics on stable isotopes in precipitation observed in Southern Meghalaya, NE India, *Earth and Planetary Science Letters*, *292*(1-2), 212–220, doi:10.1016/j.epsl.2010.01.038.

Brijker, J., S. Jung, G. Ganssen, T. Bickert, and D. Kroon (2007), ENSO related decadal scale climate variability from the Indo-Pacific Warm Pool, *Earth and Planetary Science Letters*, *253*(1-2), 67–82, doi:10.1016/j.epsl.2006.10.017.

Brook, G., S.-W. Sheen, M. Rafter, L. Railsback, and J. Lundberg (1999), A high-resolution proxy record of rainfall and ENSO since AD 1550 from layering in stalagmites from Anjohibe Cave, Madagascar, *The Holocene*, *9*(6), 695–705, doi:10.1191/095968399677907790.

Brown, J. R., A. F. Moise, and R. A. Colman (2013), The South Pacific Convergence Zone in CMIP5 simulations of historical and future climate, *Climate Dynamics*, *41*(7-8), 2179–2197, doi:10.1007/s00382-012-1591-x.

Cai, W., M. Lengaigne, S. Borlace, M. Collins, T. Cowan, M. J. McPhaden, A. Timmermann, S. Power, J. Brown, C. Menkes, A. Ngari, and M. J. Vincent, Emmanuel M.and Widlansky (2012), More extreme swings of the South Pacific convergence zone due to greenhouse warming, *Nature*, *488*, 365–369, doi:10.1038/nature11358.

Chakraborty, S., N. Sinha, R. Chattopadhyay, S. Sengupta, P. M. Mohan, and A. Datye (2016), Atmospheric controls on the precipitation isotopes over the Andaman Islands, Bay of Bengal, *Scientific Reports*, *6*(January), 19,555, doi:10.1038/srep19555.

Chung, P. H., and T. Li (2013), Interdecadal relationship between the mean state and El Niño types, *Journal of Climate*, *26*(2), 361–379, doi:10.1175/JCLI-D-12-00106.1.

Cobb, K. M., C. D. Charles, H. Cheng, and R. L. Edwards (2003), El Nino / Southern Oscillation and tropical Pacific climate during the last millennium, *Nature*, *424*(July), 271–276, doi:10.1038/nature01779.

Compo, G. P., J. S. Whitaker, P. D. Sardeshmukh, N. Matsui, R. J. Allan, X. Yin, B. E. Gleason, R. S. Vose, G. Rutledge, P. Bessemoulin, and Others (2011), The twentieth century reanalysis project, *Quarterly Journal of the Royal Meteorological Society*, *137*(654), 1–28.

Conroy, J. L., J. T. Overpeck, J. E. Cole, T. M. Shanahan, and M. Steinitz-Kannan (2008), Holocene changes in eastern tropical Pacific climate inferred from a Galapagos lake sediment record, *Quaternary Science Reviews*, *27*(11-12), 1166–1180, doi:10.1016/j.quascirev.2008.02.015.

Dansgaard, W. (1964), Stable isotopes in precipitation, *Tellus A*, *16*, 436–468, doi:10.3402/tellusa.v16i4.8993.

Fiji Meteorological Service, (2006). The climate of Fiji, *FMS Information Sheet No. 35* Retrieved from http://www.met.gov.fj/ClimateofFiji.pdf

Folland, C. K. (2002), Relative influences of the Interdecadal Pacific Oscillation and ENSO on the South Pacific Convergence Zone, *Geophysical Research Letters*, *29*(13), 2–5, doi:10.1029/2001GL014201.

Gergis, L. L. E., K. Braganza, A. Fowler, S. Mooney, and J. Risbey (2006), Reconstructing El Niño Southern Oscillation (ENSO) from high-resolution palaeoarchives, *Journal of Quarternary Science*, *21*, 707–722, doi:10.1002/jqs.

Gonfiantini, R., M. A. Roche, J. C. Olivry, J. C. Fontes, and G. M. Zuppi (2001), The altitude effect on the isotopic composition of tropical rains, *Chemical Geology*, *181*(1-4), 147–167, doi:10.1016/S0009-2541(01)00279-0.

Hijmans, Robert J and Cameron, Susan E and Parra, Juan L and Jones, Peter G and Jarvis, A. (2005), Very high resolution interpolated climate surfaces for global land areas, *International Journal of Climatology*, *25*(15), 1965–1978.

Hubert, L. F., A. F. Krueger, and J. S. Winston (1969), The Double Intertropical Convergence Zone-Fact or Fiction?, *Journal of Atmospheric Sciences*, *26*(4), 771–773, doi:10.1175/1520-0469(1969)026<0771:TDICZF>2.0.CO;2.

Kumar, R., M. Stephens, and T. Weir (2013), Rainfall trends in Fiji, *International Journal of Climatology*, *34*(5), 1501–1510, doi:10.1002/joc.3779.

Kurita, N. (2013), Water isotopic variability in response to mesoscale convective system over the tropical ocean, *Journal of Geophysical Research Atmospheres*, *118*(18), 10,376–10,390, doi:10.1002/jgrd.50754.

Kurita, N., K. Ichiyanagi, J. Matsumoto, M. D. Yamanaka, and T. Ohata (2009), The relationship between the isotopic content of precipitation and the precipitation amount in tropical regions, *Journal of Geochemical Exploration*, *102*(3), 113–122, doi:10.1016/j.gexplo.2009.03.002.

Kurita, N., D. Noone, C. Risi, G. A. Schmidt, H. Yamada, and K. Yoneyama (2011), Intraseasonal isotopic variation associated with the Madden-Julian Oscillation, *Journal of Geophysical Research Atmospheres*, *116*(24), 1–20, doi:10.1029/2010JD015209.

Lachniet, M. S. (2009), Climatic and environmental controls on speleothem oxygen-isotope values, *Quaternary Science Reviews*, *28*(5-6), 412–432, doi:10.1016/j.quascirev.2008.10.021.

Lee, X., S. Sargent, R. Smith, and B. Tanner (2005), In Situ Measurement of the Water Vapor 18 O/ 16 O Isotope Ratio for Atmospheric and Ecological Applications, *Journal of Atmospheric and Oceanic Technology*, *22*(5), 555–565, doi:10.1175/JTECH1719.1.

Lekshmy, P. R., M. Midhun, R. Ramesh, and R. a. Jani (2014), (18)O depletion in monsoon rain relates to large scale organized convection rather than the amount of rainfall., *Scientific reports*, *4*, 5661, doi:10.1038/srep05661.

Linsley, B. K., A. Kaplan, Y. Gouriou, J. Salinger, P. B. DeMenocal, G. M. Wellington, and S. S. Howe (2006), Tracking the extent of the South Pacific Convergence Zone since the early 1600s, *Geochemistry, Geophysics, Geosystems*, *7*(5), doi:10.1029/2005GC001115.

Lorrey, A., G. Dalu, J. Renwick, H. Diamond, and M. Gaetani (2012), Reconstructing the South Pacific Convergence Zone Position during the Presatellite Era: A La Niña Case Study, *Monthly Weather Review*, *140*(11), 3653–3668, doi:10.1175/MWR-D-11-00228.1.

Mataki, M., K. C. Koshy, and M. Lal (2006), Baseline Climatology of Viti Levu, Fiji and Current Climatic Trends, *Pacific Science*, *60*(1), 49–68, doi:10.1353/psc.2005.0059.

Matthews, A. J. (2012), A multiscale framework for the origin and variability of the South Pacific Convergence Zone, *Quarterly Journal of the Royal Meteorological Society*, *138*(666), 1165–1178, doi:10.1002/qj.1870.

Matthews, A. J., and H. Y. Y. Li (2005), Modulation of station rainfall over the western Pacific by the Madden-Julian oscillation, *Geophysical Research Letters*, *32*(14), 1–5, doi:10.1029/2005GL023595.

Maupin CR, Partin JW, Shen CC, Quinn TM, Lin K, Taylor FW, Banner JL, Thirumalai K, Sinclair DJ (2014), Persistent decadal-scale rainfall variability in the tropical South Pacific Convergence Zone through the past six centuries, *Climate of the Past*, *10*(4), 1319.

Meehl, G. (1987), The Annual Cycle and Interannual Variability in the Tropical Pacific and Indian Ocean Regions, *Monthly Weather Review*, *115*(1), 27–50, doi:10.1175/1520-0493(1987)115<0027:TACAIV>2.0.CO;2.

Moerman, J. W., K. M. Cobb, J. F. Adkins, H. Sodemann, B. Clark, and A. A. Tuen (2013), Diurnal to interannual rainfall δ18O variations in northern Borneo driven by regional hydrology, *Earth and Planetary Science Letters*, *369-370*, 108–119, doi:10.1016/j.epsl.2013.03.014.

Moore, M., Z. Kuang, and P. N. Blossey (2014), A moisture budget perspective of the amount effect, *Geophysical Research Letters*, *41*(4), 1329–1335, doi:10.1002/2013GL058302.

Niznik, M. J., B. R. Lintner, A. J. Matthews, and M. J. Widlansky (2015), The role of tropical-extratropical interaction and synoptic variability in maintaining the south pacific convergence zone in CMIP5 models, *Journal of Climate*, *28*(8), 3353–3374, doi:

10.1175/JCLI-D-14-00527.1.

Partin, JW and Quinn, TM and Shen, CC and Emile-Geay, J and Taylor, FW and Maupin, CR and Lin, K and Jackson, CS and Banner, JL and Sinclair, DJ and others (2005), Multidecadal rainfall variability in South Pacific Convergence Zone as revealed by stalagmite geochemistry, *Geology*, *41*(11), 1143–1146.

Permana, D. S., L. G. Thompson, and G. Setyadi (2016), Tropical West Pacific moisture dynamics and climate controls on rainfall isotopic ratios in southern Papua, Indonesia, *Journal of Geophysical Research: Atmospheres*, *121*(5), 2222–2245, doi: 10.1002/2015JD023893.

Risi, C., S. Bony, and F. Vimeux (2008), Influence of convective processes on the isotopic composition (δ18O and δD) of precipitation and water vapor in the tropics: 2. Physical interpretation of the amount effect, *Journal of Geophysical Research Atmospheres*, *113*(19), 1–12, doi:10.1029/2008JD009943.

Rozanski, K., L. Araguás-Araguás, and R. Gonfiantini (1993), Isotopic Patterns in Modern Global Precipitation, *Climate Change in Continental Isotopic Records*, *78*, 1–36, doi: 10.1029/GM078p0001.

Scholl, M. A., T. W. Giambelluca, S. B. Gingerich, M. A. Nullet, and L. L. Loope (2007), Cloud water in windward and leeward mountain forests: The stable isotope signature of orographic cloud water, *Water Resources Research*, *43*(12), 1–13, doi: 10.1029/2007WR006011.

Scholl, M. A., J. B. Shanley, J. P. Zegarra, and T. B. Coplen (2009), The stable isotope amount effect: New insights from NEXRAD echo tops, Luquillo Mountains, Puerto Rico, *Water Resources Research*, *45*(12), doi:10.1029/2008WR007515.

Stephens, M., and J. Rose (2005), Modern stable isotopic (δ18o, δ2h, δ13c) variation in terrestrial, riverine, estuarine and marine waters from north-central sarawak, malaysian borneo., *Earth Surface Processes and Landforms*, *30*(7), 901–912.

Stephens, M., S. Hodge, and J. Paquette (2013), Geoconservation of volivoli cave, fiji: a prehistoric heritage site of national significance., *Geoheritage.*, *5*(2), 123–136.

Stohl, Andreas. (1998), Computation, accuracy and applications of trajectoriesâĂŤa review and bibliography., *Atmospheric Environment.*, *32*(6), 947–966.

Takahashi, K., and D. S. Battisti (2007), Processes controlling the mean tropical Pacific precipitation pattern. Part II: The SPCZ and the Southeast Pacific dry zone, *Journal of Climate*, *20*(23), 5696–5706, doi:10.1175/2007JCLI1656.1.

Trenberth, K. E. (1976), Spatial and temporal variations of the Southern Oscillation, *Quarterly Journal of the Royal Meteorological Society*, *102*(433), 639–653.

Trenberth, K. E. (1997), The Definition of El Niño, *Bulletin of the American Meteorological Society*, (August).

van der Wiel, K., A. J. Matthews, M. M. Joshi, and D. P. Stevens (2015), Why the South Pacific Convergence Zone is diagonal, *Climate Dynamics*, *46*(5), 1683–1698, doi: 10.1007/s00382-015-2668-0.

Vincent, (1997), The South Pacific Convergence Zone (SPCZ): A review, *Monthly Weather Review*, *122*(9), 1949–1970.

Vincent, E. M., M. Lengaigne, C. E. Menkes, N. C. Jourdain, P. Marchesiello, and G. Madec (2009), Interannual variability of the South Pacific Convergence Zone and implications for tropical cyclone genesis, *Climate Dynamics*, *36*(9-10), 1881–1896, doi:10.1007/s00382-009-0716-3.

Vuille, M., Bradley, R. S., Werner, M., Healy, R., and Keimig, F. (2003), Modeling δ^{18}O in precipitation over the tropical Americas: 1. Interannual variability and climatic controls, *Journal of Geophysical Research: Atmospheres*, *108*(D6).

Vuille, M., Werner, M., Bradley, R. S., and Keimig, F. (2005), Stable isotopes in precipitation in the Asian monsoon region, *Journal of Geophysical Research: Atmospheres*, *110*(D23).

Widlansky, M. J., P. J. Webster, and C. D. Hoyos (2011), On the location and orientation of the South Pacific Convergence Zone, *Climate Dynamics*, *36*, 561–578, doi:

10.1007/s00382-010-0871-6.

Wilson, Cook, D'Arrigo, Riedwyl, Evans, Tudhope, and Allan (2010), Reconstructing ENSO: the influence of method, proxy data, climate forcing and teleconnections, *Journal of Quaternary Science*, *25*(1), 62–78.

Wolter, K., and M. S. Timlin (2011), El Niño/Southern Oscillation behaviour since 1871 as diagnosed in an extended multivariate ENSO index (MEI. ext), *International Journal of Climatology*, *31*(7), 1074–1087.

Yoshimura, K., T. Oki, N. Ohte, and S. Kanae (2003), A quantitative analysis of short-term 18O variability with a Rayleigh-type isotope circulation model, *Journal of Geophysical Research*, *108*(D20), 4647, doi:10.1029/2003JD003477.

Zinke, J., W.-C. Dullo, G. Heiss, and a. Eisenhauer (2004), ENSO and Indian Ocean subtropical dipole variability is recorded in a coral record off southwest Madagascar for the period 1659 to 1995, *Earth and Planetary Science Letters*, *228*(1-2), 177–194, doi: 10.1016/j.epsl.2004.09.028.

Chapter 5

Variability of the SPCZ recorded in South Pacific speleothem.

5.1 Introduction

Heat and moisture are redistributed around the global climate system by deep atmospheric convection over the Indo-Pacific Warm Pool (Refer to Section 1.1), which is highly variable and strongly coupled to the Pacific Walker Circulation (PWC), El Niño Southern Oscillation (ENSO), and the Interdecadal Pacific Oscillation (IPO) (Julian and Chervin, 1978; Wang and Mehta, 2008; Henley et al., 2015). Changes to IPWP convection impacts global climate by influencing the position of the Intertropical Convergence Zone (ITCZ). The drivers and mechanisms in this complex system have been the subject of much research (e.g. by meteorologists, climate modellers and palaeoclimate proxy specialists) in recent years (see references in section 1.1). However, climate models cannot yet reliably resolve the shape or behaviour of the SPCZ (Widlansky et al., 2011; Brown et al., 2013; Niznik et al., 2015; van der Wiel et al., 2015), and proxy records yet published are few, short, and both geographically

and temporally sparse, due to the lack of landmasses in the region, and only recent establishment of environmental monitoring.

5.1.1 Motivation for research

The motivation for this part of the research has three parts:

- Is it possible to construct a meaningful quantitative transfer function for speleothem oxygen isotopes (δ^{18}O) based on the amount effect?
- Could a speleothem transect of the South Pacific islands provide robust proxy records for past variability of the SPCZ?
- Is it possible to construct a reliable centre-of-action ENSO proxy from Pacific Island speleothem data, or an improvement on current understanding?

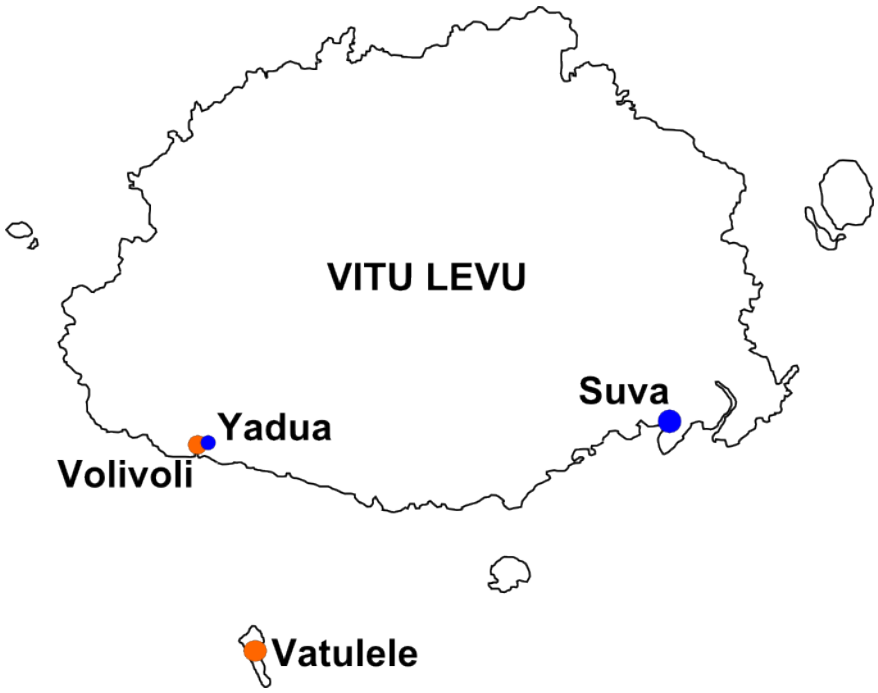

Figure 5.1: Locations of rain (blue) and speleothem (orange) sampling sites in Fiji. See Chapter 4 for details of water sampling. Volivoli cave and Yadua village are within 3 km, so the water sampling location marker is small so as not to obscure the speleothem sampling marker.

5.2 Locations and geological settings

Locations in the South Pacific were chosen for this research: Fiji and the Cook Islands (Figure 5.4a). The SPCZ is the main driver of weather conditions for both areas (a full discussion can be found within Chapter 4), with Fiji towards the north west, proximal to where the SPCZ splits from the ITCZ, and the Cook Islands lie towards the distal end.

In Fiji, field sites are located on Vitu Levu and Vatulele Islands (Figure 5.1), and in the southern group of the Cook Islands, on Atiu, 5.4b. For a full discussion on the climatological context, refer to Chapter 4

5.2.1 "Big Cave", Vatulele Island, Fiji

"Big Cave", on Vatulele island (Figure 5.2) was visited 2nd March 2013 by Prof. Dave Mattey and team, on a day of heavy rainfall. Outside the cave, CO_2 was measured at 250 ppm. At the entrance, a doline with additional

breakdown, cave air ventilates outward at 26.1°C, with CO_2 concentration measured at 1300 ppm, and relative humidity at 96% (data supplied from D. Mattey's field notes).

Within the cave, 14 m from the entrance, pCO_2 was measured at 11,280 ppm, relative humidity between 87.9 - 100%, and temperature at 26.0°C. At the lowest accessible point in the cave, fissured boulders and breakdown are visible (Figure 5.2), with deep undecorated fissures from which > 10,000 ppm of CO_2 was measured upwelling. Further from the entrance, but closer to the surface, airflow is along the ceiling with pCO_2 much lower, between 670 - 750 ppm, suggesting the existence of a small secondary entrance allowing chimney type ventilation. At this point, the ceiling of the cave is highly decorated with stalactites covering a broad area, indicating diffuse flow of water through the karst in this area (Baker and Fairchild, 2012) and dry rim-stones cover part of the cave floor (See Figure 1.1 for examples). A loose stalagmite was taken from here and labelled Vat13a.

Three speleothem samples were obtained, one of which, Vat13a, was analysed and the results are presented in this chapter.

5.2.2 Volivoli cave, Vitu Levu, Fiji

Field report of the cave and local environment

Volivoli cave is located on the south west coast of Vitu Levu, in Miocene elevated reef carbonates (Watling and Pernetta, 1978), overlooking the Sigatoka valley, near Yadua village (Figure 5.1). Native woodland and some cleared grassland overlie the cave, and a dry or ephemeral valley immediately overlies the main entrance. Some substantial tree roots penetrate through the entrance, and continue deep into the cave. For much of the year, Volivoli cave is primarily dry, although after heavy rains, water enters the upper cave entrance and flows through, exiting at the lower entrance, acting as an ephemeral

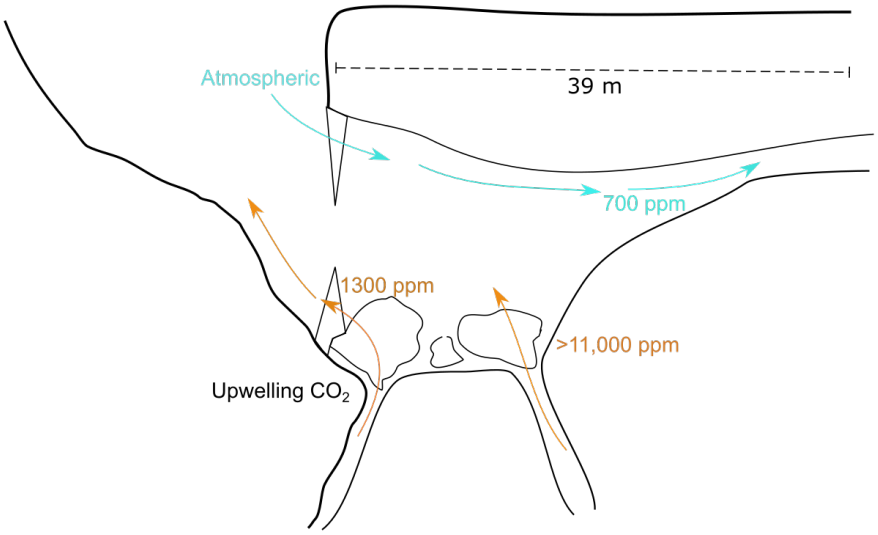

(a) Big Cave profile view with ventilation patterns. Carbon dioxide upwells from fissures at the deepest part of the cave, and ventilates out through the base of the entrance. Fresh atmospheric air enters the cave at ceiling level and flows through and along passage.

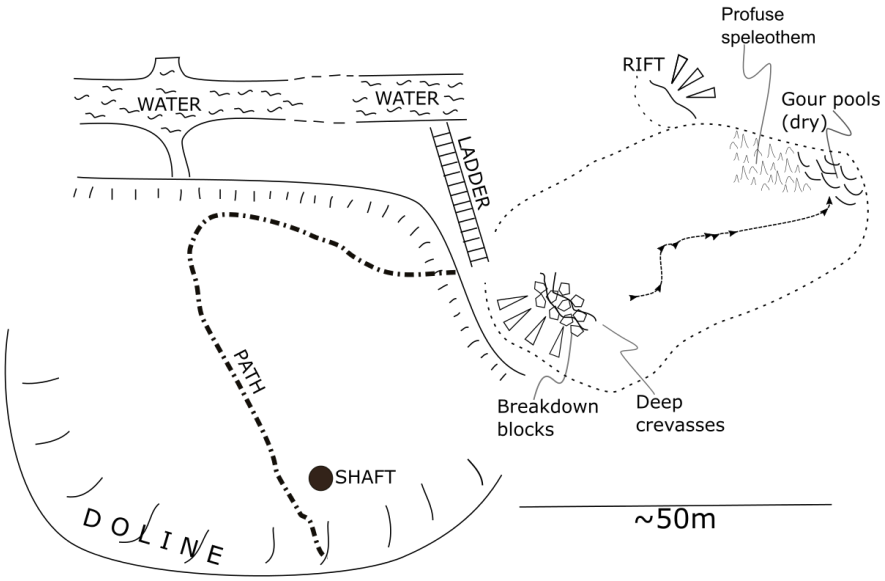

(b) Big Cave plan view, deep crevasses and breakdown blocks where carbon dioxide upwells, measured at 11280 ppm and then offscale.

Figure 5.2: Vatulele Big Cave profile and sketch plan (modified from field notes provided by D. Mattey).

stream flow. Water drainage patterns and ventilation dynamics suggest the existence of small egress at the end of the fissure leading from the deepest part of the cave towards the sea facing cliff, which overlooks Sigatoka Dunes National Park to the SE.

Monitoring (For details of equipment and methods, please refer to Chapter 2, section 2.2.1) has been under way in Volivoli cave since 2010 when three Tiny-tags were deployed to collect temperature and humidity data, along with two "Stalagmate" drip loggers (Collister and Mattey, 2008). These devices are carefully located underneath the drip site of interest and were retrieved in September 2014 for data download and maintenance, then replaced. The logger placed on the VV10 drip site was completely covered by a shell of calcite approximately 2 mm thick, although the data indicate that this did not impair the drip logging ability of the logger. Tiny-tag 1 was located under the overhang of a boulder outside the cave entrance, Tiny-tag 2 was located in the speleothem chamber, above the VV10a drilling site, and Tiny-tag 3 was deployed in the end chamber, before the final crawl (See Figure 5.3 for cave map and logger positions). "Stalagmate" drip loggers were retrieved from on top of the coring site, measuring the VV10 drip, and in the end chamber near Tiny-tag 3 logging the upper of two active drips in this chamber.

Carbon dioxide partial pressure was measured, using a GM70 Vaisala CO_2 probe, at fixed locations along a transect from outside the cave, to the end of the last crawl (as shown in Figure 5.3b). On this visit (September 2014) background air was measured at 250 ppm, and cave air peaked at 1960 ppm at the limit of the crawl, where a strong inward air flow was indicated by a smoke pen. CO_2 concentration peaked at 2820 ppm in VV10a stalagmite chamber (see Figure 5.3) where smoke indicated some airflow into a small fissure in the ceiling.

Volivoli has red clay deposits of variable depth, on the floor and lower walls of the cave, with pebble deposits as evidence of ephemeral stream flow. Red clay

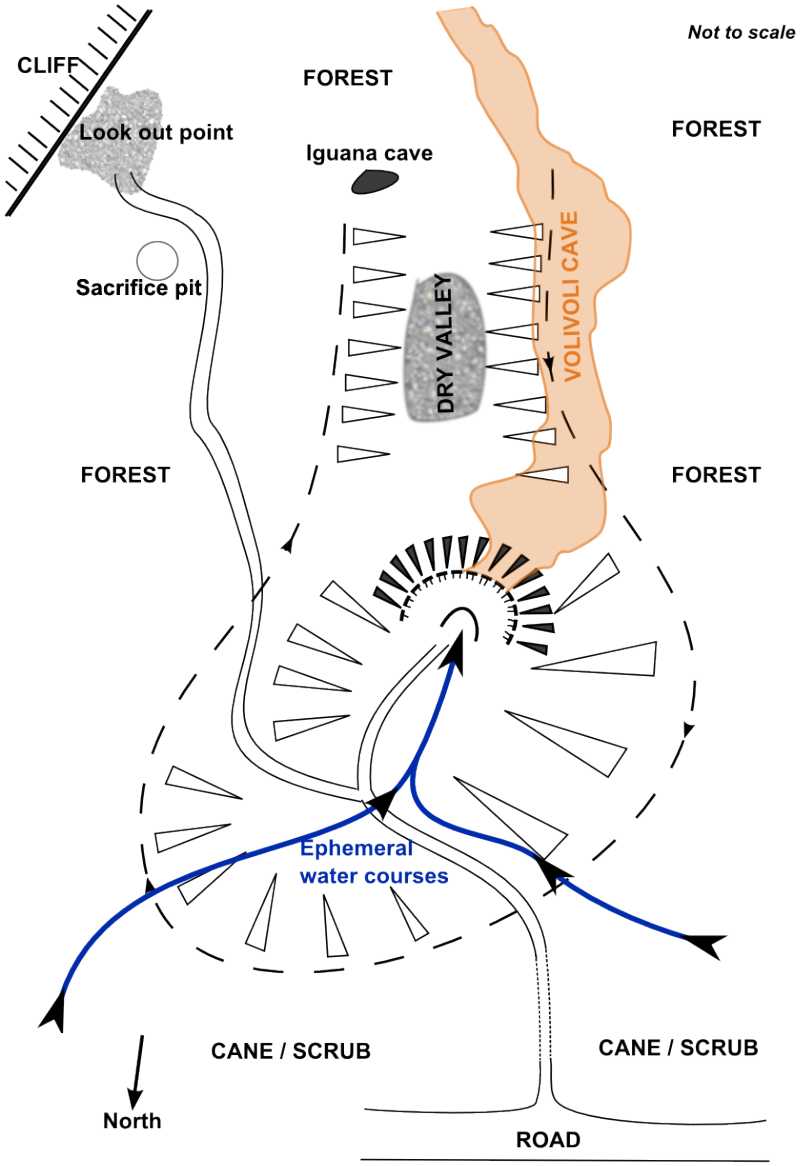

(a) Volivoli cave location plan, not to scale. Ventilation indicates a resurgence zone where the cave intersects with the cliff to the southeast.

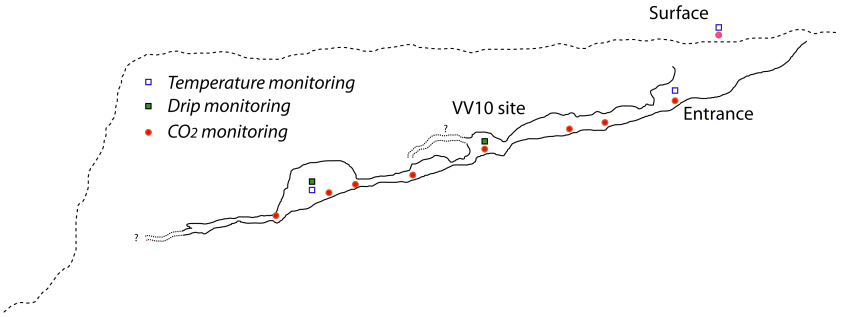

(b) Volivoli cave profile with positions of ongoing environmental loggers, and locations of carbon dioxide spot measurements.

Figure 5.3: Volivoli cave (not to scale), diagrams adapted from field notes provided by D. Mattey

deposits also contain whole shells and coral fragments.

Rain monitoring site: Yadua village

Rain monitoring equipment, a Pluvimate piezometric rain drop logger, was deployed in Yadua village, located 3 km SW of Volivoli cave, in 2010, and is in ongoing operation. It is in an open area between the bungalow frontage and the road, where trees or built infrastructure do not obstruct rainfall. During fieldwork, data recorded since the previous visit by the group were downloaded and the equipment inspected and maintained. Since this is proximal to the cave site, it is a vital resource for comparing drip rates within the cave and local surface rainfall, which can be markedly heterogenous across the island. Drip rate response to incoming recharge provides critical information on the transmission of groundwater through the unsaturated zone and into the cave.

Volivoli cave on Vitu Levu, and Big Cave on Vatulele, have some clear similarities: with ventilation from the trade winds, active deposition, proximity to the ocean, and overlying vegetation. Therefore some aspects of the ongoing environmental monitoring at Volivoli cave can be reasonably extrapolated to Big Cave. Additionally, the caves on Atiu, bear some similarities to Vatulele, in terms of terrain, host rock and ventilation, indicating that speleothem from these may be useful to compare.

5.2.3 Atiu, Cook Islands

Atiu is located (20.0°S, 158.1°W), in the Southern Group of the Cook Islands Archipelago (Figure 5.4a). Unlike most volcanic pacific islands, Atiu is moving upward due to crustal flexure following the formation of the nearby island of Rarotonga. Atiu was originally a seamount, and, as it has moved above sea level, the ocean island basalt has weathered to produce a relatively flat island, with fringing coral reefs. As the island continues to move upward, the fringing

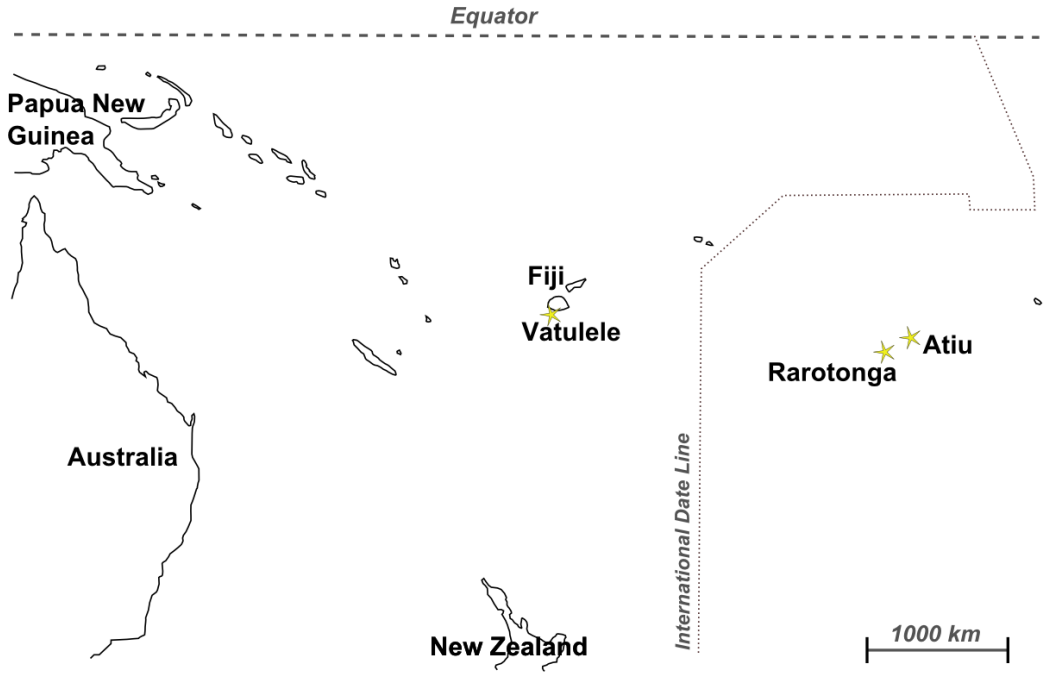

(a) Atiu Island is located in the Southern Group of the Cook Islands, and is one of the "Makatea Islands" as described by Woodroffe et al. (1991). The island is too small to be visible at this scale, but is located at the centre of the labelled star.

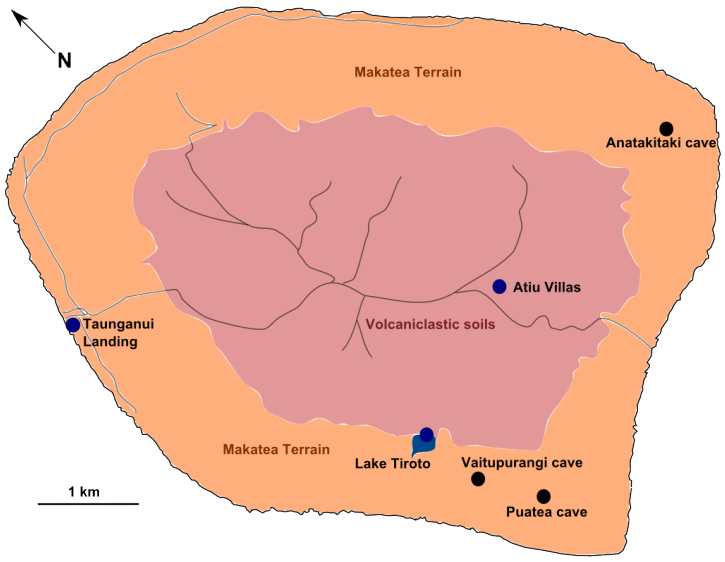

(b) Atiu island is composed of a flattened volcanic core covered by red soil (purple) and surrounding uplifted limestone (with occasional dolomitisation) reef deposits (orange). Cave field sites were established (black) and water samples taken (blue).

Figure 5.4: The location of Atiu, in the Pacific Ocean, and sampling sites and soil types on Atiu.

coral reefs are raised above sea level, and grow outward, resulting in successive layers of Pleistocene reef limestone (Woodroffe et al., 1991), deepening away from the centre of the island. There is no lagoon here, the coral reefs cling to the shore, and the beaches are entirely composed of coral fragments and shells. The beachs are bounded by low cliffs of freshly uplifted reef skeletons, with individual species clearly recognisable. Moving inland, the reef limestone has been weathered, leaving the cement behind, producing a makatea type terrain which is sharp, hazardous and frequently impassable. Dolines are common and the soil is thin or non existent in the makatea terrain. At the surface, fossil corals are visible, as well as speleothems that have been uplifted and the overlying limestone dissolved, leaving the orginal cave floor at the surface (Figure 5.5)

All caves are accessed via roof breakdown or fissures, often requiring a roped scramble, and are generally extensive and, at the time of our visit, showing little evidence of water but high humidity. All caves also show evidence of mixing corrosion (Figure 5.6c) which appears as smooth scallops, cups or scoops in the limestone that are a result of dissolution at the point that the freshwater lens overlies marine ground water, and is a common feature in flank margin caves (Mylroie, 2005). The position of this interface can change due to sea level change, storm surges, and shrinking or growing of the freshwater lens. The mixing corrosion appears distinct from the non-corroded makatea limestone, as the former is very smoothed and white, and the latter is spiky and rough. All Atiu caves also have significant deposits of red silt that we understand to be derived from the volcanic sediment from the centre of the island. Makatea is, by nature, extremely porous, so we expect reservoir storage to be limited, and flash floods to be common. We observed this during our fieldwork: the caves were nearly entirely dry during our first explorations, with drips visible but not dripping within our observation time.

A large thunderstorm, over the course of 12 hours, delivered 64.1 mm of rain as we measured, roads became impassable with red mud, and sediment was

observed to be washing along the roads and into the limestone makatea terrains. The subsequent day, drips that were previously not dripping frequently enough for us to observe began to drip at a higher rate (>1 drip per second).

Anatakitaki Cave

Entrances to Anatakitaki cave were located in a doline, leading to dry, non active but well decorated entrance chambers on all sides. Sunlight and rain has caused growth of algae on speleothem surfaces, and there are extensive tree roots from the forest floor. Echo-locating birds, kopeka, nest within the cave, using speleothems as perches and leaving their droppings near entrance areas. The cave shows evidence of flood events depositing a layer of volcanogenic red clay throughout. However, this most recent flood event was prior to 1932 according to the graffiti observed, and the layer of calcite crystals covering all flood deposits. Additionally, we see detritus-free young stalagmites growing on top of the flood surfaces, fed by pure white soda straw stalactites. There are also a number of floating flowstones observed, with the bed rock below them washed away, as well as the typical scalloped mixture corrosion surfaces (Figure 5.6d).

Vaitupurangi Cave

Vaitupurangi cave (Figure 5.7) also host kopeka birds, but in this instance also features a small but deep fissure lake that has been previously explored by cave divers, who filmed drowned stalagmites, and reported a depth greater than 40 m. Water samples were obtained from these lakes, which appeared to be fresh at the surface, but we hypothesise may be saline at depth, due to observed mixing corrosion of the host rock limestone in other locations. Additionally, we know that the only surface lake, Lake Tiroto, is a brackish lake, where rainwater runoff mixes with seawater influxing through a flooded cave system. Similar to Anatakitaki cave, Vaitupurangi also features silt coated

(a) Makatea Terrain and cave entrance

(b) Speleothems exposed on surface of forest floor

Figure 5.5: Atiu: uplifted reef limestone surface with vegetation and thin soil. Photographs by Dr A Borsato

(a) Speleothems in Anatakitaki cave. Active growth seen as new white calcite without flood deposited silt layer.

(b) Typical speleothem stump observed here: large, well formed, visibly layered and somewhat sparry. Intermittent detrital component within.

(c) Mixing corrosion: scalloped dissolution caused by mixing seawater and fresh water in the cave systems.

(d) "Floating" flowstones where the substrate has been removed by weathering, dissolution or flooding

Figure 5.6: Anantakitaki Cave, photographs provided by Dr A Borsato

(a) Vaitupurangi entrance and lakes

(b) Vaitupurangi "root-ite": a root penetrates the cave chamber and becomes a feeder stalactite for the boss stalagmite below

(c) Cross bedding observed next to mixing corrosion, indicating dissolution of bedrock with sea water and meteoric water, followed by uplift and fluvial activity depositing cross-bedded sandstone within the cave.

(d) Vaitupurangi cave has similar characteristics to Anatakitaki, with the silt staining, white active growth and mixing corrosion, but this cave has more stalagmites of the "boss variety" and appears to have more active flooding.

Figure 5.7: Vaitupurangi Cave, photographs by Dr A Borsato

limestone with new recent growth evident in the white, parasitic stalagmites, white calcite on active flowstones and boss stalagmites, and the silt fixed by a thin layer of tiny calcite crystals (Figure 5.7). The cave is relatively shallow, shown by tree roots penetrating the ceiling of the main chamber, the longest of which is covered in calcite and is acting as the feeder stalactite for the stalagmite beneath (Figure 5.7b).

Puatea Cave

Puatea cave (Figure 5.8) is similar to the Vaitupurangi, and it is suspected that the caves may link somewhere, although the 2014 expedition did not find a linking passage. The cave has been visited intermittently but this is no longer current practice.

The majority of large stalagmites had previously been hewn off or broken by the local residents to facilitate ease of passage. This meant that many of active stalagmites were still in infant stages, providing only short records. Much of the cave was dry, with active speleothems identifiable through their distinctive colour compared to the silt covered, older speleothems. Drip rates here were very slow until after the reported rain storm event, and were from soda straw stalactites only. Graffiti indicates much travel by locals to deepest part of this cave, most from the 1930s to 1970s. This graffiti has been fixed by a layer of tiny calcite crystals indicating active growth even where stalagmites are not growing.

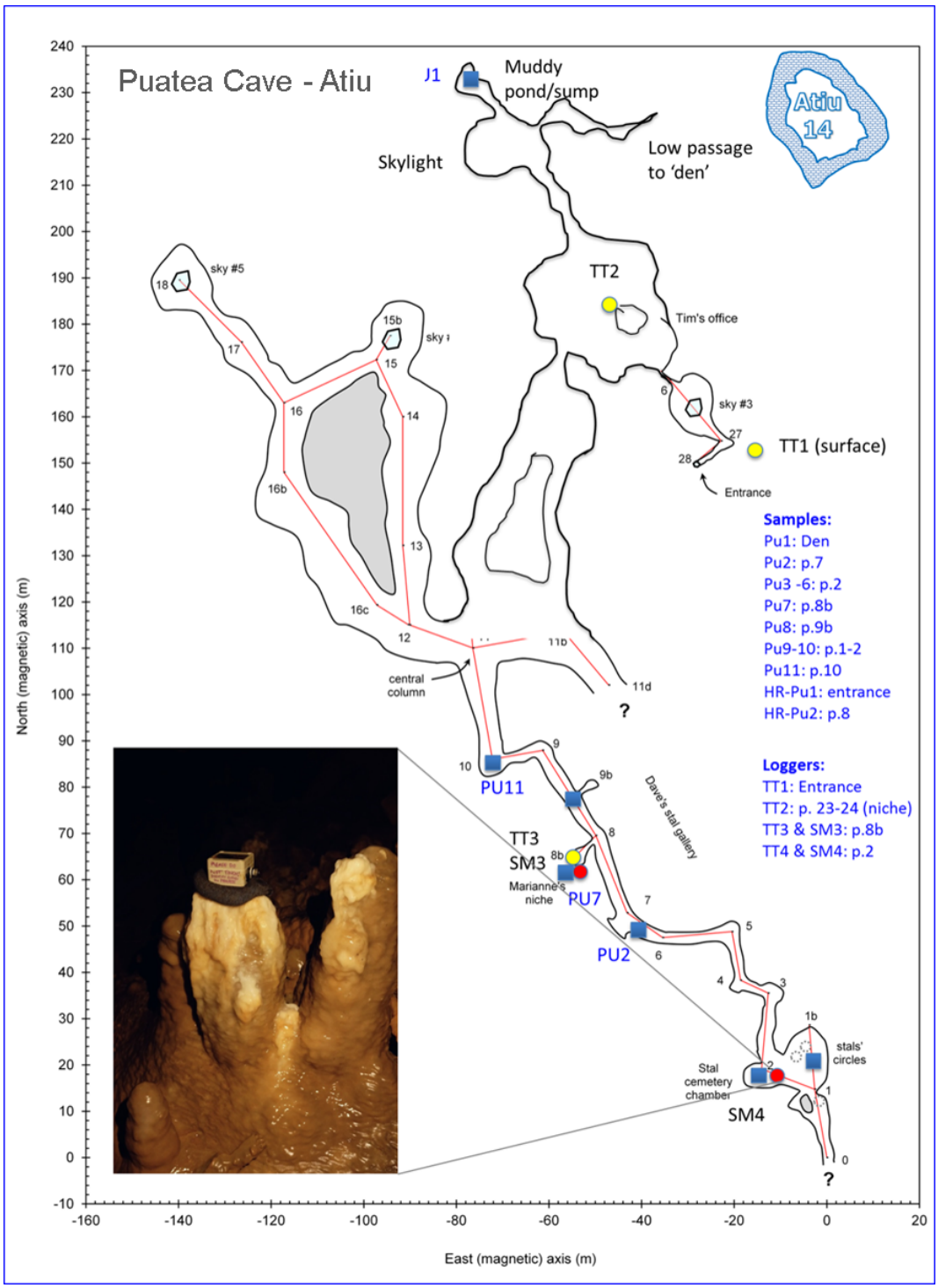

Figure 5.8: Puatea cave map with (blue squares) stalagmite sampling locations, (yellow) TinyTag locations, (red) "Stalagmate" logger locations and (inset) logger positioned on sampled stalagmite.

5.3 Pacific Island data analysis

5.3.1 Aquifer properties of uplifted lagoonal and reef limestone.

The aquifer properties of the host rock have a strong influence on the extent to which the precipitation signal is transmitted to the cave and hence the speleothem deposit. (Atkinson, 1977; Hess, 1999; McDonald and Drysdale, 2007; Hartland et al., 2012; Baker and Brunsdon, 2003; Rutlidge et al., 2014) Infiltration of water into the karst is impeded and facilitated by plants and soil cover, as well as the weather conditions. To investigate the extent to which the precipitation signal is transmitted to the cave, detailed rain and cave monitoring data from Vitu Levu and Volivoli cave are analysed as follows.

Potential evapotranspiration from the soil zone

Evapotranspiration inhibits infiltration of precipitation into the soil zone and karst aquifer, but quantifying this effect can be challenging without extensive fieldwork. In this case, the Thornthwaite equation (Thornthwaite, 1948) is used (following Mattey et al., 2008) to estimate monthly potential evapotranspiration (PET) and compare it to precipitation amount recorded at both Nacocolevu and Suva (Figure 5.9). Calculated evapotranspiration subtracted from recorded precipitation gives an estimate of effective, or infiltrating rainfall; this is the water expected to reach the karst system and influence the $\delta^{18}O$ of the drip water and hence the stalagmite. For much of the year, PET exceeds actual precipitation, resulting in a moisture deficit. During these months, especially in dry season (austral winter), little new water is expected to enter the aquifer.

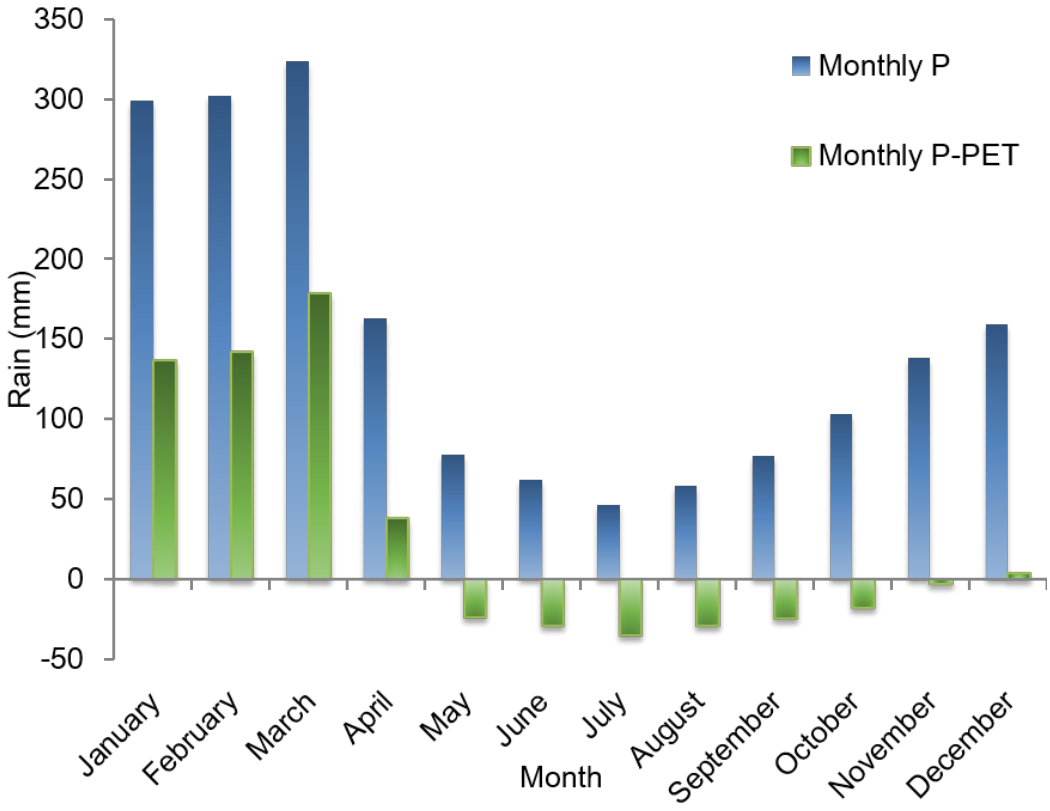

Figure 5.9: Average monthly precipitation (mm) 2008 - 2014 (blue) and "effective precipitation" (mm) (green): Precipitation - potential evapotranspiration calculated using the Thornthwaite equation. When PET is taken into account, it is clear that groundwater recharge will only occur during 3 - 4 months of the year: January to April, in austral summer.

Drip logging at Volivoli Cave

Drip loggers deployed at the stalagmite sampling site in Volivoli cave, reveal that the drip is intermittent and inactive for much of the year. Drip frequency abates throughout April, May, and June 2013, becoming inactive at the beginning of July 2013. The drip remains inactive until December 2014, when low level activity resumes after a >100 mm rain event. Drip reactivation continues in January and it remains active until well into August 2014, albeit at a low level (< 100 drips per day). The drip becomes highly active after a medium volume (>50 mm per day) rain event, if this event coincides with a drop in air temperature outside the cave, or enough smaller rain events have occurred before the medium/large event, that the PET requirement has been met, allowing water to infiltrate. The lag between rain event and peak drip rate is typically two to three days. Since rain events >50mm occur only during austral summer, December – April, this is also the time period that the drip is active. The highest drip rate recorded in 2013 – 2014 was 42631 drips per day, which, assuming that 1 drip = 0.2ml (Collister and Mattey, 2008), is a peak of 8.526L in one day. This large volume was measured on 20th March 2013 after 3 small rain events (>10 mm, < 50mm) occurred on consecutive days at the end of the wet season. In wet season (austral summer 2013 – 2014), 7 distinct drip maxima occurred, all preceded by medium or large rain events. (Figure 5.10)

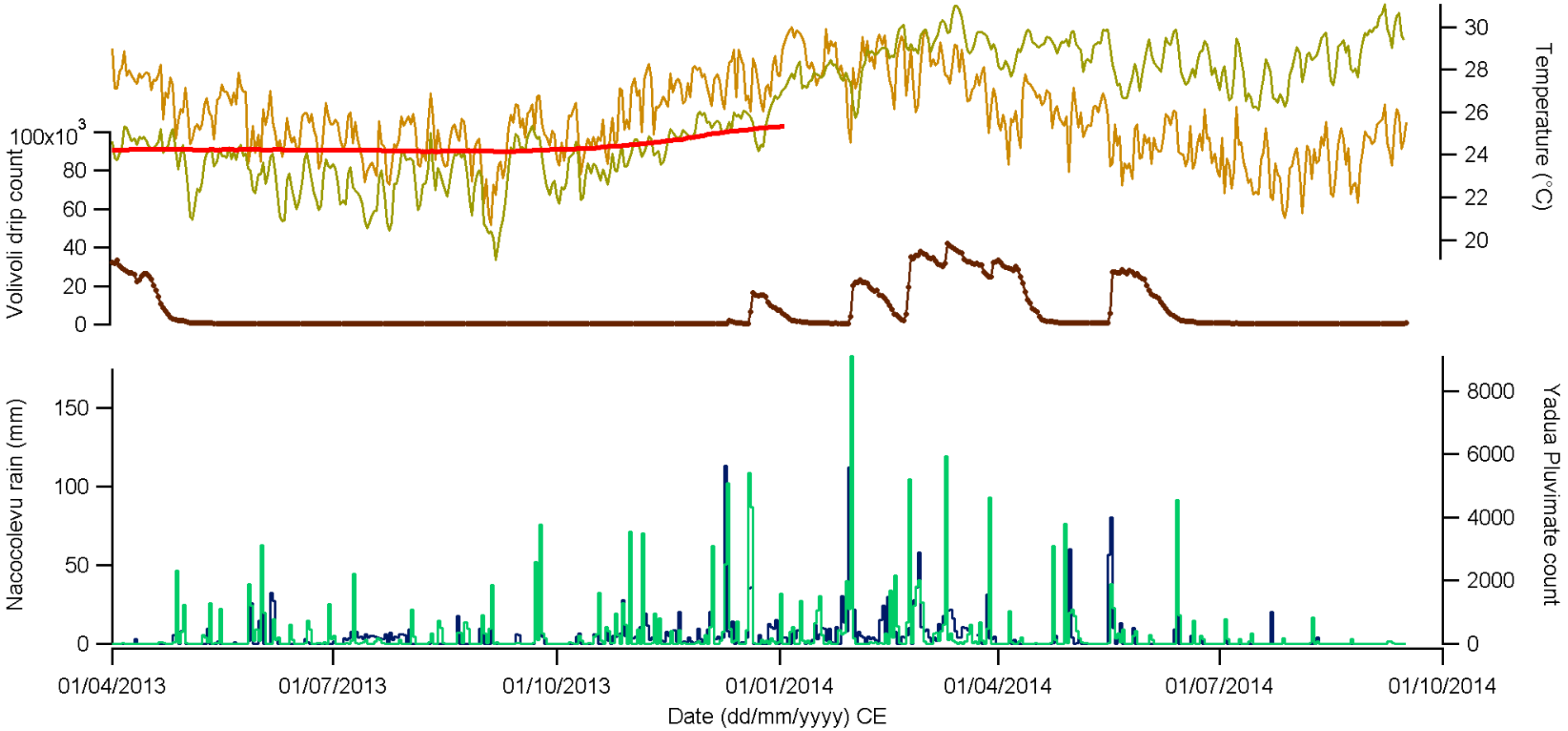

Figure 5.10: Relationship between rainfall intervals, drip discharge and cave, and surface temperatures over the three year monitoring period. Rainfall is a composite of Nacocolevu Research Station (see Chapter 4 for details) rain monitoring (left axis), and the Yadua Pluvimate raindrop counter. Surface temperature (orange) was measured in Yadua village, and outside the Volivoli cave entrance (green). Cave temperature (red) remains very consistent throughout the monitoring period.

Drip water isotopes at Volivoli Cave

$\delta^{18}O$ of drip waters from all three sampled drip sites within Volivoli cave showed little variation throughout the sampling period, ranging from -7.27‰ to -6.59—‰ (mean = -6.97, < 0.5, n = 57). Drips from the lower chamber are less depleted (average -6.75‰) than those from the speleothem chamber (average -7.07‰).

When compared with the large range in $\delta^{18}O_{precip}$ this indicates that transmission of water from surface to cave is an important filter for the precipitation $\delta^{18}O$ signal, with the drip water either being averaged within the karst by a reservoir effect, or only sampling some rain events, which have a more consistent $\delta^{18}O$ signature. A combination of both factors is likely. The difference in isotopes between the different chambers is unverified, but could be a feature of the extent of degassing, since the drips in the lower chamber fall from a greater height than the drip in the speleothem chamber. In a well-ventilated cave such as Volivoli, where pCO_2 remains very low, this fractionation effect is expected to remain consistent for each drip (Baldini et al. 2008).

When considering potential evapotranspiration, drip behaviour and drip isotopes in combination, it appears that austral summer (wet season) rainfall will infiltrate to a much greater extent than dry season rainfall, that the drips are sensitive to rainfall events over a threshold volume, and that mixing is an important feature in this cave.

This understanding has implications for reconstruction of local environmental change, since rainfall isotopes exert control on groundwater isotopes and rainfall amount also controls attenuation of the isotope signal through storage and mixing. Speleothem forming from this groundwater are therefore enabled to record long term variability of the regional convective system through $\delta^{18}O$ of calcite.

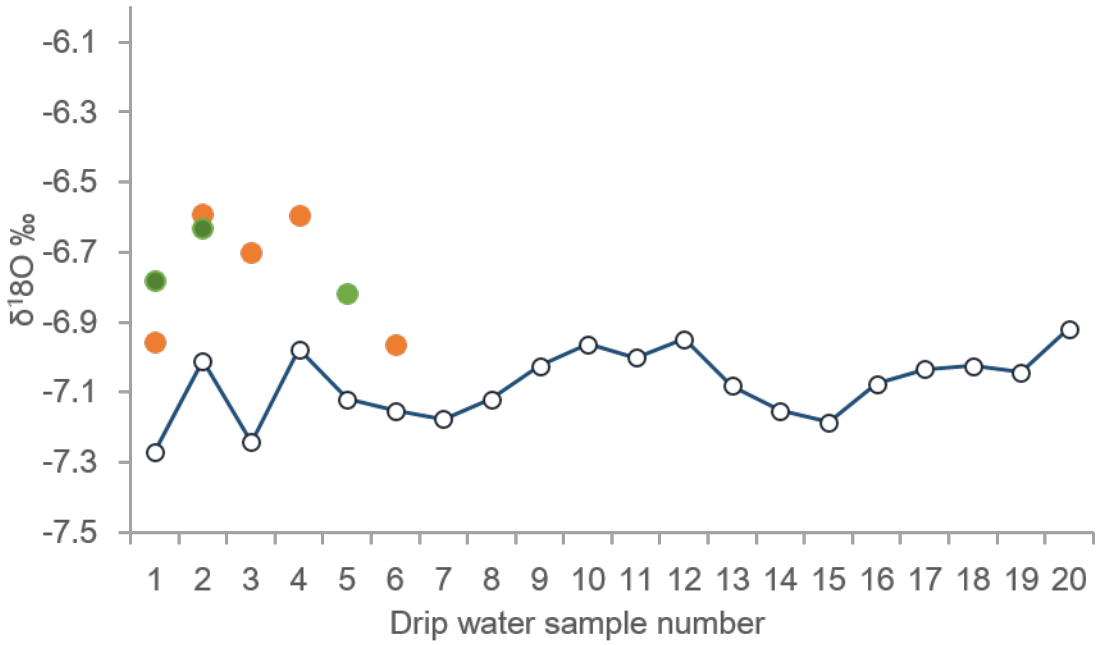

Figure 5.11: Water isotopes from two drip sites in the lower chamber of Volivoli cave (orange and green), and the speleothem chamber (blue with lines) over the 2010 - 2013.

Field observations of drip water behaviours in the Cook Islands makatea caves

The Atiu caves are located within highly porous makatea (Figure 5.4b), with thin, or no soil present, and continuous canopy cover overhead. Trees and other plants root directly into the rock, with hanging epiphytes and aerial roots providing a conduit for rain water to pour from the canopy into the porous rock. Rain water is not impeded by a soil layer but infiltrates directly, washing in what little soil there is with it, as well as plant debris. This is visible as the layer of red sediment plastering the caves across the island. Similar phenomenon are reported for other caves in the archipelago (Woodroffe et al., 1991).

Puatea cave is only approximately 6 - 10 m below the surface and the overburden very porous, as was documented during entrance and exit of the cave, thus there is very limited opportunity for groundwater storage or mixing above the cave. Drips were observed clinging to the tips of soda straws within the deeper recesses of the cave, but were not recorded actually falling, until after the

Location	Provenance	Volume	pH	Total alkalinity	Conductivity
Atiu Villas	Tap	100 ml	6.24		195 µS/cm
Anataketake	Cave lake	50 ml	7.41	144 mg/L	1281 µS/cm
Anataketake	Drip	16.5 ml	7.64	67 mg/L	
Vaitupurangi	Cave lake	100 ml	7.21	166 mg/L	1088 µS/cm
Lake Te Roto	Brackish Lake	100 ml	8.05	210 mg/L	17.43 mS/cm
Puatea	Cave pool	50 ml	7.29	112 mg/L	396 µS/cm
Pacific Ocean	Harbour	100 ml	8.00	125 µg/L	54.5 mS/cm
Puatea	Drip*	25 ml	6.61	88 mg/L	589 µS/cm

Table 5.1: Atiu field chemistry results. *each Puatea drip sample consists of water collected from the tips of several soda straw stalactites.

aforementioned storm event, whereupon the drip rate became evidently faster. Since the roof is very thin and the soil is sparse, CO_2 contribution from plant roots and microorgamisms within the karst itself must be important for establishment of the bicarbonate buffer system (Mattey et al., 2016). Throughout the caves, pCO_2 remains between 530 and 620 ppm. In Puatea cave, the cave with the most visible speleothem growth activity, the inner chamber, accessible by crawl, had elevated CO_2 up to 800 ppm, but generally it remained within the range stated above. Frequent fissures, roof breakdown and trade winds induce strong draughts within the cave, confirmed by smoke movement.

5.3.2 U-Th dating and age models

Vatulele speleothem dates and provisional age model

Six U-Th dates were determined for Vat13a (As described in section 2.7), in 2 batches. (Figure 5.12a). The first batch comprised two samples, Vat13a-top, 5 mm from the stalagmite tip, and Vat13a-base, 50 mm from the base of the stalagmite where a “clean” lamina was thick enough to sample sufficient quantity. Sample ”Vat13a-top” was reported by the lab to be lost in preparation, and sample ”Vat13a-base” was returned on 20/5/2014 at 4.62 ±0.16 ka BP

Subsequently, 5 additional samples were prepared. These were prepared using the “powder method” (see Chapter 2.7) and labelled in stratigraphic order:

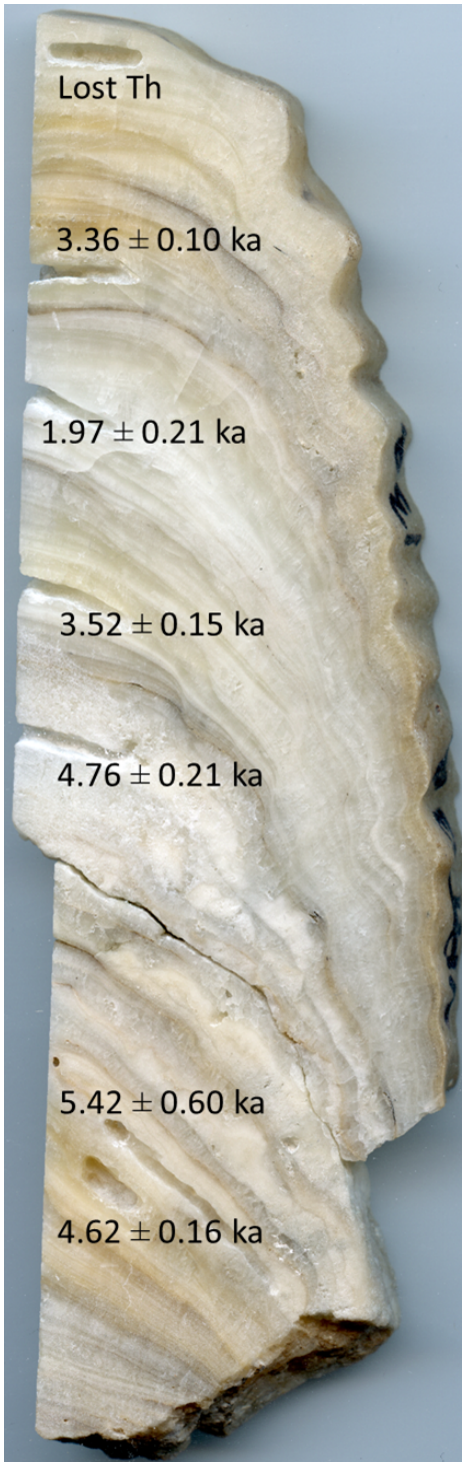

(a) Vat13a original thick sections and dating pits. Details of each in table 5.2.

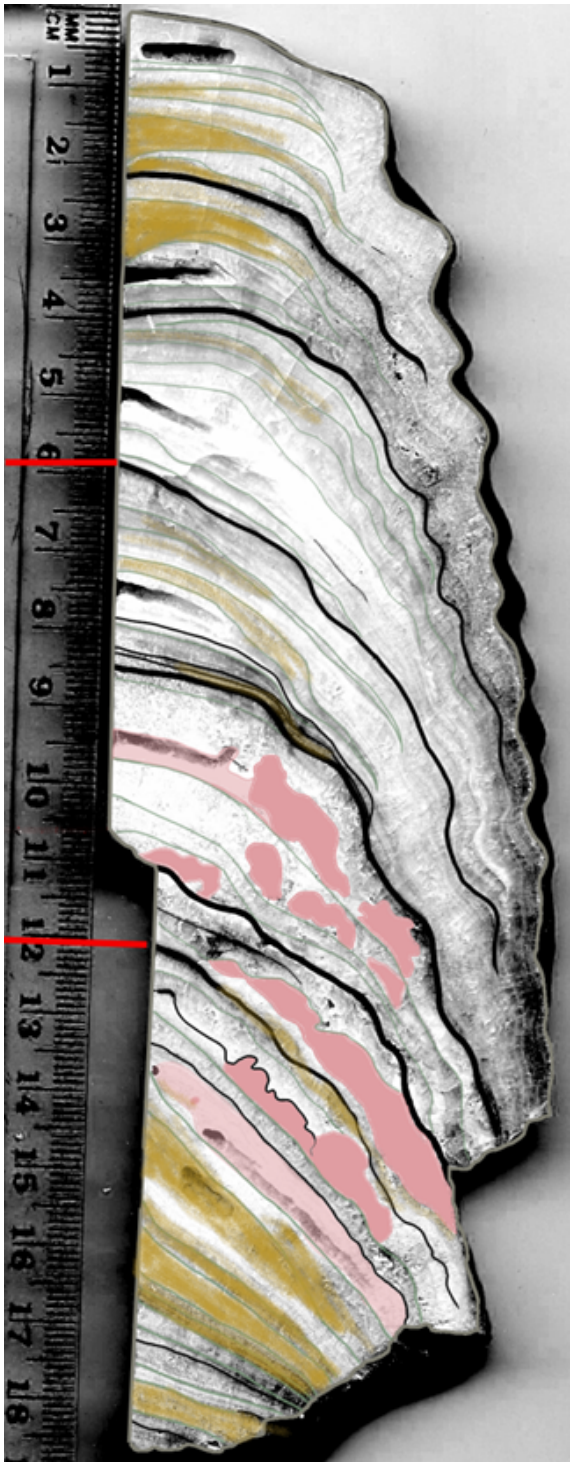

(b) Vat13a speleothem fabrics. Pink = dendritic, orange = organic-rich, black = stratigraphic discontinuities with detrital component, pale green = stratigraphic discontinuities without detrital component.

Figure 5.12: Vat13a slab with U-Th dating pits and reported ages, and the same slab with scales and summary of speleothem fabrics observed in microstratigraphic logging

Vat13a-1 to Vat13a-5. Sample names and weights are detailed in Table 5.2 and U-Th ages are not in stratigraphic order, with VAT13a-5 being measured as 800 years older than Vat13a-base despite being stratigraphically younger.

Two age models have been created (Figure 5.13), the first using a simple linear regression between all U-Th dates, and the second excluding dates sampled from within dendritic calcite (plotted in red in Figure (5.13b)). Dendritic calcite (see section 2.8.1) remains as an open system for a longer time than columnar calcite allowing the potential for uranium ions to move in or out of the system, which may introduce an error into the U-Th dates. These are preliminary age models, and further research is underway to produce a more robust age model using additional U-Th analyses and a modelling algorithm such as StalAge (Scholz and Hoffmann, 2011) or COPRA (Breitenbach et al., 2012).

Puatea speleothem dates and provisional age models

Recent and fossil corals from Atiu that remain more than 98% aragonitic have been reported to have uranium contents of 2.24 - 3.64 ppm, with coralline algae at 0.49 ppm (Woodroffe et al., 1991). However the authors noted that "many" of the coral samples collected were recrystallised to calcite and therefore they rejected those samples from their study. Gvirtzman et al. (1973) find that corals contain around 2 ppm of U regardless of species, but that the abiogenic cement can vary from aragonitic cement, at 3.6 ppm to high Mg calcite at 2.6 ppm, and that freshwater leaching and diagenesis to secondary calcite result in U content on 1.3 ppm.

This indicates that the bulk uranium content of the reefal limestone in Atiu will fall below the values measured in aragonitic samples by Woodroffe et al. (1991), and may be closer to the 1.3 ppm reported by Gvirtzman et al. (1973).

Shen et al. (2008) suggest that site specific detrital thorium corrections should be made for island reef limestones where thorium input is primarily from sea-

Lab	Label	Sample weight	U (ppm)	Th (ppm)	Activity Ratio	Date (ka)	Date (ka BP*)	±2σ(abs)	Distance (mm)
NIGL Pilot	Vat13a top						Lost	Lost	5.1
NIGL B2	VAT13a 15-1	222.17	0.03	0.000	22.0	3.42	3.36	0.10	33.4
NIGL B2	VAT13a 15-2	212.85	0.02	0.000	6.6	2.03	1.97	0.21	49.1
NIGL B2	VAT13a 15-3	206.6 1	0.02	0.000	14.6	3.58	3.55	0.15	74.2
NIGL B2	VAT13a 15-4	214.11	0.02	0.000	14.4	4.83	4.76	0.21	93.2
NIGL B2	VAT13a 15-5	214.21	0.02	0.000	6.1	5.49	5.43	0.60	143.8
NIGL Pilot	Vat13a base						4.62	0.16	150.7
NIGL B2	PU2-1	345.42	0.04	0.001	4.8	3.17	3.10	0.46	156.2
NIGL B2	PU2-2	206.34	0.06	0.002	1.8	1.09	1.03	0.67	131.0
NIGL B2	PU2-3	204.49	0.06	0.008	0.8	-0.26	-0.32	2.80	93.5
NIGL B2	PU2-4	210.28	0.07	0.001	4.5	1.61	1.54	0.26	58.9
NIGL B2	PU2-5	203.30	0.05	0.001	2.0	1.00	0.94	0.49	14.4
NIGL B1	RH C3A	190.20	0.03	0.000	21.2	1.91	1.84	0.06	7.3
UoM	Pu2 P1						0.69	0.15	7.3
UoM	Pu2 P2						4.31	0.35	152.2
NIGL B1	PU7-1	249.70	0.03	0.000	26.1	8.15	8.45	0.21	1.0
NIGL B1	PU7-2	332.90	0.10	0.000	32.1	1.932	1.87	0.04	41.5
NIGL B1	PU7-3	412.80	0.04	0.001	16.7	13.24	13.17	0.47	43.5
NIGL B1	PU7-4	239.6	0.09	0.000	229.8	12.01	11.94	0.06	175.6
NIGL B1	PU7-5	303.70	0.09	0.000	103.9	14.49	14.42	0.10	219.8

Table 5.2: U-Th dating results for Vat13a, PU2 and PU7 stalagmites, blank cells indicate unavailable data. *BP = 1950

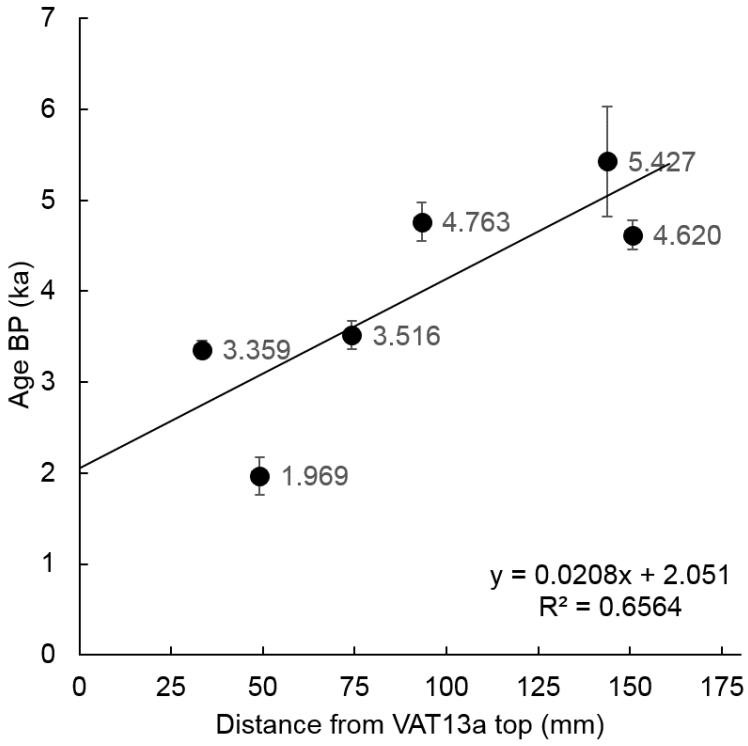

(a) Vat13a provisional age model including all reported U-Th dates.

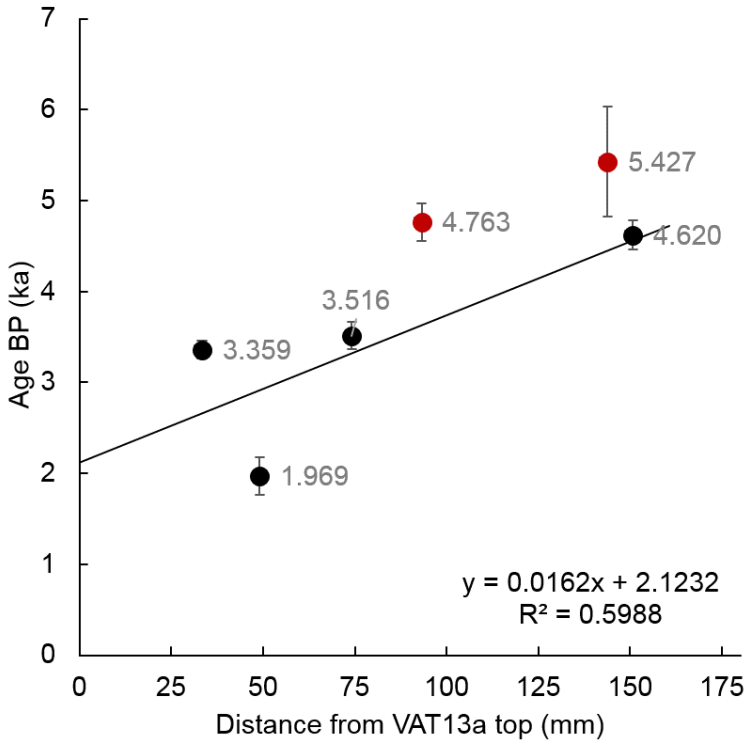

(b) Vat13a provisional age model excluding samples from dendritic calcite

Figure 5.13: U-Th dates obtained from Vat13a are not in stratigraphic order. 2 dates were sampled from dendritic fabric (plotted in red) (see Figure 5.12b) therefore can be excluded from the age modelling process due to the possibility of open system behaviour. The second age model displayed here is applied in all subsequent Vat13a timeseries.

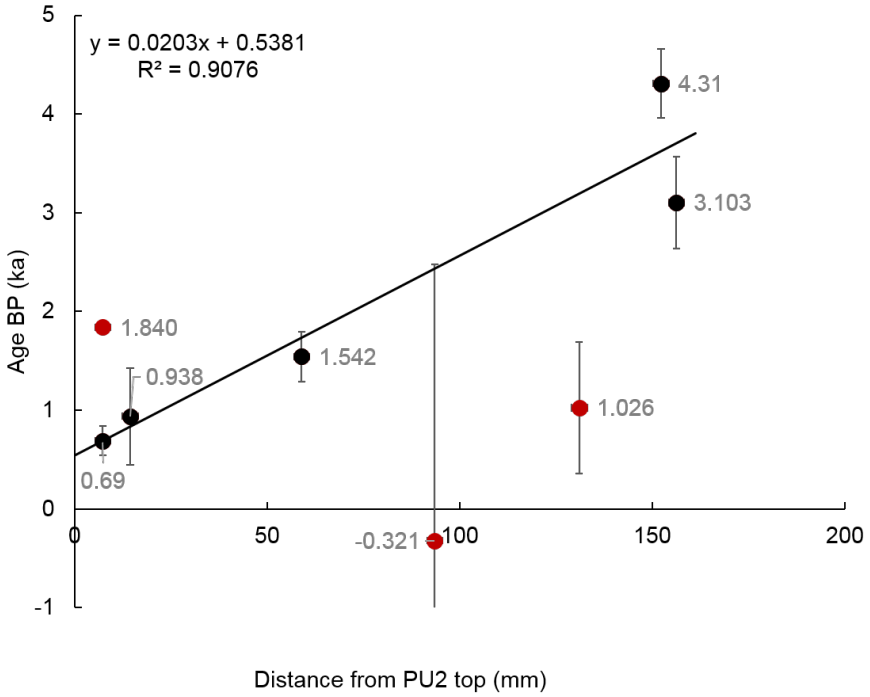

Figure 5.14: PU2 U-Th dates and preliminary age model using linear fit through accepted dates (black). Rejected dates were based on high degrees of error or stratigraphic implausibility.

water, rather than using continental crust derived values, which are suitable for site where the main thorium input is from terrestrial sediment input. The combination of young stalagmites, low uranium content of the host rock, highly mobile soluble behaviour, and more uncertainty of detrital thorium correction, provide challenges for U-Th dating in this situation.

PU2, a core sample, was sampled for dating in 8 places (Figure 5.15b) and the results detailed in table 5.2. They do not lie in stratigraphic order and two have large uncertainties associated with them, and may be discarded. One date was sampled within a dendritic layer which may be problematic, as open system behaviour may allow movement of uranium out of the system, but a higher degree of defect sites allows more uranium to partition into the dendritic calcite. A preliminary age model (Figure 5.14) has been constructed using a linear fit between the accepted dates and propagating the slope for the length of the speleothem.

PU7 has been sampled for dating ten times (Figure 5.15a), with five resulting

(a) PU7 calcite sampling for U-Th dating was carried out using a wire saw to cut from a polished section (See Methods for more detail). Samples were inspected to ensure absence of detrital material before being shipped to the dating facility.

(b) PU2 scan and U-Th sampling (both powder and wire saw methods used). The 1 mm contiguous isotope sampling traverse is also visible.

Figure 5.15: PU7 and PU2 scans & U-Th dating.

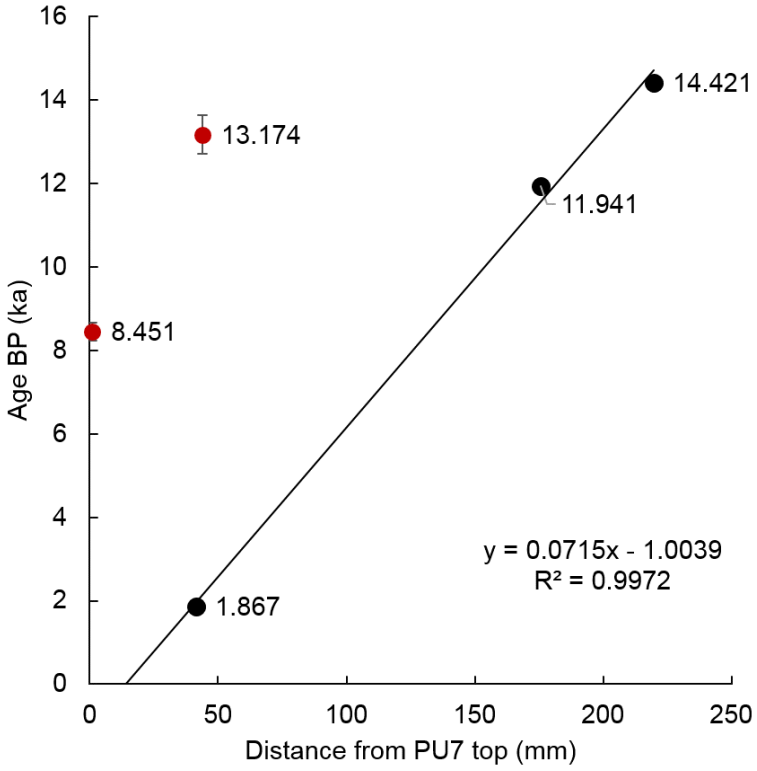

(a) PU7 U-Th dates with ±2sd, and preliminary age model using accepted dates (black). Rejected dates (red) not in stratigraphic order. This age model results in the speleothem tip being deposited 942 years in the future.

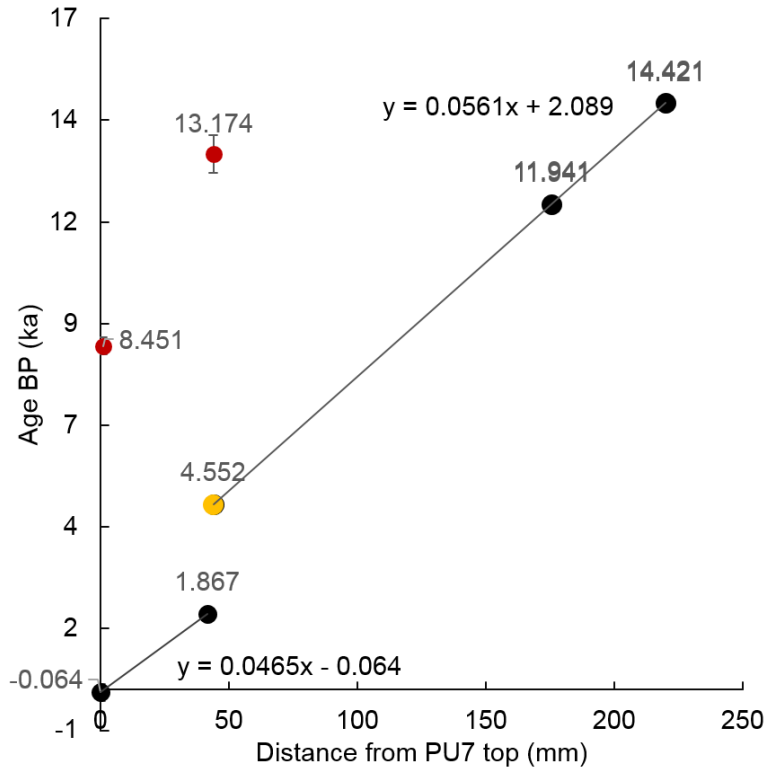

(b) Provisional age model v2, with hiatus. Hypothesised age (yellow), rejected ages (red), accepted ages (black), including a stalagmite tip date of -0.064 ka BP, or 2014 yrs CE, when sample was collected.

Figure 5.16: PU7 U-Th sampling and provisional age models

dates, not in stratigraphic order. Dates were sampled from the transparent sparry calcite at the growth axis to avoid the detrital material toward the cortex. Thin section analysis shows no sign that detrital material has influenced the core of the speleothem except at three distinct places.

Tentative age models were constructed: Figure 5.16a from 3 dates in stratigraphic order, and (Figure 5.16b), where additional time constraints are added to the accepted U-Th ages: The stalagmite was active at time of collection, so the tip has been set to the date 2014, or -0.064ka BP (1950). Thin section microscopy indicates a major stratigraphic discontinuity at the upper prominent detrital layer, which suggests a lengthy break in growth. The hypothetical age (yellow on 5.16b) allows both a lengthy hiatus where observed in the microstratigraphy, and consistent extension rate in the lower portion of the stalagmite. This interpretation, whilst tentative, is upheld by the microstratigraphic observations detailed below.

5.3.3 Vatulele speleothem microstratigraphy

Detailed microstratigraphic logging was carried out for the lower half of Vat13a as detailed in Chapter 2, section 2.8. The sample is primarily composed of open and compact calcite, with several detritally associated stratigraphic hiatuses, and several areas of dendritic fabric (Figure 5.12b)

Organic staining evident in Vat13a, predominantly as a yellow-brown tinge to the calcite in hand specimen or thick section, which is indiscernible in thin section. However, this organic staining is not associated with any fabric change; neither compact or open calcite show different morphologies in the stained vs unstained sections.

Some U-Th sampling was carried out prior to microstratigraphic logging, resulting in some dates having been taken from dendritic type fabric. This may have contributed to the ages not appearing in stratigraphic order, as dendritic

calcite may allow open system behaviour of some elements, therefore introducing uncertainty into age modelling. Sampling in areas with detrital components may also introduce error due to detrital Th contamination, although the sampling strategy for U-Th dating was designed to avoid this.

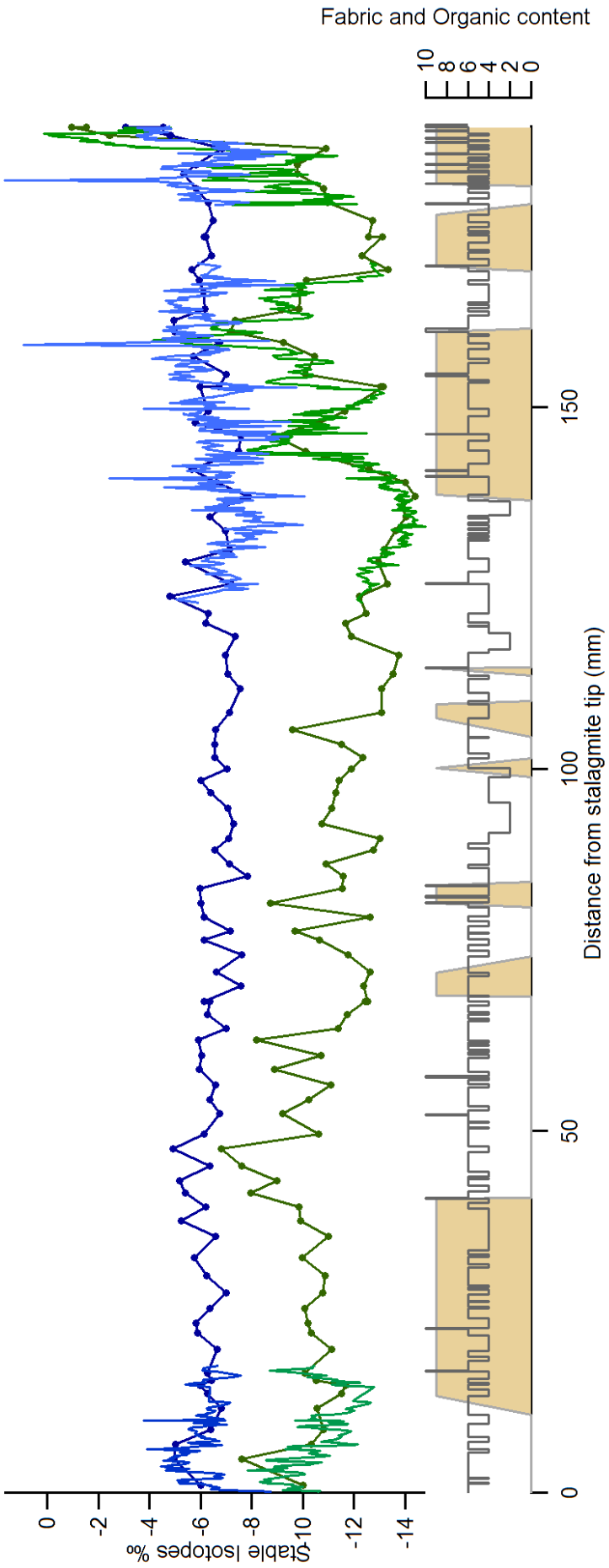

Figure 5.17: VAT13a Stable isotopes, high and low resolution: oxygen isotopes (blue) and carbon isotopes (green). Fabric and organic content.

5.3.4 Vatulele speleothem stable isotopes

Carbon and oxygen stable isotopes were analysed at 1 mm resolution for the length of the Vat13a, and at 0.1 mm resolution for regions near the top and base (For details of methods see section 2.5). The higher resolution isotopic analyses match well with the full traverse, indicating that the record is not aliased and that the lower resolution traverse acts somewhat as a low pass filter of the true variability. The base of the speleothem transitions to a flowstone and there is a distinct change in isotopes and fabric at this point, with much less depleted carbon and oxygen isotope signatures, and more open calcite and detrital material. The change in isotopes reflects the enhanced fractionation associated with flow deposits. There is little observable coherence between fabric and isotopes, and presence of the yellow-brown stained calcite, or dendritic calcite, appears to be independent of either isotope or fabric changes. Abrupt excursions, both positive and negative, are visible within the high resolution $\delta^{18}O$ timeseries, which are not replicated in the carbon isotope timeseries. There are also positive excursions in the carbon isotope data, but they are not coincident with those in the oxygen isotopes timeseries.

Covariance of stable isotopes within a speleothem record can be the result of either local or regional processes (Lachniet, 2009; Dreybrodt and Scholz, 2011; Riechelmann et al., 2013). Kinetic fractionation within the cave can result in isotope covariance and overprint the regional climatic signal, but carbon and oxygen isotopes can also be independent variables of a common driver, also resulting in covariance. If the isotopes are never in phase, then they are likely to have different drivers, or limiting factors throughout the record. To investigate this, least squares spectral analysis was performed on both raw and detrended isotope data, returning significant ($p<0.01$) peaks for 595, 88 and 77 year periodicities for both isotope datasets, as well as several peaks not replicated in across both isotopes (Figure 5.18). Based on the spectral analysis, rolling correlations at a 100 year timescale was applied to high resolution isotope

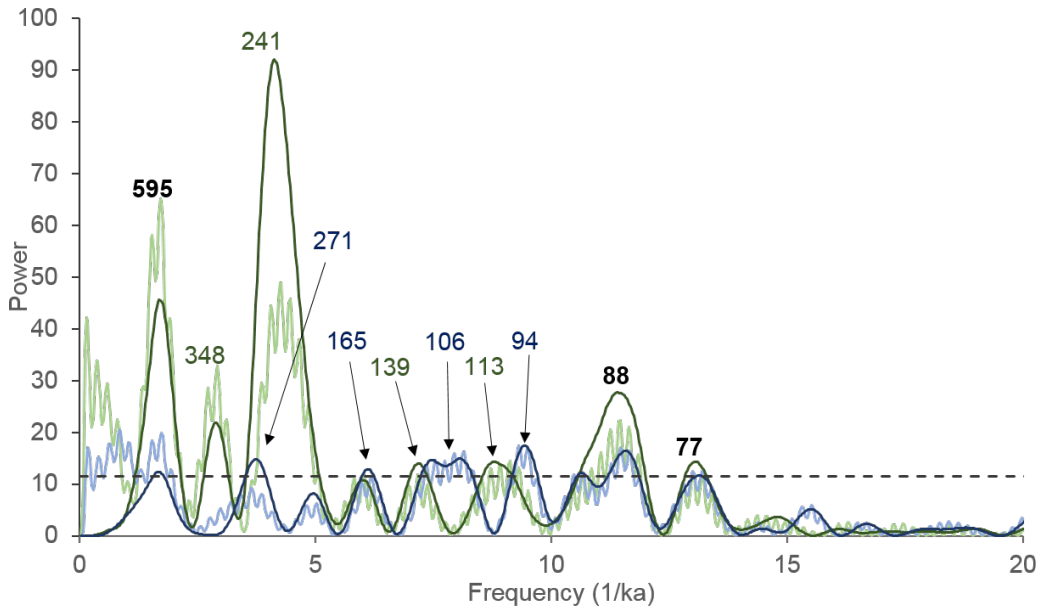

Figure 5.18: Lomb Scargle Periodogram (Pardo-Igúzquiza and Rodríguez-Tovar, 2012): Least Squares Spectral Analysis for VAT13a oxygen (blue) and carbon (green) isotope time series. The power axis is in units proportional to the square of the amplitudes of the sinusoids present in the data. The time-series were normalised prior to spectral analysis to ensure a mean of 0, $p<0.01$ at 11.44 (dashed line)

timeseries, (Figures 5.19 and 5.20).

Carbon and oxygen have an in-phase relationship for much of the time series (Figure 5.19) but the degree of correlation again appears uncorrelated with fabric changes or organics at these time scales. Again, the transition to flow-stone shows the highest level of correlation, but for the remainder of the record, there is a switching between in-phase behaviour indicating a common driver, and independent behaviour, at multidecadal or centennial timescales. A 200 year rolling correlation shows similar in-out phase switching to the 100 year correlation.

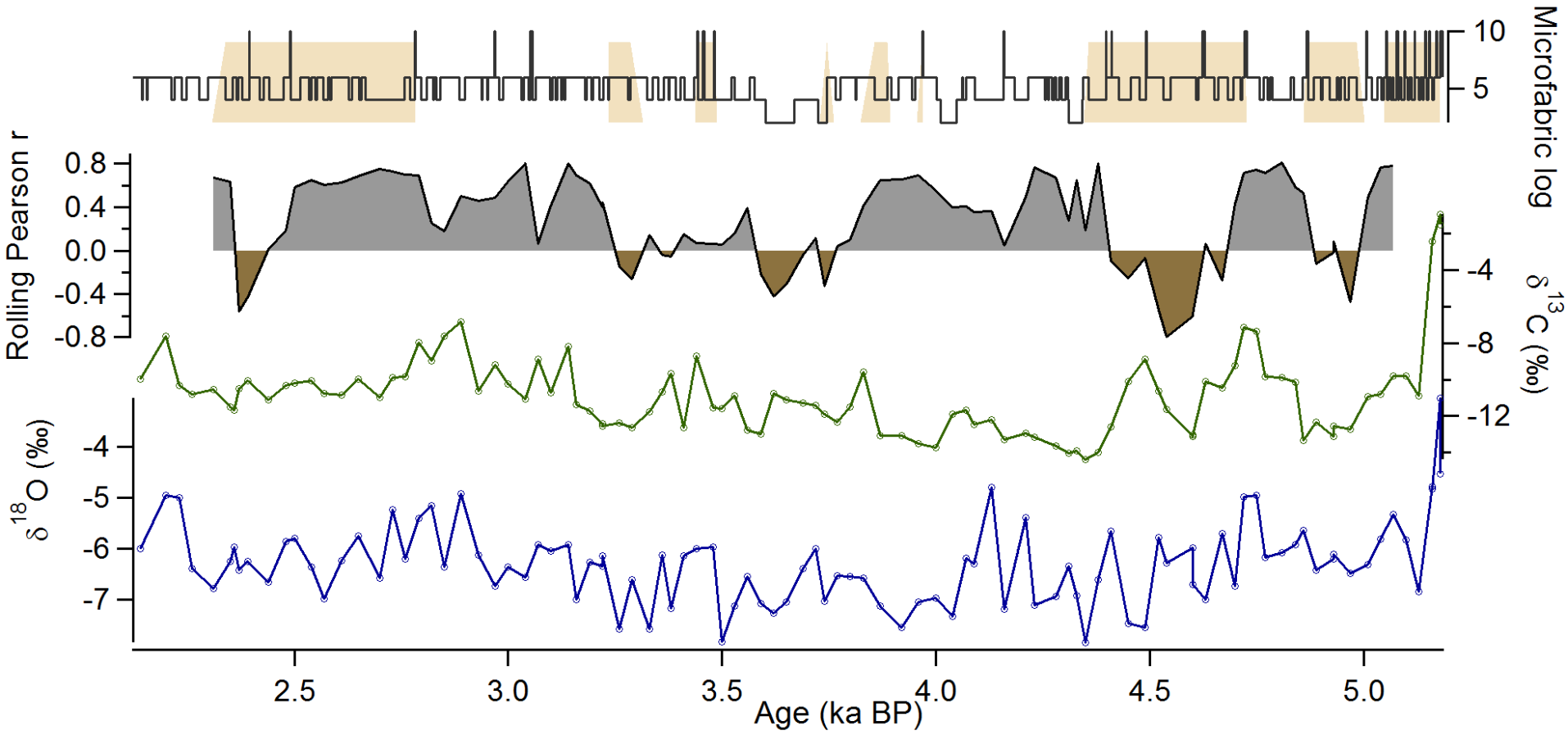

Figure 5.19: Vatulele stable isotope time series with 250 years rolling correlation (Pearson) and microfabric/organics log.

Isolating the higher resolution data (Figure 5.20), the correlations calculated are stronger, especially for the negative relationships, presumably due to the higher resolution of the record over the same 100 year rolling correlation. Again, there are long periods (50 - 200 years), where an in-phase relationship prevails, with abrupt forays into an opposition phase. A stratigraphic discontinuity and detrital layer (10 on the microfabric scale) appears close to most of these opposition phases, although the positioning of them is not consistent; and this may be an artefact of either the fabric logging process or the rolling correlation calculations.

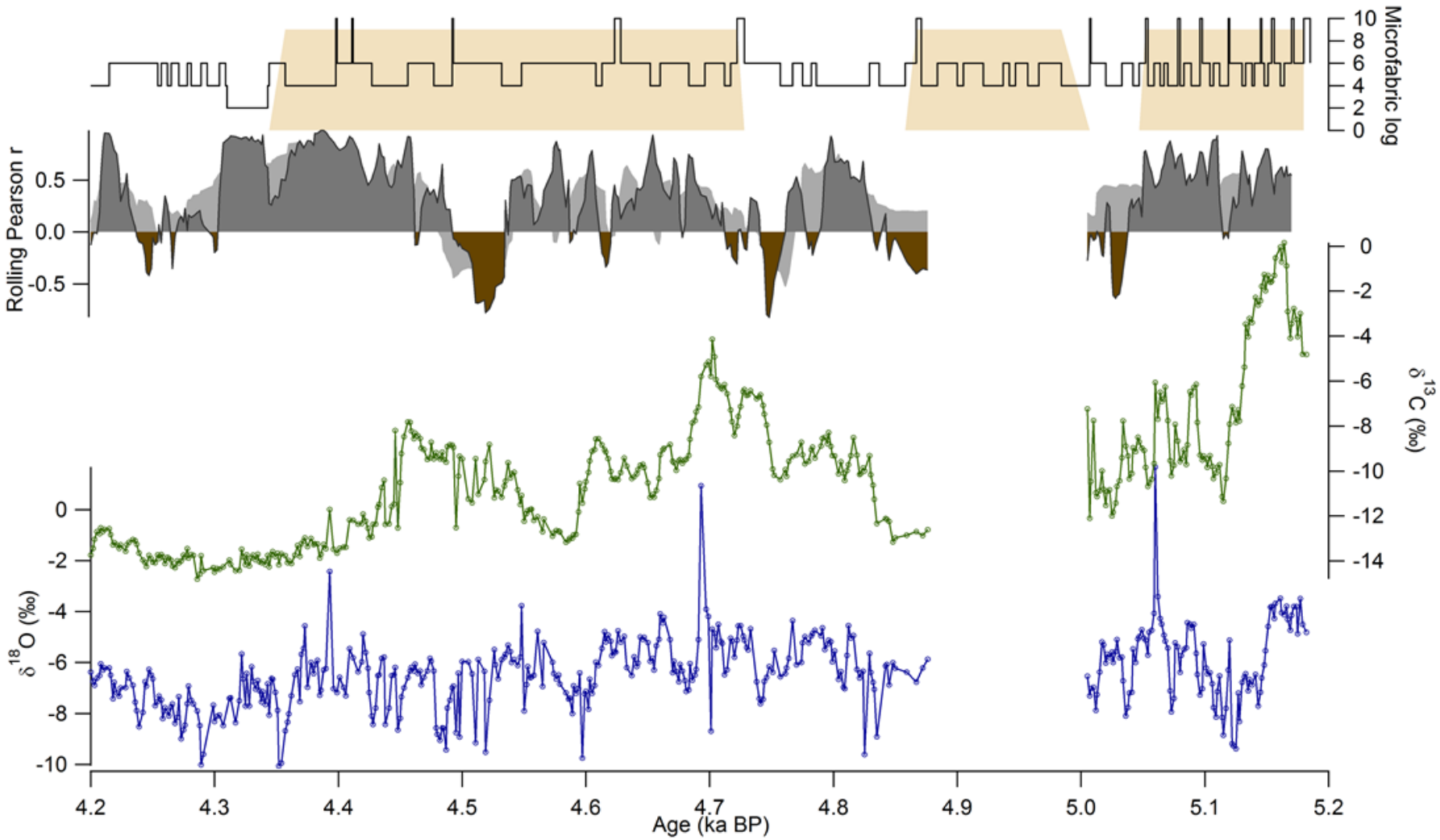

Figure 5.20: Vatulele 0.1mm resolution stable isotope time series with 20 years rolling correlation (-ve brown and +ve grey) and 100 year rolling correlation (light grey) (Pearson) and microfabric/organics log.

5.3.5 Vatulele speleothem trace elements

Traditionally, stable isotopes have been considered sufficient to make an interpretation from speleothem records, but a multi-proxy approach includes trace element analysis to investigate local environmental conditions that affect the speleothem growth. Sections of Vat13a were analysed using LA-ICPMS (see Methods: section 2.6), in six tracks along two sections from the lower half of Vat13a (Figure 2.9). Tracks were designed to cross perpendicular to laminae to maintain the highest resolution possible, and the subsequent processing involved lamina matching as closely as possible for each track, however, there is some offset between the high resolution isotopes and trace elements (Figure 5.22). However, the offset is not problematic for using trace elements to understand local environmental controls on stalagmite growth.

For such a large suite of trace elements, we are looking for coherence between sets of elements that have common associations. Mg, Sr and Ba are all double charged ions that can substitute for Ca ions in the calcite crystal lattice, but also compete with each other. They are indicators of extent of Prior Calcite Precipitation (PCP) (Oster et al., 2012) where they covary, especially if they are also in phase with carbon isotopes. F, Y, Pb, Cu, Zn, P and Br are all associated with an "autumnal flush" in temperate forested regions (Borsato et al., 2007)), but P alone can be an indicator of soil productivity, which may be variously associated with water availability, temperature, or human activities (Baldini et al., 2012). Uranium can be in phase with P due to the solubility of uranyl-phosphate complexes, but could instead be in phase with Sr and Ba due to the lower-than-unity partition coefficient (Fairchild and Treble, 2009) into calcite.

Principal component analysis

Principal Component Analysis (PCA) was used to separate the elements into suites with common drivers (following Rutlidge et al., 2014; Jamieson et al.,

2015), which could then be used for speleothem proxy interpretation. PCA of Vat13a trace elements produces variable results depending on the data window selected, as it is not robust to outliers created by crystal edges or detrital layers. If outliers are included, PC1 is 0.98 correlated with Al, and the PC2 is correlated with Mg. If outliers are excluded, PC1 explains 80% of the variance and is correlated with Mg (strongly) and Sr (weakly), and PC2 explains 10% of the variance, and is correlated with all elements except for Mg, Sr and Ba. The other principal components fall outside the 95% confidence interval when bootstrapped with 100 iterations of PCA.

At any resolution, and at any part of the record, the first principal component, is strongly correlated with Mg, which indicates that growth rate is the primary control for incorporation of trace elements in this speleothem.

Prior calcite precipitation

Mg and Sr abundances in the Vat13a show considerable coherence with 1 mm resolution $\delta^{13}C$ for the coincident part of the proxy record. While it appears that $\delta^{13}C$ lags the changes in Mg and Sr by approximately a century, this difference is most likely due to uncertainties in translating the raw LA-ICPMS data into timeseries format. However, it is clear that Mg and, to a lesser extent, Sr abundances follows the stable isotopes, increasing in the transition to flowstone at the base of the speleothem. Covariation of Mg and Sr with $\delta^{13}C$ is diagnostic of a hydrological control (Fairchild et al., 2000); when increased, they indicate lower water balance because the preferential loss of calcium cations, instead of Mg or Sr cations, from solution, raises the relative abundance of Mg and Sr concentrations in drip water, which is then transmitted to the speleothem calcite. When water input to the karst is higher, prior calcite precipitation is reduced and thus too are Mg and Sr relative abundances.

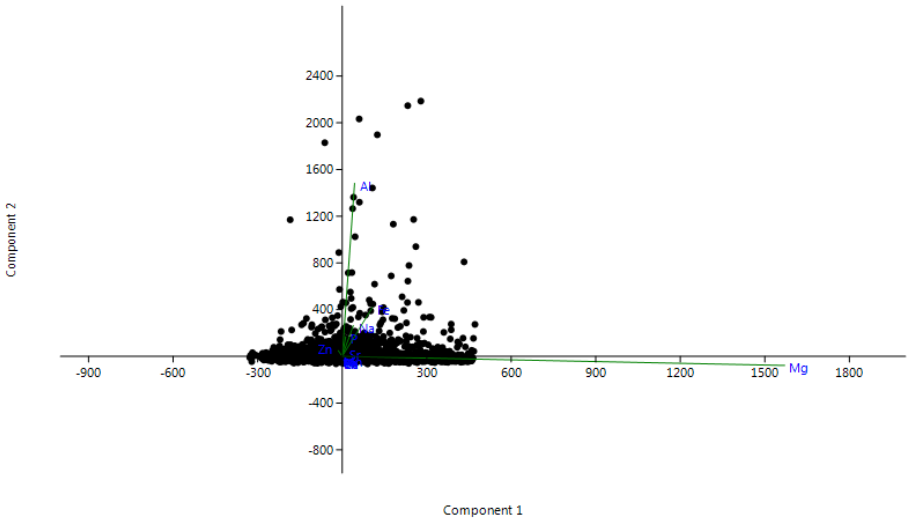

(a) PC1 vs PC2; Vat13a trace elements graph

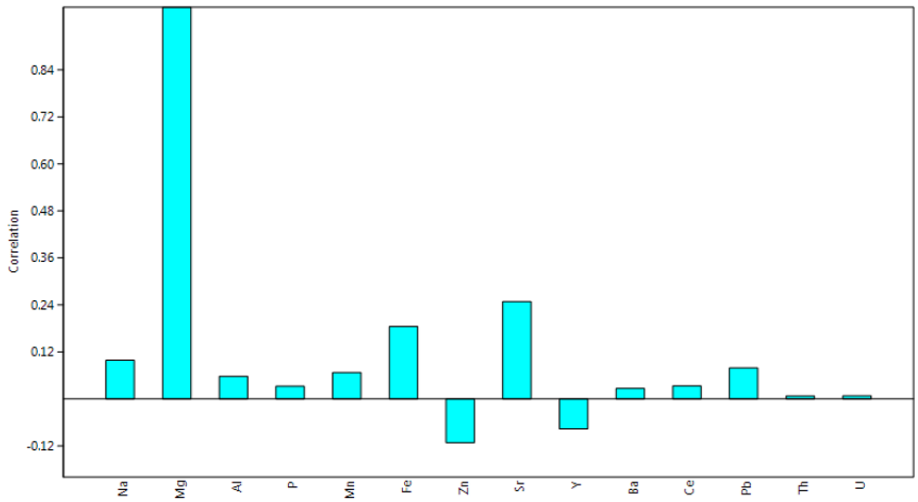

(b) Principle component 1 loadings plot

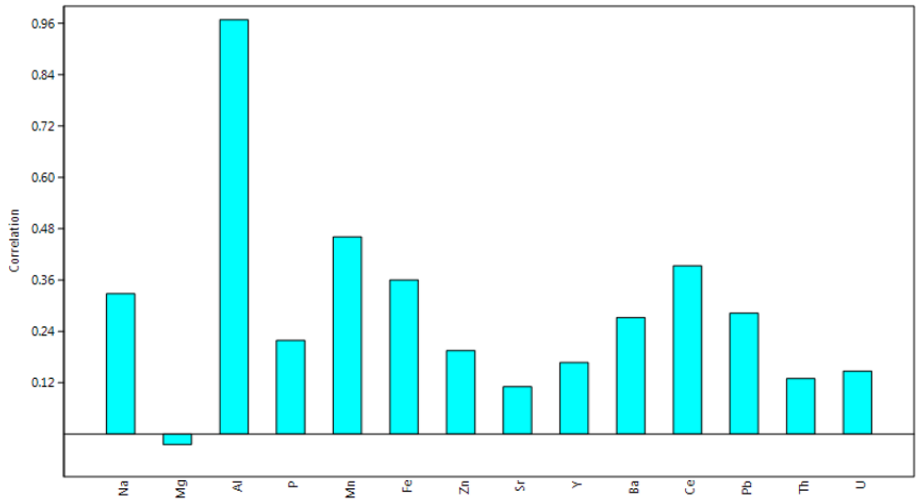

(c) Principal component 2 loadings plot

Figure 5.21: Principal Components Analysis of LA-ICPMS trace elements from VAT13a following Jamieson et al. (2015). PC1 explains 66.93% of the variance within the dataset: R^2 with Mg > 0.9

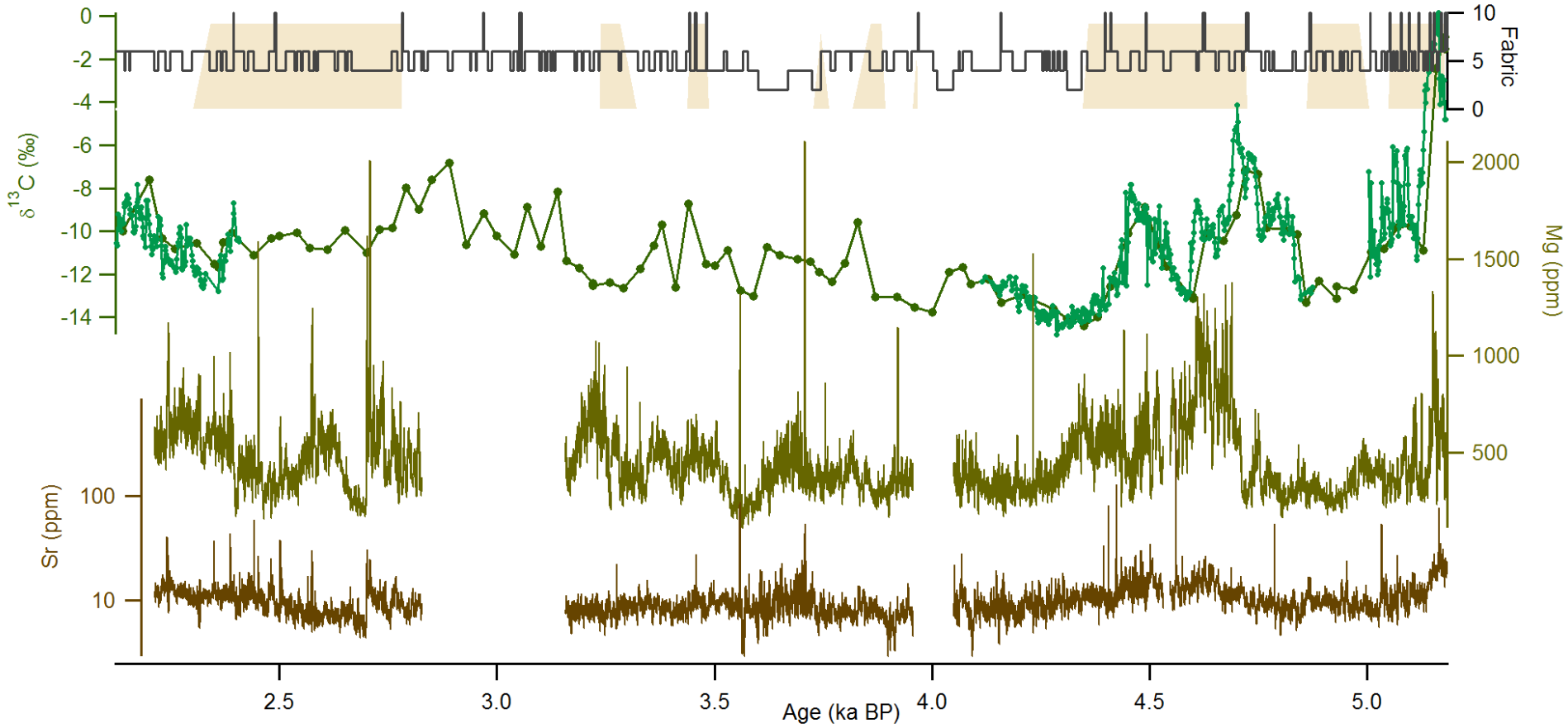

Figure 5.22: Stable isotopes, Mg and Sr trace elements indicating PCP and ICD driven by water balance. Mg, Sr and $\delta^{13}C$ show in phase relationship.

5.3.6 Puatea speleothem stable isotopes and trace elements

PU2 has been contiguously sampled at 1 mm resolution for the length, deviating from the growth axis to avoid macropores (Figure 5.15b). Oxygen isotopes range from -7.40‰ to -3.43‰ V-PDB, with an average of -5.26‰. Carbon isotopes range from -14.34‰ to -11.28‰ V-PDB with an average of -13.05‰. The preliminary age model has been used to create an isotope time series (Figure 5.23) and a 100 year rolling correlation applied. The isotopes abruptly oscillate between in phase and anticorrelated, with -0.5 > R > 0.5 for much of the record. The sawtooth nature of the graph indicates that some aliasing may have occurred and high resolution isotopic analysis would solve this. The timescale of this oscillation is slightly variable, which may be an artefact of the preliminary age model, but they appear on the decadal to centennial scale. The significance of this is, in part due to the similarity with the Vat13a record, where there is a 94-106 year periodicity in the oxygen isotope record. Here, this cyclicity is shown in the 100 year oscillation between in and out of phase correlation between the stable isotopes.

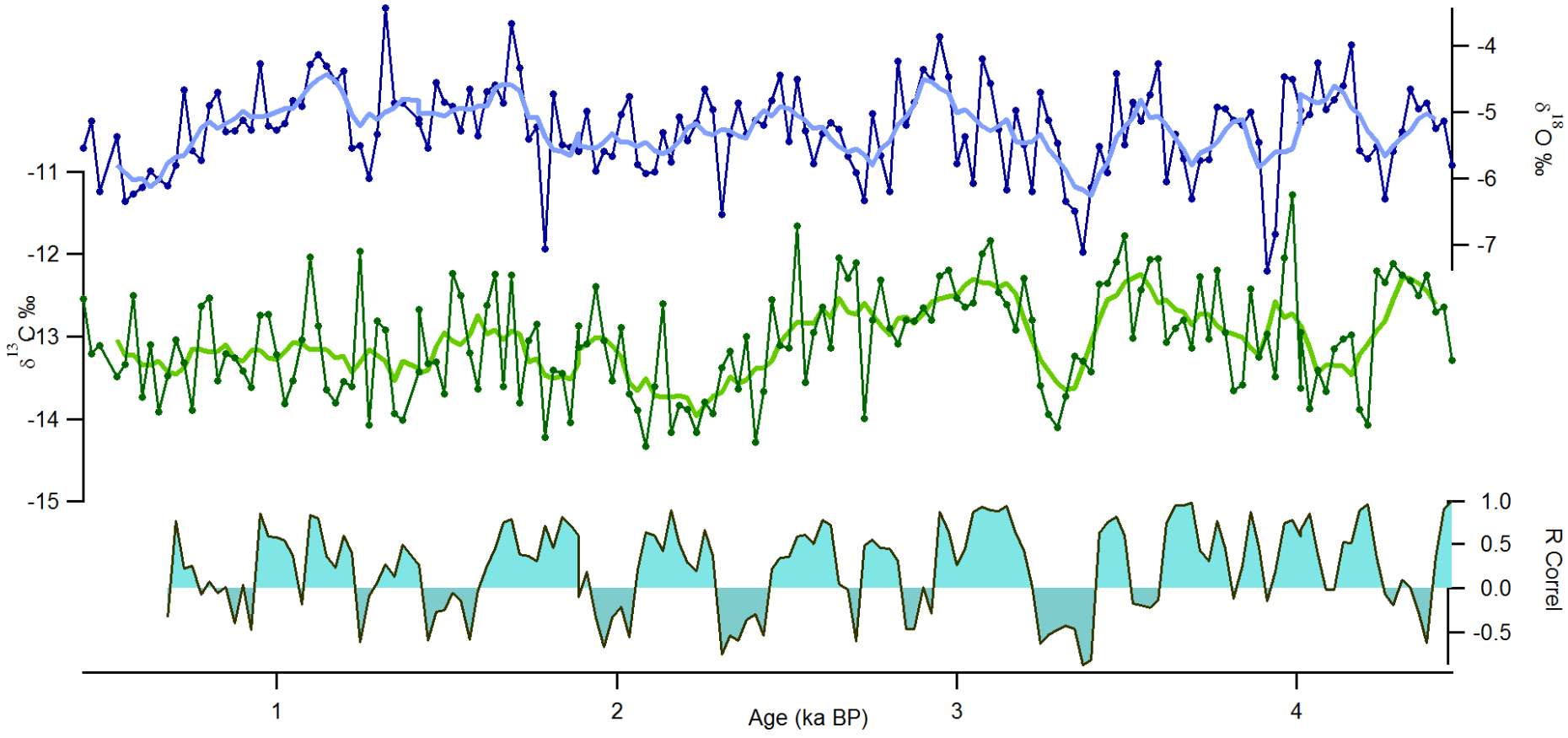

Figure 5.23: PU2 oxygen isotopes (blue), carbon isotopes (green) and 100 year rolling correlation (Pearson) applied.

Decoupling of the carbon and oxygen isotopes rules out systematic kinetic fractionation but since factors operating independently on carbon and oxygen isotopes may work in the same sense, correlated C-O is not necessarily indicative of kinetic fractionation.

Oxygen isotopes at the tip of the stalagmite are more depleted than average, and the long term average is lower than at any other time except for one excursion at 3.3 ka, where both oxygen and carbon show a large negative excursion, with oxygen lagging carbon. In the recent portion, carbon isotopes show no extra depletion, whereas oxygen isotopes show a steady march towards more negative values, with a possible reversal in the last 200 years.

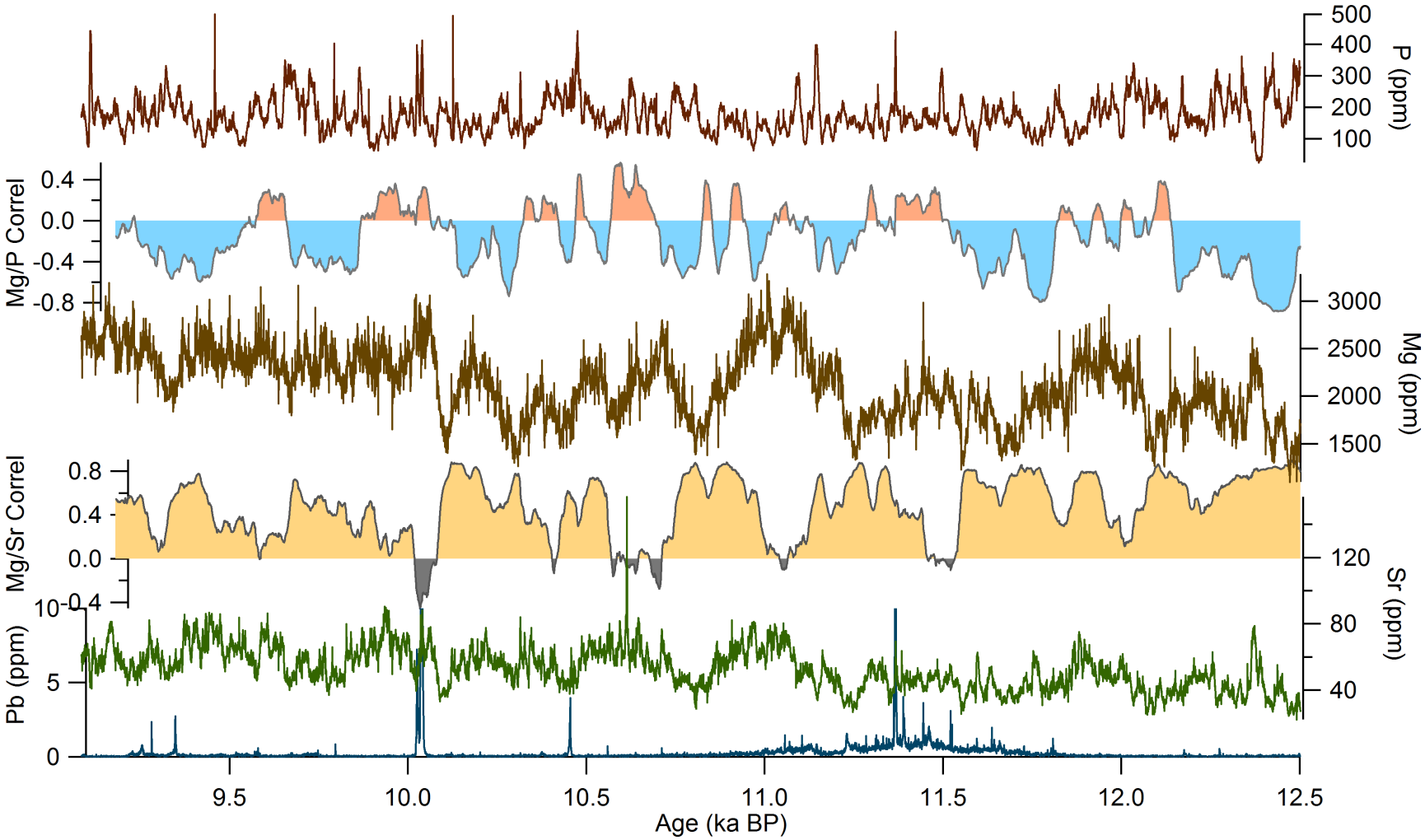

Figure 5.24: PU7 trace elements timeseries: Mg and Sr are highly correlated reflecting PCP, or dryness. Mg and P are mainly anticorrelated, showing opposite drivers: P usually associated with extent of biological activity flushed with rain. Pb marks point events probably associated with flooding.

5.4 Discussion

5.4.1 Karst residence and isotope signal

Since speleothems grow dripwise, constraining the relationship between precipitation isotopes and drip $\delta^{18}O$ allows either qualitative or quantitative interpretation of speleothem $\delta^{18}O$ in relationship to past rainfall. Precipitation amount and temperature outside the cave, in conjunction with drip rate measurements (Figure 5.10), and drip isotope sampling within the cave (Figure 5.11), record that the drips respond directly to high volume rainfall, returning swiftly to base, low frequency drips. This indicates that, in a well ventilated cave, stalagmite growth will occur primarily in the "wet season" and that annual growth rate will vary with annual rainfall variability. It therefore follows that the movement of the SPCZ will be recorded in the growth rate of the speleothem from this cave. The drip isotopes, as described above, vary only by 1.5‰ over the sampling period, indicating that the aquifer is well mixed and has a reservoir effect such that larger rain events overtop the reservoir and induce higher drip rates. As we see in the drip rate data, at the end of the dry season, the first large rain events do not cause a drip rate change, indicating that the reservoir becomes depleted over the dry season, likely due to a stressed water budget at the surface, so the first events serve to refill the reservoir. $\delta^{18}O$ drip, therefore, is likely to reflect a mixture of the previous wet season's average rainfall signature, and, as the wet season progresses, the drip water isotopes will increasingly move towards the current year' s seasonal average. This value of course will mostly reflect the larger rainfall events, as evapotranspiration inhibits the infiltration of smaller rainfall events.

By constraining the controls on rainfall isotopes and amounts within the "wet season" in Fiji, we can relate the speleothem isotopes and growth rate to the intensity (extent to which the SPCZ overlies and brings deep convective events) of the rainy season, and the relative position of the SPCZ, bringing more or less

rainfall to the island. Since the position of the SPCZ is influenced by ENSO and the position of the ITCZ, the conditions are positive for reconstructing the long term variability of the SPCZ using the stalagmite proxy record from this location.

Pending confirmation from ongoing data collection, the "Fiji model" of SPCZ control on precipitation isotope values, can be applied to other islands in the area that show similar patterns of precipitation anomalies. Furthermore, similarities in karst morphology and ventilations, suggest that speleothem growth characteristics - and therefore preservation of environmental signals - will be comparable.

5.4.2 The SPCZ and spatial variability of rainfall

Spatial variability of rainfall in the West Pacific Warm Pool (WPMP) is controlled by the position of the SPCZ therefore the spatial precipitation anomaly reflects the variability of the SPCZ as a function of the zonal sea surface temperature gradient (Chapter 4). Precipitation gradients in the SPCZ area of influence are very strong, so small departures from average position result in large precipitation anomalies for islands in the South Pacific (Gouriou and Delcroix, 2002).

Precipitation anomalies for December-February were plotted for recent El Niño and La Niña years, and two neutral years (Figure 5.25) to assess the changing precipitation gradient, under different ENSO conditions, and test the seasonal data against Vincent et al. (2011); Lorrey et al. (2012)'s comprehensive research. They match well, summarised in tables 5.3 and 5.4, indicating that the mechanism works well on both seasonal and interannual timescales. The N-S displacement of the SPCZ relative to the Pacific Islands, also matches well with the NE-SW (absolute) displacements reported by (Folland, 2002). The expansion and contraction of the SPCZ, and the E-W components of it's movement, are unlikely to be recorded in this study due to the positions of the

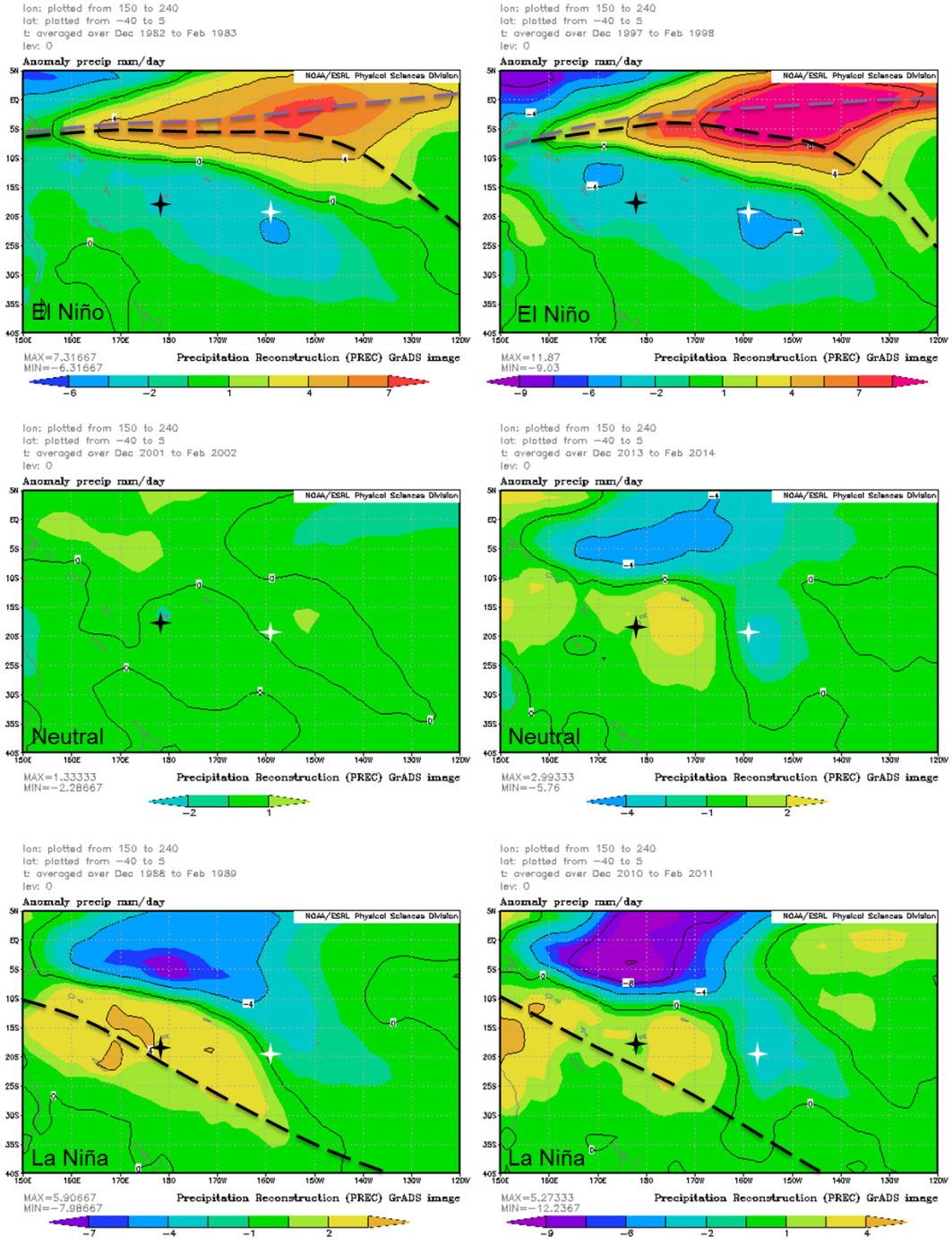

Figure 5.25: Precipitation Anomalies (DJF) for recent El Niño, Neutral and La Niña states and locations of Vatulele (Black star) and Atiu (White star). The position of the SPCZ is suggested with black dashed lines, and that of the ITCZ with purple. Relationships summarised in Table 5.3. Images provided by Physical Sciences Division, Earth System Research Laboratory, NOAA, Boulder, Colorado, from their Web site at http://www.esrl.noaa.gov/psd/ using data from NOAA's Precipitation Reconstruction (Chen et al., 2002)

	Fiji	Atiu
El Niño	< rain, SPCZ far N	< rain, SPCZ far N
Neutral	normal rain, SPCZ normal range	normal rain, SPCZ normal range
La Niña	> rain, SPCZ S/overlying	≤ rain, SPCZ S/overlying

Table 5.3: Differences of ENSO impact between Fiji and Atiu as seen in precipitation anomalies in Figure 5.25

	Fiji	Atiu
El Niño	≤ rain, SPCZ far N	≤ rain, SPCZ far N
Neutral	average rain, SPCZ normal range	average rain, SPCZ normal range
La Niña	≥ rain, SPCZ overlies	≥ rain, SPCZ overlies

Table 5.4: Differences of ENSO impact between Fiji and Atiu as reported by Vincent et al. (2011); Lorrey et al. (2012)

islands relative to the length of the convergence zone, but could be investigated using speleothem from islands under the influence of the distal part, extending the speleothem isotope transect further.

5.4.3 South Pacific Island Transect: Fiji and Cook Islands coeval records

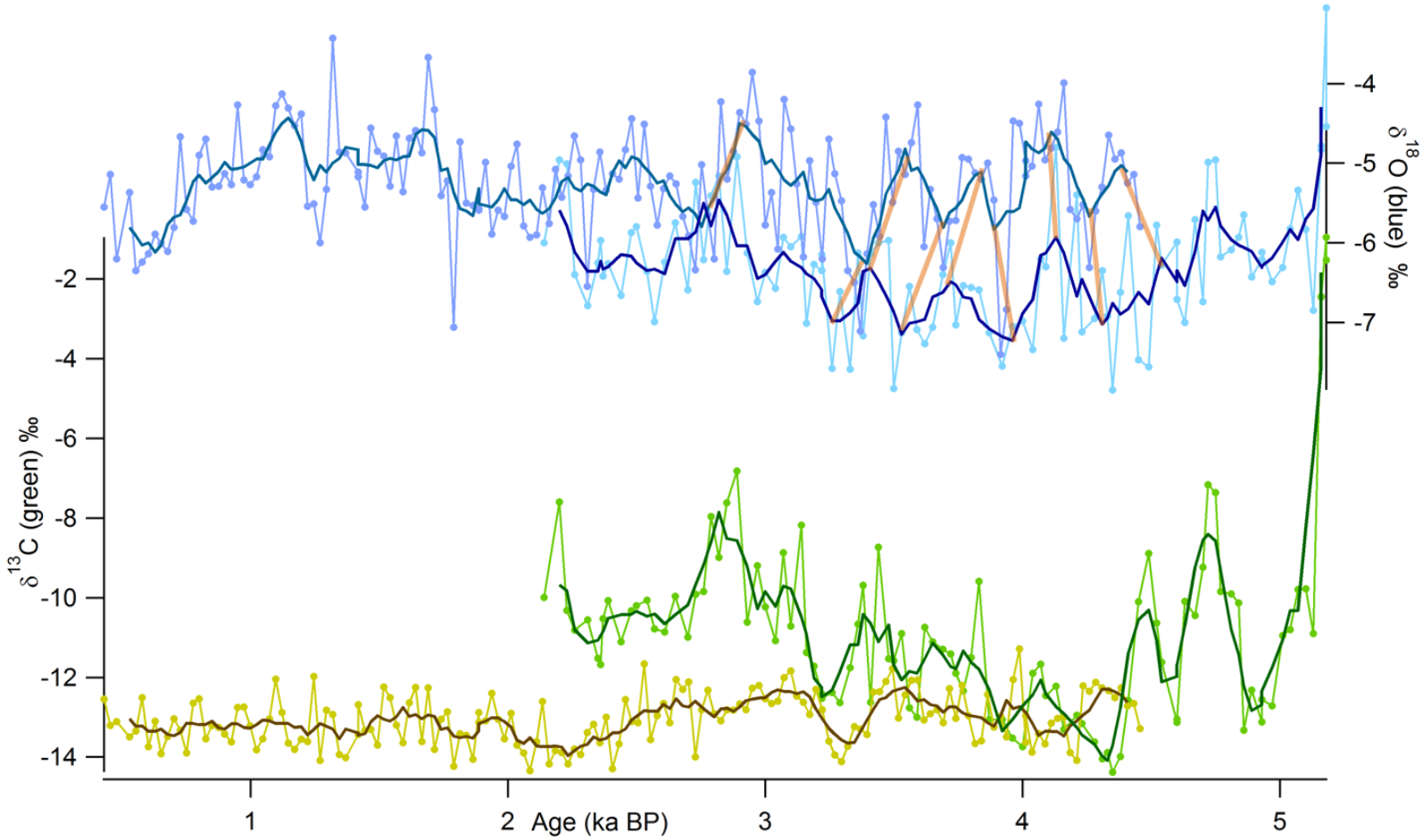

Figure 5.26: Vat13a (Fiji) and PU2 (Atiu) isotope time series: Vat13a oxygen isotopes (dark blue) are more negative than PU2 oxygen isotopes (light blue), but both exhibit similar ranges over the coeval portions, and appear to have similar variability on a centennial timescale (indicated by orange lines). Plotting both on the same x-axis, is perhaps a fallacy due to the tentative nature of the age models. Carbon isotope timeseries' (Vat13a green and PU2 yellow) bear little similarity to each other.

Despite the tentative age models, comparison of the proxy records from Fiji (Vat13a) and the Cook Islands (PU2) display some similarities in their centennial-scale oscillations for the coeval portions (Figure 5.26) Modern precipitation is currently being sampled at daily resolution from Atiu to compare with the rainfall collectd in Fiji (Chapter 4) and verify the relationship in the modern day.

A proposed mechanism for this is illustrated schematically in figure 5.27 and described as follows: If the SPCZ lies anywhere to the north of the islands, the trade winds dominate, and rainfall oxygen isotopes are consistently less depleted. When the SPCZ overlies or moves south, rain can also come from deep convective clouds, which typically bring more depleted rainfall. This results in a more diverse isotopic signature, driving the a seasonal $\delta^{18}O$ average to more depleted values. If the angle of the SPCZ is shallow, both islands fall on the same side of the SPCZ, so the isotopes move in the same sense and maintain the spatial isotopic gradient. When the SPCZ angle increases and falls between the islands, each island is affected by a different hydrological regime, which changes the isotopic gradient between the islands, narrowing the difference. This may be possible to replicate in a stalagmite situation. Carbon isotopes, however, are independent archives of local conditions, reflecting water balance, plant productivity and ventilation, often also driven by SPCZ variability.

When allowing for a more flexible age modelling approach, it is clear that oxygen isotope time series are in phase on a centennial timescale, and it is possible to speculate on using this record for an SPCZ reconstruction. The degree of long term cohesion between these records suggests that, on the centennial timescale, they must have a common driver, which can only be the variability in the position of the SPCZ reflected in the $\delta^{18}O$ of the rainfall and recorded in the speleothem calcite. This represents a three thousand year proxy record of SPCZ variability. The precipitation studies in Fiji (See Chapter 4), were conducted in a period of extended drought, so the measured drip water isotopes are likely to reflect "dry" conditions, with the SPCZ to the north of Fiji

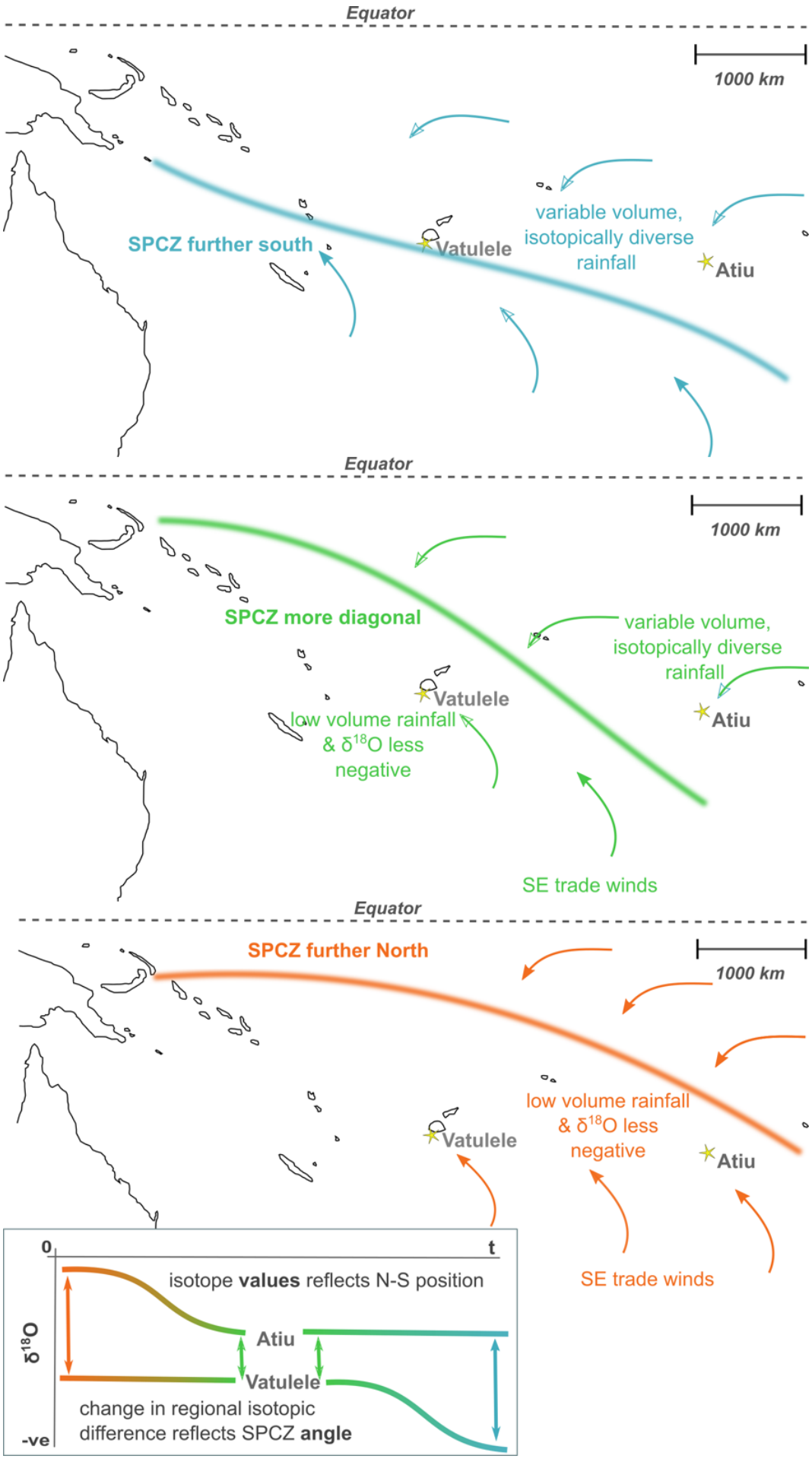

Figure 5.27: A schematic diagram to show the proposed mechanism for Vatulele and Atiu speleothem to record the N-S and diagonal variability of the SPCZ through the change oxygen isotopic difference between the two islands.

for most of the year in the modern analogue, and recharge to the aquifer over only 4 months of the year. Were the SPCZ to spend a higher proportion of the year overlying or to the south of Fiji, there would be larger number of isotopically depleted rain events, and more of them would infiltrate, resulting in lower PCP, and therefore more negative $\delta^{13}C$, as well as more negative $\delta^{18}O$, reflecting the deeper convection to the north of the SPCZ as discussed in Chapter 4.

To illustrate this, Figure 5.28 matches the centennial scale oscillations between the records, by adjusting the offset in the age models, and adds context by indicating significant anthropological events. There is no implication of a link between them, as that is outside the scope of the research, rather it is to put the record into context with human pre-history. Some of the events marked are outside the Central Pacific, but relevant as parts of human pre-history and to the the discussion in the introduction of the global ramifications of changes in the IPWP.

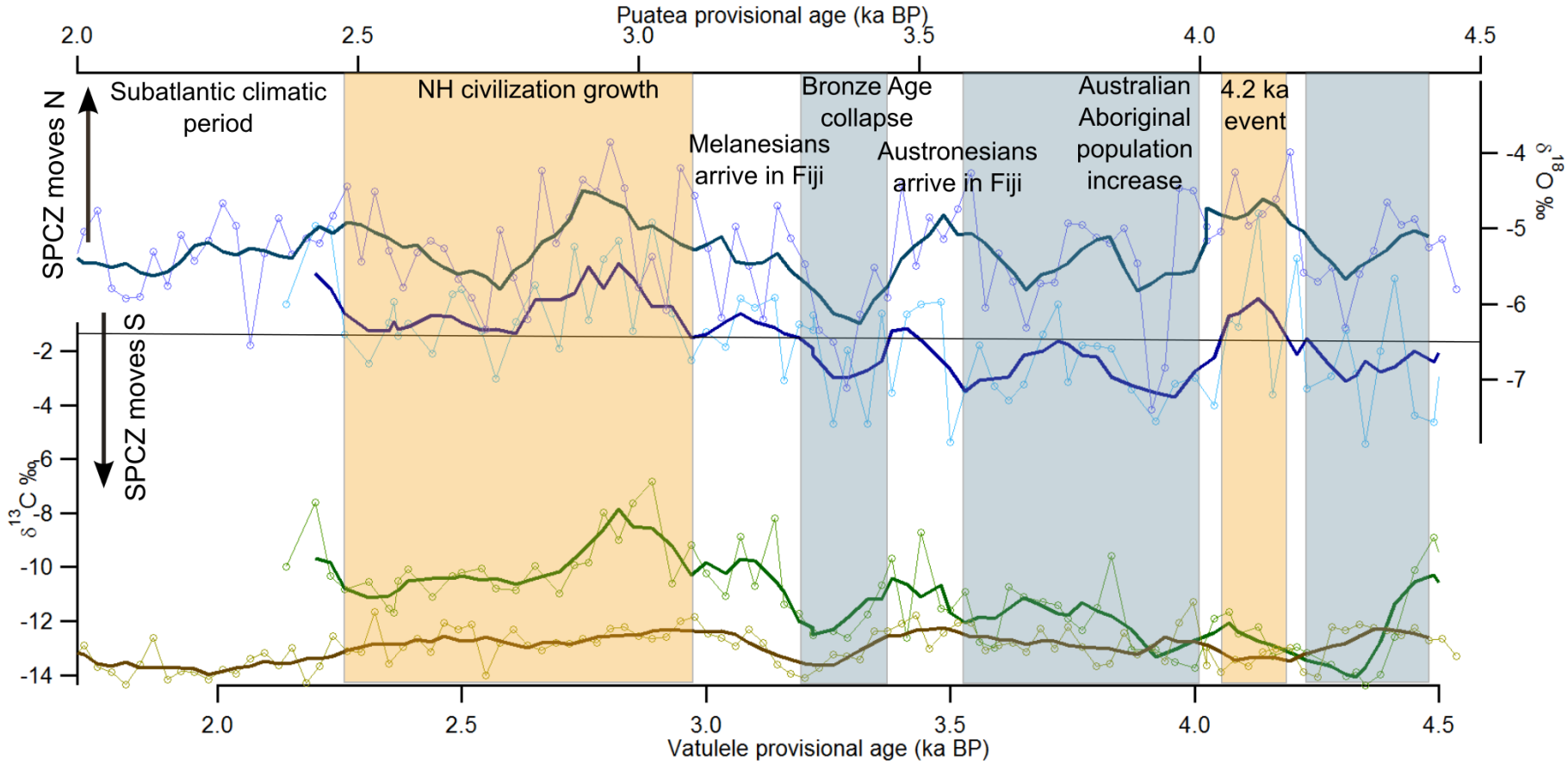

Figure 5.28: Vat13a and PU2 with flexible age models, showing a good match on centennial time scales. The longer record is PU2, and the shorter from Vat13a. Orange fill indicates time periods where oxygen isotopes in Fiji move above the -6.5 per mille threshold of modern day values, indicating a more northerly average position of the SPCZ. Blue fill indicates time periods where Fiji oxygen isotopes move below the threshold value, indicating the SPCZ ranging further to the south of modern day positions. Some archaeological events are indicated for reference, although timeframes for such are still under investigation by the archaeological community.

5.4.4 Limitations of interpretations

The assumption is that the SPCZ affects the rainfall amount and isotopes in a similar way on Atiu as on Fiji - although with an as yet unquantified offset - and there is ongoing monitoring there to assess if this is the case. However, it is reasonable to expect a similar mechanism, due to the similarities between the islands and their situations in the Pacific, proximity to the SPCZ, seasonal rainfall and cave and karst morphologies.

The interpretations presented are based on very preliminary age models, which are no more than a simple linear regression through a small number of dates. Additional analyses are expected imminently, whereupon more detailed age models can be constructed. Once this is successful, statistical analysis between the records can be used to show the relative position of the SPCZ at a higher resolution based on the variability of the difference in $\delta^{18}O$ between the two records. Additional speleothem records from both islands are also being constructed independently of this project, in an attempt to duplicate the findings and verify the regional signal.

Currently the interpretation is limited to only whether the SPCZ has spent more or less time to the north rather than overlying or south of Fiji. This is quite crude and simplistic, but nevertheless an advance of knowledge. Further work must be done to address this and is discussed in the conclusions and critical analysis sections.

5.5 Conclusions

The isotopic signature of the rainfall in Fiji is controlled both by the position of the SPCZ and the amount of rainfall, the latter which is of itself a product of the position of the SPCZ. Isotopic signature of the rainfall is highly variable, but has a consistently greater range, and more depleted signature austral sum-

mer, when the amount of rainfall is also higher. Summer rainfall infiltrates the karst, and recharges the aquifer, where mixing takes place, causing the isotopic signature of cave drips in Volivoli cave to reflect the weighted average of the summer rainfall isotopes. When measured in a speleothem from Fiji, once corrected for kinetic and equilibrium fractionation, speleothem calcite $\delta^{18}O$ will reflect the variability of the position of the SPCZ, with more negative values indicating a more southerly SPCZ position.

The same mechanisms are expected to be true for speleothems from other pacific islands that lie under the influence of the SPCZ. Speleothem $\delta^{18}O$ from Atiu match well with the Fiji speleothem, indicating common drivers and a regional control on hydroclimate. The combined record of speleothem $\delta^{18}O$ from the two islands provide the first multi-sample, teleconnected proxy record of the SPCZ in the late Holocene and show that there is variability on a multidecadal and centennial timescale.

Chapter 6

Critical Evaluation

6.1 Evaluation of samples

Samples can be divided into heritage and new samples. Heritage samples were available for the project and had some existing data as detailed in section 2.1. New samples were collected during the 2014 field work as detailed in section 2.2.

UMS10 was an unusual and frustrating sample, with some tantalising hints of excitement. The laminated couplets indicated a consistent growth rate for much of the sample, and, with low visible detrital content and regular morphology, it seemed promising. Since there were already some preliminary dates, and sections of laser data, it was the obvious step to try to extract a proxy record from it.

Constructing an age model for UMS10 was highly complex due to the frequent hiatuses (see Chapter 3 and section 6.2 for discussion of U-Th dating) but the challenge of getting a meaningful result provided a unique learning experience, which was the provocation to investigate diverse analytical options, and to try to understand the implications of using different age modeling algorithms.

Whilst UMS10 was very frustrating, in a context of doctoral training, it was

probably more useful in forcing me to scrutinise assumptions and techniques than a more "straight forward" sample would have been. With unusual fabrics, splash cups, hiatuses, diagenesis and very high porosity, it provided a lot of learning opportunities.

With the other speleothems, I was able to apply the learning outcomes of working on UMS10, and work in a more efficient and targeted manner. I also found it easier to start with a whole sample. Conducting fieldwork after having worked on some samples also helped me to ensure I knew what I wanted to look for in the field, both in terms of speleothem samples and surrounding environment.

Rainfall measurements from North East Hill University cover 2010 - 2012 but have some inconsistencies: Rainfall volume is provided but without units, and is missing for some months and the whole of 2011. Additionally data are omitted for November - March, without explanation as to whether that was due to no rainfall at all, or lack of available personnel for sampling. As such, these data are only indicative rather than reliable for supporting conclusions.

6.2 Evaluation of methods

6.2.1 U-Th: lessons learned

U-Th dating of the speleothem samples was a large stumbling block for this thesis, but also a valuable learning opportunity. For a discussion of the dating UMS10, see Chapter 3, section 3.5. In addition to the information there, it is worth discussing the challenges of obtaining U-Th dates here.

U-Th dating was carried out under a series of NERC funded grants:

- *U-series dating of speleothem calcite and evaluation of climate recording of S. Asian monsoon intensity in Mawmluh Cave, Cherrapunji, NE*

India. Mattey, D. Natural Environment Research Council (NERC): £13,000 1/09/10 31/08/11

- *A 3000 year annually resolved speleothem record of monsoon intensity from the Shillong plateau, NE India: frequency and duration of drought and teleconnections to regional climate modes* (NERC IP-1551-0515 £20,600) PI, Mattey, D, Co-I Brett 1/01/14 31/12/14

- *Mapping South Pacific Convergence Zone variability using Holocene speleothem from Fiji and the Cook Islands* (NERC IP-1540-0515, £12,000) PI Mattey, D, Co-I Brett 1/09/15 31/08/16

UMS10 samples have been analysed for U-Th disequilibrium dating in a series of batches and in two different labs, all returned dates are in Figure 6.1, and an additional batch was lost in preparation. As can clearly be seen, the dates are not in stratigraphic order, precision varies widely, and the 2012 dates are offset from the rest of the data. Vat13a, PU2, and PU7 have all been sampled for dating multiple times with similar challenges. In the following paragraphs, I will discuss why.

At the beginning of the research, I was using the "powder method" for sampling for U-Th dating, which is described in section 3. When I attended the Karst Record VII conference, I was made aware that this is not considered best practice, as it may introduce error by introducing calcite from non-target lamina, may allow dust or other particles to contaminate the sample if not in a clean lab, and does not allow the specialist at the dating lab to inspect the sample. I was advised to switch to a cutting method, preferred by specialist speleothem geochronology labs, so that the geochronologist receives a piece of calcite and may inspect for calcite fabric, detrital components, staining or foreign objects, and clean as necessary.

When on a study visit to University of Newcastle NSW, learning about confocal microscopy and speleothem microstratigraphic logging, I learnt that some fabrics are to be avoided when dating. Previously, I had known to avoid areas

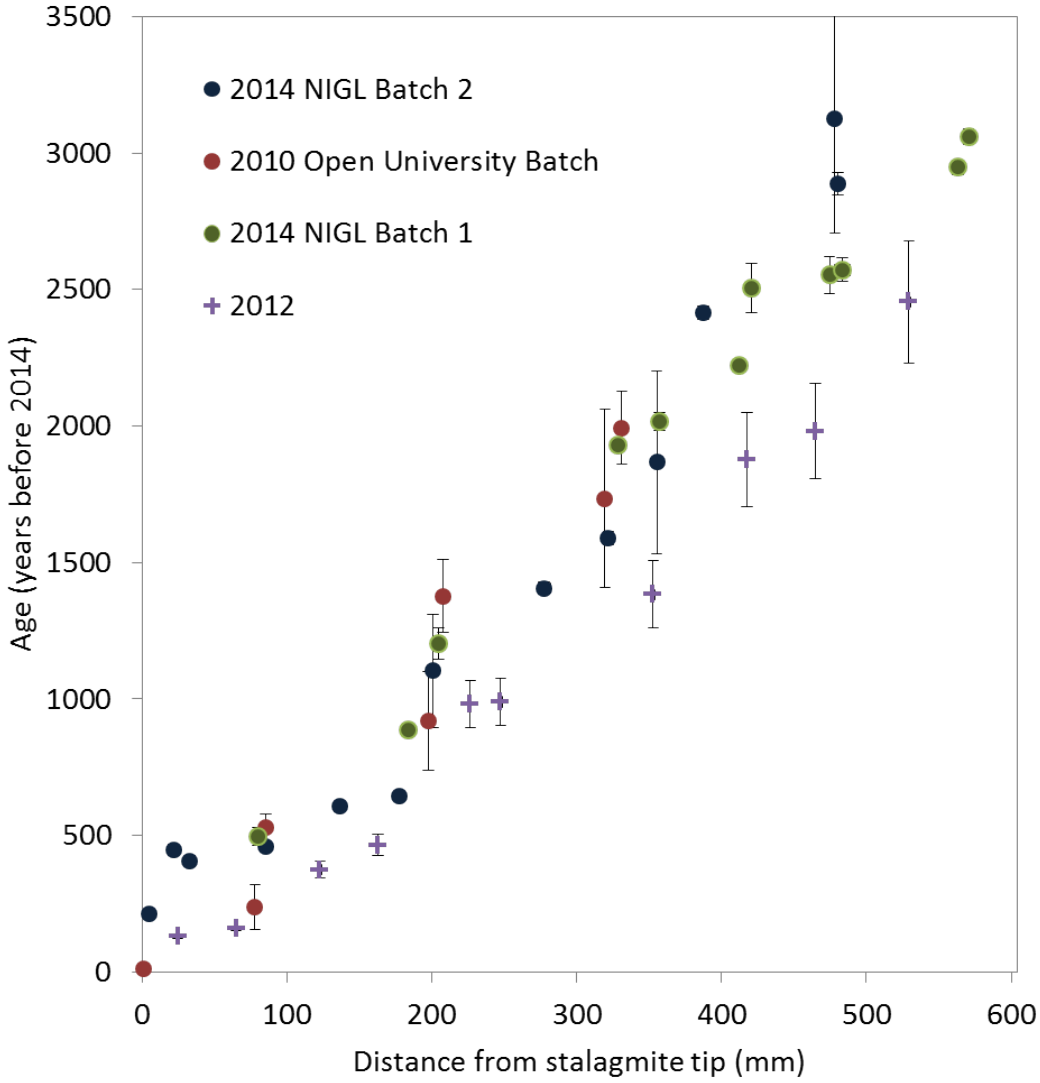

Figure 6.1: All U-Th dates returned for UMS10 with error bars: With dates from the Open University in red (2010) and purple (2012) and the two batches from NIGL in green and blue. Where no error bars are visible, reported precision is better than the size of the graph marker

with visible particles, dirt or discolouration, but was unaware of the extent to which fabric can affect U-Th dating accuracy. Diagenetic fabrics, or any fabric that is associated with open system behaviour should be avoided, as uranium can be remobilised and lost to the system.

We were the fortunate recipients of a series of NERC small grants (detailed above) in collaboration with the National Isotope Geochemistry Laboratory (NIGL), an interdisciplinary geochronology laboratory with experience in speleothem dating (Nehme et al. 2015, Smith et al. 2016). This lab is much in demand for work done under Research Councils UK (RCUK), leading to sample turnaround of several months.

So, in summary, my method of sample preparation was flawed, introducing spatial uncertainties and possible detrital Th, and I was targeting unsuitable calcite, however, in collaboration with NIGL, we have produced novel datasets that provide useful insights into environmental change in their target areas, which are in preparation for publication.

Without funding constraints, and in hindsight, when outsourcing specialist analysis, best practice would include seeking advice and collaboration with sample specific geochronologists, working in uniquely specialised labs. An example of the desired outcome can be found in the supplementary material of (Wang et al., 2008). This is one of the key learning outcomes from the doctoral training process for me.

6.2.2 Other methods

I think the stable isotope methodology used in this thesis could not have been much improved with the resources available, and I am proud of the systematic and thorough methodology used. Every one of the thousands of calcite samples for this research was individually weighed to ensure it fell within the bounds indicated when the linearity of the IRMS was tested, and to explore

the possibility that calcite density could be a proxy record by itself (with this methodology, not possible). One of the highlights of the PhD experience has been learning to run, maintain and troubleshoot the Isotope Ratio Mass Spectrometers in the Stable Isotope Lab at RHUL, although I am yet a novice.

It would have been advantageous to extend all the techniques used for the full length of all samples, especially high resolution stable isotope and trace element data, and to have far more U-Th dates, but the former wouldn't extend the conclusions without the latter, which is out of our hands.

There were a lot of methods of speleothem analysis that we didn't use. Examples include:

- Micro X-Ray Diffraction (XRD) for confirmation of mineralogy (e.g. Finch et al., 2001).

- Fluid inclusion methodologies such as palaeotemperature work (Kluge et al., 2008), or isotope analysis (Dennis et al., 2001).

- Micro X-Ray Fluorescence for validation of elemental concentrations of major elements (e.g. Wu et al., 2012).

- Sulphur isotope analysis (Wynn et al., 2008)

- Clumped isotopes analysis (e.g. Kluge and Affek, 2012)

Most of these methods were excluded purely to limit the scope of the research, and to maximise use of in-house facilities. However, in hindsight, UMS10 may have been much more valuable if it had been scanned by micro-CT for three dimensional porosity analysis, and then used for fluid inclusion work, making the large pores an asset rather than a challenge.

6.3 Evaluation of data

6.3.1 Accuracy and precision

Precision and reproducibility of $\delta^{18}O_{water}$ was not ideal (with standard deviations of individual sample repeats between 0.03 and 0.9, averaging σ=0.37) but samples were repeated up to twelve times to ensure accuracy and bring down the standard deviation. When calibrated by new water reference materials, precision of the CF-IRMS was 0.085 per mille. Both the Dual Inlet -IRMS and CF-IRMS return precisions around 0.03 per mille. All geochemical analyses were calibrated to reference materials obtained from the International Atomic Energy Agency (IAEA): Vienna-Standard Mean Ocean Water 2 (V-SMOW2), Greenland Ice Sheet Precipitation (GISP) and Standard Light Antarctic Precipitation 2 (SLAP2), for water samples; NBS19 TS-Limestone (Friedman et al., 1982) and LSVEC lithium carbonate (Stichler, 1995) Details of all reference materials used can be obtained from the IAEA website and in the appendices. Stable isotopes results were in good agreement between high and low resolution analyses, as well as reproducible in repeat samples. Reported precision of U-Th dates are very good (see Table 5.2), even to sub-annual in some cases, but the accuracy is more difficult to determine as discussed at the start of this section.

6.3.2 Limitations of conclusions and comparison with existing work

Limitations of the conclusions are discussed within the relevant sections: Chapter 3 discusses the limitations and complexity of stalagmite research, and Chapter 5 discusses the limitations of the interpretations made in section 5.4.4.

Chapter 7

Conclusion

7.1 Summary of Conclusions

Conclusions of this research are summarised below:

- The "amount effect" is not a causative relationship, instead, where it exists, it is a product of regional convective processes affecting both the amount of rain and the oxygen isotope signature of that rain. Studies that do not have specific evidence of a clear amount effect at their own site, should exercise caution when interpreting the relationship between oxygen isotopes and rainfall amount in speleothem proxy records.

  This conclusion has been reached before, by meteorologists and palaeoclimatologists (see Chapter 4, section 1), but this study set out to find a place where "the amount effect" was a strong causative relationship that could be applied as a simple transfer function to speleothem as paleorainfall proxy, and returned the null hypothesis.

- The oxygen isotope signature of precipitation in NE India is controlled by the increasing moisture availability as the monsoon progresses, and is not related to rainfall amount of a daily, monthly or annual timescale. It is also not related to the freshening of the Bay of Bengal, as had

previously been suggested. This highlights the first conclusion; that the amount effect as a control for oxygen isotopes in rainfall is not a safe assumption to make without local evidence presented to support that claim.

- In neither a "complex" continental monsoon scenario, nor a more "simple" oceanic island setting, is the precipitation isotope signature controlled by the amount of rain fall, rather they are both the consequence of regional convective processes.

- A multi-proxy approach is essential for speleothem research, for robust confirmation of the extent of the preservation of local and regional environmental signals within the sample. In the case of UMS10, this approach forced the confrontation of limitations, if not for the multi-proxy approach, the complexity may have not been fully appreciated and instead a rather dubious "palaeorainfall" record could have been produced which would not have been a good approximation of reality.

- The position of the South Pacific Convergence Zone in relation to Fiji, can be described as a function of the zonal sea surface temperature gradient between Fiji and the Nino4 sector, and is therefore evidence that the ocean-atmosphere coupling is driven by the oceanic component in this area and on the timescales studied.

- A speleothem transect of the karst terrains of South Pacific islands has the potential to allow reconstruction of the past variability in both position and angle of the SPCZ, through the changing isotopic gradient between islands. This is an exciting opportunity for further research.

7.2 Summary of Thesis Achievements

- Co-authored papers; all involving international collaborations and interdisciplinary research:
  - Jamieson, R. A., Baldini, J. U., Brett, M. J., Taylor, J., Ridley, H. E., Ottley, C. J., ... & Breitenbach, S. F. (2016). Intra-and interannual uranium concentration variability in a Belizean stalagmite controlled by prior aragonite precipitation: A new tool for reconstructing hydro-climate using aragonitic speleothems. *Geochimica et Cosmochimica Acta*, 190, 332-346.
  - M Brett, S Breitenbach, N Harris, T Ahmad, N Grassineau, S Noble, S Frisia, D Mattey, Annually Laminated speleothem from India, in prep.
  - M Brett, D Mattey & M Stephens, Oceanic conditions drive the atmospheric component over Fiji, submitted to *Journal of Geophysical Research: Atmospheres*.
- Conference proceedings
  - Karst Record VII, Melbourne Australia, oral presentation
  - American Geophysical Union, Fall Meeting 2015, poster presentation
- Study visits
  - University of Newcastle, New South Wales studying confocal microscopy under Prof. Silvia Frisia
  - National Isotope Geochemistry Laboratory, BGS Keyworth, studying U-Th disequilibrium dating chemical separation processes under Dr Diana Sahy and Dr Steve Noble.

7.3 Further work and ongoing challenges

There are a number of questions that are raised as a result of the research presented here:

Does the oceanic component consistently drive the atmospheric component of the SPCZ through time? If the ITCZ deviates further to the south, does the atmospheric component enhance, modulate, or overide the oceanic driver? Is the extent of the oceanic-atmospheric coupling the primary control of the diagonal angle of the SPCZ? If it is, can a speleothem transect of the Pacific Islands provide a record of palaeovariability of SPCZ ocean-atmosphere coupling as changes in the differences between oxygen isotopes on each of the islands?

Some of these questions have been discussed in section 5.4.2 but a more thorough investigation can commence when the next round of U-Th dates are delivered, which are due imminently. This will allow for more robust age modelling of all the samples. Subsequently, high resolution isotope and trace element analyses of the Atiu samples and comparison with both Vat13a and VV10a will test the SPCZ island transect hypothesis.

Bibliography

Akers, P. D., Brook, G. A., Railsback, L. B., Liang, F., Iannone, G., Webster, J. W., Reeder, P. P., Cheng, H., and Edwards, R. L. An extended and higher-resolution record of climate and land use from stalagmite MC01 from Macal Chasm , Belize , revealing connections between major dry events , overall climate variability , and Maya sociopolitical changes. *Palaeogeography, Palaeoclimatology, Palaeoecology*, 459:268–288, 2016. ISSN 0031-0182. doi: 10.1016/j.palaeo.2016.07.007.

Alonso-Zarza, A. M., Martin-Perez, A., Martin-Garcia, R., Gil-Pena, I., Melendez, A., Martinez-Flores, E., Hellstrom, J., and Munoz-Barco, P. Structural and host rock controls on the distribution , morphology and mineralogy of speleothems in the Castanar Cave (Spain). *Geological Magazine*, 148(2):211–225, 2011. doi: 10.1017/S0016756810000506.

Annamalai, H. Intrinsic problems in the seasonal prediction of the Indian summer monsoon rainfall. *Meteorology and Atmospheric Physics*, 55(1-2):61–76, 1995. ISSN 01777971. doi: 10.1007/BF01029602.

Asmerom, Y., Polyak, V., Burns, S., and Rassmussen, J. Solar forcing of Holocene climate: New insights from a speleothem record, southwestern United States. *Geology*, 35(1):1–4, jan 2007. ISSN 0091-7613.

Atkinson, T. C. Diffuse flow and conduit flow in limestone terrain in the Mendip Hills, Somerset (GB). *Journal of Hydrology*, 35:93–110, 1977.

Baker, A. and Fairchild, I. Drip water hydrology and speleothems. *Nature Education Knowledge*, 3(5):16, 2012.

Baker, A. and Brunsdon, C. Non-linearities in drip water hydrology : an example from Stump Cross Caverns , Yorkshire. *Journal of Hydrology*, 277:151–163, 2003. doi: 10.1016/S0022-1694(03)00063-5.

Baker, A., Smith, C. L., Jex, C., Fairchild, I. J., Genty, D., and Fuller, L. Annually laminated speleothems: A review. *International Journal of Speleology*, 37(3):193–206, 2008. ISSN 03926672. doi: 10.5038/1827-806X.37.3.4.

Baldini, J. U. L., McDermott, F., Baker, A., Baldini, L. M., Mattey, D. P., and Railsback, L. B. Biomass effects on stalagmite growth and isotope ratios: A 20th century analogue from Wiltshire, England. *Earth and Planetary Science Letters*, 240(2), 2005. doi: 10.1016/j.epsl.2005.09.022.

Baldini, J. U. L., McDermott, F., Hoffmann, D. L., Richards, D. a., and Clipson, N. Very high-frequency and seasonal cave atmosphere P-CO2 variability: Implications for stalagmite growth and oxygen isotope-based paleoclimate records. *Earth and Planetary Science Letters*, 272(1-2):118–129, jul 2008. ISSN 0012821X. doi: 10.1016/j.epsl.2008.04.031.

Baldini, J. U. L., McDermott, F., Baldini, L. M., Ottley, C. J., Linge, K. L., Clipson, N., and Jarvis, K. E. Identifying short-term and seasonal trends in cave drip water trace element concentrations based on a daily-scale automatically collected drip water dataset. *Chemical Geology*, 330:1–16, nov 2012. ISSN 00092541. doi: 10.1016/j.chemgeo.2012.08.009.

Belli, R., Frisia, S., Borsato, a., Drysdale, R., Hellstrom, J., Zhao, J.-x., and Spötl, C. Regional climate variability and ecosystem responses to the last deglaciation in the northern hemisphere from stable isotope data and calcite fabrics in two northern Adriatic stalagmites. *Quaternary Science Reviews*, 72:146–158, jul 2013. ISSN 02773791. doi: 10.1016/j.quascirev.2013.04.014.

Berkelhammer, M., Sinha, A., Mudelsee, M., Cheng, H., Edwards, R. L., and Cannariato, K. Persistent multidecadal power of the Indian Summer Monsoon. *Earth and Planetary Science Letters*, 290(1):166–172, 2010.

Boch, R. and Spötl, C. Reconstructing palaeoprecipitation from an active cave flowstone. *Journal of Quaternary Science*, 26(7):675–687, 2011. ISSN 02678179. doi: 10.1002/jqs.1490.

Borsato, A., Frisia, S., Fairchild, I. J., Somogyi, A., and Susini, J. Trace element distribution in annual stalagmite laminae mapped by micrometer-resolution X-ray fluorescence: Implications for incorporation of environmentally significant species. *Geochimica Et Cosmochimica Acta*, 71(6):1494–1512, 2007. doi: 10.1016/j.gca.2006.12.016.

Breitenbach, S. F. M., Rehfeld, K., Goswami, B., Baldini, J. U. L., Ridley, H. E., Kennett, D. J., Prufer, K. M., Aquino, V. V., Asmerom, Y., Polyak, V. J., Cheng, H., Kurths, J., and Marwan, N. Constructing proxy records from age models (COPRA). *Climate of the Past*, 8(5):1765–1779, 2012. ISSN 18149324. doi: 10.5194/cp-8-1765-2012.

Breitenbach, S. *Changes in Monsoonal Precipitation and Atmospheric Circulation During the Holocene Reconstructed from Stalagmites from Northeastern India*. PhD thesis, Deutsches GeoForschungsZentrum GFZ, 2010.

Brijker, J., Jung, S., Ganssen, G., Bickert, T., and Kroon, D. ENSO related decadal scale climate variability from the Indo-Pacific Warm Pool. *Earth and Planetary Science Letters*, 253(1-2):67–82, jan 2007. ISSN 0012821X. doi: 10.1016/j.epsl.2006.10.017.

Brown, J. R., Moise, A. F., and Colman, R. A. The South Pacific Convergence Zone in CMIP5 simulations of historical and future climate. *Climate Dynamics*, 41(7-8):2179–2197, 2013. ISSN 09307575. doi: 10.1007/s00382-012-1591-x.

Cailleau, G., Verrecchia, E. P., Braissant, O., and Emmanuel, L. The biogenic origin of needle fibre calcite. *Sedimentology*, 56(6):1858–1875, 2009. ISSN 00370746. doi: 10.1111/j.1365-3091.2009.01060.x.

Campbell, I., Wilde, R., Wilson, A., Frisby, R. H., and McCormack, D. Soil map of atiu, cook islands. 1980.

Chen, M., Xie, P., Janowiak, J. E., and Arkin, P. A. Global land precipitation: A 50-yr monthly analysis based on gauge observations. *Journal of Hydrometeorology*, 3(3): 249–266, 2002.

Chen, S. S. and Houze Jr, R. A. Diurnal variation and life cycle of deep convective systems over the tropical Pacific warm pool, 1997. ISSN 1477870X.

Collister, C. and Mattey, D. Controls on water drop volume at speleothem drip sites: An experimental study. *Journal of Hydrology*, 358(3-4):259–267, 2008. ISSN 00221694. doi: 10.1016/j.jhydrol.2008.06.008.

Cosford, J., Qing, H., Mattey, D., Eglington, B., and Zhang, M. Climatic and local effects on stalagmite delta C-13 values at Lianhua Cave, China. *Palaeogeography Palaeoclimatology Palaeoecology*, 280(1-2), 2009. doi: 10.1016/j.palaeo.2009.05.020.

Dai, A. and Wigley, T. M. L. Global patterns of ENSO-induced precipitation. *Geophysical Research Letters*, 27(9):1283–1286, 2000. ISSN 00948276. doi: 10.1029/1999GL011140.

Dansgaard, W. Stable isotopes in precipitation. *Tellus A*, 1964. ISSN 0280-6495. doi: 10.3402/tellusa.v16i4.8993.

De Boever, E., Brasier, A. T., Foubert, A., and Kele, S. What do we really know about early diagenesis of non-marine carbonates? *Sedimentary Geology*, 2017.

De Deckker, P. The Indo-Pacific Warm Pool: critical to world oceanography and world climate. *Geoscience Letters*, 3(1):20, 2016. ISSN 2196-4092. doi: 10.1186/s40562-016-0054-3.

Deininger, M. *The European Holocene Climate from the Speleothem's View: Investigating*

spatio-temporal coherent changes in European speleothem proxy time series. PhD thesis, Heidelberg, 2013.

Dennis, P., Rowe, P., and Atkinson, T. The recovery and isotopic measurement of water from fluid inclusions in speleothems. *Geochimica et Cosmochimica Acta*, 65(6):871–884, 2001.

Denniston, R. F., Gonzalez, L. A., Baker, R. G., Asmerom, Y., Reagan, M. K., Edwards, R. L., and Alexander, E. C. Speleothem evidence for Holocene fluctuations of the prairie-forest ecotone, north-central USA. *Holocene*, 9(6), 1999. doi: 10.1191/095968399674716399.

Domínguez-Villar, D., Baker, A., Fairchild, I. J., Edwards, R. L., Dominguez-Villar, D., Baker, A., Fairchild, I. J., and Edwards, R. L. A method to anchor floating chronologies in annually laminated speleothems with U-Th dates. *Quaternary Geochronology*, 14:57–66, 2012. ISSN 18711014. doi: 10.1016/j.quageo.2012.04.019.

Dorale, J. A. and Liu, Z. Limitations of hendy test criteria in judging the paleoclimatic suitability of speleothems and the need for replication. *Journal of Cave and Karst Studies*, 71(1):73–80, 2009. ISSN 10906924. doi: PNR61.

Dorale, J. A., Lawrence Edwards, R., Ito, E., and Gonzalez, L. A. Climate and Vegetation History of the Midcontinent from 75 to 25 ka: A Speleothem Record from Crevice Cave, Missouri, USA. *Science*, 282(5395):1871–1874, 1998. doi: 10.1126/science.282.5395.1871.

Dreybrodt, W. Chemical kinetics, speleothem growth and climate. *Boreas*, 28(3):347–356, jan 1999. ISSN 0300-9483. doi: 10.1080/030094899422073.

Dreybrodt, W. and Scholz, D. Climatic dependence of stable carbon and oxygen isotope signals recorded in speleothems: From soil water to speleothem calcite. *Geochimica et Cosmochimica Acta*, 75(3):734–752, feb 2011. ISSN 00167037. doi: 10.1016/j.gca.2010.11.002.

Evans, D. and Muller, W. LA-ICPMS elemental imaging of complex discontinuous carbonates: An example using large benthic foraminifera. *Journal of Analytical Atomic Spectrometry*, 28(7):961–1132, 2013. doi: 10.1039/c3ja50053e.

Fairchild, I. J. and Baker, A. *Speleothem Science: From Process to Past Environments*. John Wiley & Sons, 2012.

Fairchild, I. J. and Treble, P. C. Trace elements in speleothems as recorders of environmental change. *Quaternary Science Reviews*, 28(5-6):449–468, mar 2009. ISSN 02773791. doi: 10.1016/j.quascirev.2008.11.007.

Fairchild, I. J., Borsato, A., Tooth, A. F., Frisia, S., Hawkesworth, C. J., Huang, Y., McDermott, F., and Spiro, B. Controls on trace element (sr–mg) compositions of carbonate cave waters: implications for speleothem climatic records. *Chemical Geology*, 166(3-4): 255–269, 2000.

Fairchild, I. J., Frisia, S., Borsato, A., and Tooth, A. Speleothems. In Nash, D. J. and McLaren, S. J., editors, *Geochemical Sediments and Landscapes*, chapter 7, pages 1–21. Wiley-Blackwell, 2007. ISBN 978-1-4051-2519-2.

Fairchild, I., Smith, C., Baker, A., and Fuller, L. Modification and preservation of environmental signals in speleothems. *Earth-Science ...*, 44(January):1–41, 2006.

Finch, A. A., Shaw, P. a., Weedon, G. P., and Holmgren, K. Trace element variation in speleothem aragonite: potential for palaeoenvironmental reconstruction. *Earth and Planetary Science Letters*, 186(2):255–267, mar 2001. ISSN 0012821X. doi: 10.1016/S0012-821X(01)00253-9.

Fleitmann, D., Burns, S. J., Mangini, A., Mudelsee, M., Kramers, J., Villa, I., Neff, U., Al-Subbary, A. A., Buettner, A., Hippler, D., and Matter, A. Holocene ITCZ and Indian monsoon dynamics recorded in stalagmites from Oman and Yemen (Socotra). *Quaternary Science Reviews*, 26(1-2):170–188, jan 2007. ISSN 02773791. doi: 10.1016/j.quascirev.2006.04.012.

Folland, C. K. Relative influences of the Interdecadal Pacific Oscillation and ENSO on the South Pacific Convergence Zone, 2002. ISSN 0094-8276.

Frappier, A. B., Sahagian, D., Carpenter, S. J., González, L. a., Frappier, B. R., and Gonzalez, L. A. Stalagmite stable isotope record of recent tropical cyclone events. *Geology*, 35(2):111–114, 2007. ISSN 0091-7613. doi: 10.1130/g23145a.1.

Friedman, I., O'Neil, J., and Cebula, G. Two New Carbonate StableIsotope Standards. *Geostandards and Geoanalytical Research*, 6(1):11–12, 1982.

Frisia, S. Microstratigraphic logging of calcite fabrics in speleothems as tool for palaeoclimate studies. *International Journal of Speleology*, 2015.

Frisia, S. and Borsato, A. Calcite fabrics, growth mechanisms, and environments of formation in speleothems from the Italian Alps and southwestern Ireland. *Journal of ...*, 2000.

Gao, H., Wang, Y., and He, J. Weakening significance of ENSO as a predictor of summer precipitation in China. *Geophysical Research Letters*, 33(9):2–5, 2006. ISSN 00948276. doi: 10.1029/2005GL025511.

Gascoyne, M. Palaeoclimate determination from cave calcite deposits. *Quaternary Science Reviews*, 11(6):609–632, 1992. ISSN 02773791. doi: 10.1016/0277-3791(92)90074-I.

Gergis, L. L. E., Braganza, K., Fowler, A., Mooney, S., and Risbey, J. Reconstructing El Nino Southern Oscillation (ENSO) from high-resolution palaeoarchives. *Journal of Quaternary Science*, 21:707–722, 2006. doi: 10.1002/jqs.

Gouriou, Y. and Delcroix, T. Seasonal and ENSO variations of sea surface salinity and temperature in the South Pacific Convergence Zone during 19762000. *Journal of Geophysical Research: Oceans*, 107, 2002.

Griffiths, M. L., Drysdale, R. N., Gagan, M. K., Frisia, S., Zhao, J.-x., Ayliffe, L. K., Hantoro, W. S., Hellstrom, J. C., Fischer, M. J., and Feng, Y.-X. Evidence for Holocene changes in AustralianIndonesian monsoon rainfall from stalagmite trace element and stable isotope ratios. *Earth and Planetary Science Letters*, 292(1-2):27–38, mar 2010. ISSN 0012821X. doi: 10.1016/j.epsl.2010.01.002.

Gröning, M., Dargie, M., and Winckler, G. Reference sheet for reference materials. Technical report, International Atomic Energy Agency (IAEA), 2007.

Gupta, A. K., Anderson, D. M., and Overpeck, J. T. Abrupt changes in the Asian southwest monsoon during the Holocene and their links to the North Atlantic Ocean. *Nature*, 421 (6921):354–357, 2003. ISSN 0028-0836. doi: 10.1038/nature01340.

Gvirtzman, G., Friedman, G. M., and Miller, D. S. Control and Distribution of Uranium in Coral Reefs During Diagenesis. *Journal of Sedimentary Petrology*, 43(4):985–997, 1973.

Ham, Y. G., Choi, J. Y., and Kug, J. S. The weakening of the ENSOIndian Ocean Dipole (IOD) coupling strength in recent decades. *Climate Dynamics*, 49(1-2):249–261, 2017. ISSN 14320894. doi: 10.1007/s00382-016-3339-5.

Harmon, R. S., Schwarcz, H. P., Gascoyne, M., Hess, J. W., and Ford, D. C. Palaeoclimate information from Speleothems: the present as a guide to the past. In *Studies of Cave Sediments*, pages 199–226. Springer Berlin Heidelberg, 2004. doi: /10.1007/978-1-4419-9118-8.

Hartland, A., Fairchild, I. J., Lead, J. R., Borsato, A., Baker, A., Frisia, S., and Baalousha, M. From soil to cave: Transport of trace metals by natural organic matter in karst dripwaters. *Chemical Geology*, 304:68–82, apr 2012. ISSN 00092541. doi: 10.1016/j.chemgeo.2012.01.032.

Hausfather, Z., Menne, M. J., Williams, C. N., Masters, T., Broberg, R., and Jones, D. Quantifying the effect of urbanization on u.s. Historical climatology network tempera-

ture records. *Journal of Geophysical Research Atmospheres*, 118(2):481–494, 2013. ISSN 21698996. doi: 10.1029/2012JD018509.

Hendy, C. H. The isotopic geochemistry of speleothems-I . The calculation of the effects of different modes of formation on the isotopic composition of speleothems and their applicability as palaeoclimatic indicators. *Geochimica et Cosmochimica Acta*, 35(386), 1971.

Henley, B. J., Gergis, J., Karoly, D. J., Power, S., Kennedy, J., and Folland, C. K. A Tripole Index for the Interdecadal Pacific Oscillation. *Climate Dynamics*, pages 3077–3090, 2015. ISSN 0930-7575. doi: 10.1007/s00382-015-2525-1.

Hess, J. W. *Karst Modelling*. Karst Waters Institue, 1999. ISBN 0964025841.

Hut, G. Consultants' group meeting on stable isotope reference samples for geochemical and hydrological investigations. Technical report, International Atomic Energy Agency, 1987.

Jamieson, R. A., Baldini, J. U. L., Frappier, A. B., and M??ller, W. Volcanic ash fall events identified using principal component analysis of a high-resolution speleothem trace element dataset. *Earth and Planetary Science Letters*, 426:36–45, 2015. ISSN 0012821X. doi: 10.1016/j.epsl.2015.06.014.

Jochum, K. P., Scholz, D., Stoll, B., Weis, U., Wilson, S. a., Yang, Q., Schwalb, A., Börner, N., Jacob, D. E., and Andreae, M. O. Accurate trace element analysis of speleothems and biogenic calcium carbonates by LA-ICP-MS. *Chemical Geology*, 318-319:31–44, jul 2012. ISSN 00092541. doi: 10.1016/j.chemgeo.2012.05.009.

Julian, P. R. and Chervin, R. M. A Study of the Southern Oscillation and Walker Circulation Phenomenon, 1978. ISSN 0027-0644.

Kluge, T., Marx, T., Scholz, D., Niggemann, S., Mangini, A., and Aeschbach-Hertig, W. A new tool for palaeoclimate reconstruction: Noble gas temperatures from fluid inclusions in speleothems. *Earth and Planetary Science Letters*, 269(3):408–415, 2008.

Kluge, T. and Affek, H. P. Quantifying kinetic fractionation in Bunker Cave speleothems using D 47. *Quaternary Science Reviews*, 49:82–94, 2012. ISSN 0277-3791. doi: 10.1016/j.quascirev.2012.06.013.

Kumar, K. K. On the Weakening Relationship Between the Indian Monsoon and ENSO. *Science*, 284(5423):2156–2159, jun 1999. ISSN 00368075. doi: 10.1126/science.284.5423.2156.

Lachniet, M. S. Climatic and environmental controls on speleothem oxygen-isotope values.

Quaternary Science Reviews, 28(5-6):412–432, 2009. ISSN 02773791. doi: 10.1016/j.quascirev.2008.10.021.

Lachniet, M. S., Burns, S. J., Piperno, D. R., Asmerom, Y., Polyak, V. J., Moy, C. M., and Christenson, K. A 1500-year El Niño/Southern Oscillation and rainfall history for the Isthmus of Panama from speleothem calcite. *Journal of Geophysical Research D: Atmospheres*, 109(20):1–8, 2004. ISSN 01480227. doi: 10.1029/2004JD004694.

Li, H.-C., Lee, Z.-H., Wan, N.-J., Shen, C.-C., Li, T.-Y., Yuan, D.-X., and Chen, Y.-H. The delta O-18 and delta C-13 records in an aragonite stalagmite from Furong Cave, Chongqing, China: A-2000-year record of monsoonal climate. *Journal of Asian Earth Sciences*, 40(6):1121–1130, 2011. doi: 10.1016/j.jseaes.2010.06.011.

Liang, F., Brook, G. A., Kotlia, B. S., Railsback, L. B., Hardt, B., Cheng, H., Edwards, R. L., and Kandasamy, S. Panigarh cave stalagmite evidence of climate change in the Indian Central Himalaya since AD 1256 : Monsoon breaks and winter southern jet depressions. *Quaternary Science Reviews*, 124:145–161, 2015. ISSN 0277-3791. doi: 10.1016/j.quascirev.2015.07.017.

Lintner, B. R., Langenbrunner, B., Neelin, J. D., Anderson, B. T., Niznik, M. J., Li, G., and Xie, S.-P. Characterizing cmip5 model spread in simulated rainfall in the pacific intertropical convergence and south pacific convergence zones. *Journal of Geophysical Research: Atmospheres*, 121(19), 2016.

Lorrey, A., Dalu, G., Renwick, J., Diamond, H., and Gaetani, M. Reconstructing the South Pacific Convergence Zone Position during the Presatellite Era: A La Niña Case Study. *Monthly Weather Review*, 140(11):3653–3668, nov 2012. ISSN 0027-0644. doi: 10.1175/MWR-D-11-00228.1.

Madden, R. A. and Julian, P. R. Observations of the 40-50-day Tropical Oscillation - A Review. *Monthly Weather Review*, 122:814–837, 1994.

Mattey, D. P., Atkinson, T. C., Barker, J. A., Fisher, R., Latin, J., Durrell, R., and Ainsworth, M. Carbon dioxide , ground air and carbon cycling in Gibraltar karst. *Geochimica et Cosmochimica Acta*, 184:88–113, 2016. ISSN 0016-7037. doi: 10.1016/j.gca.2016.01.041.

Mattey, D., Lowry, D., Duffet, J., Fisher, R., Hodge, E., and Frisia, S. A 53 year seasonally resolved oxygen and carbon isotope record from a modern gibraltar speleothem: reconstructed drip water and relationship to local precipitation. *Earth and Planetary Science Letters*, 269(1):80–95, 2008.

Maupin, C. R., Partin, J. W., Shen, C.-C., Quinn, T. M., Lin, K., Taylor, F. W., Banner, J. L., Thirumalai, K., and Sinclair, D. J. Persistent decadal-scale rainfall variability in the tropical South Pacific Convergence Zone through the past six centuries. *Climate of the Past*, 10(4):1319–1332, jul 2014. ISSN 1814-9332. doi: 10.5194/cp-10-1319-2014.

McDermott, F. Palaeo-climate reconstruction from stable isotope variations in speleothems : a review. *Quaternary Science Reviews*, 23:901–918, 2004. doi: 10.1016/j.quascirev.2003.06.021.

McDonald, J. and Drysdale, R. Hydrology of cave drip waters at varying bedrock depths from a karst system in southeastern Australia. *Hydrological Processes*, 21:1737–1748, 2007. ISSN 08856087. doi: 10.1002/hyp.6356.

Medina-Elizalde, M., Burns, S. J., Lea, D. W., Asmerom, Y., von Gunten, L., Polyak, V., Vuille, M., and Karmalkar, A. High resolution stalagmite climate record from the Yucatan Peninsula spanning the Maya terminal classic period. *Earth and Planetary Science Letters*, 298(1-2):255–262, 2010. ISSN 0012821X. doi: 10.1016/j.epsl.2010.08.016.

Mehterian, S., Pourmand, A., Shari, A., Lahijani, H. A. K., Naderi, M., and Swart, P. K. Speleothem records of glacial / interglacial climate from Iran forewarn of future Water Availability in the interior of the Middle East. *Quaternary Science Reviews*, 164:187–198, 2017. doi: 10.1016/j.quascirev.2017.03.028.

Meyer, K. W., Feng, W., Breecker, D. O., Banner, J. L., and Guilfoyle, A. Interpretation of speleothem calcite d13C variations: Evidence from monitoring soil CO2, drip water, and modern speleothem calcite in central Texas. *Geochimica et Cosmochimica Acta*, 142 (August):281–298, 2014. ISSN 00167037. doi: 10.1016/j.gca.2014.07.027.

Muñoz-García, M., López-Arce, P., Fernández-Valle, M., Martín-Chivelet, J., and Fort, R. Porosity and hydric behavior of typical calcite microfabrics in stalagmites. *Sedimentary Geology*, 265:72–86, 2012.

Mylroie, J. E. Coastal Caves. *Speleogenesis and Evolution of Karst Aquifers*, 4(1):155–161, 2005. doi: 10.1016/B978-0-12-374144-8.00055-2.

Nehme, C., Verheyden, S., Noble, S., Farrant, A., and J-J, D. Contribution of an accurate growth rate reconstruction of a stalagmite from the Kanaan Cave-Lebanon to the understanding of humidity variations in the Levant during the MIS 5. *Geologica Belgica*, 18 (2-4):102–108, 2015.

Niznik, M. J., Lintner, B. R., Matthews, A. J., and Widlansky, M. J. The role of tropical-extratropical interaction and synoptic variability in maintaining the south pacific conver-

gence zone in CMIP5 models. *Journal of Climate*, 28(8):3353–3374, 2015. ISSN 08948755. doi: 10.1175/JCLI-D-14-00527.1.

Oppo, D. W., Rosenthal, Y., and Linsley, B. K. 2,000-year-long temperature and hydrology reconstructions from the Indo-Pacific warm pool. *Nature*, 460(7259):1113–6, aug 2009. ISSN 1476-4687. doi: 10.1038/nature08233.

Ortega, R., Maire, R., Devès, G., and Quinif, Y. High-resolution mapping of uranium and other trace elements in recrystallized aragonite–calcite speleothems from caves in the pyrenees (france): implication for u-series dating. *Earth and Planetary Science Letters*, 237(3):911–923, 2005.

Oster, J. L., Montanez, I. P., and Kelley, N. P. Response of a modern cave system to large seasonal precipitation variability. *Geochimica Et Cosmochimica Acta*, 91, 2012. doi: 10.1016/j.gca.2012.05.027.

Pardo-Igúzquiza, E. and Rodríguez-Tovar, F. J. Spectral and cross-spectral analysis of uneven time series with the smoothed Lomb-Scargle periodogram and Monte Carlo evaluation of statistical significance. *Computers and Geosciences*, 49:207–216, 2012. ISSN 00983004. doi: 10.1016/j.cageo.2012.06.018.

Partin, J. W., Quinn, T. M., Shen, C.-C., Emile-Geay, J., Taylor, F. W., Maupin, C. R., Lin, K., Jackson, C. S., Banner, J. L., Sinclair, D. J., and Huh, C.-a. Multidecadal rainfall variability in South Pacific Convergence Zone as revealed by stalagmite geochemistry. *Geology*, 41(11):1143–1146, sep 2013. ISSN 0091-7613. doi: 10.1130/G34718.1.

Perrin, C., Prestimonaco, L., Servelle, G., Tilhac, R., Maury, M., and Cabrol, P. Aragonite–calcite speleothems: identifying original and diagenetic features. *Journal of Sedimentary Research*, 84(4):245–269, 2014.

Pfeiffer, M., Timm, O., Dullo, W.-C., and Garbe-Schönberg, D. Paired coral Sr/Ca and δ18O records from the Chagos Archipelago: Late twentieth century warming affects rainfall variability in the tropical Indian Ocean. *Geology*, 34(12):1069, 2006. ISSN 0091-7613. doi: 10.1130/G23162A.1.

Rasbury, M. and Aharon, P. ENSO-controlled rainfall variability records archived in tropical stalagmites from the mid-ocean island of Niue, South Pacific. *Geochemistry, Geophysics, Geosystems*, 7(7):n/a–n/a, jul 2006. ISSN 15252027. doi: 10.1029/2005GC001232.

Rehfeld, K., Marwan, N., Breitenbach, S. F. M., and Kurths, J. Late Holocene Asian Summer Monsoon dynamics from small but complex networks of palaeoclimate data. *Climate Dynamics*, 41(1):3–19, 2012. ISSN 0930-7575. doi: 10.1007/s00382-012-1448-3.

Riechelmann, D. F., Deininger, M., Scholz, D., Riechelmann, S., Schröder-Ritzrau, A., Spötl, C., Richter, D. K., Mangini, A., and Immenhauser, A. Disequilibrium carbon and oxygen isotope fractionation in recent cave calcite: Comparison of cave precipitates and model data. *Geochimica et Cosmochimica Acta*, 103:232–244, feb 2013. ISSN 00167037. doi: 10.1016/j.gca.2012.11.002.

Rutlidge, H., Baker, A., Marjo, C. E., Andersen, M. S., Graham, P. W., Cuthbert, M. O., Rau, G. C., Roshan, H., Markowska, M., Mariethoz, G., and Jex, C. N. Dripwater organic matter and trace element geochemistry in a semi-arid karst environment: Implications for speleothem paleoclimatology. *Geochimica et Cosmochimica Acta*, 135:217–230, 2014. ISSN 00167037. doi: 10.1016/j.gca.2014.03.036.

Saji, N. H., Goswami, B. N., Vinayachandran, P. N., and Yamagata, T. A dipole mode in the tropical Indian Ocean. *Nature*, 401(6751):360–3, sep 1999. ISSN 0028-0836. doi: 10.1038/43854.

Scholz, D. and Hoffmann, D. L. StalAge An algorithm designed for construction of speleothem age models. *Quaternary Geochronology*, 6(3-4):369–382, jun 2011. ISSN 18711014. doi: 10.1016/j.quageo.2011.02.002.

Sharp, Z. *Principles of Stable Isotope Geochemistry.* Pearson, 2nd edition, 2017. ISBN 978-0130091390.

Shen, C. C., Li, K. S., Sieh, K., Natawidjaja, D., Cheng, H., Wang, X., Edwards, R. L., Lam, D. D., Hsieh, Y. T., Fan, T. Y., Meltzner, A. J., Taylor, F. W., Quinn, T. M., Chiang, H. W., and Kilbourne, K. H. Variation of initial 230Th/232Th and limits of high precision U-Th dating of shallow-water corals. *Geochimica et Cosmochimica Acta*, 72(17):4201–4223, 2008. ISSN 00167037. doi: 10.1016/j.gca.2008.06.011.

Short, M. B., Baygents, J. C., Beck, J. W., Stone, D. A., Iii, R. S. T., and Goldstein, R. E. Stalactite Growth as a Free-Boundary Problem : A Geometric Law and Its Platonic Ideal. *Physical Review Letters*, 018501(January):14–17, 2005. doi: 10.1103/PhysRevLett.94.018501.

Sinha, A., Cannariato, K. G., Stott, L. D., Cheng, H., Edwards, R. L., Yadava, M. G., Ramesh, R., and Singh, I. B. A 900-year (600 to 1500 A.D.) record of the Indian summer monsoon precipitation from the core monsoon zone of India. *Geophysical Research Letters*, 34(16), 2007. ISSN 00948276. doi: 10.1029/2007GL030431.

Smith, A. C., Wynn, P. M., Barker, P. A., Leng, M. J., Noble, S. R., and Tych, W. North atlantic forcing of moisture delivery to europe throughout the holocene. *Scientific reports*, 6, 2016.

Smith, C. L., Fairchild, I. J., Spötl, C., Frisia, S., Borsato, A., Moreton, S. G., Wynn, P. M., and Spoetl, C. Chronology building using objective identification of annual signals in trace element profiles of stalagmites. *Quaternary Geochronology*, 4(1):11–21, feb 2009. ISSN 18711014. doi: 10.1016/j.quageo.2008.06.005.

Spötl, C. and Mangini, A. Stalagmite from the Austrian Alps reveals Dansgaard - Oeschger events during isotope stage 3 : Implications for the absolute chronology of Greenland ice cores. *Earth and Planetary Science Letters*, 203:507–518, 2002.

Stichler, W. Interlaboratory comparison of new materials for carbon and oxygen isotope ratio measurements. *Reference and intercomparison materials for stable isotopes of light elements*, pages 67–74, 1995.

Stolper, D. A., Bender, M. L., Dreyfus, G. B., Yan, Y., and Higgins, J. A. A Pleistocene ice core record of atmospheric O2 concentrations. *Science*, 353(6306):1427–1430, 2016. ISSN 0036-8075. doi: 10.1126/science.aaf5445.

Thornthwaite, C. W. An Approach toward a Rational Classification of Climate. *Geographical Review*, 38(1):55–94, 1948. doi: 10.2307/210739.

Tokinaga, H., Xie, S.-P. P., Deser, C., Kosaka, Y., and Okumura, Y. M. Slowdown of the Walker circulation driven by tropical Indo-Pacific warming. *Nature Research Letter*, 491 (7424):439–443, 2012. ISSN 0028-0836. doi: 10.1038/nature11576.

van der Wiel, K., Matthews, A. J., Joshi, M. M., and Stevens, D. P. Why the South Pacific Convergence Zone is diagonal. *Climate Dynamics*, 2015. ISSN 0930-7575. doi: 10.1007/s00382-015-2668-0.

Vilhena, D. A. and Smith, A. B. Spatial Bias in the Marine Fossil Record. *PLoS ONE*, 8 (10):e74470, 2013. ISSN 1932-6203. doi: 10.1371/journal.pone.0074470.

Vincent, E. M., Lengaigne, M., Menkes, C. E., Jourdain, N. C., Marchesiello, P., and Madec, G. Interannual variability of the South Pacific Convergence Zone and implications for tropical cyclone genesis. *Climate Dynamics*, 36(9-10):1881–1896, dec 2011. ISSN 0930-7575. doi: 10.1007/s00382-009-0716-3.

Walczak, I. W., Baldini, J. U., Baldini, L. M., McDermott, F., Marsden, S., Standish, C. D., Richards, D. A., Andreo, B., and Slater, J. Reconstructing high-resolution climate using CT scanning of unsectioned stalagmites: A case study identifying the mid-Holocene onset of the Mediterranean climate in southern Iberia. *Quaternary Science Reviews*, 127: 117–128, 2015. ISSN 02773791. doi: 10.1016/j.quascirev.2015.06.013.

Wang, H. and Mehta, V. M. Decadal variability of the Indo-Pacific warm pool and its

association with atmospheric and oceanic variability in the NCEP-NCAR and SODA reanalyses. *Journal of Climate*, 21(21):5545–5565, 2008. ISSN 08948755. doi: 10.1175/2008JCLI2049.1.

Wang, Y., Cheng, H., Edwards, R. L., Kong, X., Shao, X., Chen, S., Wu, J., Jiang, X., Wang, X., and An, Z. Millennial- and orbital-scale changes in the East Asian monsoon over the past 224,000 years. *Nature*, 451(7182):1090–3, 2008. ISSN 1476-4687. doi: 10.1038/nature06692.

Watling, D. and Pernetta, J. Limestone caves in the sigatoka valley, viti levu, fiji. *Studies in Speleology*, 3:78–86, 1978.

Weller, E., Min, S.-k., Cai, W., Zwiers, F. W., Kim, Y.-h., and Lee, D. Human-caused Indo-Pacific warm pool expansion. *Science Advances*, 2(7):1–8, 2016.

Widlansky, M. J., Webster, P. J., and Hoyos, C. D. On the location and orientation of the South Pacific Convergence Zone. *Climate Dynamics*, 36:561–578, 2011. ISSN 09307575. doi: 10.1007/s00382-010-0871-6.

Winograd, I. J., Coplen, T. B., Landwehr, J. M., Riggs, A. C., Ludwig, K. R., Szabo, B. J., Kolesar, P. T., and Revesz, K. M. Continuous 500,000-year climate record from vein calcite in devils hole, nevada. *Science (New York, N.Y.)*, 258(5080):255–60, 1992. ISSN 0036-8075. doi: 10.1126/science.258.5080.255.

Woodroffe, C. D., Short, S. A., Stoddart, D. R., Spencer, T., and Harmon, R. S. Stratigraphy and chronology of late pleistocene reefs in the Southern Cook Islands, south Pacific. *Quaternary Research*, 35(2):246–263, 1991. ISSN 10960287. doi: 10.1016/0033-5894(91)90071-C.

Wu, J. Y., Wang, Y. J., Cheng, H., Kong, X. G., and Liu, D. B. Stable isotope and trace element investigation of two contemporaneous annually-laminated stalagmites from northeastern China surrounding the 8 . 2 ka event . *Climate of the Past*, 8:1497–1507, 2012. doi: 10.5194/cp-8-1497-2012.

Wynn, P. M., Fairchild, I. J., Baker, A., Baldini, J. U., and McDermott, F. Isotopic archives of sulphate in speleothems. *Geochimica et Cosmochimica Acta*, 72(10):2465–2477, 2008.

Yadava, M. G. and Ramesh, R. Monsoon reconstruction from radiocarbon dated tropical Indian speleothems. *The Holocene*, 15(1):48–59, 2005. doi: 10.1191/0959683605h1783rp.

Yuan, D., Cheng, H., Edwards, R. L., Dykoski, C. A., Kelly, M. J., Zhang, M., Qing, J., Lin, Y., Wang, Y., Wu, J., Dorale, J. A., An, Z., and Cai, Y. Transitions of the Last Interglacial Asian Monsoon. *Science*, 304(April):575–578, 2004. doi: 10.1126/science.1091220.

Zisu, N. S., Schwarcz, H. P., Konyer, N., Chow, T., and Noseworthy, M. D. Macroholes in stalagmites and the search for lost water. *Journal of Geophysical Research: Earth Surface*, 117(3):1–14, 2012. ISSN 21699011. doi: 10.1029/2011JF002288.

Appendices

A Relating to methodology

Appendices relating to the methodological chapter are detailed below and can be found on the enclosed compact disc in folder Appendix A Methods.

File name	Type	Description
Past3	.exe	Paleontological Statistics Software from Øyvind Hammer, University of Oslo. Version 3. Used for all statistical analysis within the thesis.
Past3manual	PDF	Past3.16 reference manual. Includes references and explanations of all statistical functions.
CFIRMS Calcite Reference Materials	.xlsx	Batch results sheet for stretch calibration of CF-IRMS output to reference materials NBS19 and LSVEC, with internal lab standard RHBNC, and type samples from Vat13a.
CFIRMS Linearity test	.xlsx	Results sheet for CFIRMS linearity tests ascertaining acceptable peak height window for precise results.
CFIRMS Water Standards Calibration	.xlsx	Results for calibration tests between two batches of international reference materials, plus internal lab standards "DEW" and "MX"

File name	Type	Description
GHCN Gauhati	.csv	Global Historical Climatology Network (GHCN), Gauhati station rainfall data
GHCN Jowai station rainfall	.xlsx	GHCN Jowai station rainfall data 1901 - 1968
GNIP SHILLONG	.xlsx	Global Networks of Isotopes in Precipitation, Station 4251600, Shillong, 1966 - 1978
SB DM IMD data	.xlsx	Compilation of data from Breitenbach's 2010 data, monsoon reports from the Indian Department of Meteorology and data from NEHU
Monsoon rain analysis	.xlsx	Rain isotopes both from Breitenbach and analysed here, plus regional comparisons with other datasets.
Shillong HYSPLIT output	.ppt	Collection of trajectory frequency plots from the HYSPLIT model, for different months of 2010, 2011 and 2012. Point of origin nearby rain sampling site.

B Relating to India

B.1 India Rain data

Global Historical Climatology Network data accessed from the National Climatic Data Center, National Oceanic Atmospheric Administration.

Menne, M.J., I. Durre, R.S. Vose, B.E. Gleason, and T.G. Houston, 2012: An overview of the Global Historical Climatology Network-Daily Database. Journal of Atmospheric and Oceanic Technology, 29, 897-910, doi.10.1175/JTECH-D-11-00103.1.

B.2 Heritage Stal data

All data within folder "B2 Heritage Stal Data" is from work produced prior to commencement of doctoral training. The creators of these data are credited in file name and table below.

File name	Type	Description
Hodkin Laminae Counts	.xlsx	UMS10 Lamina counting data including extension rates (Dave Hodkin), StalAge age model (Dave Hodkin) and preliminary COPRA age model (Brett).
Stable isotopes UMS10	.xlsx	Work of Grassineau, Hodkin and Mattey. Micromilled 0.1 mm and 4 mm resolution stable isotope traverses for UMS10 are found here.
Trace elements B4 Grassineau	.xlsx	Section B4 trace element traverses using LAICPMS. Work of Nathalie Grassineau, with additional work by D Mattey.
Trace elements UMS Hodkin4	.xlsx	Trace element traverse using LAICPMS by D Hodkin.
Trace elements UMS Hodkin6	.xlsx	Trace element traverse using LAICPMS by D Hodkin.

B.3 Trace elements and Isotopes

Folder "B3 Trace elements Isotopes" contains stable isotope data, and trace element statistical analysis produced by the candidate.

File name	Type	Description
Master 1mm stable isotopes	.xlsx	1mm contiguous isotope traverse of UMS10 including plots, fabrics and Hendy tests.
UMS10 TEs PCA	.xlsx	UMS10 trace elements Principal Component Analysis summary and loadings, using Past3 as Appendix A

B.4 Age modelling

File name	Type	Description
2014 U series data batch a	.xlsx	Uranium series dating results from NIGL. Batch 1 (of 2) analysed in 2014.
2014 U series data batch b	.xlsx	Uranium series dating results from NIGL. Batch 2 (of 2) analysed in 2014.
Composite age model final	.xlsx	Final version of composite age model with isotopes, based on development in "time series development.xlsx"
COPRA 2010 dates	.xlsx	COPRA output with only the 2010 Open University ages.
COPRA all good dates	.xlsx	COPRA output using 2010, 2014a and 2014b U-Th ages
Stalage 2010 dates	.xlsx	StalAge output with only the 2010 Open University ages.
StalAge all good dates	.xlsx	StalAge output using 2010, 2014a and 2014b U-Th ages
Time series development	.xlsx	Use of annual layering extension rates, COPRA and StalAge output to create time series and compare with other proxy records
U-Th dates master	.xlsx	All U-Th data from all batches including Open University 2010 and 2012, and NIGL 2014a and 2014b

B.5 Imaging

File name	Type	Description
Microscopy	Folder	Stereomicroscopy video images of UMS10 thin sections arranged by slide number. Both XPL and PPL in individual file names, and scale bars within image.
UVF	Folder	Ultraviolet Fluorescence confocal microscopy output from UMS10 thick sections. Slide number indicated in individual file name.
UMS10 spliced	.jpg	UMS10 scanned after dissection and spliced together, to allow accurate measurement of sections distance from tip.

B.6 Other records

File name	Type	Description
2004 Dongge	.txt	Yuan, D., et al., 2004. Dongge Cave Stalagmite Oxygen Isotope Data
2006 Dongge	.txt	Wang, Y. et al. 2006. Dongge Cave Stalagmite High-Resolution Holocene d18O Data
2650 Beijing	.txt	Tan, M., et al., 2003, 2650-Year Beijing Stalagmite Layer Thickness and Temperature Reconstruction
dasuopu2000	.xls	Thompson, L.G., et al. 2011. Dasuopu Ice Core 1000 Year d18O, Dust and Accumulation Data.
dunde2006	.xls	Thompson, L.G., et al. 2012. Dunde Ice Core 1500 Year d18O, Dust, Anion, and Accumulation Data.
East Rongbuk Ice Core	.txt	Hou Shugui, et al., 2003, East Rongbuk Glacier, Mt. Everest, Chemistry and Stable Isotope Data
jhumar-wah-shikar2011	.xlsx	Sinha, A., et al. 2011. Central and Northeast India 1000 Year Stalagmite Oxygen Isotope Data.
mawmluh2012	.xls	Berkelhammer, M., et al. 2012. Mawmluh Cave, India Holocene Stalagmite d18O Data.
Moberg NHT reconstruction	.doc	Highly variable Northern Hemisphere temperatures reconstructed from low- and high-resolution data by Moberg, A., Sonechkin, D.M., Holmgren, K., Datsenko, N.M & Karlen, W
PDSI	.xlsx	The Palmer Drought Severity Index (PDSI) uses readily available temperature and precipitation data to estimate relative dryness.
Proxy data compilation	.xlsx	UMS10 timeseries with composite age model, with all other proxy records mentioned in this appendix, in one workbook.
Qunf2007	.txt	Fleitmann, D., et al. 2007. Qunf Cave, Oman Stalagmite Oxygen Isotope Data.
rongbuk2007	.xls	Kaspari, S., et al. 2008. East Rongbuk Glacier Col Ice Core 1,000 Year Geochemical Data.
Wanxiang2009	.txt	Zhang, P. et al. 2009. Wanxiang Cave, China Stalagmite Oxygen Isotope Data.

C Relating to Precipitation in Fiji

C.1 Rain sample logs

File name	Type	Description
Water Sample Records Jan-Jul 2013	.doc	Water sampling records January - July 2013, from University of the South Pacific Suva Campus, gathered, compiled and documented by Mark Stephens
Water Sampling Records Jan-Sep 2012	.doc	Water sampling records January - Sep 2012, from University of the South Pacific Suva Campus, gathered, compiled and documented by Mark Stephens

C.2 Isotopes

File name	Type	Description
Fiji Rain Isotopes	.xlsx	Oxygen isotope analyses from precipitation samples collected in Suva by Mark Stephens, using CF-IRMS and corrected to international reference materials.

C.3 HYSPLIT

File name	Type	Description
yymm Fiji Month yy frequency 24hours	.jpg	HYSPLIT back trajectory matrix outputs. Individual file names indicate year, month, starting location, and frequency of sampling.

C.4 Analysis

File name	Type	Description
Fiji water analysis 1 LOCKED	.xlsx	some columns redacted due to terms of usage of meteorological data supplied by Fiji Meterological Service. Fiji rain isotope and meteorological data analysed with SST, SST anomaly, Nino4 measurements, Multivariate ENSO Index, and Aquarius Sea Surface Salinity data.
Fiji water analysis 2 LOCKED	.xlsx	some columns redacted due to terms of usage of meteorological data supplied by Fiji Meterological Office. Fiji rain data analysed by wind direction, non-confidential rain data and summary statistics.
FMS Data & Product Agreement	PDF	Fiji Meteorological Service Data and Product agreement for release of meteorological data.
FMS Data & Product Request & Disclosure Form	PDF	Fiji Meteorological Service Product Request and Disclosure Form for release of meteorological data for this research.
README	.txt	READ BEFORE OPENING LOCKED SPREADSHEETS
Thornthwaite PET calcs	.xlsx	Output from Thorthwaite PET calc spreadsheet using Nacocolevu meterological data.
Thornthwaite PET method	.xlt	Computation template for potential evapotranspiration using the Thornthwaite method. Andre K Lehre (1994) Dept. of Geology, Humboldt State University.

C.5 Other data

File name	Type	Description
Fiji synoptic data and outputs	folder	netCDF files and .png visualisations of parameters: daily precipitable water, mean daily v wind, ensemble mean u wind, Omega 600mbar and outgoing longwave radiation. Visualised data date indicated on individual file
Aquarius SSS	.xlsx	Sea Surface Salinity data from Aquarius satellite data for coastal areas around Fiji. No wraparound possible for extracting, so separated either side of 180 degrees.
GNIP d18O precipitation islands	.xlsx	Compilation of GNIP data for Pacific Islands. Graphing by Dave Mattey
Nausori airport data	.xlsx	Meteorological data for Nausori Airport.
Nino4 data	.xlsx	Data is from PSD using the HadISST1 dataset. Rayner et al., 2003, Global analyses of sea surface temperature, sea ice, and night marine air temperature since the late nineteenth century, J. Geophys. Res., 108. and extrapolation to daily using Past3.
Radiosonde data	.xlsx	Radiosonde data from January 2012 Lat 17.75S177.45E Lon 18

D Relating to Pacific speleothem

D.1 Speleothem and Drip Stable Isotopes

File name	Type	Description
PU2 stable isotopes	.xlsx	1mm isotope traverse from speleothem core sample PU2, Atiu, Cook Islands
Vat13a Stable Isotopes	.xlsx	Vat13a Stable Isotopes master sheet including 2mm and 0.1mm resolution traverses
Volivoli cave drip isotopes	.xlsx	Volivoli cave drip water isotopes, collected by Mark Stephens and others, analysed at RHUL

D.2 Trace elements

File name	Type	Description
PU7 S2 NIST610	.xlsx	Laser ablation traverse data for slide 2, track 1 of sample PU7, Atiu, Cook Islands, corrected to NIST610 glass.
Vat13a Section A and B w NIST610	.xlsx	Vat13a Laser ablation data corrected to NIST610 glass from sections A and B.
Vat13a Section C and D w NIST610	.xlsx	Vat13a Laser ablation data corrected to NIST610 glass from sections C and D.

D.3 U series data

File name	Type	Description
2015 9 Atiu dates	.xlsx	U-Th disequilibrium raw data from September 2015 Atiu samples including PU7
161210 Vat13a and PU2 dates	.xlsx	U-Th disequilibrium raw data from September 2015 Atiu samples including PU2 and Vat13a
Age data	.xlsx	PU2, PU7 and Vat13a U-Th and preliminary age models.

D.4 Imaging

File name	Type	Description
PU2 microscopy	folder	Stereomicroscopy video images of PU2 thin sections arranged by slide number. Both XPL and PPL in individual file names, and scale bars within image.
PU7 microscopy	folder	Stereomicroscopy video images of PU7 thin sections arranged by slide number. Both XPL and PPL in individual file names, and scale bars within image.
Vat13a microscopy	folder	Stereomicroscopy video images of Vat13a thin sections arranged by slide number. Both XPL and PPL in individual file names, and scale bars within image.
MRI Scan Images	.ppt	functional Magnetic Resonance Imaging of Pu11.

D.5 Other

File name	Type	Description
Atiu rainfall and ONI	.xls	Atiu rainfall data and Oceanic Nino Index. Data from Andrew Lorrey, graphing by Dave Mattey
Fabric density working	.xlsx	test document to see if a density proxy record can be made from micromilled calcite weights.
Vat13a Lomb periodogram output	.xlsx	Vat13a isotopes lomb scargle periodogram ouput. calculated using Past3.